LBL-8862 c.2

A UNIFIED NUMERICAL MODEL FOR SATURATED-UNSATURATED GROUNDWATER FLOW

T. N. Narasimhan
(Ph. D. thesis)

RECEIVED
LAWRENCE
BERKELEY LABORATORY

APR 24 1979

LIBRARY AND
DOCUMENTS SECTION

February 1975

Prepared for the U. S. Department of Energy
under Contract W-7405-ENG-48

TWO-WEEK LOAN COPY

This is a Library Circulating Copy
which may be borrowed for two weeks.
For a personal retention copy, call
Tech. Info. Division, Ext. 6782

LAWRENCE BERKELEY LABORATORY
UNIVERSITY OF CALIFORNIA
BERKELEY

LBL-8862 c.2

LEGAL NOTICE

This report was prepared as an account of work sponsored by the United States Government. Neither the United States nor the Department of Energy, nor any of their employees, nor any of their contractors, subcontractors, or their employees, makes any warranty, express or implied, or assumes any legal liability or responsibility for the accuracy, completeness or usefulness of any information, apparatus, product or process disclosed, or represents that its use would not infringe privately owned rights.

A Unified Numerical Model
for Saturated-Unsaturated Groundwater Flow

Ph.D. Dissertation

in

Engineering Science, Civil Engineering

By

T.N. Narasimhan

Department of Civil Engineering
University of California
Berkeley
1975

I dedicate this work
to the memory of
my parents

TABLE OF CONTENTS

	Page
ABSTRACT	ii
TABLE OF CONTENTS	v
LIST OF FIGURES	x
LIST OF TABLES	xiv
NOMENCLATURE	xv
ACKNOWLEDGEMENTS	xx
I. INTRODUCTION	1
A. Motivation	1
B. The Problem	1
C. Purpose and Scope	4
D. Previous Work	5
II. PHYSICS OF SATURATED-UNSATURATED GROUNDWATER MOTION	9
A. Introduction	9
B. Governing Equation	12
1. Equation of motion	12
2. Equation of state	14
3. Conservation of matter	15
4. Divergence and divergence theorem	16
5. Equation of continuity	18
a. Differential form	18
b. Integral form	19
c. The dependent variable	20

Page

C. Initial and Boundary Conditions 21

1. Initial conditions 21

2. Boundary conditions 21

a. No-flow boundary 21

b. Prescribed flux boundary 21

c. Prescribed potential boundary 22

3. Sources and sinks 22

D. Fluid Mass Capacity of Porous Media 23

1. Compressibility of water 24

2. Deformation of soil skeleton 25

a. One-dimensional consolidation theory . 26

b. The concept of effective stress 27

c. Effective stress in the unsaturated region 29

d. Stress-strain relationships in soils . 33

e. The deforming volume element 40

f. Extension to multidimensional stress fields 44

3. Desaturation of soil skeleton 47

4. Final expression for fluid mass capacity of volume element 50

E. Integral Form of Governing Equations for Saturated-Unsaturated Groundwater Motion . . . 51

1. Variation of permeability in the saturated region 51

2. Variation of permeability in the unsaturated region 52

3. Complete governing equation for an isotropic medium 54

4. Equation of flow for an anisotropic medium 56

Page

F. Governing Equation for the Isotropic Case Based on Moisture Content, θ 57

III. METHODS OF SOLVING THE GOVERNING EQUATION 61

A. General Remarks 61

B. Numerical Methods 64

Integral formulations 65

C. Physical Basis of Development 66

D. Mathematical Development 70

1. Non-overlapping subdomains 77

2. Measurement of gradients 78

3. The Integrated Finite Difference Scheme . . 79

4. The Galerkin method and the IFD 80

5. Isoparametric elements 94

6. Advancing in the time domain 100

7. Matrix inversion versus iteration techniques 103

8. Choice of a suitable method 104

IV. DESCRIPTION OF THE NUMERICAL MODEL 109

A. Introduction 109

B. Numerical Formulation 110

1. Explicit and Implicit schemes 115

2. Explicit scheme and stability 116

3. Implicit method of solution 119

4. The parameters λ and γ 127

5. Evaluation of nonlinear coefficients . . . 128

Page

6. Boundary conditions 129

a. Prescribed potential and prescribed flux boundaries 129

b. Seepage face 130

c. Evaporation and evapotranspiration boundaries 130

7. Control of accuracy 132

8. Organization of computer program TRUST . . 135

V. RESULTS OBTAINED WITH THE NUMERICAL MODEL 140

1. Radial flow to a well 141

2. Continuous point source 143

3. One-dimensional consolidation of London clay 148

4. One-dimensional consolidation of clay slurry 154

a. Lagrangian formulation 160

b. Horizontal and vertical columns 162

c. Departure from experimental results . . 166

d. Accuracy and adjustment of nodal distances 168

e. Deforming and non-deforming coordinates 172

5. Rainfall infiltration 173

6. One-dimensional column drainage 178

Moisture suction and effective stress . . . 185

7. Drainage from a sand box 188

a. Material properties 190

b. Role of deformation of the soil skeleton 193

c. Comparison of experimental and numerical results 199

Page

8. Excavation in soft clay 212

9. Flow to a soil probe 223

VI. CONCLUSIONS AND RECOMMENDATIONS 233

A. Conclusions 233

1. Physics of the problem 233

2. Differential versus integral equations . . 233

3. Numerical methods 234

4. Development of computer program TRUST . . . 235

5. Testing of computer program and applications 235

B. Recommendations 236

1. Use of computer program TRUST 236

2. Improvements to the numerical model 237

a. Improvements to the calculational model 238

b. Improvements to the physics of the governing equation 238

REFERENCES 240

LIST OF FIGURES

Figure		Page
1.	Deep weathering patterns near Jos, northern Nigeria (after Ollier, 1969)	3
2.	Fluxes crossing boundary surface of an arbitrary subregion of the flow region	15
3.	Schematic representation of effective stress in the saturated and the unsaturated domains	30
4.	Variation of the parameter χ with saturation for four compacted, partly saturated clays	32
5.	Plot of void ratio, e, versus effective stress, σ', for San Francisco Bay Mud (data from Prof. W.N. Houston, University of California, Berkeley)	34
6.	Semi-log plot of void ratio, e, versus effective stress, σ', for San Francisco Bay Mud (data from Prof. W.N. Houston, University of California, Berkeley)	38
7.	Hysterisis between saturation and pressure head for Del Monte sand (after Liakopoulos, 1965)	48
8.	Hydraulic conductivity as a function of void ratio for saturated soils (after Lambe and Whitman, 1969)	53
9.	Hysterisis between hydraulic conductivity and pressure head for Del Monte sand (after Liakopoulos, 1965)	55
10.	Nodal points and their associated subregions; A. Independent subregions, B. Overlapping subregions	69
11.	Primary and Secondary elements	73
12.	Discretization of flow region into triangular elements	82
13.	Blow-up of triangle II of figure 12 and scheme for numerical integration	82
14.	Division of secondary element II into independent subregions	87

Figure		Page
15.	The non-overlapping subdomain of influence of nodal point m	87
16.	Disposition of nodes (elements) and nodal points in the Integrated Finite Difference scheme	93
17.	Curved isoparameteric quadrilaterals; A. Quadratic element, B. Cubic element	95
18.	Scheme for integration over a curved iso-parametric element	95
19.	Network of subregions	111
20.	Nodal points within subregions	111
21.	Points that govern the calculation of $\Delta\phi_n^{p+1}$	125
22.	Finite element and IFD meshes for radial flow to a well	142
23.	Radial flow to a well; comparison of numerical and analytical results	144
24.	Three-dimensional network of elements for the continuous point source problem	146
25.	Continuous point source; comparison of IFD and analytical solutions, A. time-drawdown plot, B. distance-drawdown plot	147
26.	Consolidation of non-homogeneous clay; initial and boundary conditions	150
27.	Consolidation of non-homogeneous clay; material properties	151
28.	Consolidation of non-homogeneous clay; comparison of numerical results	152
29.	Consolidation of non-homogeneous clay; volumetric strain-rate as a function of depth	153
30.	Consolidation of clay slurry; initial and boundary conditions	157

Figure		Page
31.	Consolidation of clay slurry; material properties, A. void ratio versus effective stress, B. void ratio versus permeability	159
32.	Consolidation of clay slurry; comparison of numerical and experimental results	164
33.	Consolidation of clay slurry; volumetric strain-rates of some typical elements	165
34.	Consolidation of clay slurry; relation between λ and e for a vertical column	167
35.	Consolidation of clay slurry; effect of ignoring nodal point displacements on the rate of consolidation, A. permeability uncorrected, B. permeability multiplied by 1.75	170
36.	Rainfall infiltration; initial and boundary conditions	174
37.	Rainfall infiltration; material properties (after Rubin et al., 1964)	175
38.	Rainfall infiltration; moisture profiles as a function of time	179
39.	Column drainage in Del Monte sand; intitial and boundary conditions	181
40.	Column drainage in Del Monte sand; material properties, A. moisture content versus pressure head, B. saturation versus pressure head, C. permeability versus pressure head	182
41.	Column drainage in Del Monte sand; comparison of numerical and experimental results, A. rigid sand, B and C. deformable sand	184
42.	Column drainage in Del Monte sand; comparison of numerical and experimental drainage rates	187
43.	Drainage from a sand box; initial and boundary conditions	189
44.	Drainage from a sand box; material properties, A. mean curves of moisture content versus pressure head, B. mean curve of permeability versus moisture content (after Vachaud et. al., 1971)	191

Figure		Page
45.	Drainage from a sand box; material properties used in the simulation, A. moisture content versus pressure head, B. saturation versus pressure head, C. permeability versus pressure head	192
46.	Drainage from a sand box; initial distribution of pressure head at different abcissa (after Vachaud et. al., 1971)	194
47.	Drainage from a sand box; initial distribution of moisture content at different abcissa (after Vachaud et. al., 1971)	195
48.	Drainage from a sand box; initial distribution of pressure head and saturation used in the simulation	196
49.	Drainage from a sand box; discretization of the flow region	197
50.	Drainage from a sand box; effect of different values of C_c on the evolution of the surface, $\psi = 0$	200
51.	Drainage from a sand box; comparison of numerical and experimental results of the evolution of the surface, $\psi = 0$	201
52.	Drainage from a sand box; cumulative depletion from storage as a function of time	203
53.	Drainage from a sand box; experimentally observed evolution of isopotentials	204
54.	Drainage from a sand box; numerically computed evolution of isopotentials	205
55.	Drainage from a sand box; deviation of computed potentials from observed potentials	208
56.	Drainage from a sand box; contribution to cumulative depletion from storage by some parts of the flow region	210

Figure		Page
57.	Excavation in soft clay; initial and boundary conditions	213
58.	Excavation in soft clay; material properties, A. void ratio versus effective stress, B. void ratio versus permeability	216
59.	Excavation in soft clay; discretization of the flow region	218
60.	Excavation in spft clay; evolution of isopotentials and the surface, $\psi = 0$	219
61.	Excavation in soft clay; pattern of consolidation and swelling	221
62.	Excavation in soft clay; time-rates of strain of four typical elements in the flow region	222
63.	Flow to a soil probe; physical description of the model	226
64.	Flow to a soil probe; material properties	227
65.	Flow to a soil probe; distribution of pressure head as a function of time	228
66.	Flow to a soil probe; distribution of moisture content as a function of time	230
67.	Flow to a soil probe; cumulative volume of effluent as a function of time	231
68.	Flow to a soil probe; percent contribution to cumulative depletion from storage by one cm. wide shells of the flow region	232

LIST OF TABLES

Table		Page
V.I	Compressibility and related coefficients at $t = 0$ for a node located at an elevation of 1.05 m. above the bottom of the sand box	198

NOMENCLATURE

Symbol	Description	Dimensions
A	General term used for hydraulic conductivity in discussing numerical formulations	L/T
$\bar{A}$	Parameter proposed by Skempton for calculating change in pore pressure due to change of loading under undrained conditions	1
a	Arbitrary variable used in writing divergence theorem and Green's First identity	
a_v	Coefficient of compressibility	LT^2/M
B	i) Parameter proposed by Skempton for calculating change in pore pressure due to change in loading under undrained conditions	1
	ii) General term used for fluid mass capacity per unit volume in discussing numerical methods	M/LL^3
b	Arbitrary variable used in writing divergence theorem and Green's First identity	
C	Specific Moisture Capacity (in the zone of partial saturation)	$1/L$
C_c	Compression Index; slope of the best-fitting straightline on the e versus log effective stress plot	1
C_k	Slope of the best-fitting straightline on the e versus log k plot	1
C_s	Swelling Index; slope of the best-fitting straightline on the e versus log effective stress plot in the rebound region	1
C_v	Coefficient of consolidation, used in soil mechanics literature	L^2/T

Symbol	Description	Dimensions
D	Diffusivity of the soil, used in soil physics literature	L^2/T
D_m	Transformed Diffusivity in material coordinates, used in the clay slurry problem	L^2/T
D'	General term used for fluid mass capacity in discussing numerical methods	M/L
$d_{n,m}$	Distance between nodal points n and m	L
E_n	Difference between the values of potential of nodal point n for two successive iterations	L
e	Void Ratio	1
F	Material identification label	
G	Intensity of source or sink, integrated over a finite subregion	M/T
g	Accelaration due to gravity	L/T^2
K	Hydraulic conductivity	L/T
k	Absolute permeability	L^2
M_c	Fluid mass capacity of a finite subregion	M/L
m	Material coordinate in the clay slurry problem	L
m_c	Specific fluid mass capacity; M_c per unit volume	M/LL^3
m_v	Coefficient of volumetric compressibility	LT^2/M
n	Porosity	1
$\vec{n}$, $\vec{n}_i$	unit outer normal	
p	i) Pressure	M/LT^2
	ii) when used as a superscript, denotes iteration number	
p_o	Reference pressure	M/LT^2

Symbol	Description	Dimensions
$\vec{q}$	Specific Flux or Darcy velocity	L/T
S	i) Saturation	1
	ii) Surface of integration	L^2
S_s	Coefficient of specific storage, used in groundwater literature	1/L
t	Time	T
U	Degree of consolidation, used in soil mechanics literature	1
$U_{n,b}$	Surface conductance between node n and boundary node b	M/T
$U_{n,m}$	Surface conductance between node n and node m	M/T
u	Pore pressure in soil mechanics literature	M/LT^2
	ii) General term for hydraulic potential in discussing numerical methods	L
V	Bulk volume of soil	L^3
V_s	Volume of soilds	L^3
V_v	Volume of voids	L^3
x_i	Space coordinate	L
Z_n	Sum of the surface conductances of all the surfaces bounding node n	M/T
z	Elevation head	L
z_o	Reference datum	L
β	Coefficient of water compressibility	LT^2/M
γ	Accelaration parameter used in the iterative scheme	1

Symbol	Description	Dimensions
γ_w	Specific weight of water	ML/T^2
$(\Delta t)_n$	Time constant or stable time step for node n	T
ε_v	Volumetric strain	1
ζ	Space coordinate	L
η	Space coordinate	L
θ	Volumetric mositure content	1
λ	i) Parameter determining the weight of backward differencing scheme in the implicit method	1
	ii) Boltzman's transformation	$L/T^{1/2}$
μ	Viscosity of water	M/LT
ν	i) Poisson's ratio	1
	ii) Arbitrary parameter in some empirical relationships	1
ξ_n	Linear coefficient to characterize variation of potential over a elemental region	1
ρ	Mass density	M/L^3
ρ_o	Reference density at p = 0	M/L^3
σ	i) Total stress at a point	M/LT^2
	ii) when used as $d\sigma$, in a surface integral, denotes differential surface area	L^2
$\sigma_1, \sigma_2, \sigma_3$	Principal stresses	M/LT^2
$\sigma_{m,n}$	Surface area between nodes m and n	L^2
σ'	Effective stress	M/LT^2
$(\sigma)_w$	Total stress expressed in equivalent height of water column	L
$(\sigma')_w$	Effective stress expressed in equivalent height of water column	L

Symbol	Description	Dimensions
τ	Volume of small elemental sub-region, in writing divergence	L^3
Φ	Hydraulic potential or Fluid potential or Buckingham-Hubbert potential	L^2/T^2
ϕ	Hydraulic head	L
χ	Coefficient proposed by Bishop to calculate effective stress in the unsaturated zone	1
ψ	Pressure head; pore pressure expressed in equivalent height of column of water	L
ω	i) Weighting function, in the Method of Weighted Residuals	1
	ii) Some arbitrary experimental parameters	1

ACKNOWLEDGEMENTS

I would first like to express my gratitude to Prof. P.A. Witherspoon for his sustained interest, encouragement and patience which contributed greatly to my education. I have had his invaluable guidance in every phase of this work. To Prof. W.N. Houston, I am grateful for many stimulating discussions on soil mechanics, for valuable suggestions during the course of the research work and for his final critique of the manuscript. Through many hours of thought-provoking discussions on the fundamentals of flow through variably saturated porous media, Prof. P.R. Day has significantly contributed to the present work. I am indebted to him for this and for his final critical evaluation of the manuscript. My sincere thanks are due to Prof. D.K. Todd for constructive suggestions and for his final perusal of the manuscript.

As a close friend and fellow student, Donald Helm has been a constant source of strength and inspiration to me. For this and for a careful scrutiny of the final manuscript, I convey him my sincere feelings of appreciation. My special thanks are due to Dr. A.L. Edwards of the Lawrence Livermore Laboratory. Through several discussions with him I gained a better understanding of the phenomenon of mass transfer in porous media. Dr. D.E. Smiles of the CSIRO, Canberra, Australia, very willingly helped me with fruitful discussions on water movement in swelling soils, for which I am very thankful to him. For an in-depth criticism of the third and the fourth chapters of the manuscript, I am indebted to my friend and colleague, Dr. Shlomo Neuman.

It has been my great previlege to have had, as my fellow-students, several energetic and enthusiastic minds. I fondly recall many interesting exchange of ideas with Marcelo Lippman, Tom Lasseter, Ardeshir Asfari, John Gale, Mike Sorey, Gregg Korbin, Yoshi Moriwaki, Dai Watkins and P.N. Sundaram. It is a pleasure to acknowledge the help of Ms. Gloria Pelatowski, who, with patience and care, drafted all the figures.

With gratitude, I acknowledge the financial assistance received from the Earl C. Anthony Fellowship, the Neshan Zovick Fellowship, the Jane Lewis Felloship and the Geological Engineering Foundation.

The efforts and the sacrifice of the members of my family in connection with the present work exceed my own individual efforts. With humor and forbearance, my wife Vijayalakshmi (Vijaya) and my son Lakshminarayanan (Ravi) have given me strength at times of frustration and have shared the joys of my successes. With pride and affection, I convey to them my deep sense of gratitude.

During the period of my studies at Berkeley there arose several occasions when my family and I should have been back home in India to share emotions with our closest relatives. The memory of these events make me feel particularly humble at the time of completing this thesis.

CHAPTER I

INTRODUCTION

A. MOTIVATION

The present work is an attempt to develop a numerical model for analyzing the transient flow of groundwater in fully or partially saturated, multidimensional heterogeneous porous media. The motivation for this effort originated with the author's experiences as a hydrogeologist in studying the occurrence of groundwater in the hard rock areas of peninsular India. However, the numerical model itself, which has been developed from the fundamental concepts of fluid flow in porous media, has proved to be applicable to a wide class of problems in the fields of soil mechanics, hydrogeology, and soil physics. In the following pages, a description of this model and its possible applications in various fields will be presented.

B. THE PROBLEM

In order to introduce the problem, it is appropriate to briefly describe the occurrence of groundwater in the hard rock areas of peninsular India.

The Indian peninsula forms part of an ancient geological shield and is mostly occupied by hard rocks such as granites, gneisses and basalts. Since these rocks lack primary porosity, the groundwater occurrence in them is chiefly governed by the formation of secondary porosity. The development of such secondary pore spaces may occur either due to structural deformation (fissures, fractures,

joints and faults) or due to the effects of weathering. The groundwater reservoir in the hard rock areas of India is therefore made up of the weathered mantle grading below into the fractured rock. Experience has shown that, when well developed, the zone of weathering can provide valuable space for the accumulation and movement of groundwater. For this reason, the zone of weathering is eagerly sought after for siting domestic, irrigation, and industrial water wells.

A complete model of the groundwater reservoir in a hard rock area of peninsular India should therefore take into consideration the weathered zone as well as the jointed rock below. However, since the treatment of flow of water in fractures is in itself a complex subject and since the weathered zone, whenever it is well developed, stores the bulk of the available groundwater, we will restrict our attention to the nature of the weathered zone.

Physically, the weathered zone is very irregular in extent, the depth of weathering varying considerably even over short distances (figure 1). Also, due to the variable nature of the weathering processes, the weathered material is heterogenous with respect to its physical properties such as porosity and permeability. In order to mathematically simulate groundwater movement in such an irregular, heterogenous system, one would require a general, multidimensional model.

Moreover, the weathered zone is generally a near surface phenomenon and in the semi-arid Indian peninsula the seasonal waterlevel fluctuations in it are often considerable in relation to the overall depth of weathering. As a result, it seems reasonable to infer that

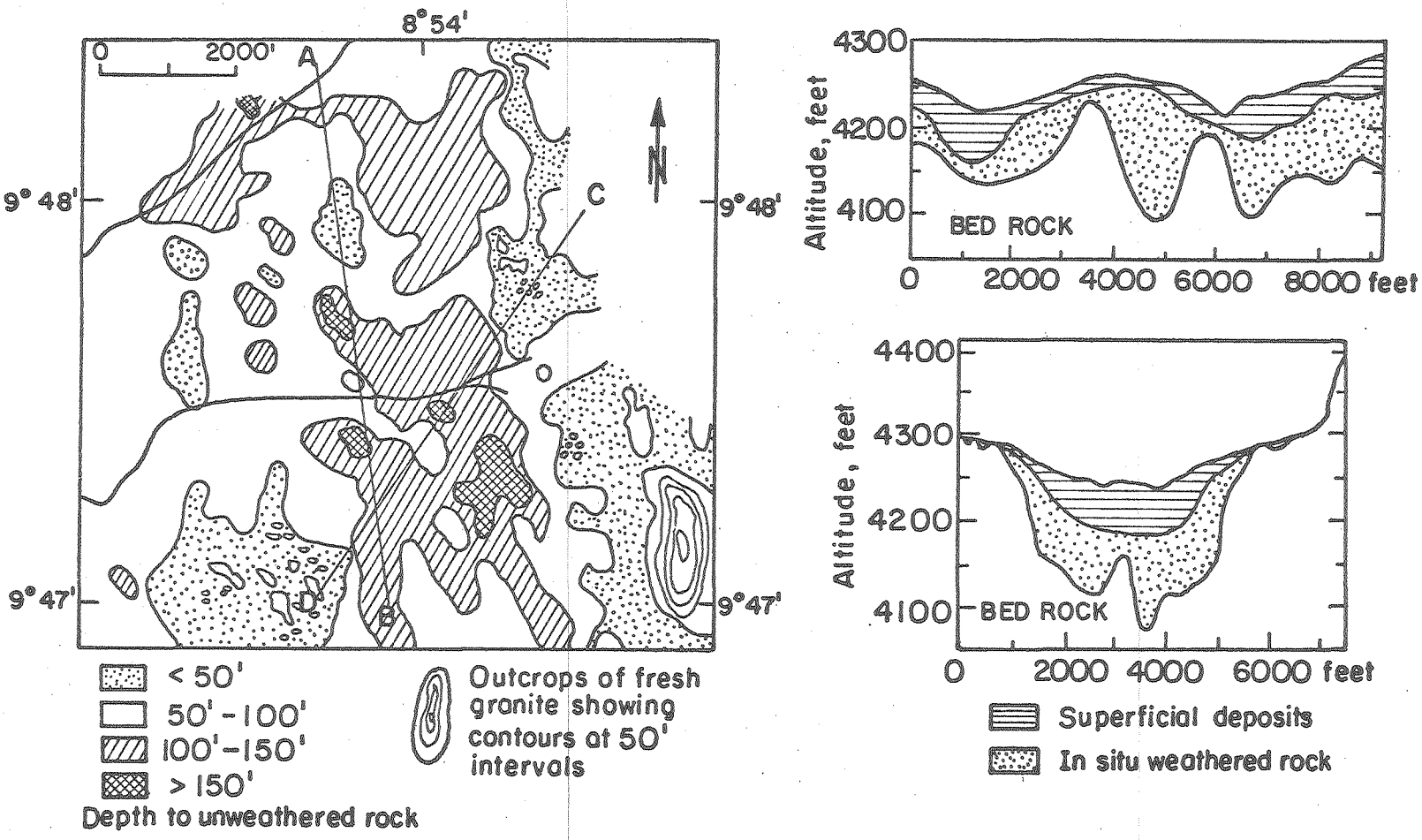

Fig. 1. Deep weathering patterns near Jos, northern Nigeria (after Ollier, 1969)

a significant part of the available groundwater may occur in the zone of partial saturation, above the water table.

For India, as well as many other agriculturally oriented countries having hard rock terranes, a proper management of the limited groundwater supplies available in the weathered zone is of vital economic importance. It seems therefore very worthwhile to direct one's efforts towards the problem of a detailed study of groundwater occurrence in the weathered zone, using a numerical model. In the light of the features of the weathered zone described in the last paragraph, the problem initially reduces to one of developing a general, transient, multidimensional model for the flow of fluids in variably saturated, heterogeneous porous media.

C. PURPOSE AND SCOPE

The present work is essentially an attempt to develop a suitably general mathematical model for analyzing transient, multidimensional fluid flow in variably saturated, heterogenous porous media. Towards this end, the physical principles of groundwater motion in variably saturated porous media is first considered in detail. This is followed by an examination of the available mathematical tools of analysis and the selection of an appropriate tool for the present study. Then, the mathematical model chosen for the present study is described. In order to check the validity of this approach, the model is then used to solve several typical problems for which solutions have already been obtained and published in the literature and the results are compared for consistency. Having looked into the reasonableness and validity of

the model, the possible applications of the model are finally described. Thus, the principal effort is to develop a general mathematical model and demonstrate its application.

D. PREVIOUS WORK

Up until a few years ago, very little attention seems to have been paid to the development of an unified saturated-unsaturated flow model, giving due considerations to the factors peculiar to each regime of flow. Indeed, until recently, the unsaturated domain of flow has mainly interested the soil physicists, concerned with the movement of water in soils in so far as it directly affects the well being of plants. On the other hand, both groundwater geologists and soil engineers have devoted a greater part of their research efforts to study the flow of water in the saturated zone. The phenomena by which water is absorbed or released from storage by the soil differ significantly in the saturated and in the partially saturated zones. In the saturated zone, water is released from or taken into storage because of the deformation of the soil skeleton and a consequent change in the porosity of the soil. In the unsaturated zone water is released from storage primarily through a process of desaturation, although some deformation of the soil skeleton may occur. In dealing with unsaturated flow, soil physicists generally tend to ignore the deformation characteristics of the soil skeleton, while the soil engineers and hydrogeologists, concentrating on the saturated zone, generally neglect the effects of desaturation.

It stands to reason that in order to model a flow region where both saturated and unsaturated regimes coexist, one should combine the physical features governing the nature of each of these important phenomena.

Since the early 1950's, research work on numerical modelling of flow through unsaturated or saturated porous media has been growing at an ever accelerating pace, with the contemporaneous development of high speed digital computers. The earliest efforts were limited to the study of simple one-dimensional models which subsequently evolved into the study of either two-dimensional models or three-dimensional models with radial symmetry. The construction of three-dimensional models was somewhat a later development because of the large size of computer storage and computations involved. Nevertheless, since the late 1960's, computers with sufficiently large capacity, speed, and precision have been available and this has facilitated the study of general, multidimensional, transient groundwater flow models, simultaneously considering saturated and unsaturated regimes of flow.

So far as is known, the only three-dimensional saturated-unsaturated flow model available in the literature is that of Freeze (1971). Freeze's model is a finite difference model, which takes into account the effects of hysteresis in the moisture content-pressure head and in the moisture content-permeability relationships in the unsaturated zone. In the saturated zone, consideration is given to the compressibility of the different materials making up the flow region. In addition, Freeze also considers the density and the viscosity of the fluid as fundamental quantities, so that the model

could equally well handle the flow of other fluids.

Being a finite difference model, Freeze's model is less convenient to use in the case of flow regions of arbitrary geometry. Moreover, while his model takes into account the compressibility of the soil, it does not treat the more basic relationships between compressibility and the state of stress, a feature which may be of considerable importance in shallow, consolidating systems.

The present work seeks to overcome these two limitations by developing a method for handling arbitrary geometries with ease and modelling stress-strain relationships of the soil skeleton more faithfully.

The combined, saturated-unsaturated flow phenomena encompass a wide spectrum of problems, having relevance in the fields of soil mechanics, hydrogeology, and soil physics. At one extreme is the problem of diffusion in porous media of extremely low saturation. At the other extreme is the problem of flow of electrolytes in extremely swelling soils. There is every reason to believe that the physical and physico-chemical processes governing these two extremes are widely different and to synthesize them in a single calculational model would be a very complex and possibly an uneconomical task. However, most problems encountered by the soil engineer or the hydrogeologist or even the soil physicist do not lie at these extremes. A wide class of their problems deal with materials of moderate compressibility at moderate to high levels of saturation. These problems, as can be judged from the works of Freeze (1971), Braester et al.(1971), Neuman (1972) and others, can in fact be brought into the folds of a single workable,

calculational model. The present work, which has been a venture to develop such a model has not only suggested the practibability of such a general model but also, apparently, has provided a common base for a free interaction between the disciplines of soil mechanics, soil physics and hydrogeology. From what can be gathered from available literature, such an interaction appears to have been very limited in the past.

CHAPTER II

PHYSICS OF SATURATED-UNSATURATED GROUNDWATER MOTION

A. INTRODUCTION

The foundation for an unified treatment of transient groundwater flow in variably saturated soils was given by Edgar Buckingham (1907) who was a soil physicist with U.S. Bureau of Soils, who introduced the concept of capillary potential. Buckingham's concept was the starting point for much of the subsequent work in the field of soil physics, including the classical contribution of L.A.Richards (1931) on the capillary conduction of liquids in porous mediums. Almost an identical concept of fluid potential was independently developed by M.K. Hubbert (1940), who was probably unaware of the earlier work of Buckingham in the field of soil physics. The concept of fluid potential, coupled with Darcy's Law lies at the base of almost all present day analysis of isothermal flow of liquids in porous media.

In nature, groundwater is in a constant state of motion, obeying Newtonian laws. For a quantitative study of this motion, it is convenient to assume that groundwater moves from suitably defined "higher" to a "lower" state. Buckingham's capillary potential and Hubbert's fluid potential are both measures of this "state". Simply stated, the fluid potential at a point in the flow region is the amount of mechanical energy stored in an unit mass of the fluid. Some soil physicists prefer to define capillary potential as energy per unit weight of water (see, for example, Phillip, 1972).

In an isothermal system, a unit mass of water derives energy from three sources, namely, a) potential energy, by virtue of its position in the gravitational field, b) elastic energy, due to the elastic compressibility of the mass due to hydrostatic pressures, and c) kinetic energy by virtue of its velocity of motion.

Now, Darcy's law, which is fundamental to the theory of groundwater motion, is a statistical, macroscopic concept. It has been shown by Hubbert (1940) that in order to derive this statistical concept from the complex flow phenomena occurring in the microscopic pores, one has to realize a scale change of several orders of magnitude without destroying the kinematic properties of the flow system. It has further been shown by Hubbert that in order for the kinematics of the microscopic and macroscopic systems to be identical, the kinetic energy of the unit mass of water should be negligible in comparison with its potential and elastic energies. In most natural groundwater systems, the velocity of motion is so small that the kinetic energy component can, in fact, be safely neglected. Therefore, the mechanical energy per unit mass of water in an isothermal system reduces to the sum of its potential energy and its elastic energy. Thus, we have,

$$\Phi = g\,(z - z_o) + \int_{p_o}^{p} dp/\,\rho(p) \qquad \text{(II.1)}$$

where, Φ is the fluid potential

g is the gravitational constant

z is the elevation above datum, z_o

p is the hydrostatic pressure above the datum, p_o

and ρ is the density of the fluid, which is a unique function of the hydrostatic pressure p

If we set p_o equal to atmospheric pressure and define it to be zero, equation (II.1) reduces to,

$$\Phi = gz + \int_o^p dp/\ \rho(p) \qquad \text{(II.2)}$$

The pressure dp exerted by a column of fluid of height $d\psi$ and at an average hydrostatic pressure p is given by,

$$dp = \rho(p)\ g\ d\psi \qquad \text{(II.3)}$$

Substituting (II.3) into (II.2) and factoring out $\rho(p)$ in the numerator and in the denominator, we get,

$$\Phi = gz + \int_o^\psi g\ d\psi$$

$$= gz + g\psi = g\ (z + \psi) \qquad \text{(II.4)}$$

where, ψ can be conveniently termed the pressure head, which can be experimentally determined by inserting a manometer (piezometer) at the point of interest and letting the fluid rise in the manometer. We can conveniently factor out g in equation (II.4) and write,

$$\phi = \Phi/g = z + \psi \qquad \text{(II.5)}$$

where ϕ can be called the hydraulic potential and is a measure of the fluid potential.

In saturated porous media the hydrostatic pressure exerted by the fluid is greater than atmospheric and hence, in such media, $\psi \geq 0$. However, when the medium is not fully saturated, ψ is negative. In soil physics literature, negative pressure heads are customarily termed as moisture "suction" or "tension".(*) Experimental determination of such soil moisture suction can be carried out with the help of "tensiometers", instead of the simpler "piezometer".

The quantity ϕ is a scalar and is a function of space and time ($\phi = \phi(x_i, t)$). The force that causes groundwater to move originates in the spatial gradient of this scalar potential. At any given point in the flow region, therefore, the velocity of groundwater motion is directly proportional to the gradient of ϕ.

B. GOVERNING EQUATION

1. Equation of Motion

The quantitative relationship existing between the potential gradient and the velocity of groundwater motion in a soil is expressed by the equation of groundwater motion. It was experimentally

---

(*) The present work, which originated in the field of hydrogeology has culminated with some interactions between the fields of soil mechanics, soil physics and hydrogeology. Therefore, in the selection of nomenclature and symbols in this work, efforts have been made towards a standardization, conforming as closely as possible to common usages in these disciplines.

observed by Henry Darcy in 1856 that in the case of sands, the velocity of groundwater seepage was directly proportional to the gradient of ϕ. The validity of this observation has since been confirmed for a wide class of soils, provided that the flow is laminar and there is no turbulence. For isotropic media, Darcy's law is simply expressed as

$$\vec{q} = -K \vec{\nabla}\phi \qquad \text{(II.6)}$$

in which $\vec{q}$ is the specific flux or Darcy velocity

K is the constant of proportionality and is called hydraulic conductivity or coefficient of permeability

and the negative sign denotes that flow is in the direction of decreasing potential.

The quantity K in (II.6) is actually a lumped parameter, combining the properties of the flow region as well as the fluid. Again, as demonstrated by Hubbert (1940), K can be decomposed into its more basic components as follows:

$$K = k\rho g/\mu \qquad \text{(II.7)}$$

where, k is the specific permeability, which is a fundamental property of the porous medium

and μ is the coefficient of viscosity of the fluid and is a constant in isothermal systems

Substituting (II.7) and (II.5) into (II.6), we get,

$$\vec{q} = -(k\rho g/\mu)\,\vec{\nabla}(z + \psi) \qquad \text{(II.8)}$$

Darcy, who was concerned with a saturated medium, proposed the equation in the form (II.6). However, it was probably Buckingham (1907) who first separated the gravitational and pressure components and wrote the equation in the form (II.8). For this reason, L.A. Richards (1960) suggested that equation (II.8) be named after Buckingham. However, as Swartzendruber (1969) reasoned, (II.8) should probably be named after both Darcy and Buckingham.

2. Equation of State

In (II.8) the quantity ρ which denotes fluid density is in itself a function of hydrostatic pressure. The dependence of ρ on hydrostatic pressure is the equation of state for water, which is given by the relation (Muskat, 1937),

$$\rho = \rho_o\, e^{\beta(p - p_o)} \qquad \text{(II.9)}$$

where β is the compressibility of water. If we let p_o be atmospheric pressure and define it to be zero, then, (II.9) reduces to

$$\rho = \rho_o\, e^{\beta p} \qquad \text{(II.10)}$$

Since water has very low compressibility, we can let $p \simeq \rho_o g\psi$ and thus,

$$\rho \simeq \rho_o e^{\beta \rho_o g \psi} \tag{II.11}$$

Equation (II.11) can be considered an adequate expression for the equation of state for water.

3. Conservation of matter

In transient groundwater motion, the distribution of potential within the flow region undergoes continual change with time. The nature of the time-dependence of this potential field is governed by the law of conservation of mass, subject to the constraints of the equations of motion and of state. The conservation law as applied to fluid flow or heat transfer is also known as the equation of continuity.

Consider a finite subregion of the flow region as depicted in figure 2.

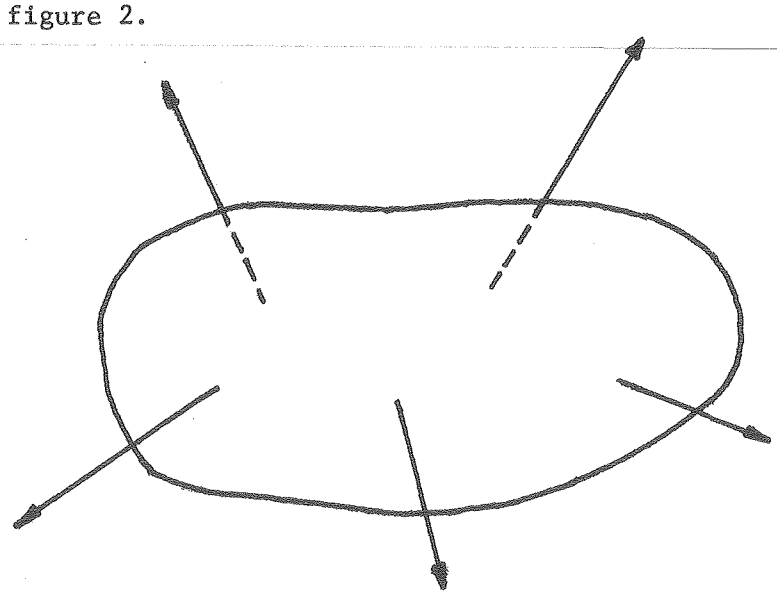

Fig. 2. Fluxes crossing boundary surface of an arbitrary subregion of the flow region

Under transient conditions of flow, water enters and leaves the flow region at different rates at different parts of the enclosing surface. The nature of transient flow is such that if we sum up all the mass that enters and leaves the system across the bounding surface over a small interval of time, there would result either a mass excess or a mass deficiency. The special case, when the inflow exactly equals the outflow so that there is neither a mass excess nor a mass deficiency, is the phenomenon of steady state flow.

Since mass can neither be created nor destroyed, the mass excess or deficiency arising from a particular flow condition has to be absorbed into or released from the particular small part of the flow region under consideration. The equation of continuity, then, is a statement, equating the summation of the rates at which mass enters or leaves a closed subregion of the flow region and the rate at which mass is absorbed by the subregion.

Before expressing the equation of continuity in mathematical form, it is advantageous to introduce the concept of divergence.

4. Divergence and divergence theorem

The concept of divergence is introduced as a measure of the rate per unit volume at which fluid is accumulating within an infinitesimally small closed subregion, whose maximum dimension tends to zero. Divergence is defined (Sokolnikoff and Redheffer, 1966) as,

$$\operatorname{div} \vec{q} = \lim_{T \to 0} 1/\tau \int_S \vec{q} \cdot \vec{n} \, d\sigma \qquad \text{(II.12)}$$

where $\vec{q}$ is the velocity of the fluid

T is the maximum dimension of the elemental volume

τ is the volume of the element

$\vec{n}$ is the unit normal

S is the closed surface bounding the element

and $d\sigma$ is the differential surface area

An advantage in using the concept of divergence that its definition is independent of any coordinate system and hence it is invariant. Note that by definition, divergence relates to an infinitesimal volume element. However, in numerical modelling one deals with larger, macroscopic elements. In order to extend the concept of divergence to macroscopic elements, we make use of the fundamental relation called divergence theorem or Gauss' theorem, which relates a volume integral to a surface integral. According to Sokolnikoff and Redheffer (1966), divergence theorem can be stated as,

$$\int_S \vec{q} \cdot \vec{n} \, d\sigma = \int_V \operatorname{div} \vec{q} \, dV \qquad \text{(II.13)}$$

Physically, the right hand side of (II.13) amounts to dividing a finite region V into a large number of small volume elements and summing up the rate of fluid increase in each element in order to obtain the overall fluid mass increase in V. The left hand side of (II.13) on the other hand, amounts to subdividing the bounding surface S into a large number of surface segments and algebraically summing up the fluid fluxes that leave the system. The equality

sign in (II.13) simply states that the fluid excess arising out of transient flow of fluid across the bounding surface of the element (left hand side of (II.13)) is accomodated by an equivalent increase in the fluid content within the element (right hand side of (II.13)). This is but a restatement of the conservation equation. Note also that the left hand side of (II.13) is the cause and the right hand side is the effect.

5. Equation of continuity

a. Differential form

In soil physics literature, Richards (1931) was probably the earliest to express the equation of continuity for transient soil water movement in the form of a parabolic, partial differential equation. Familiarly known as the Richard's equation, it can be written in cartesian coordinates as,

$$- \text{div}\, \vec{q} = - \vec{\nabla} \cdot \vec{q} = \partial\theta/\partial t \qquad \text{(II.14)}$$

where θ is the volumetric moisture content, defined as the volume of water per unit volume of soil

and $\vec{q}$ is specific flux or Darcy velocity

In (II.14) the density of water has been omitted assuming that variations in the density of water can be practically neglected. It is easy to see that Richard's equation is also an expression of the conservation of mass.

b. Integral form

The differential equation in (II.14) is the starting point for solving most problems of groundwater flow using analytical techniques. It is also the starting point for the finite difference schemes of numerical analysis. However, the numerical model which we shall eventually develop in the present work is based on the study of interactions between adjacent macroscopic volume elements in space. For such purpose, it is more natural to express the continuity equation in the form of an integral equation, rather than a differential equation. Thus, we have (see, for example, Encyclopedia of Science and Technology, McGraw Hill, vol. 5, p. 45, 1960),

$$-\int_V \operatorname{div} \vec{q}\, dV = -\int_S \vec{q} \cdot \vec{n}\, d\sigma = \frac{\partial}{\partial t} \int_V \theta dV$$

$$= \frac{\partial}{\partial t} (V\theta), \qquad \text{(II.15)}$$

assuming that θ represents an average value over the subregion. Introducing the density term into (II.15) we get the following integral equation for mass balance,

$$-\int_V \operatorname{div} \rho\vec{q}\, dV = -\int_S \rho\vec{q} \cdot \vec{n}\, d\sigma = \frac{\partial}{\partial t} (V\rho\theta) \qquad \text{(II.16)}$$

where, ρ is the mass density of the fluid.

The amount of moisture contained in a unit volume of the soil, θ, is a function of porosity, n, and saturation, S. Thus $\theta = nS$.

Substituting this expression for θ into (II.16), we get,

$$-\int_V \operatorname{div} \rho\vec{q}\, dV = -\int_S \rho\vec{q} \cdot \vec{n}\, d\sigma = \frac{\partial}{\partial t}(V\rho nS) \qquad \text{(II.17)}$$

The usefulness of these expressions will be apparent from the following paragraphs.

c. The dependent variable

In practical problems of fluid flow in porous media, the most easily measured physical parameter is the fluid potential. Also, in itself, the variation in fluid potential is a phenomenon of considerable interest in studying flow through porous media. Hence, in the practical use of (II.17), it is convenient to make fluid potential the dependent variable. Thus, substituting (II.8) into (II.17), assuming that z is a constant during the time interval and applying the chain rule of differentiation to the time derivative on the right hand side of (II.17), we obtain,

$$\int_V \operatorname{div} \left[\rho\frac{k\rho g}{\mu}\vec{\nabla}(z+\psi)\right] dV = \int_S \rho\frac{k\rho g}{\mu}\vec{\nabla}(z+\psi)\cdot\vec{n}\, d\sigma$$

$$= \frac{d}{d\psi}(V\rho nS)\frac{\partial\psi}{\partial t} \qquad \text{(II.18)}$$

In using equation (II.18), one seeks to solve for the time derivative $\partial\psi/\partial t$ of the dependent variable at selected points in the flow region, with a priori knowledge of all the other variables.

C. INITIAL AND BOUNDARY CONDITIONS

1. Initial conditions

Let us now consider the surface integral in (II.18). At any instant of time t_o, there is an initial distribution of ψ_o within the flow region bounded by the surface S. This region may be a part or all of the flow region. This distribution of ψ_o forms the intial condition for the transient fluid flow problem.

2. Boundary conditions

The flow region as a whole communicates across its boundaries with its surroundings. The nature of this communication is reflected in the conditions that exist on the boundary of the flow region. The nature of these conditions are termed boundary conditions and, in general, these are of three types. In addition, there may exist "mixed boundary conditions" of special types, which we will omit for the present.

a. No-flow boundary

When no fluid enters or leaves the flow region across its boundary, the boundary is called a no-flow boundary. In fluid flow, an impermeable barrier or a plane of symmetry of flow is an impermeable boundary. Mathematically, this is identical to the condition that there is no gradient in potential across this boundary and hence, $\partial\phi/\partial\vec{n} = 0$, in which $\vec{n}$ denotes the normal to the boundary.

b. Prescribed flux boundary

It may so happen that the flow region receives fluid from or discharges fluid to its surroundings at a known or prescribed rate. For example, a soil may be receiving rainfall infiltration at a constant rate or a well may be discharging the flow region at a

constant or variable rate. Such a condition is known as a prescribed flux boundary condition. Mathematically, this amounts to saying that, for a unit surface area of the boundary, $\partial\phi/\partial\vec{n}$ is known. Such a condition is called a Neumann problem in potential theory. Indeed, the no flow boundary condition, (a), can be considered as a special case of the Neumann problem.

c. Prescribed potential boundary

The third type of boundary condition arises when the flow region interacts with a very large reservoir of the fluid and receives fluid from or discharges fluid into this practically infinite reservoir. In this case, the potential on the boundary will be determined by the fluid potential in the infinite reservoir, which may fluctuate in time in a known, prescribed manner. This type of boundary condition is called a Dirichlet problem in potential theory.

In most problems of practical interest different parts of the boundary of a flow region may experience different types of boundary conditions and thus these problems are mixed initial-boundary-value problems.

3. Sources and Sinks

In addition to the movement of fluid that is caused by the initial and boundary conditions, fluid may be arbitrarily extracted from or added to the flow region at one or more locations. Such locations, usually of very small or infinitesimal spatial extent are called sinks or sources. When present, sources and sinks materially affect the mass balance expressed by (II.18). Hence their effects would have to be duly incorporated into (II.18), as will be done subsequently.

D. Fluid Mass Capacity of Porous Media

In describing initial and boundary conditions, we considered the left hand side of the continuity equation (II.18). We shall now turn our attention to the right hand side of this equation.

The quantity $\partial\psi/\partial t$ in (II.18) represents the time rate of change in pressure head within the region of interest bounded by the surface of integration. The magnitude of the change in pressure head, however, is actually an expression of the ability of the flow region of interest to absorb the mass excess arising out of ground-water movement into and out of it. The expression $d(\rho nSV)/d\psi$, occuring on the right hand side of (II.18) quantitatively defines this ability of the flow region to absorb mass excess, per unit change in pressure head, ψ. We can therefore conveniently define a term $M_c = d(\rho nSV)/d\psi$ and call it "Fluid Mass Capacity" of the finite flow region. Thus, fluid mass capacity is defined as the mass of water absorbed or released by finite subregion of volume V, for a unit change in the pressure head. The factors that govern the magnitude and variation of M_c are of considerable importance to the physics of transient fluid flow and merit careful consideration.

By the chain rule of differentiation we have,

$$M_c = \frac{d\ (V\rho nS)}{d\psi}$$

$$= [VnS\frac{d\rho}{d\psi} + \rho S\frac{d(nV)}{d\psi} + V\rho n\frac{dS}{d\psi}] \qquad \text{(II.19)}$$

where M_c is a unique function of ψ.

Physically, the ability of the flow region to absorb or discharge fluid is governed by three different physical phenomena. First and quantitatively the least important from the point of view of flow of water, is the ability of water to expand in response to changes in ψ and thus undergo changes in mass density. This phenomenon is represented by the first of the three quantities on the right hand side of (II.19).

Secondly, the skeleton of the porous medium undergoes deformation in response to changes in ψ and the consequent changes in the stress distribution. As a result, the void spaces available for the fluid to occupy also undergoes a change. The deformation characteristics of the soil skeleton are incorporated in the second of the three terms on the right hand side of (II.19).

Lastly, at values of ψ less than the so called "air entry" value of the soil, the soil releases moisture by a process of desaturation. The capacity of the soil to absorb or release moisture due to saturation changes is expressed by the last of the three terms on the right hand side of (II.19).

We shall now consider each of these terms separately.

1. Compressibility of water

As already stated, the density of fluid is related to its hydrostatic pressure by the equation of state, (II.11). Differentiating (II.11) with respect to ψ, we get,

$$\frac{d\rho}{d\psi} \simeq \rho_o \beta g \left(e^{\beta \rho_o g \psi}\right) = \rho \rho_o \beta g \qquad \text{(II.20)}$$

Substituting (II.20) into the first term on the right hand side of (II.19) we get,

$$VnS \frac{d\rho}{d\psi} = VnS\rho\rho_o\beta g \qquad \text{(II.21)}$$

2. Deformation of soil skeleton

Any natural soil is under some state of stress and it deforms in response to changes in the state of stress. The relation between stress and deformation, usually termed "stress-strain" relationship, is fundamental to the study of soil deformation and soil mechanics. It may be fairly stated here that in handling the fluid mass capacity term, groundwater hydrologists have, in general, avoided a detailed consideration of these stress-strain relationships. However, as more and more data are collected from shallow groundwater systems, especially those involving aquitards (for example, Witherspoon et al., 1971; Helm, 1974) and clayey sediments, it is becoming increasingly clear that the stress-strain relationships have to be given much greater consideration than has hitherto been done.

If we consider a finite volume element and assume that the total change in the bulk volume of the solid phase is negligible (an assumption generally valid for most sediments) then, all the volume changes occurring in the volume element would be accounted for an equal change in the volume of the void spaces. The amount of void spaces present in a given soil can be expressed either by its void ratio, e, or by its porosity, n, and we have the following relations:

$$e = V_v/V_s$$

$$n = V_v/V$$

$$V = V_v + V_s$$

$$n = e/(1 + e)$$

$$e = n/(1 - n) \qquad \text{(II.22)}$$

where, V_v is the volume of voids

V_s is the volume of solids

and V is the bulk volume of the soil

We also define the volume element to be fixed in the solid phase, so that V_s is always a constant for a particular volume element.

a. One-dimensional consolidation theory

The most general and detailed way of considering the state of stress at a point in the soil is to consider it in three dimensions. This would require that stress be treated as a second order tensor (in the case of orthotropic porous media). However, in a great many natural field situations, because of the commonly large lateral extent of the soil masses being investigated, it can be reasonably assumed that the lateral strains resulting from changes in stress state are essentially zero. Under these conditions, the stress-strain

relation can be modelled as one-dimensional. This reasoning is the basis for the well-known "one-dimensional consolidation" theory developed by Terzaghi (1925). Work by numerous researchers in the field of soil mechanics over the past five decades have confirmed the reasonableness of the Terzaghi theory for most field situations. In the development of the present work, the Terzaghi model will be utilized. In a subsequent subsection, an attempt will be made to examine a conceptual possibility for handling general multi-dimensional deformations in soils.

b. The concept of effective stress

When a soil is fully saturated with fluid (also to some extent when it is partially saturated), its skeleton is subjected to two principal types of forces. The first is the weight of the overburden, which tends to compress the skeleton and hence reduce its volume. Opposing this is the pore-fluid pressure, which is hydrostatic and acts outward in all directions, tending to dilate the skeleton and therefore increase its volume. Since these two forces oppose each other, the stress that is effectively transmitted to the soil skeleton is the difference between these two stresses. As a consequence, we define the quantity, σ', as the "effective stress".

$$\sigma' = \sigma - u \qquad \text{(II.23)}$$

where σ' is the effective stress acting on the soil skeleton

σ is the total stress acting on the soil skeleton due to overburden weight, which includes the weight of any water present. For a horizontal ground surface, the total stress at depth z is essentially equal to z times

the average unit weight of the material above the point of consideration

and u is the pore-water pressure

Or, if we express stresses in equivalent heights of column of water,

$$(\sigma')_w = (\sigma_w) - \psi \qquad \text{(II.24)}$$

where $(\sigma')_w$ and $(\sigma)_w$ are stresses expressed in units of length and $\psi = (u/\rho g)$ is the pressure head previously defined.

In (II.24), $(\sigma')_w$ and $(\sigma)_w$ are defined to be positive in compression and ψ, positive in tension.

Now, since the water that is drained from the soil is distributed over a fairly large volume of the flow region and since the volume of water drained is generally small relative to the bulk volume of the soil, it can further be assumed that the change in water content of the soil mass due to drainage has negligible effect on the total stress due to overburden weight at any point in the soil mass; i.e., σ and $(\sigma)_w$ remain essentially constant at any point in the soil mass, providing no external loading of the soil mass occurs. Therefore, we can say that $(\sigma')_w + \psi =$ constant at any point within the soil mass and hence,

$$\Delta(\sigma')_w = -\Delta\psi \qquad \text{(II.25)}$$

where, $\Delta(\sigma')_w$ is the change in effective stress measured in equivalent height of column of water and $\Delta\psi$ is the change in pressure head.

Equation (II.25) implies that if the pore pressure increases, effective decreases by an identical magnitude and vice versa.

When Terzaghi (1925) first introduced the concept of effective stress, he demonstrated that the deformation of the soil skeleton is entirely governed by changes in effective stress, rather than total stress. Thus, for the case where the total stress is unchanging, deformations are governed by changes in pore pressures or pressure heads.

c. Effective stress in the unsaturated region

Equation (II.25) indicates that a plot of $(\sigma')_w$ versus ψ should have a slope of -1 as shown in figure 3. While this appears to be true in the saturated zone (and in the region of very high saturation), (II.25) fails to hold as ψ assumes increasingly large negative values (higher suction and lower saturation). The reason for this discrepancy in the mechanical behavior of the pore pressures in the zones of saturation and partial saturation is not yet fully known, although such a discrepancy has been experimentally observed by many workers (Bishop 1959; McMurdie and Day,1960; Bishop and Donald,1961; Day and Forsythe,1962; Bishop and Blight, 1963; Blight,1965; Matyas and Radhakrishna,1968; and others). Intuitively it would appear that as the degree of saturation drops the negative pore water pressure operates on a progressively small percentage of the gross cross-sectional area, thus contributing less to the effective stress. However, indications are such that the mechanism is more complex than this. In order to handle the aforesaid condition, Bishop (1959) suggested a modification of (II.23). Thus

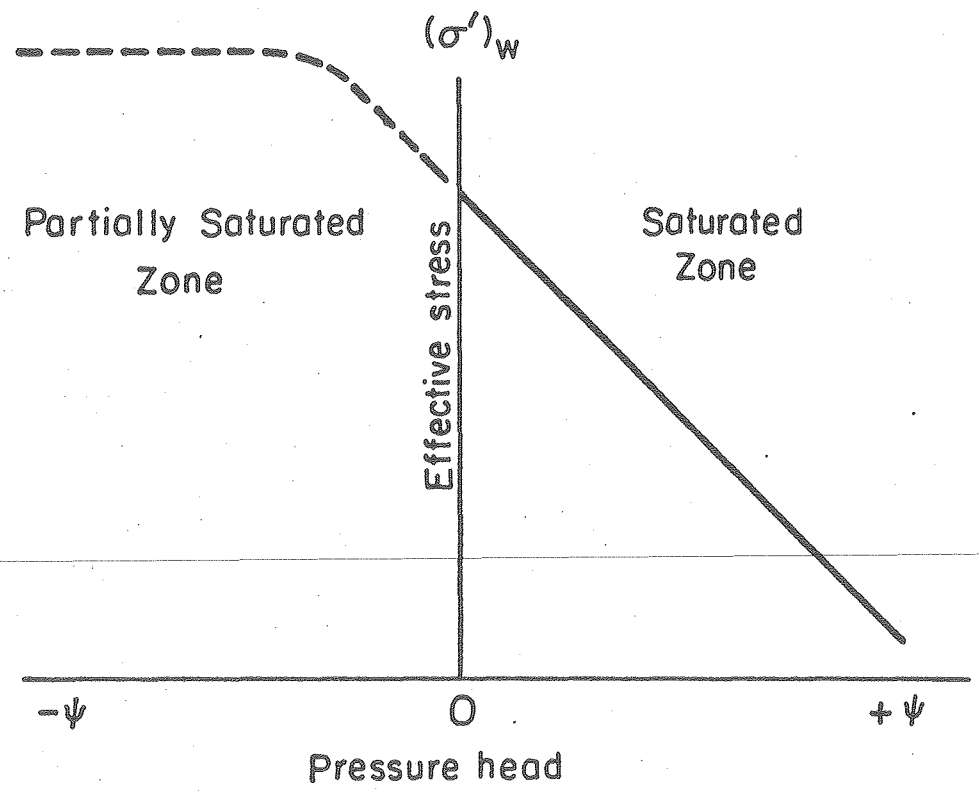

Fig. 3. Schematic representation of effective stress in the saturated and the unsaturated domains

he proposed,

$$\sigma' = \sigma - u_a + \chi(u_a - u_w) \qquad \text{(II.26)}$$

where u_a and u_w are pore-air and pore-fluid pressures and χ is a parameter, depending on soil properties and degree of saturation. If we assume the air-phase in the soil to be at atmospheric pressure (which is commonly the case) and set $u_a = 0$, then (II.26) reduces to, $\sigma' = \sigma - \chi u_w$ and hence,

$$\Delta(\sigma')_w = -\chi\Delta\psi \qquad \text{(II.27)}$$

McMurdie and Day (1960) independently suggested an identical expression based on triaxial tests on soils under soil moisture suction. It appears that the parameter χ can be determined reliably only by means of experiments.

The parameter χ depends on saturation, soil structure, cycle of wetting and drying and stress changes leading to that saturation (Sircar, 1973). The value of χ should be intuitively expected to vary between 0 and 1. However, values less than 0 or greater than 1 may sometimes be observed. Bishop and Blight (1963) plotted χ as a function of saturation for some compacted, saturated clays (figure 4) and their results indicate χ to be strongly non-linear in relation to saturation. The significance of the parameter χ is that in the partially saturated zone, mechanical stresses and suction stresses are not physically equivalent. Hence there is reason to believe that for accurate prediction of flow in the zone of partial saturation, due consideration must be given to the manner in which mechanical stresses and suction stresses are related in that zone.

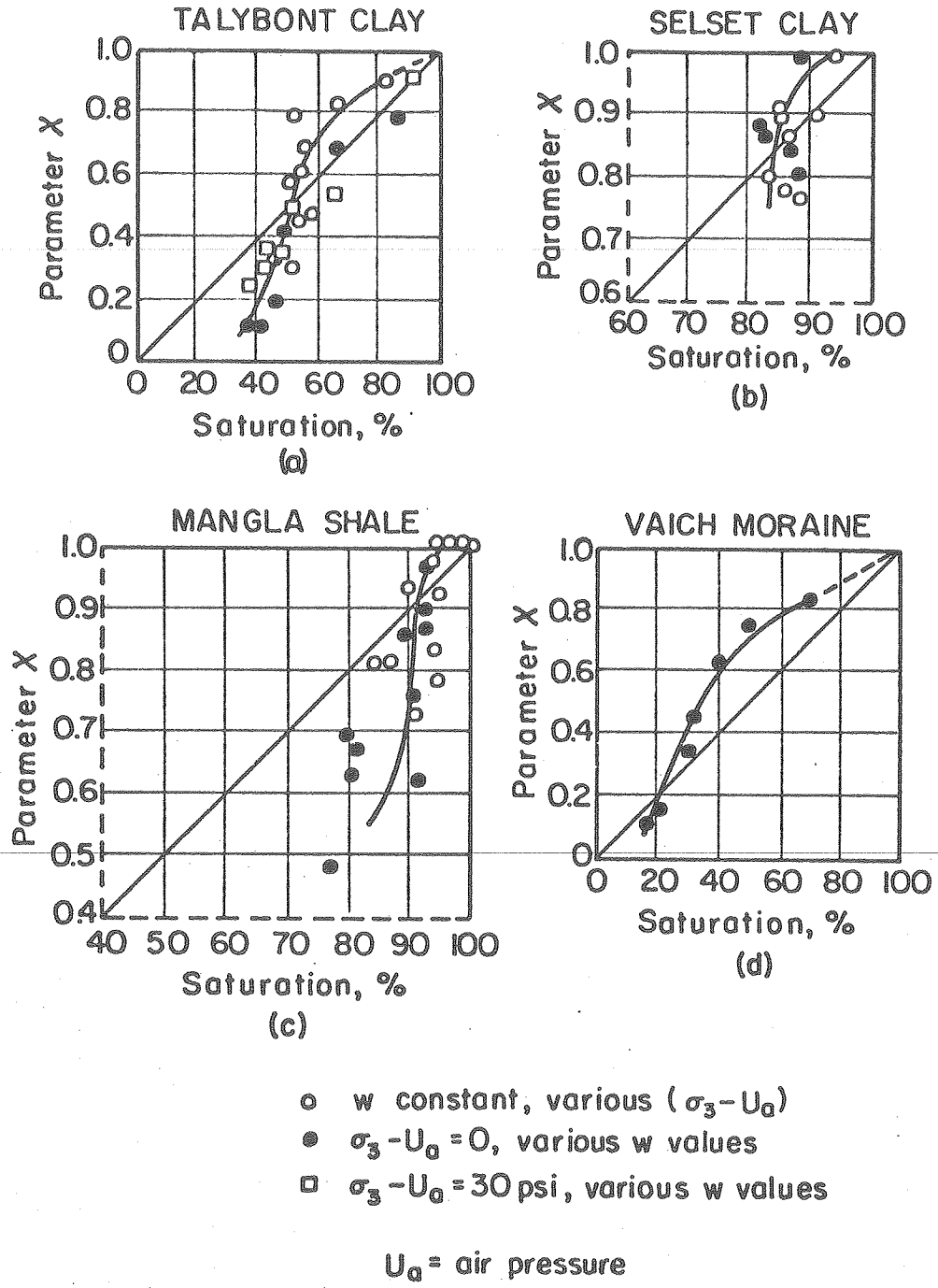

Fig. 4. Variation of the parameter χ with saturation for four compacted, partly saturated soils

d. Stress-strain relationships in soils

In soil mechanics literature it is customary to express stress-strain relationships in soil (on the basis of the effective stress concept) with the help of a plot of void ratio versus effective stress or void ratio versus versus the log of effective stress. Since void ratio is uniquely related to porosity (equation (II.22)), the relation between porosity and effective stress, σ', can always be inferred from the e versus σ' plot. Since almost all stress-strain data on soils is provided by soil engineers, in the present work we shall use the e versus σ' plot (or, the e versus log σ' plot), as the standard way of expressing stress-strain relationships in soils.

It should be noted that stress-strain relationships for a variety of boundary conditions are of interest in special cases. For example, the response of a soil element to an increasing axial stress (major principal stress, σ_1) when the minor and intermediate stresses, σ_2 and σ_3, are held constant and equal to each other as in the triaxial test, is often measured. A much more common boundary condition for field loading, however, is one in which the strains in the intermediate and minor principal stress directions are essentially negligible. In the present work, attention will be confined to the stress-strain relationships for this latter case where the strains are essentially one-dimensional.

A simple example of the e versus σ' plot is shown in figure 5 for a soft clay. Point B in figure 5 represents the state of the soil in situ, as it occurred in the field at the time of sampling. On being removed from its location (sampled), transported to the laboratory and trimmed and prepared for testing, a reduction in effective

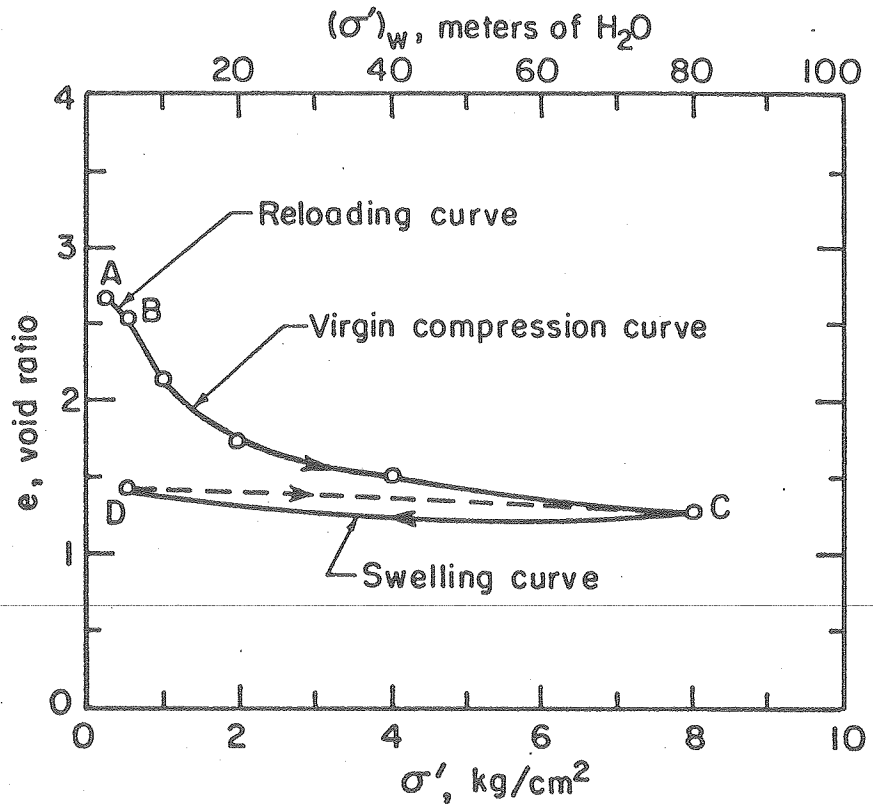

Fig. 5. Plot of void ratio, e, versus effective stress, σ', for San Francisco Bay Mud (data from Prof. W.N. Houston, University of California, Berkeley)

is unavoidable. In addition, it is standard practice to allow the sample to rebound to lower effective stress, while absorbing water, so that the reloading curve can be determined. Therefore, at the commencement of the one-dimensional compression test, the state of stress of the sample is represented by point A. As the vertical stress is increased, the sample follows the reloading curve AB. In this region, the soil is in a state of overconsolidation. The maximum stress the soil had ever experienced before the test was the stress level at point B. Once the laboratory loading exceeds the stress level at B, the soil experiences a magnitude of loading it had never experienced before and the void ratio decreases along the curve BC, which is usually called the virgin compression curve. As it lies on BC, the soil is said to be normally consolidated. At the point C, further loading is stopped and a gradual unloading of the soil is commenced. The stress level at point C now becomes the new preconsolidation pressure and the sample, instead of moving along the curve CB, moves along the curve CD (solid line), which is called the swelling curve or rebound curve. If the sample were to be again reloaded at D, it would follow the dotted line connecting D and C. That the paths followed by the virgin curve and the swelling curve are different shows that the phenomenon of soil deformation is not elastic, in that part of the deformation is non-recoverable. Such inelastic behavior is exhibited by sands as well as clays.

The slope of the virgin curve or the swelling curve at any given point on the e versus σ' plot is called the coefficient of compressibility,

$$a_v = - de/d\sigma' \qquad \text{(II.28)}$$

where, a_v is the coefficient of compressibility, e is the void ratio and σ' is the effective stress.

Closely related to the coeffcient of compressibility is the parameter, volumeteric compressibility, m_v, defined by,

$$m_v = -d\varepsilon_v/d\sigma' \qquad \text{(II.29)}$$

where, ε_v is the volumetric strain = $\Delta V_v/V_o$

ΔV_v is the change in void volume

and V_o is the bulk volume of the soil at the start of the compression increment for which m_v is computed

The quantities, a_v and m_v are related by,

$$a_v = m_v(1 + e_o)$$

$$\text{and} \quad m_v = a_v/(1 + e_o) \qquad \text{(II.30)}$$

It is easily seen from figure 5 that e versus σ' relation is non-linear and that the slope of the curve BC varies markedly along the curve, the variations being particularly pronounced for lower values of effective stress. Thus, the compressibility parameters, a_v and m_v, are both functions of σ', a fact which cannot be ignored in dealing with deformations at low levels of effective stress. However, if the stress increment is very small, the curve could be approximated by a short straight line segment and the slope of the line segment can be considered a reasonable value of a_v.

It is pertinent to mention here that within the saturated zone, and ignoring the compressibility of water, the coefficient of specific storage (S_s), used extensively in groundwater literature, is equivalent to the coefficient of volume compressibility, m_v. Thus, S_s is actually based on a linear relationship between e and σ'. As we have seen, such an assumption is reasonable only when the anticipated changes in effective stress are very small, in comparison to the original magnitude of effective stress.

Analysis of a large number of experimental data on one-dimensional consolidation indicates that the stress-strain relation, with e on the arithmetic scale and σ' on the logarithmic scale plots approximately linearly (figure 6). The slope of the best fitting straight-line is called the compression index (C_c) in the case of the virgin curve or the swelling index (C_s) in the case of the swelling curve. In general, C_c may be larger than C_s by one or more orders of magnitude. The values of C_c and C_s are determined by observing the change in void ratio for one log cycle of change in σ'.

An advantage in using C_c and C_s whenever possible is that these are dimensionless parameters and are independent of the units used for expressing effective stress. In addition, they enable easy definition of the stress-strain relationships with few parameters.

Although the e versus σ' plot and the e versus log σ' plots are the most widely used, other methods of expression have also been employed in the literature. For example, Schultze and Moussa (1961), in studying the factors affecting compressibility of sands, have proposed an exponential relationship between stress and strain such that,

$$m_v = 1/\nu\sigma'^{\omega}$$

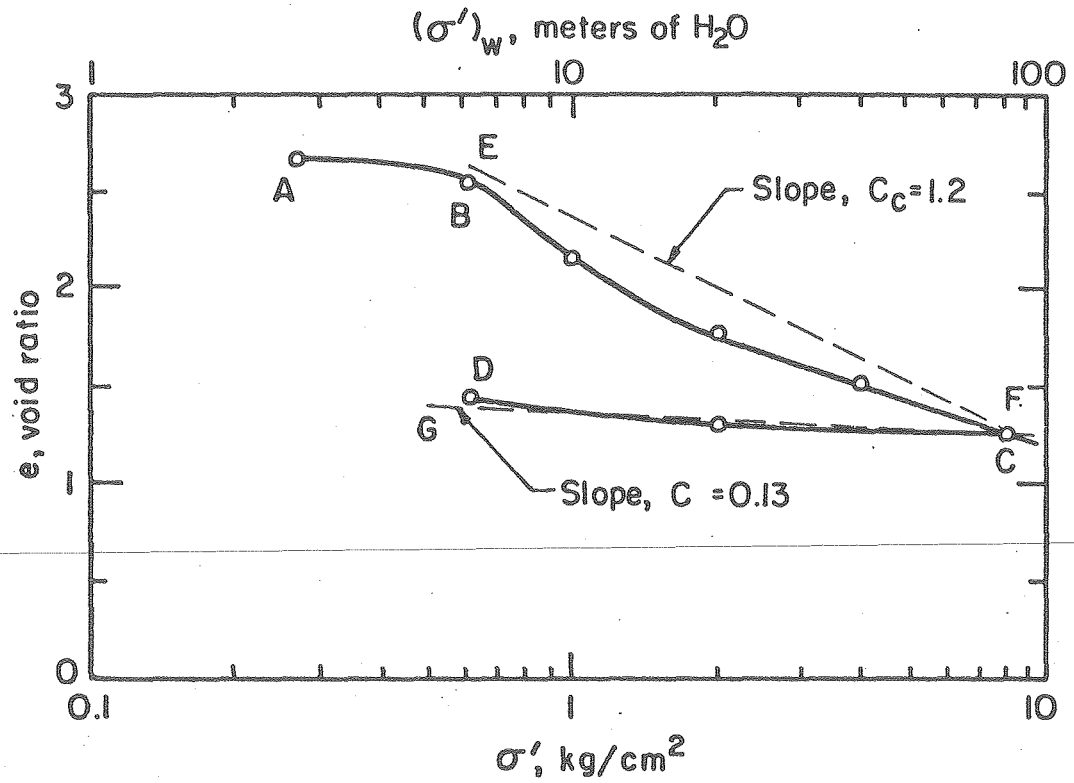

Fig. 6. Semi-log plot of void ratio, e, versus effective stress, σ', for San Fracisco Bay Mud (data from Prof. W.N. houston, University of California, Berkeley)

where, ν and ω are experimentally determined parameters.

Using the chain rule of differentiation, we can easily establish the unique correspondence between C_c and a_v. Thus,

$$C_c = -\frac{de}{d(\log_{10}\sigma')}$$

$$= -\frac{de}{d\sigma'} \cdot \frac{d\sigma'}{d(\log_e \sigma')} \cdot \frac{d(\log_e \sigma')}{d(\log_{10} \sigma')}$$

$$= a_v \, \sigma' \, (2.303)$$

$$= 2.303 \, \sigma' a_v \qquad \text{(II.31)}$$

We now revert to evaluate the second of the three terms on the right hand side of (II.19). Noting that $n = e/(1 + e)$ and that $V = V_s(1 + e)$ (equation (II.22)) and also that $\Delta\psi = -\Delta(\sigma')_w/\chi$ (from equation (II.27)) we get,

$$\rho S \frac{d(nV)}{d\psi} = -\rho S V_s \chi \frac{de}{d(\sigma')_w}$$

$$= -\rho S \frac{V}{1 + e} \chi \frac{de}{d\sigma'} \frac{d\sigma'}{d(\sigma')_w} \qquad \text{(II.32)}$$

But, $d\sigma'/d(\sigma')_w = \rho_o g = \gamma_w$ (where γ_w is the specific weight of water) and from (II.31), $a_v = -de/d\sigma' = C_c/2.303\,\sigma'$. Substituting these into (II.32) we obtain,

$$\rho S \frac{d(nV)}{d\psi} = -\rho SV \frac{1}{1+e} \chi \left[-\frac{C_c}{2.303\sigma'}\right]\gamma_w$$

$$= \rho SV \frac{\chi}{1+e} \frac{C_c \gamma_w}{2.303\sigma'}$$

$$= \frac{V\rho S}{(1+e)} \frac{\chi C_c}{2.303(\sigma')_w} \qquad \text{(II.33)}$$

since $(\sigma')_w = \sigma'/\gamma_w$

e. The deforming volume element

In giving detailed consideration to the deformation of the soil skeleton, we have taken into account the changes in the volume of the arbitrarily chosen volume element in response to changes in stress. This suggests that in order to be consistent, we have to consider the effects of such deforming element on the surface integral or on the volume integral on the left hand side of (II.18).

The consequence of deformation is that in addition to a change in volume, there are also accompanying changes in surface areas and spatial distances. If we look at the surface integral in (II.18),

$$\int_S \rho \frac{k\rho g}{\mu} \vec{\nabla}(z+\psi) \cdot \vec{n}\, d\sigma$$

we note that the changes in spatial distances consequent upon deformation will affect the gradient term, while the changes in surface areas would affect the term $d\sigma$. Now, while the changes in the total volume of the chosen element is a scalar quantity, the spatial distances as well as surface areas are associated with directions and

orientations. Thus a single magnitude of volume change (volumetric strain) can be associated with a variety of combinations of changes in spatial distances and surface areas. In other words, for the same magnitude of volume strain, the shape of the volume element could change in a variety of ways. The type of change occurring in a particular problem would depend on the nature of the stress changes and boundary conditions.

Another consequence of the deformation of the flow region is the relation between deformation and Darcy's law. It has been pointed out (Cooper,1966; Freeze,1971) that Darcy's law pertains actually to the velocity of the fluid relative to the velocity of the soil grains. Therefore, the velocity calculations inside the surface integral in question would need to be corrected with respect to the velocity of the soil grains. At a given location and at a given instant of time, the correction would depend on the direction of movement of the fluid and the direction of movement of the grains. The direction of movement of the grains would, in turn, depend on the nature of the forces causing the grains to move and the boundary conditions to which the grains are subjected. A rigorous model of the phenomenon should take into consideration these factors. In order to achieve this rigorous treatment, alternate formulations (other than the diffusion equation) may need to be considered. In this regard, the essence of the problem appears to be one of choosing a proper material or Lagrangian coordinate system. Attempts have been made to develop consolidation theories based on this reasoning (Gambolati,1973a, 1973b; Helm, 1974), but these efforts have been restricted to the simple one dimensional case.

In the case of numerical modelling of deforming, multidimensional regions, one possible way of achieving a more accurate simulation would be to progressively adjust the surface areas and spatial distances with each cycle of calculation, based on a knowledge of the boundary conditions (and hence, the relation between volume change and shape change) or using some reasonable assumption of uniform dilatation or preferential deformation (e.g. one-dimensional deformation).

Customarily, these corrections are not made and it is of interest to examine, if only qualitatively, the type and magnitude of error that may arise as a result. We will consider two cases.

First, consider one-dimensional consolidation. In this case, the flow region is a simple vertical column and adjoining subregions communicate with each other across planes normal to the direction of consolidation, which is also the direction of fluid movement. As consolidation proceeds, there occurs a shortening of spatial distances in the direction of consolidation; however, the surface areas normal to this direction do not change. Therefore, in calculating the flux across any such surface area, if we ignored spatial shortening, we would tend to underestimate gradients of potential. In this case, the calculated flux would be less than the actual flux.

As a second example, consider a multidimensional element in a uniformly shrinking or dilating flow region. In this case, if we consider any elemental surface area and its normal direction, both the surface area and spatial distance along the normal decrease or increase at the same time. Hence, if the surface area decreases, gradients should increase and vice versa. It seems reasonable to

infer, therefore, that in the case of uniform contraction or dilation in all directions, in so far as flux calculations are concerned, the changes of surface areas and nodal distances tend to oppose each other. Qualitatively, therefore, ignoring these changes in flux calculations may not cause large errors.

In any other system undergoing arbitrary deformation, it is not easily apparent as to whether such compensations may or may not take place.

By Darcy's law, the flux across any surface area is the product of permeability, surface area and the gradient in potential along the normal to the surface. Therefore, it seems possible to compensate for any possible errors in the calculation of surface areas and gradients by making an equivalent gross correction to the permeability term. The exact magnitude of such a correction would be a function of the boundary conditions as well as the deformation parameters of the soil and may have to be determined empirically or with the help of detailed parametric studies. In chapter V, while dealing with the problem of consolidation of a clay slurry, we shall see that such a correction is indeed possible in the case of a highly deforming one-dimensional column of clay. Nevertheless, Gambolati's work (1973b) as well as the results of the present study seem to indicate that for most field situations, ignoring the changes in surface areas and spatial distances in evaluating the spatial integral on the left hand side of (II.18) may not cause significant errors and that the diffusion equation is adequate for most field problems.

f. Extension to multidimensional stress fields

The analysis of the deformation of the soil skeleton carried out in the preceding pages was based on the one-dimensional consolidation theory of Terzaghi. This theory suffices for most field situations and therefore, the mathematical model which will be developed in the present work is based on this theory. Nonetheless, it seems appropriate at this point to examine the type of approach that one might follow to handle multidimensional stress fields resulting due to arbitrarily applied external loads. In order to do this we have to examine, a) how a soil may react to external loading and b) what is the logical framework of the diffusion equation in relation to deformation.

Suppose a saturated or nearly saturated soil is in equilibrium with its ambient stress field. In this state, part of the load is borne by the soil skeleton and part, by the pore-fluid. The part borne by the latter will be expressed by the pore-fluid pressure, which is hydrostatic. Suppose now that at an instant, t_o, the stresses are suddenly changed to a new level, giving rise to a new distribution of total stresses (σ_1, σ_2, σ_3, τ_{12} etc.) over the flow region. From known behavior of soils, the instantaneous reaction of the soil to this changed loading appears to be governed by its "undrained" behavior, in the following manner. The pore fluid pressure quickly changes to compensate the change in total stress, while the soil skeleton does not "feel" any change in effective stress in the undrained state; in some cases, the soil skeleton may experience a slight decrease in effective stress immediately after the changed loading. Therefore, if the external loading is increased, the pore pressures rise up suitably and vice versa. Due to the change

in pore pressures, the field of fluid potential is disturbed and if the soil is allowed to drain, the fluid pressures would change towards a new state of equilibrium as governed by the diffusion equation and with the change in fluid pressures, the effective stress distribution within the soil would gradually undergo change. From the foregoing, it would appear as though the pore water acts as a liaison between the external load and the reaction of the soil skeleton.

In handling this problem with the diffusion equation, the first step is to find the new distribution of pressures at t_o^+, owing to the stepwise change in the stresses. An important information required for this purpose is the relation between stress change and pore pressure change. In the case of the simple one-dimensional model, this relation is easily expressed by (II.25). But, in the case of multidimensional stress problems, the relationship is more complex than (II.25). Skempton (1954) attempted to relate, empirically, the relation between stress change and pore pressure change under "undrained"conditions. He separated the total stress change to a hydrostatic and a deviatoric components and, superposing the effects of each of these on pore pressure change, proposed,

$$\Delta u = B\Delta\sigma_3 + \bar{A}(\Delta\sigma_1 - \Delta\sigma_3) \qquad \text{(II.34)}$$

where, Δu is the pore pressure change and B and $\bar{A}$ are parameters to be experimentally determined.

Alternatively, from physical considerations, Skempton (1954)

also proposed,

$$\Delta u = B\left(\frac{1}{3}(\Delta\sigma_1 + 2\Delta\sigma_3) + \frac{3A - 1}{3}(\Delta\sigma_1 - \Delta\sigma_3)\right) \qquad \text{(II.35)}$$

In this case, for a material behaving in accordance with elastic theory, with $A = 1/3$, the pore pressure change depends solely on "the mean principla stress", whereas in soils with $A \neq 1/3$ in general, the pure shear stress has marked effect on pore pressure changes.

The calculation of instantaneous pore pressure changes, due to applied stress changes is external to the diffusion equation. But, once this information is generated, it forms the basic input for solving the diffusion equation, which is an initial-boundary value problem.

For a moment, if we neglect the compressibility of water and the desaturation of the soil skeleton, the rate of dissipation of pore pressure is governed by the change of void ratio in response to the stress changes. In a multidimensional stress field, then, the term, "compressibility" is a function of the slope of the surface representing the relationship between void ratio and the principal effective stresses.

The stresses acting on the soil skeleton continuously change as the pore pressure changes in general. Assuming that the changes in pore pressure and the changes in boundary conditions can be used to ascertain changes in effective stress, the direction in which the skeletal stresses will change in response to pore pressure change can be determined and the slope of the void ratio surface in this direction will provide a measure of the soil"compressibility" value to be used in computing fluid mass capacity (equation (II.19)).

From this point on, the calculational procedure will be identical to that of the one-dimensional model already described.

If this reasoning is indeed correct,then , one segment of the basic input data needed in the diffusion equation would be to express void ratio , e, as an unique function of the effective stresses, σ_1', σ_2' and σ_3',based on elaborate laboratory tests on the soil. Obviously, this relation would be subject to the same "inelastic" phenomena exhibited by the one-dimensional compression samples. No doubt, analytical use of such data would be very complex. But, numerical handling of such data, when suitably tabulated, is well within the reach of modern digital computers. Therefore, it seems quite possible to extend the diffusion model to handle arbitrary external loading, providing that suitable experimental data relating void ratio change to arbitrary change in stresses can be obtained and numerically described.

3. Desaturation of soil skeleton

The third and the last phenomenon by which a soil may absorb or release water from storage is by a process of saturation change. Change of saturation in soils is a phenomenon having thermodynamic implications. For less than one hundred per cent saturation, with the pore-air pressure at atmospheric pressure, the pore-water pressure in soils assumes negative values, usually called moisture suction or moisture tension. Due to the complex nature of the configuration of the liquid phase in volved, the functional relationship between pressure head, ψ, and saturation, S, is not unique, but is characterized by a multiple-valued, hysteresis relationship as depicted in figure 7.

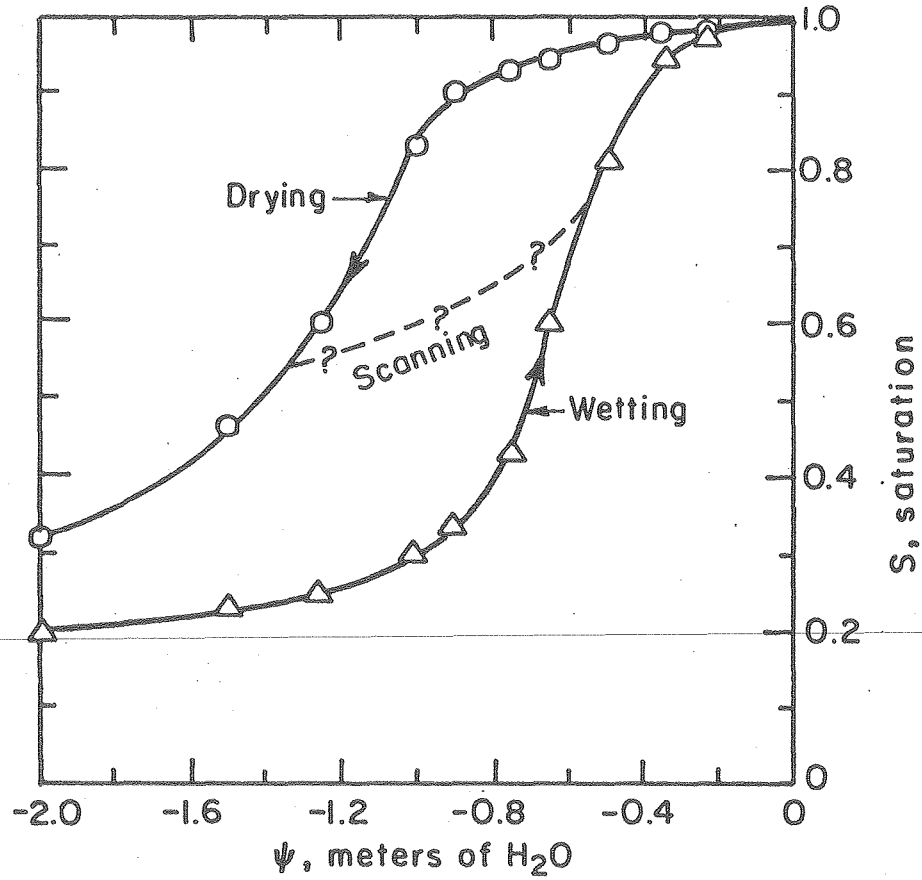

fig. 7. Hysterisis between saturation and pressure head for Del Monte sand (after Liakopoulos, 1965)

If we consider a soil with $\psi = 0$ (saturation 100% and $S = 1$) and apply suction, the soil does not physically desaturate until the applied suction passes a critical value called the "air-entry" value. In figure 7, the air-entry value for the drying curve is approximately -0.15 m of water. Between zero suction and the air-entry value, the soil remains saturated but has negative pore pressures. The capillary fringe occurring in natural soils occurs in that part of the soil where the pressure head is between the air-entry value and zero.

Once suction exceeds air-entry value, the S versus ψ relation changes along the drying curve, as indicated on figure 7. If, at any point on the drying curve the process is reversed, hysterisis, as shown by the scanning curve in figure 7, is exhibited. The S versus ψ relation moves along the scanning curve until it meets the wetting curve and then moves up the wetting curve (i.e. towards higher values of S). The drying and the wetting curves form the boundary of the "hysterisis loop", within which the soil can assume any value of saturation and ψ, depending on the past history of the saturation process.

The slope of the S versus ψ curve , $dS/d\psi$ (on the drying, wetting or scanning curve)at any point in the S versus ψ relation is a measure of the ability of the soil to absorb or release water from storage due to saturation changes. If we assume the porosity of the partially saturated soil to be constant, then,

$$n \frac{dS}{d\psi} = \frac{d(nS)}{d\psi} = \frac{d\theta}{d\psi} = C \qquad \text{(II.36)}$$

The quantity C is called Specific Moisture Capacity in soil physics literature. Because of the hysteresis relation, the quantity, $dS/d\psi$ varies with ψ, with an additional constraint imposed by past saturation history. It is to be noted here that the S versus ψ is to be determined empirically for each soil.

We now recall the equation for fluid mass capacity of the volume element, (II.19). Substituting (II.36) into the last term on the right hand side of (II.19), we see that,

$$\rho nV \frac{dS}{d\psi} = \rho V \frac{d(nS)}{d\psi} = \rho VC \qquad \text{(II.37)}$$

providing that n is a constant.

4. Final expression for fluid mass capacity of volume element

Equations (II.21), (II.33), and (II.36) are the final expressions, expressing the ability of the arbitrary volume element to release or absorb water from storage, respectively due to water compressibility, soil compressibility and saturation change, in response to changing pressure head. Combining these quntities, therefore, we have the final expression for the fluid mass capacity (M_c) of a volume element:

$$M_c = VnS \frac{d\rho}{d\psi} + \rho S \frac{d(nV)}{d\psi} + V\rho n \frac{dS}{d\psi}$$

$$= VSn\rho\rho_o\beta g + \frac{V\rho S\chi C_c}{2.303(1+e)(\sigma')_w} + V\rho n \frac{dS}{d\psi}$$

$$= V[Sn\rho\rho_o\beta g + \frac{\rho S\chi C_c}{2.303(1+e)(\sigma')_w} + \rho n \frac{dS}{d\psi}] \qquad \text{(II.38)}$$

Or, since, from (II.31), $a_v = C_c/2.303\ \sigma'$, we have,

$$M_c = V[Sn\rho\rho_o\beta g + \frac{\rho S\gamma_w \chi a_v}{(1+e)} + \rho n \frac{dS}{d\psi}] \qquad \text{(II.39)}$$

Note that in (II.38) and in (II.39), the quantities, V, ρ, S, $(\sigma')_w$, e and n are all functions of ψ. It is worth mentioning here that the functional relationships between the parameters, $(\sigma')_w$, e and n and the pressure head, ψ, are somewhat indirect in that ψ affects these parameters only in so far it affects effective stress. Now, since total stress varies from point to point within the flow region, for a given value of ψ, the effective stress may also vary from point to point. Hence, effective stress and, consequently, e, n and a_v cannot be expressed as unique functions of ψ.

A consequence of this is that in the field of groundwater hydrology, in which the concept of specific storage (S_s) is extensively used, and in which the relation between ψ effective stress is totally ignored, it is not possible to accurately treat the variation of S_s in space and in time. Such variations, it appears, may be very important in some shallow groundwater bodies.

E. INTEGRAL FORM OF GOVERNING EQUATIONS FOR SATURATED-UNSATURATED GROUNDWATER MOTION

1. Variation of permeability in the saturated region

We have so far considered all the parameters in (II.18) excepting permeability, k. For a given isotropic soil, the quantity k is a function of ψ. The functional relationships between ψ and k is direct and characterized by hysterisis in the unsaturated zone, but is somewhat indirect in the saturated zone.

As we have seen, the skeletal structure of the soil changes with effective stress and this is reflected in the changes in void ratio and porosity. Now, since the absolute permeability, k, of the porous medium is a function of the skeletal structure, it stands to reason that there must be a functional relationship between permeability and effective stress. The dependence of permeability on void ratio was studied by Terzaghi as early as 1925 (Terzaghi, 1925b). Experimental work by numerous workers in the field of soil mechanics (Lamb and Whitman, 1969) has shown that permeability is indeed a pronounced function of void ratio (and hence, effective stress), especially for the finer sediments.

It has also been found by experimentalists in soil mechanics that void ratio usually plots a straightline with log of permeability (figure 8). This enables us to express permeability as an exponential function of void ratio as follows:

$$k = k_o \exp \left[\frac{e - e_o}{(C_k/2.303}\right] \qquad \text{(II.40)}$$

where C_k is the slope of the best-fitting strainghtline on the e versus log k plot, and (e_o, k_o) is a convenient reference point on the straight line.

2. Variation of permeability in the unsaturated region

While permeability is related to mechanical stresses in the saturated zone, it is a function of the proportion of the two phases (water and air) occupying the pore spaces in the unsaturated zone. As the water saturation decreases, hydraulic conductivity K decreases. However, the relationship between saturation and K is not

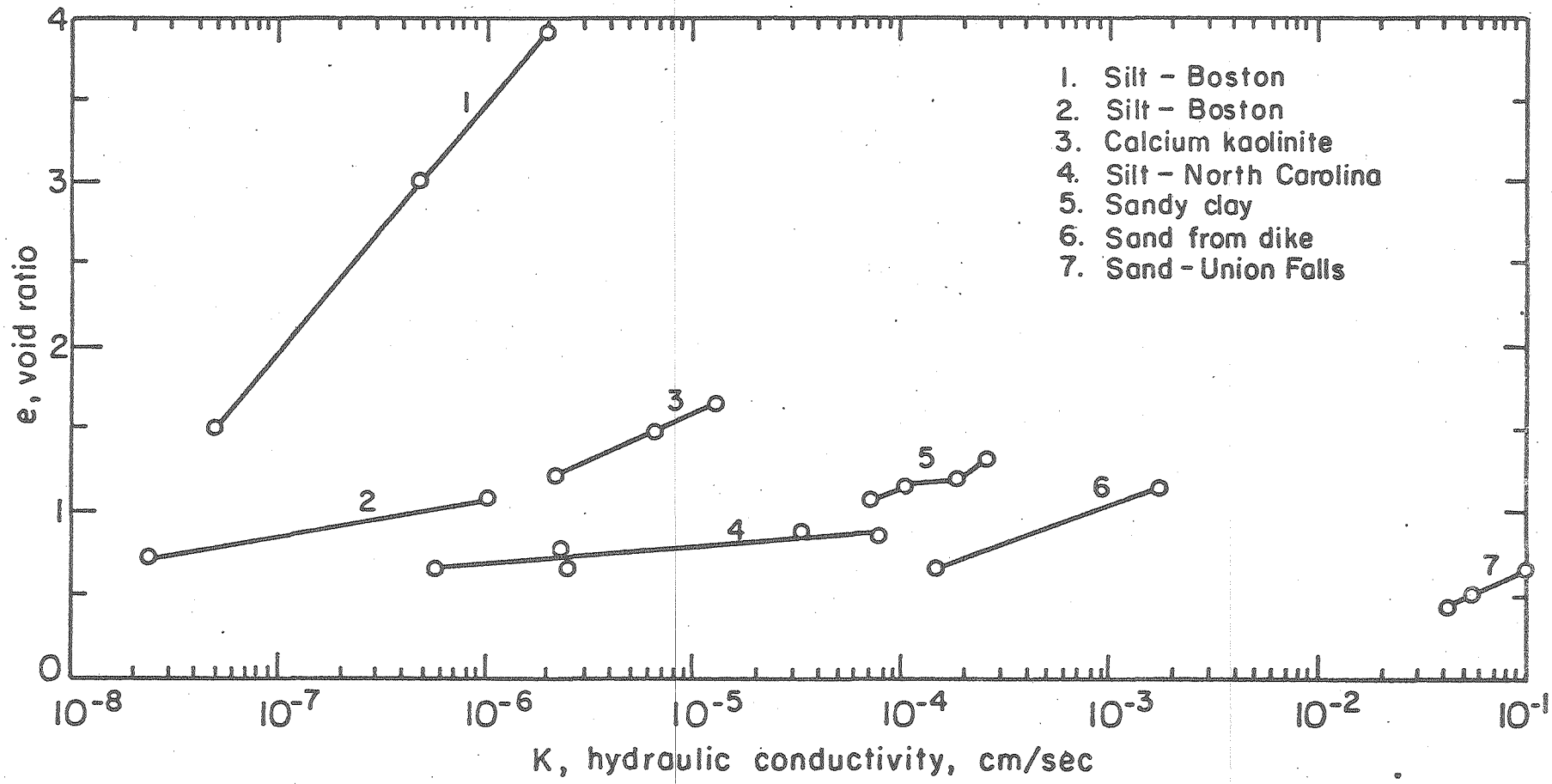

Fig. 8. Hydraulic conductivity as a function of void ratio for saturated soils (after Lambe and Whitman, 1969)

unique and is characterized by hysterisis, as in the case of the saturation versus pressure head relationship. Since there is a functional relationship between saturation and pressure head, there is also a hysteritic relationship between hydraulic conductivity and pressure head as shown in figure 9. Here too one must know the past history of the variation of pressure head before one could determine the value of K or k for a given value of ψ.

3. Complete governing equation for an isotropic medium

We can now write the complete governing equation of transient groundwater motion in an integral form:

$$\int_V \mathrm{div}\rho\frac{k\rho g}{\mu}\vec{\nabla}(z+\psi)\,dV + G = \int_S \rho\frac{k\rho g}{\mu}\vec{\nabla}(z+\psi)\cdot\vec{n}\,d\sigma + G$$

$$= V\left(Sn\rho\rho_o\beta g + \frac{\rho S\chi C_c}{2.303(1+e)(\sigma')_w} + \rho n\frac{dS}{d\psi}\right)\frac{\partial\psi}{\partial t}$$

$$= V\left(Sn\rho\rho_o\beta g + \frac{\rho S\gamma_w\chi a_v}{(1+e)} + \rho n\frac{dS}{d\psi}\right)\frac{\partial\psi}{\partial t} \qquad \text{(II.41)}$$

where G signifies the strength of the source or sink, integrated over the volume element. The first two integrals in (II.41) are alternate forms for the same physical phenomenon. The last two quantities in (II.41) are also identical, except for the difference in the soil deformation parameter. For purposes of actual solution, either of the integrals can be used in conjunction with either of the last two quantities in (II.41).

Equation (II.41) can also be applied to a heterogeneous flow region, having more than one isotropic material. When more than one isotropic material is present, care should be taken to evaluate

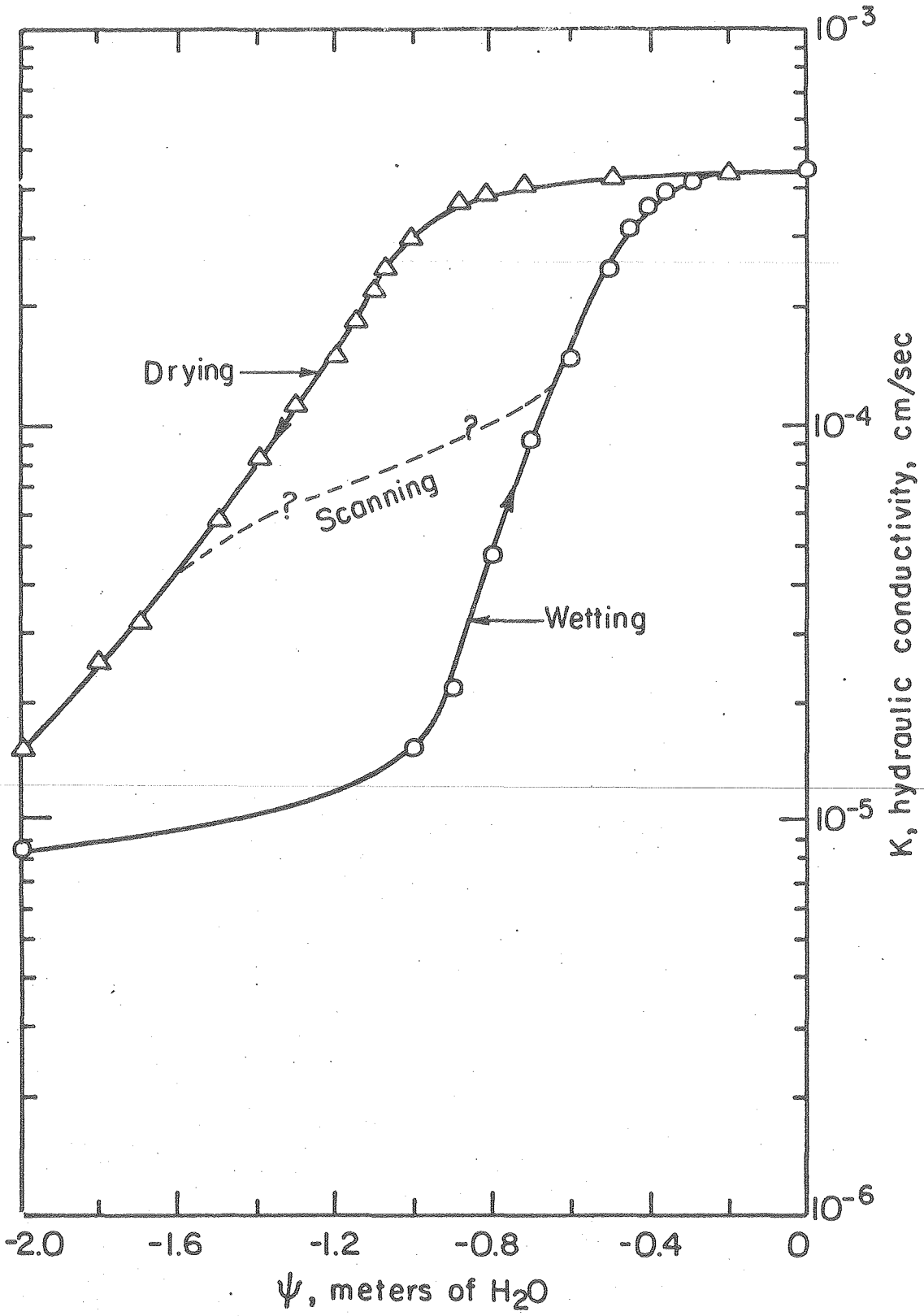

Fig. 9. Hysterisis between hydraulic conductivity and pressure head for Del Monte sand (after Liakopoulos, 1965)

the mean permeability, $\bar{k}$, and the mean density, $\bar{\rho}$, while computing the flux at the surface between two different materials.

Assuming that the different materials making up the flow region are all isotropic, we have the following functional dependencies:

$$k = k\ (F,\psi)$$

$$\rho = \rho\ (\psi)$$

$$V = V\ (\psi)$$

$$S = S\ (F,\psi)$$

$$e = e\ (F,\psi)$$

$$n = n\ (F,\psi)$$

$$C_c = C_c\ (F)$$

$$a_v = a_v\ (F,\psi)$$

and $$G = G\ (t)$$

where F is material identification number

4. Equation of flow for an anisotropic medium

Equation (II.41) would need to be modified if one or more materials making up the flow region were anisotropic. In order to handle anisotropy, k in (II.41) would have to be replaced by the cartesian tensor, k_{ij}. In addition, the gradient operator, $\vec{\nabla}$, would also have to be replaced by $\vec{\partial}/\partial x_j$. Thus, for anisotropic media, (II.41) becomes,

$$\int_V \frac{\vec{\partial}}{\partial x_j} \rho \frac{\rho g}{\mu} k_{ij} \frac{\vec{\partial}}{\partial x_i} (z + \psi)\ dV \quad + \quad G$$

$$= \int_S \rho \frac{\rho g}{\mu} k_{ij} \frac{\vec{\partial}}{\partial x_i} (z + \psi) \cdot \vec{n}_j\ d\sigma \quad + \quad G \quad = \quad M_c \frac{\partial \psi}{\partial t} \qquad \text{(II.42)}$$

In the present work we shall restrict coverage mainly to isotropic, heterogenous media and hence we shall be concerned only with equation (II.41) instead of (II.42)

F. GOVERNING EQUATION FOR THE ISOTROPIC CASE BASED ON MOISTURE CONTENT, θ

In the development of the governing equation (II.41) we made ψ the dependent variable (ψ-based equation). However, soil physicists, mainly interested in the zone of partial saturation have used θ as the dependent variable instead of ψ (θ-based equation) [e.g. Bruce and Klute (1956), Rubin and Steinhardt (1963), Swartzendruber (1969)]. Using this approach and in the light of (II.8), Richard's Equation (II.14) can be written as follows (Neuman (1972)):

$$\frac{\vec{\partial}}{\partial x_i}\left[K \frac{\vec{\partial}}{\partial x_i}(z+\psi)\right] = \frac{\vec{\partial}}{\partial x_i}\left[K \frac{\vec{\partial} z}{\partial x_i} + K \frac{d\psi}{d\theta} \frac{\vec{\partial}\theta}{\partial x_i}\right]$$

$$= \frac{\vec{\partial}}{\partial x_i}\left[K \frac{\vec{\partial} z}{\partial x_i} + D(\theta) \frac{\vec{\partial}\theta}{\partial x_i}\right] = \frac{\partial \theta}{\partial t} \qquad \text{(II.43)}$$

The quantity, $D(\theta) = K \frac{d\psi}{d\theta}$ is called "soil moisture diffusivity" in soil physics literature. As can be seen, it is a lumped parameter, combining hydraulic conductivity and the reciprocal of specific moisture capacity, both of which are functions of θ .

The advantages of the θ-based equation are two-fold. First, there is no non-linear coefficient on the right hand side of (II.43). Secondly, the dependence of D on θ is much less non-linear, for soils of low saturation, than the dependence of K or C on θ. As a result, the mathematical problem is much easier to solve.

Moreover, the physics of the flow mechanism at low saturations appears to be much more "linear" with reference to moisture content (or saturation) than with reference to fluid potential. In other words, whereas the fluid potential may vary rapidly over short distances, the moisture content or saturation is likely to vary more gradually. For this reason too, it seems more appropriate for using the θ-based equation in the case of soils of low saturation.

However, the diffusivity concept and the θ - based equation have some disadvantages. As pointed out by Klute (1972), this equation is applicable only to uniform soils, uniformly drying or wetting.

The concept of diffusivity completely breaks down (unless an alternate interpretation is given to it) when ψ is in the range, air-entry value $\leq \psi \leq 0$. Since, in this range, no desaturation can take place, $dS/d\psi = 0$ and, if porosity is assumed constant, $d\theta/d\psi = 0$, which means that $d\psi/d\theta = \infty$. Therefore, close to $\psi = 0$, $D(\theta) = K \frac{d\psi}{d\theta} \rightarrow \infty$. However, in solving practical problems, $D(\theta)$ can be arbitrarily made finite at or close to $\psi = 0$.

The anomaly, however, can be overcome, if we take into account the deformation of the soil skeleton at or near full saturation. Indeed, the only process by which water can be drained from a soil at or above the air-entry value is by soil deformation, since desaturation is not possible. Hence, in the range, air-entry value $\leq \psi \leq 0$, the diffusivity term $K \frac{d\psi}{d\theta}$ should actually represent $K \frac{d\psi}{dn}$, where n is porosity. Following this line of reasoning, it can be shown that for the above range of values of ψ, $D(\theta)$ is identical with C_v, where C_v is the coefficient of consolidation extensively used in soil mechanics literature.

The proof of this identity is as follows:

By definition, $D = K \frac{d\psi}{d\theta}$. For $\psi >$ air-entry value, $S = 1$. Hence, for $\psi >$ air-entry value, $\theta = n$, and,

$$D = K \frac{d\psi}{dn} = \frac{K}{dn/d\psi} \qquad \frac{K(1 + e_o)}{de/d\psi}, \tag{II.44}$$

if change in void volume is << bulk volume of soil.
Also, by definition (Lamb and Whitman (1969)), coefficient of consolidation,

$$C_v = \frac{K}{\gamma_w m_v} = \frac{K(1 + e_o)}{\gamma_w a_v} = \frac{K(1 + e_o)}{\gamma_w(- de/d\sigma')} \tag{II.45}$$

But, noting that $\Delta\psi = -\Delta\sigma'/\gamma_w$, we finally have,

$$C_v = \frac{K(1 + e_o)}{de/d\psi}$$

which is identical to the final expression (II.44), obtained for D. Failing to recognize this equivalence between diffusivity and coefficient of consolidation can give rise to a logical difficulty in effecting mass balance.

For example, consider a vertical column of sand, initially just saturated and with water freely flowing downward so that throughout the column $\psi = 0$. Then, the supply of water at the top end of the column is cut off and the column is allowed to drain. Now suction begins to develop near the top and it is possible to visualize an early period during which suction has no where exceeded the air-entry value of the sand. Therefore, nowhere in the column has

the sand begun to desaturate and the only way to account for the water draining at the bottom of the column is to account for the deformation of the soil skeleton.

As has been pointed out, the θ - based equation is in general not suited for heterogenous, saturated-unsaturated media, such as those considered in the present work. However, because of the extremely non-linear behavior of the ψ - based equation at low saturations, it seems desirable to examine if the θ - based equation could, in some fashion, be transformed into an equivalent, ψ-based form. Such a transformation seems possible as shown below.

In the simple one dimensional case, if θ varies linearly between two known points, then, the quantity, $d\theta/dx$ is known, from the initial conditions. Moreover, from the known relation between ψ and θ, we can also evaluate the quantity, $d\psi/d\theta$ at any appropriate average value of θ between the points. Now, the product, $(d\psi/d\theta)(d\theta/dx) = d\psi/dx$ actually provides us with an equivalent gradient of ψ in the direction x. If we can use this equivalent gradient in the ψ - based equation, instead of using the gradients on the basis of linear variation of ψ, we can reap the benefits of the θ - based equation. Although this approach is also applicable only to uniform media, the advantage here is that it can be used in numerical models for those parts of the flow region where the soil is uniform and at low saturations.

In the preceding pages we have examined in detail, the physics of transient groundwater motion in deformable, saturated-unsaturated porous media. We shall now examine the numerical methods that can be used to solve the governing equation that has been developed.

CHAPTER III

METHODS OF SOLVING THE GOVERNING EQUATION

A. GENERAL REMARKS

The governing equation for transient, saturated-unsaturated groundwater motion can be expressed in a differential form or in an integral form as follows:

Differential form:

$$\vec{\nabla} \cdot A\vec{\nabla}u = B\ \partial u/\partial t \tag{III.1}$$

Integral form:

$$\int_V \vec{\nabla} \cdot A\vec{\nabla}u\ dV = \int_S A\vec{\nabla}u \cdot \vec{n}\ d\sigma$$

$$= \int_V B(\partial u/\partial t)\ dV \tag{III.2}$$

where S is the surface bounding the region V. If we assume that B and $(\partial u/\partial t)$ represent average values for the small region V, then, these can be taken out of the integral sign and we will have,

$$\int_V \vec{\nabla} \cdot A\vec{\nabla}u\ dV = \int_S A\vec{\nabla}u \cdot \vec{n}\ d\sigma = D'(\partial u/\partial t) \tag{III.3}$$

where, $D' = BV$

In (III.2) and (III.3),

$$A = \rho \frac{k\rho g}{\mu}$$

$$B = [Sn\rho\rho_o\beta g + \frac{\rho S\chi\gamma_w a_v}{(1+e)} + \rho n \frac{dS}{d\psi}]$$

$$D' = M_c, \text{ fluid mass capacity}$$

and $u = z + \psi$

Equations (III.1) through (III.3) are non-linear equations, since the coefficients, A, B and D' are functions of the dependent variable, u. In solving any of these equations, one would need to give due considerations to the intial and boundary conditions,

$$u = U_o(x_i), \quad t = 0$$

$u = U(x_i, t)$ on S_1, where S_1 is a prescribed potential boundary

$\frac{\partial u}{\partial \vec{n}} = V(x_i, t)$ on S_2, where S_2 is a prescribed flux boundary and $(\partial u/\partial \vec{n})$ is the gradient along the outer normal to S_2

(III.4)

The earliest investigators attempted to solve (III.1) by finding analytical solutions, using such techniques as separation of variables, Laplace transformation, Green's Functions and conformal mapping. A distinct advantage of such analytical methods is that the solutions

are derived in algebraic forms and it is easy to study the behavior of the systems in terms of convenient dimensionless variables. However, the process of finding an analytical solution becomes cumbersome and difficult except in the case of simple initial and boundary conditions and material composition of the flow region. Most natural field situations are such that a description of the problem in terms of simple conditions may not be possible. Hence, researchers felt the need for alternate methods of solution, capable of handling realistic field problems, involving complex intitial and boundary conditions and material properties. This desire gave birth to a new approach in which each complex problem was posed and solved as a specific numerical problem, obtaining approximate solutions of any desired accuracy. Although only one problem could be handled by it at a time, the new numerical approach had the capability of handling complex problems, which was far beyond the reach of analytical methods. The growth of the new numerical approach required the development of a suitable approximation theory, appropriate techniques of averaging and, above all, an ability to rapidly carry out a large number of calculations. Although the theory of approximations had been under development over a long period of time, it did not, by itself, spur the growth of the numerical approach. The explosive development of the numerical approach in recent times has been mainly due to the rapid evolution of high speed digital computers in the last twenty-five years. Thanks to the numerical approach, in several fields of science and technology, complex problems have now come within the reach of critical analysis. In the present work, we shall follow the numerical approach in order to solve the initial-boundary value problems of saturated-unsaturated groundwater motion.

B. NUMERICAL METHODS

The oldest of the numerical methods is that of finite differences. The origin of this method goes back to Isaac Newton (Schneid (1968)). The central concept in the finite difference approach is that the gradient of a function between two points is equal to the difference in the value of the function at the given points divided by the distance in between. For example, if $y = f(x)$, then,

$$\left.\frac{dy}{dx}\right|_{x_{+\frac{1}{2}}} = \frac{f(x)_{+1} - f(x)_0}{x_{+1} - x_0} \qquad \text{(III.5)}$$

where the subscripts, +1 and o denotes the locations at which x is evaluated and +1/2 denotes a location midway between them. As is commonly employed in heat conduction and fluid flow studies, the finite difference method of numerical analysis basically consists in a direct approximate solution of the differential equation (III.1).

On examination of (III.1) it is noted that the left hand side of the equation involves the evaluation of a second derivative of the variable u at a given point in space. In the light of (III.5) it follows that in order to evaluate the second derivative at a given point and in a given direction, we must have three collinear points in that direction, the central point being the point of interest. Now, since the evaluation of derivatives at each point involves its neighbors, it follows that to employ the finite difference technique the points of interest be generally arranged parallel to the cartesian co-ordinate axes, filling the general three-dimensional space with orthorhombic boxes. Hence, in the finite difference technique, all flow regions, whatever be the complexity of shape, is usually

discretized in terms of orthorhombic boxes (in three-dimensions) or rectangular blocks (in two-dimensions). Experience showed that this restriction was often a handicap in handling flow regions with complex configurations. Therefore, attention was soon directed to alternate techniques, which enabled easy handling of complex boundary shapes.

It was recognized that in this connection that by integrating (III.1) over finite subregions, and by having the resulting integral form (III.2) or (III.3) as the basic governing equation, one could get over the restriction inherent in the finite difference technique in handling complex geometries. As a result of this possibility, a great deal of interest was generated in the study of such integral equations and the post 1960's has witnessed the establishment of such integral schemes as powerful tools of numerical analysis of continuum problems.

Integral formulations

Although we shall not dwell upon details, the integral formulations were conceived and developed by several workers in different disciplines such as heat transfer, hydraulics, physics and structural mechanics (Finlayson, 1972). Depending on their particular nature, integral formulations have been variously termed, variational methods, collocation methods, Galerkin procedure, finite element method, method of weighted residuals, etc. However, Finlayson (1972) shows how most of them could be grouped under a single broad technique of the method of weighted residuals.

In the field of groundwater flow, the finite element method, developed on the basis of variational principles or Galerkin procedure is widely used. Less well known are collocation procedures, which too have been occasionally employed. Conceptually, these approaches have a great deal in common and each of these has its advantages in handling specific classes of problems.

For the type of the general multidimensional problems envisaged in this thesis, a form of the integral formulation, similar to the collocation procedure was found to be especially suitable and hence was chosen as the basic calculational model. Before its final choice, however, considerable effort was spent on an examination of the theoritical bases of this technique and the finite element method. The rest of this chapter will be devoted to a consideration of the results of such an examination.

C. PHYSICAL BASIS OF DEVELOPMENT

In developing mathematical models, it is customary in the literature to make use of concise mathematical expressions and operations. However, for convenience, we shall first consider the physical description of the mathematical model before making use of the mathematical notations. Hopefully, this approach would not only describe the particular method of solution more clearly, but also render a physical comparison of different models more easy.

Consider the governing equation in an integral form, as in (III.3), which is a mass conservation equation. On the right hand side of (III.3) is the quantity, $\partial u/\partial t$, which is the time derivative of the dependent variable, u at some spatial location. This is the unknown

quantity sought to be solved for by the initial-boundary value problem. The left hand side of (III.3) mathematically expresses the factors which cause the time derivative to change from place to place and from time to time. Also, on the left hand side we have two equivalent spatial integrals - one, a volume integral and the other, a surface integral. Since the right hand side of the equation relates to a particular point in the flow domain, it follows that either of the two space integrals on the left hand side pertains to a small subregion immediately surrounding the spatial location at which $\partial u/\partial t$ is evaluated. As already demonstrated in chapter II, the volume integral signifies the summation of the time-rate of mass change over the subregion involved, while, equivalently, the surface integral signifies the summation of all the fluxes that enter and leave the subregion across its bounding surface. Indeed, as far as the diffusion process is concerned, one seems justified in stating that the surface integral is the cause of the transient fluid flow phenomenon, since any change of mass within the subregion can take place only due to fluxes entering or leaving the subregion of interest through the surface segments that enclose the latter. At any rate, in order to solve (III.3) for any point in space, we have to associate a finite subregion with each point of interest. Furthermore,in order to extend the solution to the entire flow region, a convenient set of points (nodal points) could be distributed throughout the flow region. A finite subregion could then be associated with each of these nodal points, so that the total space of the flow region is composed of the sum of the various sub regions. After choosing the points of interest and the associated subregions, we

could solve (III.3) for each subregion, subject to the important constraint of assuring compatibility between the calculations with respect to adjoining subregions.

If we take an arbitrary flow region and choose a set of nodal points, there are two possible ways of associating subregions with each nodal point. Thus, in figure 10A, we consider two nodal points 1 and 2 and the subregions associated with these nodal points are mutually exclusive. As a result, the fluxes entering into the mass balance calculations of one subregion are not repeated in the mass balance calculations of the other, except along their common interface, where the fluxes cancel each other, being of the same magnitude but of opposite sign. If we extend this manner of subdivision to the entire flow region, we will finally have a set of mutually exclusive subregions.

In figure 10B, the subregion for each nodal point is defined by lines connecting its immediate neighbors. As seen from the figure, this results in an overlap between subregions of adjoining nodal points. In carrying out mass balance calculations, therefore, care should be taken to remove the effects of this overlap on mass balance.

Once we have divided the flow region into subregions and associated nodal points, the simplest procedure of solution is to repeat the logical continuity process of evaluating the rate of mass increase within the subregion, either by evaluating the surface integral or by evaluating the volume integral on the left hand side of (III.3) and obtain the required quantity, $\partial u/\partial t$ for the associated nodal point by a simple explicit relation,

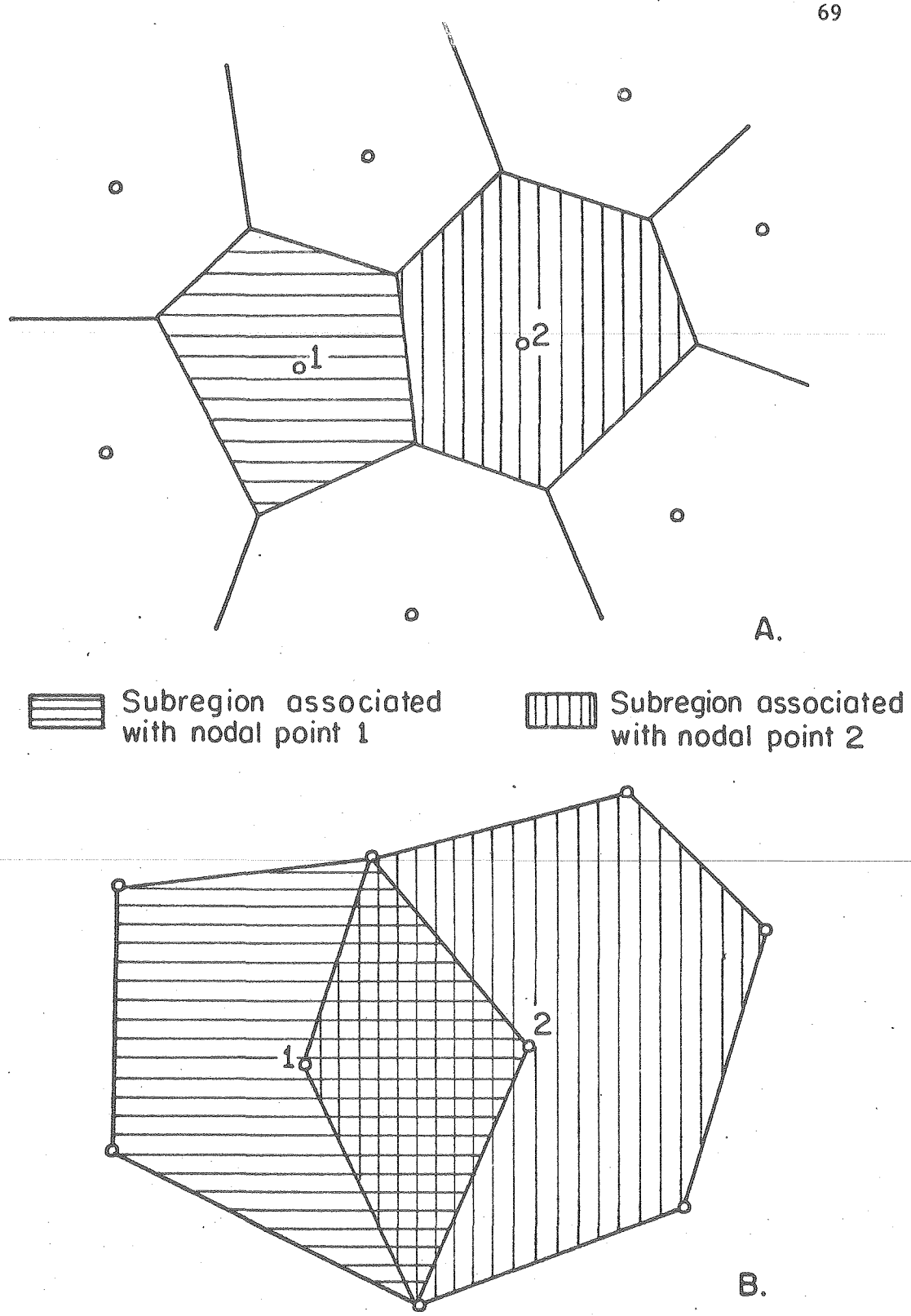

Fig. 10. Nodal points and their associated subregions: A. Independent subregions, B. Overlapping subregions

$$\frac{\partial u}{\partial t} = \frac{1}{D'} \int_S A\vec{\nabla}u \cdot \vec{n}\, d\sigma \qquad \text{(III.6)}$$

Or, in the light of the equivalence between volume and surface integrals, one could use, instead of (III.6),

$$\frac{\partial u}{\partial t} = \frac{1}{D'} \int_V \vec{\nabla} \cdot A\vec{\nabla}u\, dV \qquad \text{(III.7)}$$

D. MATHEMATICAL DEVELOPMENT

The mathematical development of the solution of integral formulations involves translation of the physical development discussed in the previous section into mathematical formalism. If we assume that the manner of defining subregions with overlap is a more general case and we consider the mutually exclusive subregions as as having zero overlap, they can be treated in a single logical process of discussion.

As discussed earlier, in the case of overlapping subregions, some form of compensation would have to be effected in mass balance calculations in order to correct for the overlap between subregions of adjoining nodal points. Mathematically, one way of effecting such compensation is to "weigh" each addend with suitable "weighting" factor while carrying out the integration with reference to each nodal point (that is, evaluating the volume integral or the surface integral). Sufficient mathematical theory is now available to incorporate this "weighting factor" into the integral itself, so that the weighted averaging process becomes inherent in the process of numerical

integration. The incorporation of the weighting factor into the integral equation gives rise to a very general approach called the method of weighted residuals (MWR) (Finlayson, 1972), including in itself most of the integral equations currently used for numerical analysis of heat flow and fluid flow problems.

1. The method of weighted residuals

In order to apply, let us rewrite (III.2) as,

$$\int_V (\vec{\nabla} \cdot A\vec{\nabla}u - B \frac{\partial u}{\partial t}) \, dV = 0 \qquad \text{(III.8)}$$

We now multiply the integral by a weighting factor and get,

$$\int_V \omega \, (\vec{\nabla} \cdot A\vec{\nabla}u - B \frac{\partial u}{\partial t}) \, dV = 0 \qquad \text{(III.9)}$$

where $\omega = \omega(x_i)$ and $u = u(x_i)$ are both space variables.

Before developing (III.9) further, it should be noted that the coefficients A and B, as they relate to saturated-unsaturated flow problem, are dependent on u and hence, (III.9) is a non-linear integral equation. Now, the theoritical basis for the theory of weighted residuals is generally developed for linear equations and their application to non-linear equations is not entirely rigorous. Hence, for purposes of our discussions in this chapter, we will restrict ourselves to linear equations and assume that A and B are constants, independent of u.

We shall now revert to (III.9). Since this is an initial-boundary value problem, in principle, we need to know the initial distribution of u as a function of the space variables. While the variation of u over the entire flow region may not be a simple function, it is reasonable to imagine that within an appropriately small subregion, the variation may be simple enough so that its distribution could be approximated by a simple polynomial expression, usually of the first degree. Physically, such a polynomial approximation would imply a "plane" surface representing the variation of u over the subregion. Suppose we have an appropriately small two-dimensional subregion involving a nodal point and its immediate neighbors, as in figure 11. We can divide the subregion, which happens to be a pentagon, into five smaller triangles, designated by the Roman numerals, I - V. As was suggested in the last section, in setting up the continuity equation for the central nodal point (nodal point 1 in figure 11), we have to consider the entire pentagonal region and hence we will call it a "primary" element. The triangular elements, each of which forms part of the primary element, could be called "secondary" elements. Within each secondary element, which is sufficiently small, we can assume that, at any instant of time, u varies approximately linearly, satisfying a first degree polynomial equation. For instance, at any point (x_i) within triangle I, we will have, at a given instant of time, t,

$$u(x_i,t) = \xi_1(x_i)u_1(t) + \xi_2(x_i)u_2(t) + \xi_3(x_i)u_3(t) \tag{III.10}$$

where ξ_1, ξ_2 and ξ_3 are certain linear coefficients which can be

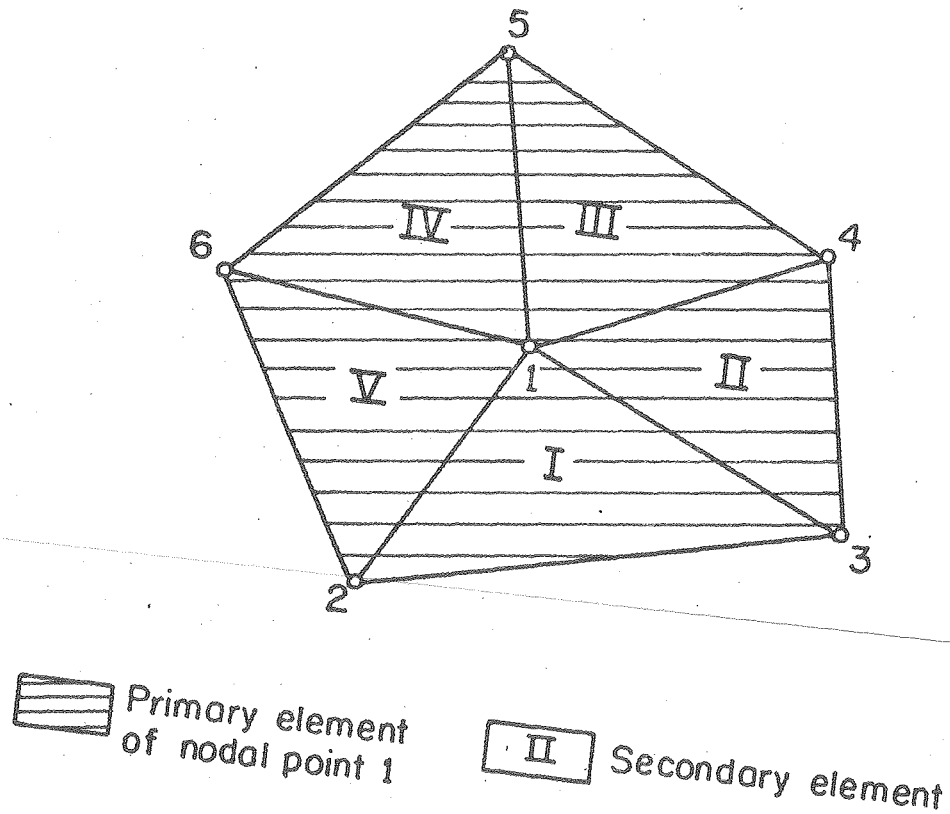

Fig. 11. Primary and secondary elements

determined from geometric considerations. Generalizing this and using the concise subscript notation, we can write,

$$u(x_i,t) \simeq \xi_n(x_i)u_n(t), \qquad n = 1,2,3,\ldots\ldots \qquad \text{(III.11)}$$

in which, the repeated subscript indicates summation over n, as shown in (III.10). Substituting (III.11) into (III.9) we get,

$$\int_V \omega(x_i)\ [\vec{\nabla} \cdot A\vec{\nabla}\xi_n u_n - B\frac{\partial \xi_n u_n}{\partial t}]\ dV = 0 \qquad \text{(III.12)}$$

Equation (III.12) is a form of the method of weighted residuals. In (III.11) and (III.12), the subscripts m and n denote labels of specific points in the flow region. If, in (III.11), $\xi_n u_n$ is exactly equal to u (instead of being approximate), then, the term within the square bracket in (III.12) will identically vanish and hence, (III.12) will be exactly satisfied. On the other hand, if (III.11) is satisfied only approximately, as indicated, then, the right hand side of (III.12) will no more be zero and will assume some finite "residual" value. How close this residual value would be to zero would depend on how closely the approximating function, $\xi_n u_n$, satisfies the actual function u. Conversely, one could force the residual to be zero on the right hand side of (III.12) and obtain an approximate solution for $u(x_i,t)$.

In (III.12), the weighting factor ω can be chosen in many ways and each choice leads to a particular method of solution and to a different approximate solution of the function u. For example, if one sets $\omega(x_i) = \xi(x_i)$, the result is the Galerkin approach, which, when used with the spatial discretization suggested in figures 10B and 11, is one way of developing the finite element equations.

Again, if one sets $\omega(x_i) = 1$ within the elemental subregion and zero everywhere else, the result is the subdomain collocation method. If one sets $\omega(x_i) = 1$ at specific points in the flow region but zero elsewhere, the resulting approach is the point collocation scheme.

In this manner, we have the following equations for the Galerkin and the subdomain collocation schemes:

Galerkin scheme:

$$\int_V \xi_m [\vec{\nabla} \cdot A\vec{\nabla}\xi_n u_n - B \frac{\partial \xi_n u_n}{\partial t}] \, dV = 0 \qquad \text{(III.13)}$$

Subdomain collocation scheme:

$$\int_V \omega_m [\vec{\nabla} \cdot A\vec{\nabla}\xi_n u_n - B \frac{\partial \xi_n u_n}{\partial t}] \, dV = 0 \qquad \text{(III.14)}$$

in which,

$$\omega_m = \begin{cases} 1, & \text{over subregion associated with nodal point } m \\ 0, & \text{elsewhere} \end{cases}$$

Since we are restricting ourselves to linear problems with A as constant, we can rewrite (III.13) as,

$$\int_V [A\xi_m \vec{\nabla}^2 \xi_n u_n - B\xi_m \frac{\partial \xi_n u_n}{\partial t}] \, dV = 0 \qquad \text{(III.15)}$$

We could remove the second derivative in the first term within the square brackets with the help of divergence theorem. However, since

we have two spatial functions, ξ_m and ξ_n in the expression, we make use of Green's first identity (Sokolnikoff and Redheffer, 1966),

$$\int_V a\vec{\nabla}^2 b \, dV = -\int_V \vec{\nabla}a \cdot \vec{\nabla}b \, dV + \int_S a\vec{\nabla}b \cdot \vec{n} \, d\sigma$$

which is a corollary of the divergence theorem. Thus, applying Green' first identity to (III.15) we arrive at the final expression for the Galerkin scheme,

$$-\int_V A\vec{\nabla}\xi_m \cdot \vec{\nabla}\xi_n u_n \, dV - \int_V B\xi_m \frac{\partial \xi_n u_n}{\partial t} \, dV$$

$$+ \int_S A\xi_m \vec{\nabla}\xi_n u_n \cdot \vec{n} \, d\sigma = 0 \qquad \text{(III.16)}$$

In the case of (III.14), since there is only one space variable, ξ_n, (ω_m is a constant), we can directly apply the divergence theorem (Sokolnikoff and Redheffer, 1966),

$$\int_V \vec{\nabla} \cdot a\vec{\nabla}b \, dV = \int_S a\vec{\nabla}b \cdot \vec{n} \, d\sigma$$

to the first term within the square brackets in (III.14) and obtain the final expression for the subdomain collocation scheme,

$$\int_S \omega_m A\vec{\nabla}\xi_n u_n \cdot \vec{n} \, d\sigma - \int_V \omega_m B \frac{\partial \xi_n u_n}{\partial t} \, dV = 0 \qquad \text{(III.17)}$$

Equation (III.16) and (III.17) relate to the primary element associated with nodal point m in figure 11. The subscript m can therefore be

recognized as the nodal point associated with the primary element and the subscript n denotes, in turn, each of the nodal points occurring in the primary element, including m.

Now, if we carefully define ξ_m to be non-zero only within the primary element and zero everywhere else in the flow region, then, the integral suggested in (III.16) and (III.17) can be imagined for all practical purposes, as carried out over the whole flow region, since the effect of the summation outside of the primary element has only the effect of adding zeros.

In effecting the final formulations (III.16) and (III.17) for the Galerkin scheme and the subdomain collocation scheme respectively, we divided the primary element into secondary elements (figure 11). Within each secondary element we assumed a linear variation in u. Looking at figure 11, it is easy to visualize that the same secondary element would be shared by primary elements of each of the nodal points lying at its vertices. Hence, there would occur overlap between subdomains of nodal points in the Galerkin scheme and the subdomain collocation scheme. The overlap, however, is compensated for by the weighting function, ω_m.

1. Non-overlapping subdomains

Instead of discretizing the flow region into overlapping subregions, it is also possible to discretize it into mutually exclusive subregions, as suggested in figure 10A. Inasmuch as there is no overlapping of subdomains we can now dispense with the need for a weighting factor. Hence, we can directly use (III.2) and write, using the divergence theorem, for each subdomain,

$$\int_S A\vec{\nabla}u \cdot \vec{n}\, d\sigma - \int_V B\frac{\partial u}{\partial t}\, dV = 0 \qquad \text{(III.18)}$$

which is similar to the expression (II.17) for the subdomain collocation scheme except for the substitution of $u = \xi_n u_n$.

Measurement of gradients

If we ignore the introduction of the weighting factor, (whose role can be interpreted as compensating for overlap between subdomains), and if we recognize equivalence between volume and surface integrals indicated by divergence theorem, what is really fundamental to the solution is the summation of the fluxes across the boundary of each independent subdomain. These fluxes are indeed the cause of the mass redistribution within each subdomain and the consequent transient behavior of the system.

Now, according to the equation of motion, Darcy's law, in order to calculate flux in a given direction (say, along the normal to some surface of interest), we require a knowledge of the gradient of the potential u in that direction. Therefore, we need to calculate the quantity, $\vec{\nabla}u \cdot \vec{n}$, where, $\vec{n}$ is the unit outer normal to the surface of interest. As will be seen presently, the manner of evaluating the gradient $\vec{\nabla}u \cdot \vec{n}$ is different in the finite difference and the finite element approaches.

In the simple finite difference approach, gradient is measured by the relation (III.5), dividing Δu by the distance between the nodal points. This requires that in order to measure gradients in a given direction, we must have two nodal points aligned in that

direction.

Another way of measuring gradient in any given direction is to take three or more non-collinear points and fit a surface for the variation of the potential, u, within the region "enclosed" by the points. Once the equation of this surface is known, the gradient in any specific direction and at any specific point within the region can always be computed from the equation of the surface. This is the approach that is followed in the "finite element" approach, as it is commonly understood. The advantage of this approach is that the evaluation of gradient is somewhat more general and this approach is somewhat more amenable to using higher order polynomial equations for the variation of u within a secondary element. This approach is also convenient in a general handling of anisotropy, involving tensorial quantities. On the other hand, the simpler finite difference approach is generally well-suited for first-degree approximation to gradient. In principle, higher-order approximations could be obtained with the finite difference scheme by considering several successive points along a straightline, but the procedure, apparently, is not very convenient to use.

3. The Integrated Finite Difference Scheme

The mathematical model which has been developed for the present study is an integral formulation (III.3). In this model, the flow region is discretized into non-overlapping subregions in the manner suggested in figure 10A. In addition, the technique of evaluating gradients used in this model is based on the finite difference approach. Descriptively, it seems appropriate to call this method as

The Integrated Finite Difference scheme (IFD). Perhaps the earliest to use this approach was MacNeal (1953), who termed it an "asymmetrical finite difference network". Subsequently, this approach seems to have been extensively used in heat-transfer calculations (Dusinberre 1961; Edwards, 1969).

Having divided the flow region into appropriate subregions, equation (III.3) is directly applied to each subregion by evaluating the surface integral . Because of the use of non-overlapping subdomains, the IFD does not use a weighting factor and hence the resulting governing equation is very similar to that of the subdomain collocation scheme.

Considering the fact that the three different approaches discussed above have the same physical basis, it is reasonable to infer that all of them should lead to the same general result, although by somewhat different paths and may be expected to yield results which are of comparable accuracy. If we simply look at the mathematical expressions, however, the basic similarities, for example, between the Galerkin scheme on the one hand and the IFD on the other are not immediately obvious. In the next section, we will examine their mathematical expressions for a more detailed comparison.

4. The Galerkin method and the IFD

Since the IFD uses first degree approximation for measuring gradient (linear variation of potential between adjoining nodal points), we shall, for purposes of comparison, consider Galerkin scheme in conjunction with first degree coordinate functions. We will begin with the development of the Galerkin equations for an arbitrary subregion.

On the basis of the results so obtained, we will relate the Galerkin scheme to the IFD scheme.

For easy reference, let us reproduce the Galerkin equation,

$$- \int_V A\vec{\nabla}\xi_m \cdot \vec{\nabla}\xi_n u_n \, dV - \int_V B\xi_m \frac{\partial \xi_n u_n}{\partial t} \, dV$$

$$+ \int_S A\xi_m \vec{\nabla}\xi_n u_n \cdot \vec{n} \, d\sigma = 0 \qquad \text{(III.16)}$$

Consider now an arbitrary two-dimensional flow region as shown in figure 12. Since we are assuming linear variation in u between adjoining nodal points, and since only three points are required to adequately describe a plane surface in three dimensions, the simplest possible shape for a secondary element in two dimensions is a triangle. Therefore we discretize the flow region in terms of triangles.

The integration implied in the Galerkin equation (III.16) is over the entire flow region in figure 12. In the light of the discretization of the flow region into triangles (within each of which u varies linearly) we can replace (III.16) by a summation of the integrals evaluated over each secondary element. Thus,

$$\sum_{i=1}^{i=N} \left[- \int_{V_i} A_i \vec{\nabla}\xi_m \cdot \vec{\nabla}\xi_n u_n \, dV - \int_{V_i} B_i \xi_m \frac{\partial \xi_n u_n}{\partial t} \right.$$

$$\left. + \int_{S_i} A_i \xi_m \vec{\nabla}\xi_n u_n \cdot \vec{n} \, d\sigma \right] = 0 \qquad \text{(III.19)}$$

where N is equal to the total number of secondary elements in the flow region.

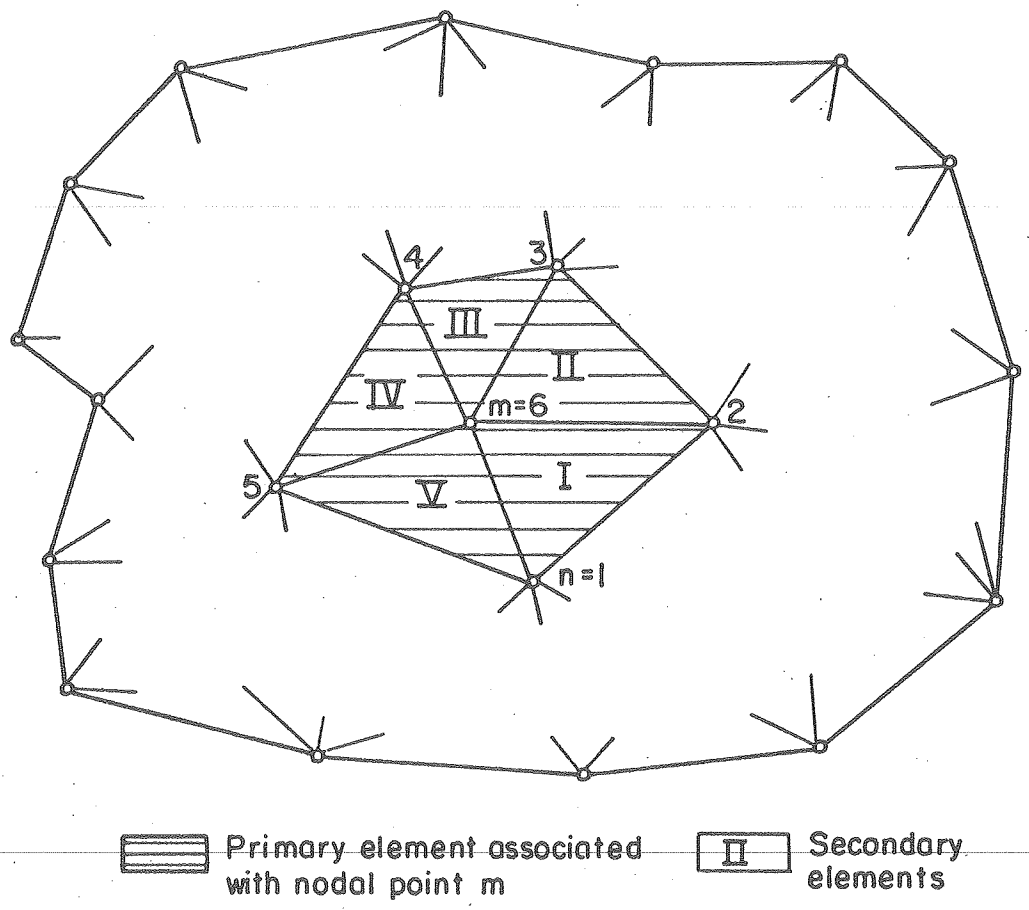

Fig. 12. Discretization of flow region into triangular elements

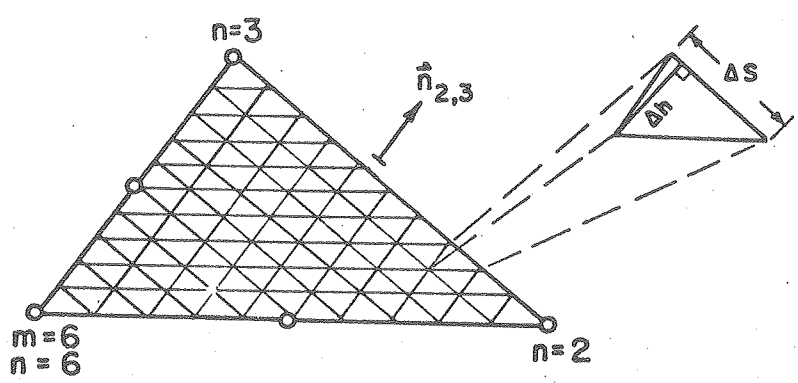

Fig. 13. Blow-up of triangle II of figure 12 and scheme for numerical integration

Now, since the primary aim of the governing equation is to estimate the time derivative of potential at each nodal point, it follows that an equation of the type (III.19) would not have to be set up for all those nodal points in the system for which potentials are prescribed in the form of boundary conditions. Therefore, (III.19) would have to be set up only for those nodal points at which u is allowed to vary with time. This would include all interior nodal points of the flow region and all those boundary nodal points lying on a boundary with prescribed flux.

In (III.16), the surface integral pertains to the outer boundary of the flow region. As will be seen presently, the nature of the function ξ_m is such that that the surface integral in (III.16) will be zero if m is an interior nodal pointand will have a known, non-zero value if m lies on a segment of a prescribed flux boundary. Hence, we will not consider the surface integral any further. Thus, we are left with only two volume integrals to consider.

Let us now consider the first volume integral in (III.19), and apply it to the secondary element II in figure 12. The secondary element II is shown in detail in figure 13.

At this point, we will pause to consider the nature of the fuction ξ_m. By definition,

$$\xi_m = \begin{cases} 1, & \text{at nodal point } m \\ 0, & \text{at all other nodal points} \end{cases}$$

Moreover, between nodal point m and an adjoining nodal point ξ_m is defined to vary linearly. Therefore, if m = 6 (figure 13), then,

$\xi_m = 1$ at nodal point 6 and $\xi_m = 0$ at nodal points 2 and 3 as well as the line connecting nodal points 2 and 3. Also, since ξ_m varies linearly along the sides of the triangle, the lines of equal value of ξ_m lie parallel to the side (2,3). Therefore, the gradient of ξ_m is directed along $\vec{n}_{2,3}$, which is the outer normal to the side (2,3). Hence, we can rewrite the first integral in (III.19) as follows:

$$-\int_{V_{II}} A\vec{\nabla}\xi_m \cdot \vec{\nabla}\xi_n u_n \, dV = -\int_{V_{II}} A\left|\frac{\partial \xi_m}{\partial \vec{n}_{2,3}}\right| \vec{n}_{2,3} \cdot \vec{\nabla}\xi_n u_n \, dV$$

$$= -\int_{V_{II}} A \left|\frac{\partial \xi_m}{\partial \vec{n}_{2,3}}\right| \nabla\xi_n u_n \cdot \vec{n}_{2,3} \, dV \qquad \text{(III.20)}$$

in which, the quantity, $\left|\frac{\partial \xi_m}{\partial \vec{n}_{2,3}}\right|$ is the magnitude of the gradient vector along the direction $\vec{n}_{2,3}$.

In figure 13, each side of the triangle is divided into ℓ equal parts ($\ell = 10$), resulting in ℓ^2 small congruent triangles. If the length of the side parallel to side (2,3) of each of these small triangles is denoted by Δs and if Δh denotes the altitude normal to Δs, then,

$$dV = \text{area of each small triangle} = \frac{1}{2}\Delta s \Delta h \qquad \text{(III.21)}$$

Also, since the gradient of ξ_m is constant over the large triangle and since the sides of the large triangle have been divided

into ℓ equal parts, within each triangle, the gradient of ξ_m can be denoted by,

$$\frac{\partial \xi_m}{\partial \vec{n}_{2,3}} = \frac{1/\ell}{\Delta h}$$

Therefore, (III.20) becomes,

$$-\int_{V_{II}} A\vec{\nabla}\xi_m \cdot \vec{\nabla}\xi_n u_n \, dV = -\int_{V_{II}} A \frac{1/\ell}{\Delta h} [\vec{\nabla}\xi_n u_n \cdot \vec{n}_{2,3} \frac{1}{2}\Delta s \Delta h]$$

$$= -\frac{1}{2} \int_{V_{II}} A \frac{1}{\ell} [\vec{\nabla}\xi_n u_n \cdot \vec{n}_{2,3}] \Delta s$$

$$= -\frac{1}{2} \sum_{\substack{\text{all small} \\ \text{triangles}}} \frac{1}{\ell} [A\vec{\nabla}\xi_n u_n \cdot \vec{n}_{2,3} \Delta s] \quad \text{(III.22)}$$

Recalling that A represents hydraulic conductivity and u is the fluid potential and noting that there are ℓ^2 small triangles in the large triangle, we have,

$$-\int_{V_{II}} A\vec{\nabla}\xi_m \cdot \vec{\nabla}\xi_n u_n \, dV = -\frac{1}{2} \ell^2 \frac{1}{\ell} [\vec{q} \cdot \vec{n}_{2,3}] \Delta s$$

$$= -\frac{1}{2} [\vec{q} \cdot \vec{n}_{2,3}] \ell \Delta s \quad \text{(III.23)}$$

But, $\ell\Delta s$ = length of side (2,3) of the large triangle (secondary

element II) and therefore,

$$-\int_{V_{II}} A\vec{\nabla}\xi_m \cdot \vec{\nabla}\xi_n u_n \, dV = -\frac{1}{2}\,[\vec{q} \cdot \vec{n}_{2,3}]\ [\text{side}(2,3)]$$

$$= -\frac{1}{2}\,[\text{flux across the side opposite nodal point m, along the outer normal, } \vec{n}_{2,3}\,] \tag{III.24}$$

Since the gradient of u is constant throughout triangle II as a consequence of the linearity assumption, (III.24) implies that,

$$-\int_{V_{II}} A\vec{\nabla}\xi_m \cdot \vec{\nabla}\xi_n u_n \, dV = -\,[\text{Flux across the line joining the mid points of sides (6,3) and (6,2) of the secondary element II, along the outer normal } \vec{n}_{2,3}\,] \tag{III.25}$$

Now, consider figure 14, in which triangle II is once again reproduced. In figure 14, G is a point so situated (centroid) that the three shaded regions have the same area. As wehave just seen from (III.25), the volume integral actually yields the flux across side AB in figure 14, which is opposite nodal point m. However, as shown by the arrows in figure 14, the flux across the line AB is exactly equal to the sum of the fluxes across the lines GA and GB, providing that the linear approximation of u implies "steady" conditions of flow within the secondary triangle II, which is indeed so. Hence, if we subdivide the secondary element II into three non-overlapping

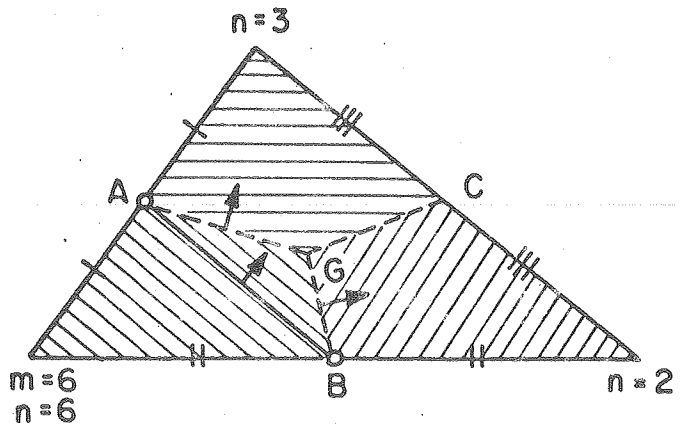

Fig. 14. Division of secondary element II into independent subregions

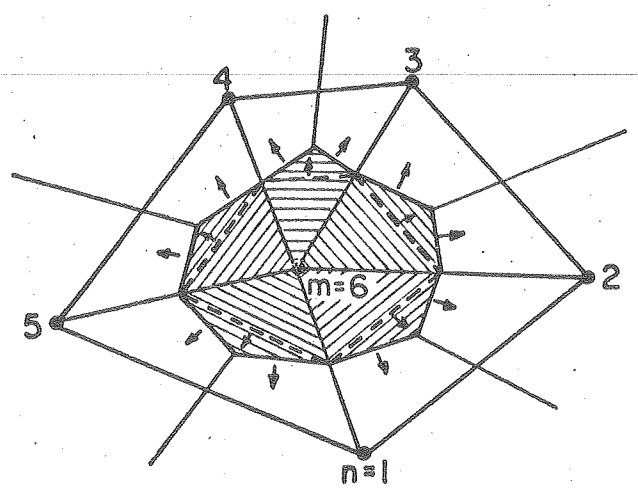

Fig. 15. The non-overlapping domain of influence of nodal point m

subregions of equal area, as shown by the dotted lines in figure 14, then, the first volume integral of the Galerkin equation (III.19) in fact yields the fluxes crossing the surface of the subregion opposite nodal point m (surface AGB).

We can now repeat this process of integration for each of the secondary elements and sum up the results to achieve the required integration for the primary element. The result is shown in figure 15.

The shaded region in figure 15 is the subregion exclusively associated with nodal point m. In a similar fashion, we could associate one such subregion exclusively with each of the nodal points in the flow region. What we have actually achieved is that we start with a set of mutually overlapping subregions, apply the Galerkin procedure (using weighting functions) and end up with the fluxes for mutually exclusive subregions. It is pertinent to point out here that in the IFD method, we start with a set of non-overlapping subregions and directly evaluate the required fluxes. In effect, therefore, the role of the weighting functions is one of compensating for overlap in carrying out mass balance calculations.

We now consider the second volume integral in (III.19), namely,

$$\int_{V_i} B_i \xi_m \frac{\partial \xi_n u_n}{\partial t} \, dV \, , \qquad i = \mathrm{I}, \mathrm{II}, \ldots . \mathrm{V}.$$

There are two possible ways in which this integral can be interpreted. The first approach (which usually involves matrix inversion of a set of implicit linear equations) is as follows:

Since $\xi_n(x_i)$ is independent of time, we have,

$$\int_{V_i} B_i \xi_m \frac{\partial \xi_n u_n}{\partial t} \, dV = \int_{V_i} B_i \xi_m \xi_n \frac{\partial u_n}{\partial t}$$

$$= B_i \frac{\partial u_n}{\partial t} \int_{V_i} \xi_m \xi_n \, dV \, , \qquad \text{(III.26)}$$

since $\partial u_n/\partial t$ is dependent only on t and since B_i is constant for the linear problem assumed in the present discussion. The last integral in (III.26) has been evaluated by Felippa (1966) and, for a triangular region it is shown to be,

$$\int_{V_i} \xi_m \xi_n \, dV = \begin{cases} \dfrac{\Delta_i}{12} \, , & m \neq n \\ \dfrac{\Delta_i}{6} \, , & m = n \end{cases} \qquad \text{(III.27)}$$

where Δ_i is the area of triangle V_i. Therefore, for a secondary element such as triangle II, (III.26) becomes,

$$\int_{V_{II}} B_{II} \xi_m \frac{\partial \xi_n u_n}{\partial t} \, dV = B_{II} \left[\frac{\Delta_{II}}{6} \frac{\partial u_6}{\partial t} + \frac{\Delta_{II}}{12} \left(\frac{\partial u_2}{\partial t} + \frac{\partial u_3}{\partial t} \right) \right]$$

(III.28)

Summation of (III.28) for the entire subregion around nodal point m (figure 12) would result in an expression involving not only the unknown time derivative of nodal point m, but also the time derivatives of nodal points 1 through 5, which are also unknown. Thus when the equations are set up for all the nodal points in the flow region, the

unknown time derivative of each nodal point will appear in more than one equation. Therefore, the resulting set of equations for the total flow region are inherently implicit in nature and would need to be solved as a set of simultaneous equations involving the unknown time derivatives.

The second approach is to interpret the second volume integral in (III.19) from physical considerations. Thus since the first volume integral in (III.19) yielded the summation of fluxes across the bounding surface of a non-overlapping subregion associated with a nodal point (figure 15), we can replace $\frac{\partial \xi_n u_n}{\partial t}$ by $\frac{\partial \bar{u}_m}{\partial t}$, where, $\frac{\partial \bar{u}_m}{\partial t}$ represents the average time rate of u within the shaded region in figure 15 that is associated with nodal point m.

The concept of using an average time rate of u is appealing for the following reason as well. Neuman (1972) has argued that the Galerkin scheme is a semi-discrete scheme (Benthien, 1973) in which the spatial variable is discretized at any instant of time. Hence, the substitution $u = \xi_n u_n$ cannot be made in the time integral (the second volume integral in (III.19)).

Thus, the second volume integral in (III.19) can be written as,

$$\sum_{i=I}^{i=V} \int_{V_i} B_i \xi_m \frac{\partial \xi_n u_n}{\partial t} dV = \frac{\partial \bar{u}_m}{\partial t} \sum_{i=I}^{i=V} B_i \int_{V_i} \xi_m \, dV \qquad \text{(III.29)}$$

By simple integration it can be shown that ,

$$\int_{V_i} \xi_m \, dV = \frac{\Delta_i}{3} \qquad \text{(III.30)}$$

where Δ_i is the area of the triangle i. Hence, (III.29) becomes,

$$\sum_{i=I}^{i=V} \int_{V_i} B_i \xi_m \frac{\partial \bar{u}_m}{\partial t} dV = \frac{\partial \bar{u}_m}{\partial t} \sum_{i=I}^{i=V} \frac{1}{3} [B_i \Delta_i] \qquad \text{(III.31)}$$

We recognize that B_i is the capacity of the material in the secondary element i to absorb fluid per unit "volume", and the quantity, $B\Delta_i$ represents the total capacity of the secondary element i. Hence,

$$\sum_{i=I}^{i=V} \int_{V_i} B_i \xi_m \frac{\partial \xi_n u_n}{\partial t} dV = \frac{1}{3} \left[\begin{array}{l}\text{capacity of primary} \\ \text{element of nodal} \\ \text{point } m\end{array}\right] \times \frac{\partial \bar{u}_m}{\partial t} \qquad \text{(III.32)}$$

Note that in figure 15, the area of the shaded region is equal to one-third the area of the large pentagonal region. Wilson's (1968) development of the FEM equations based on physical considerations leads to similar results as in (III.32). Hence, for a general, interior nodal point m, we will have two possible expressions,

$$\sum_i - \int_{V_i} A\vec{\nabla}\xi_m \cdot \vec{\nabla}\xi_n u_n \, dV - B_i \left[\frac{\Delta_i}{6}\frac{\partial u_m}{\partial t} + \frac{\Delta_i}{12} \sum_{n \neq m} \frac{\partial u_n}{\partial t}\right] = 0 \qquad \text{(III.33)}$$

or,

$$\sum_i - \int_{V_i} A\vec{\nabla}\xi_m \cdot \vec{\nabla}\xi_n u_n \, dV - \frac{1}{3} [B_i \Delta_i] \frac{\partial \bar{u}_m}{\partial t} = 0 \qquad \text{(III.34)}$$

Although (III.33) pertains to nodal point m, it contains the unknown time derivatives of the other nodal points denoted by n and so, the resulting set of equations has to be solved simultaneously for all the unknown time derivatives. In equation (III.34), on the other hand, if we assume that u_n = the known initial values, $U_n(t_o)$, then the only unknown is the time derivative of nodal point m. Equation (III.34), therefore, becomes an explicit relation capable of direct solution for each nodal point independently (see also, Emery and Carson, 1969).

We will now examine the manner in which the solution process is carried out in the IFD.

In the IFD, the nodal points and their associated non-overlapping subregions are defined at the outset, as shown in figure 16. The distribution of the nodal points and the elements (also called "nodes" in the IFD) are so chosen that the line joining any two nodal points coincides with the normal to the surface separating them. Hence, applying (III.3) to the shaded subregion in figure 16, we will have,

$$\int_S A\vec{\nabla}u \cdot \vec{n}\, d\sigma = \sum_{n=1}^{n=5} \bar{A}_{6,n} \frac{u_n - u_6}{d_{6,n}} \sigma_{6,n}$$

$$= B_6 V_6 \frac{\partial u_6}{\partial t} \qquad \text{(III.35)}$$

in which, $d_{6,n}$ is the distance between nodal points 6 and n

$\sigma_{6,n}$ is the "area" of the surface separating nodal points 6 and m

V_6 is the "volume"of nodal point m

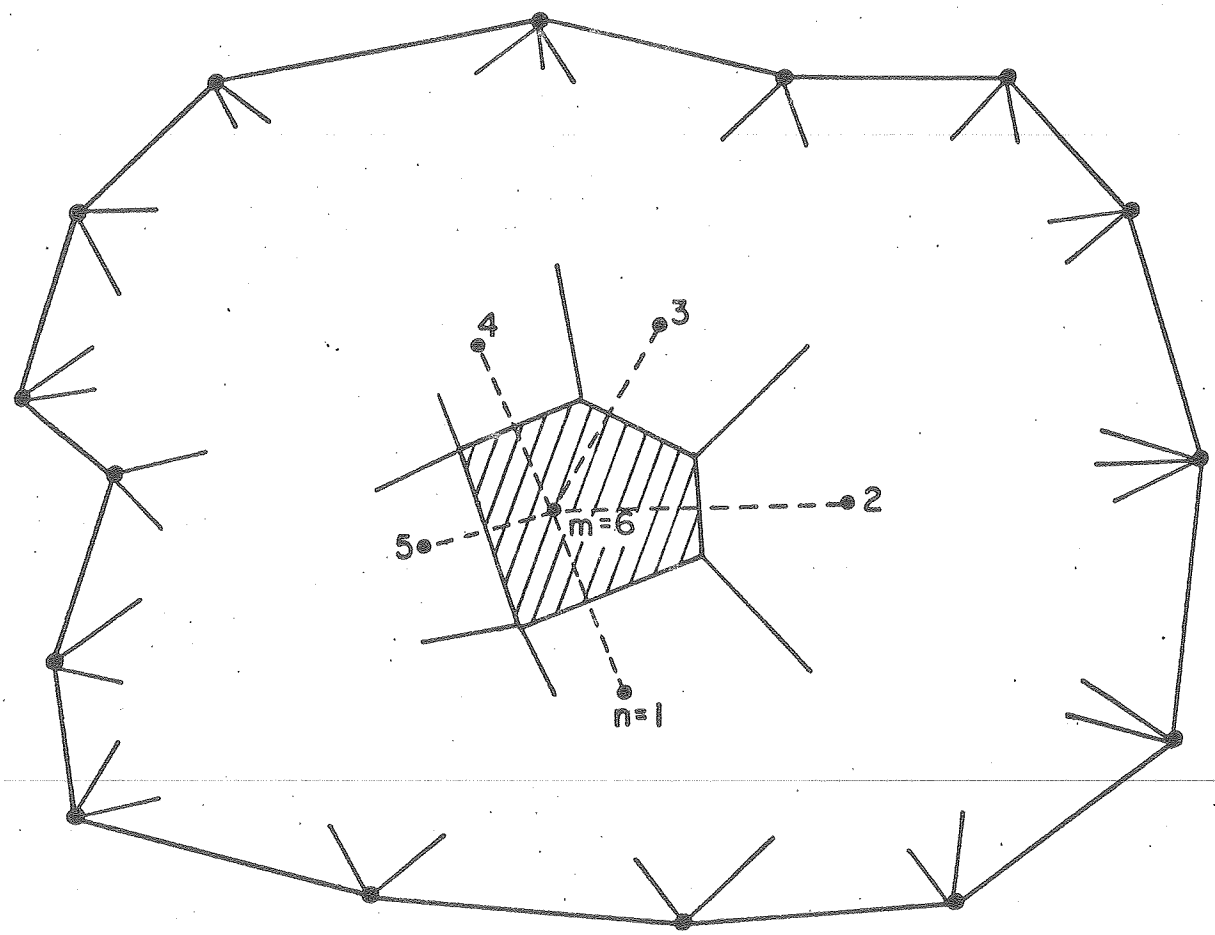

Fig. 16. Disposition of nodes (elements) and nodal points in the Integrated Finite Difference scheme

and $\bar{A}_{6,n}$ is a suitable "mean" permeability at the surface $\sigma_{6,n}$

In figures 15 and 16, the nodal points are centrally located within the non-overlapping subregions. Comparison of equations (III.34) and (III.35) and figures 15 and 16 show that except for the differences in shape and size of the subregions, both the Galerkin scheme and the IFD eventually carry out the same calculational process of summing up the surface fluxes around subregions of interest.

6. Isoparametric elements

One of the advantages of the Galerkin approach is the possibility of employing higher order approximations for the spatial variation of u within a secondary element. Also, in the case of the triangular element, a fairly large number of triangular elements may be needed to accurately approximate curved boundaries. In order to make use of higher order approximations as well as to handle curved boundaries with fewer elements, curved, "isoparametric" elements have been used in the literature (Ergatoudis et al., 1968; Zienkiewicz and Parekh, 1970; Pinder and Frind 1972). Curved, isoparametric quadrilaterals are quadrilateral elements (in two dimensions) with arbitrarily curved sides and with additional nodal points on the sides of the quadrilateral (figure 17).

The central concept in the case of curved isoparameteric elements is to treat the curved quadrilateral as a"square" or as a "cube" in a suitably transformed, new, curvilinear coordinate system. In two dimensions, let this new coordinate system be denoted by (η,ζ), whereas the real coordinate system is designated by (x,y). The co-

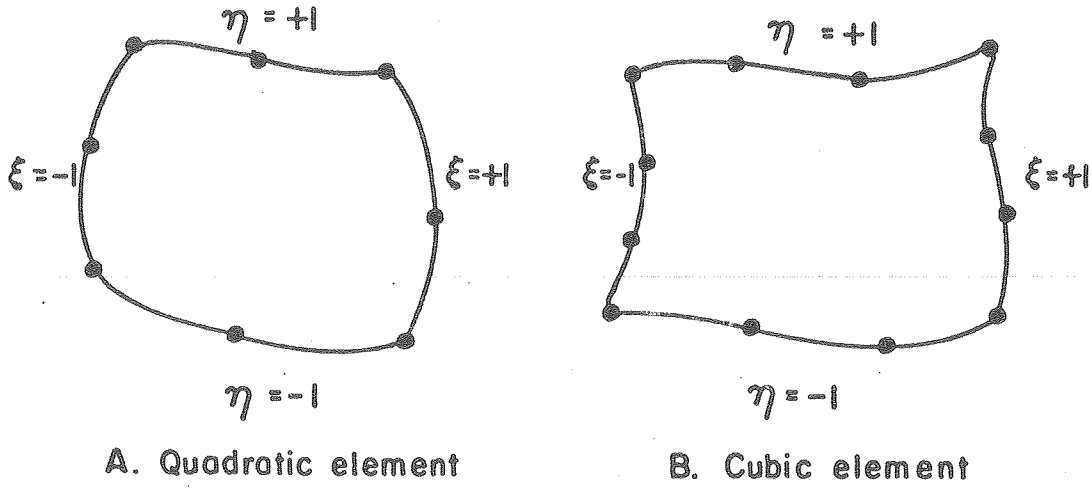

Fig. 17. Curved isoparametric quadrilaterals: A. Quadratic element, B. Cubic element

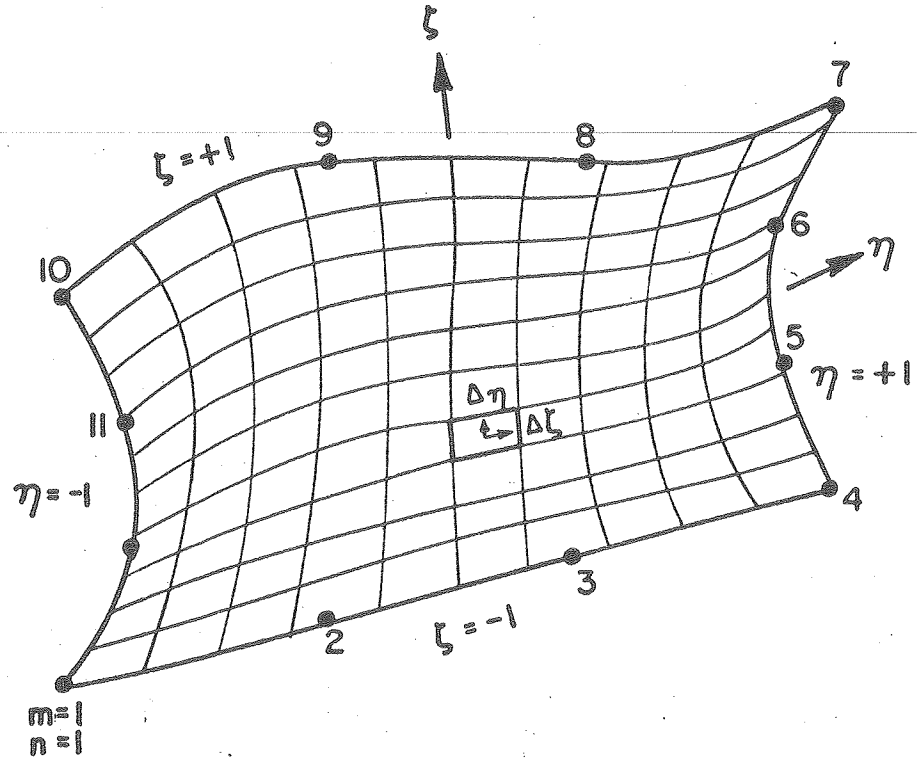

Fig. 18. Scheme for integration over a curved isoparametric element

ordinate functions $\xi(x,y)$ can be suitably transformed with the help of "metric coefficients" (Sokolnikoff and Redheffer, 1966) to a new set of functions $\xi(\eta,\zeta)$ in the new "curvilinear" space in which the isoparameteric quadrilaterals are treated as"squares". In the case of "quadratic" isoparameteric elements, ξ involves the second power of the space variable, η and ζ, while, in the case of "cubic" elements, the third powers of η and ζ are involved.

We will now discuss the consequence of applying the Galerkin equation (III.19) to a single isoparameteric element (secondary element). For convenience, we reproduce (III.19):

$$\sum_{i=I}^{i=V}\left\{-\int_{V_i} A\vec{\nabla}\xi_m \cdot \vec{\nabla}\xi_n u_n \, dV - \int_{V_i} B_i \xi_m \frac{\partial \xi_n u_n}{\partial t} \, dV + \int_{S_i} A\xi_m \vec{\nabla}\xi_n u_n \cdot \vec{n} \, d\sigma\right\} = 0 \qquad \text{(III.19)}$$

We shall apply the first integral in (III.19) to the cubic isoparametric element shown in figure 18.

If we let m = 1 in (III.19), then, by definition, $\xi_m = 1$ at nodal point 1 and $\xi_m = 0$ at all other nodal points. Moreover, ξ_m has non-zero values along the sides, $\eta = -1$ and $\zeta = -1$ (except at the intermediate nodal points on these sides) and ξ_m vanishes along the sides $\eta = +1$ and $\zeta = +1$.

Now, in the system (η,ζ) we can decompose the vector, $\vec{\nabla}\xi_m$ into,

$$\vec{\nabla}\xi_m = \left(\frac{\vec{\partial}\xi_m}{\partial\eta}, \frac{\vec{\partial}\xi_m}{\partial\zeta}\right) \qquad \text{(III.36)}$$

In the light of (III.36) we can rewrite the first integral in (III.19) as,

$$-\int_{V_i} A\vec{\nabla}\xi_m \cdot \vec{\nabla}\xi_n u_n \, dV$$

$$= -\int_{V_i} A\left(\left|\frac{\vec{\partial}\xi_m}{\partial\eta}\right|(\vec{n}_\eta),\ \left|\frac{\vec{\partial}\xi_m}{\partial\zeta}\right|(\vec{n}_\zeta)\right) \cdot \left(\frac{\vec{\partial}\xi_n u_n}{\partial\eta},\ \frac{\vec{\partial}\xi_n u_n}{\partial\zeta}\right)$$

$$= -\int_{V_i} A\left(\left|\frac{\vec{\partial}\xi_m}{\partial\eta}\right|\left(\frac{\vec{\partial}\xi_n u_n}{\partial\eta}\cdot\vec{n}_\eta\right),\ \left|\frac{\vec{\partial}\xi_m}{\partial\zeta}\right|\left(\frac{\vec{\partial}\xi_n u_n}{\partial\zeta}\cdot\vec{n}_\zeta\right)\right)$$

$$= -\int_{V_i} A\left[\left|\frac{\vec{\partial}\xi_m}{\partial\eta}\right|\left(\frac{\vec{\partial}\xi_n u_n}{\partial\eta}\right),\ \left|\frac{\vec{\partial}\xi_m}{\partial\zeta}\right|\left(\frac{\vec{\partial}\xi_n u_n}{\partial\zeta}\right)\right] dV \qquad \text{(III.37)}$$

But, in the (η,ζ) coordinate system, the "volume" of each small "square" equals (figure 18), $dV = \Delta\eta\Delta\zeta$. Using this and replacing $\partial\xi_m$, $\partial\eta$ etc. in (II.37) by $\Delta\xi_m$, $\Delta\eta$ etc., we get,

$$-\int_{V_i} A\vec{\nabla}\xi_m \cdot \vec{\nabla}\xi_n u_n \, dV$$

$$= -\sum_{\substack{\text{all small}\\ \text{squares}}} A\left[\frac{(\Delta\xi_m)_\eta}{\Delta\eta}\left(\frac{\vec{\partial}\xi_n u_n}{\partial\eta}\right),\ \frac{(\Delta\xi_m)_\zeta}{\Delta\zeta}\left(\frac{\vec{\partial}\xi_n u_n}{\partial\zeta}\right)\right]\Delta\eta\Delta\zeta$$

$$= \quad - \sum_{\substack{\text{all small} \\ \text{squares}}} A[(\Delta\xi_m)_\eta (\frac{\partial \vec{\xi}_n u_n}{\partial \eta})\Delta\zeta, (\Delta\xi_m)_\zeta (\frac{\partial \vec{\xi}_n u_n}{\partial \zeta})\Delta\eta \quad] \qquad \text{(III.38)}$$

It can be recognized that in (III.38), the quantities,

$A\ (\frac{\partial \vec{\xi}_n u_n}{\partial \eta})\Delta\zeta$ and $A\ (\frac{\partial \vec{\xi}_n u_n}{\partial \zeta})\Delta\eta$ are respectively, the fluxes along the positive η and ζ directions at the surface of a small square. The implication of (III.38) is that within each square the fluxes directed outward and away from the nodal point m (shown by arrows in figure 18) are evaluated, weighted by the quantities, $(\Delta\xi_m)_\eta$ and $(\Delta\xi_m)_\zeta$ and the resulting quantities are summed up over the entire element. Note that $(\Delta\xi_m)_\eta$ and $(\Delta\xi_m)_\zeta$ are incremental quantities, representing the change of ξ_m in each small square, in the η and the ζ directions. Hence, the process of summation over the entire isoparametric element can be expected to yield a gross weighted value of the flux directed away from the nodal point m. Or, equivalently, we could imagine this gross value as a fraction of the fluxes summed up over the surfaces $\eta = +1$ and $\zeta = +1$, which lie opposite point m. By analogy, for example, in the case of the linear triangle, this fraction turned out to be $1/2$. The exact magnitude of this fraction, however, is difficult to evaluate for an isoparameteric element, because, $\xi(\eta,\zeta)$ is not a simple function.

Let us now consider the second volume integral in (III.19) as applied to the isoparameteric element. In the manner suggested in (III.34), we replace $\frac{\partial \xi_n u_n}{\partial t}$ by the average quantity, $\frac{\partial \bar{u}_m}{\partial t}$ and get,

$$\int_{V_i} B_i \xi_m \frac{\partial \xi_n u_n}{\partial t} dV = B_i \frac{\partial \bar{u}_m}{\partial t} \int_{V_i} \xi_m \, dV \qquad \text{(III.39)}$$

Depending on the special nature of the function, $\int_{V_i} \xi_m \, dV$ could be expected to yield some value less than 1, since $\xi_m \leq 1$ over the isoparametric element. Combining the results of (III.38) and (III.39), we can write for an isoparametric element with an interior nodal point m,

$$- \int_{V_i} A \vec{\nabla} \xi_m \cdot \vec{\nabla} \xi_n u_n \, dV - \int_{V_i} B_i \xi_m \frac{\partial \xi_n u_n}{\partial t} dV$$

$$= - a \sum \begin{matrix} \text{Fluxes across sides} \\ \text{opposite nodal point m} \end{matrix} - b \, D'_m \frac{\partial \bar{u}_m}{\partial t} = 0 \qquad \text{(III.40)}$$

where a and b are some fractions, and D'_m is the capacity of the primary element associated with nodal point m. A comparison of (III.40), (III.35) and (III.34) shows that in all the cases, namely, linear Galerkin, isoparametric Galerkin and the IFD schemes, the final calculational process is the same. That is, in all these cases, a finite subregion is associated with each nodal point of interest. This is done directly in the IFD and by implication in the Galerkin scheme. Then the normal external fluxes across the boundary of the chosen subregion is summed up to arrive at the rate of accumulation of fluid due to the fluxes at the boundary surface. Again, in the IFD, the volume, and hence, the capacity of the chosen subregion

is fixed and known. In the case of the Galerkin scheme, this volume is determined by a process of weighted integration ($\int_{V_i} \xi_m \, dV$). Because the final calculational process is the same in the Galerkin scheme and the IFD scheme and since both methods are known to yield results of comparable accuracy, in choosing a numerical method for solving a particular class of problems, one has to primarily consider the computational conveniences offerred by one or the other method in relation to the class of problems under consideration.

6. Advancing in the time domain

The differences between the Galerkin and the IFD schemes lie principally in handling the spatial discretization, although, as suggested by Zienkiewicz and Parekh (1970), the Galerkin scheme has been extended by some workers to include the time domain. For advancing in the time domain both the schemes make use of the finite difference approach. If we look at (III.34), (III.35) and (III.40), the equations have the general form,

$$-\sum_{\substack{\text{surfaces of}\\ \text{subdomain of}\\ \text{nodal point } m}} \text{Flux along outer normal} = (\text{capacity})_m \frac{\Delta u_m}{\Delta t} \qquad \text{(III.41)}$$

in which, $(\Delta u_m/\Delta t)$ is the unknown quantity sought for.

In (III.41) if we use the initial distribution in potentials to calculate the fluxes, then, all the quantities needed to evaluate the left hand side are known a priori from the initial conditions. On the right hand side, the capacity term is a known quantity and the time interval Δt can be chosen conveniently. Therefore, rewriting (III.41) we have the convenient explicit relation,

$$-\frac{\Delta t}{(\text{capacity})_m} \sum_{\substack{\text{surfaces of} \\ \text{subdomain of} \\ \text{nodal point } m}} \text{Fluxes along outer normal} = \Delta u_m \qquad \text{(III.42)}$$

Once Δu_m is computed according to (III.42), it can be added to the value of u_m at the beginning of the time interval Δt to get,

$$(u_m)_{t+\Delta t} = (u_m)_t + \Delta u_m \qquad \text{(III.43)}$$

The quantity, $(u_m)_{t+\Delta t}$ becomes the initial condition for the next time step in the calculation, in which the whole process of (III.42) is repeated.

An important feature of this explicit relation is that the known initial conditions are assumed to remain fixed throughout the interval Δt. Now, if we have two adjoining subregions communicating with each other, transfer of mass takes place from one subdomain to the other due to the difference in potential prevalent. However, as the mass transfer takes place (assuming there is no interference from other subdomains), the difference in potential decreases and this affects the rate of mass transfer, as the subregions tend towards equilibrium. Therefore, if we make Δt arbitrarily large and assume the persistence of initial conditions throughout the interval as envisaged in (III.42), we would tend to overestimate mass transfer, which normally decreases with time. Indeed, if we make Δt too large, we may compute far too much mass transfer from one subdomain to the other so that the flow direction is reversed in the next time step, whereas, in the real case, the subdomains would tend to equi-

librate with each other, if there is no external interference.

Therefore, the usage of the explicit equation is subject to a limit on the choice of the size of the time interval Δt. Qualitatively, the upper limit of the size of Δt for any subdomain is governed by the time it takes to attain equilibrium with its neighbors, assuming no external interference. If the time interval chosen exceeds this upper limit, the solution for the particular subdomain becomes unstable. Such a physical interpretation of the stability criterion can be found in Dusinberre (1961) and Edwards (1969). Equivalently, the stability of the explicit relation can also be interpreted in a more sophisticated fashion in terms of error growth (O'Brien et al., 1951). The factors that govern the stable time step for a given subdomain are its capacity and the total "conductance" of its bounding surface. Often, the restrictions on the size of the time step may become so severe that the explicit method of solution may become uneconomical to use. Therefore, there is a definite need for methods which would enable the handling of conveniently large time steps. Such methods, which remove the restrictions on the size of the time step are known as "implicit" methods.

We recall that in the case of the explicit scheme, we start with the initial conditions, calculate changes in potential and from this we determine a new set of initial conditions and so, march forward in time. This scheme is therefore called the "forward differencing" scheme. In order to avoid the stability problem associated with the forward differencing scheme, the backward differencing scheme is often used to advantage. In this method (as the name suggests), the direction of marching in time is reversed and one assumes that

the change in potential during a time step, Δu_m, is governed by the fluxes that would arise due to the distribution of potential at the end of the time interval, Δt. Although logically not very appealing, the backward differencing procedure always yields stable results. In actual practice, for improved accuracy and convenience, one could use a combination of forward and backward differencing procedures. For example, if the combination is such that equal weight is given to each of the procedures, the resulting scheme is called the central differencing scheme.

Now, since the backward differencing scheme requires a knowledge of the distribution of potential at the end of the time interval, which, in fact, is the information sought by the solution process, the schemes involving the backward differencing approach generate a set of implicit equations in the unknown time derivatives of the nodal points. These implicit equations are to be solved either as a set of simulatneous equations in the unknown time derivatives or with the help of iterative techniques, using a trial and error approach.

7. Matrix inversion versus iteration techniques

As we have seen in the previous sections, the integral formulations eventually yield a set of mass balance equations, there being one equation for each nodal point in the flow region at which potential is varying with time. This set of equations is to be solved subject to compatibility between adjoining subdomains. In the case of the explicit or forward difference scheme, the compatibility problem does not arise, unless the equations are formulated in the form of (III.33) rather than (III.34). Hence, in the explicit scheme

the required change in potential is computed directly for each nodal point.

In the case of implicit formulations (those formulations involving the backward differencing approach), we are constrained to solve a set of simultaneous equations. To solve the set of simultaneous equation, it is customary to use the matrix-inversion techniques in the finite element method of solution. Such inversion techniques are especially powerful for two dimensional problems. Alternatively, the solution process could be carried out using iteration techniques, in conjunction with accelaration factors for rapid minimization of errors.

8. Choice of a suitable method

As we have seen, the Galerkin scheme (which is now widely used as a basis for developing the finite element equations) and the IFD lead to the computation of the same physical quantities, although by different calculational techniques. In choosing between either of these approaches, therefore, one would have to take into consideration such factors as ease and accuracy of mesh design, ease and generality of programming, computer storage, comprehension of the nature of the calculational model and so on, in relation to the particular class of problems that are required to be solved. Towards this end, we will now discuss some of the special features of the IFD and the finite element techniques.

First, consider the left hand side of the equation of continuity,

$$-\int_V \operatorname{div} \vec{q}\, dV = -\int_S \vec{q} \cdot \vec{n}\, d\sigma = -\int_V \vec{\nabla} \cdot \vec{q}\, dV \qquad \text{(III.44)}$$

The first integral in (III.44) is an invariant expression, independent of any coordinate system. The integrand in the second expression involves only one dimension, provided $\vec{q}$ is measured in the direction of $\vec{n}$ and the quantity $d\sigma$ is known a priori. The integrand in the third integral involves the operator, $\vec{\nabla}$, which represents divergence in the cartesian coordinate system.

The IFD seeks to make use of the second integral in (III.44) (figure 16) by designing lines joining nodal points to be normal to the surfaces in between and by providing geometric quantities such as nodal distances, surface areas and volumes as input information. As a result, the basic calculational process of evaluating fluxes ($\vec{q} \cdot \vec{n}\, d\sigma$) is locally a one-dimensional process, irrespective of whether the overall problem is one-, two- or three-dimensional.

The finite element method, seeking to make use of weighting factors, makes use of the third integral, which is bound to a cartesian coordinate system. Therefore, in the finite element method, in discretizing the flow region, one has to make use of some basic cartesian elemental shape such as a triangle, a square, a quadrilateral, an isoparametric quadrilateral etc., to subdivide the flow region. In those flow regions where mixed symmetries may exist, this aspect of the finite element method may not be a very advantageous feature. On the other hand, the locally one-dimensional IFD can handle mixed symmetries with greater flexibility.

A further consequence of the locally one-dimensional approach is that in the IFD, there is no distinction between one-, two- or three dimensional problems. The method is therefore generally multidimensional.

Normally, the finite element method is used in conjunction with matrix inversion techniques, rather than iterative techniques. In order that the sparse matrix arising out of the finite element equations be properly organized, the nodal points would have to be numbered in a an optimum sequence. The nature of the numbering sequence has a strong influence on the computer storage requirements. In the case of three dimensional problems, even with optimal numbering, the storage requirements can become inconveniently high.

The finite element method is powerful in its ability to handle higher order approximations of the spatial variation of potential and to take into account tensorial quantities such as anisotropy and dispersion. As can be seen from figure 16, in the IFD only gradients normal to surface areas are computed. But, for handling tensorial quantities such as anisotropy, one would have to take into account gradients in directions normal to the normal gradients computed in the IFD. In the finite element method, on the other hand, inasmuch as a surface is constructed for the variation of potential, the gradient in any desired direction can easily be obtained from the surface of potential variation. In the case of the IFD, gradients in directions other than the normals to surfaces would have to be generated by interpolation procedures. In a restricted way, however, this difficulty can be oversome in the IFD by designing the subregions in such way that the normals to the surfaces of the subregions coincide with the principal axes of anisotropy.

The IFD is inherently a first degree approximation scheme, like the finite difference scheme or the "linear" finite element scheme, which uses triangular elements. In the case of flow regions with

large potential gradients, the finite element method could use a coarser mesh and make use of higher order polynomials for the variation of potential, while the IFD would have to rely on finer zoning of subregions.

In the IFD, nodal point distances, surface areas, and volumes are provided as input data. In addition, care should be taken to locate nodal points are surface areas in such a way that the lines joining the nodal points are normal to the surface areas in between. In designing the mesh and in organizing the input data, these tasks may involve additional effort.

An important difference between the IFD and the Galerkin methods involves the manner of marching in the time domain. In the IFD, one can set up equations explicitly or implicitly, for each nodal point. The advantage of an explicit equation is that it is easiest and quickest to compute, whenever it is valid. When the explicit scheme is not valid, however, one would have to make use of the more time-consuming implicit scheme. In a large flow region, where the sizes of subregions may vary and where significant changes of potential are restricted to certain parts, it can so happen that the chosen time steo exceeds the stability limits of only some of the subregions and not the others. In such a situation, the most economic method of solution would be one in which the subregions whose stability limits are exceeded are treated implicitly, while the rest are treated explicitly.

Now, if we look at the form of the Galerkin equation (III.33), it is seen that because of the occurrence of the unknown time derivative of each nodal point in more than one equation, the set of equations

is always to be solved as a set of simultaneous equations. Hence, in this method, it is not possible to make use of an economical combination of explicit - implicit calculations. However, the IFD, or, for that matter, the Galerkin scheme, expressed in the form of (III.34) can accomodate an explicit or an implicit expression and hence can combine the advantages of both.

Finally, the Galerkin method is mostly developed in the literature from mathematical considerations. Mathematically, this scheme is very convenient to set up the matrix of equations. However, in this approach of setting up the equations, the physical phenomena involved in the basic problem are not readily apparent. In the case of the IFD, on the other hand, the model is developed from physical considerations and the physical aspects of the basic problem are always in focus.

Considering the various aspects outlined above,it was decided that the IFD had greater advantages in handling multidimensional, heterogeneous problems envisaged in the present study and hence was chosen as the basic tool of analysis. For implicit calculations, the IFD uses an iterative scheme rather than an inversion scheme. In the next chapter, we shall consider the IFD scheme in detail.

CHAPTER IV

DESCRIPTION OF THE NUMERICAL MODEL

A. INTRODUCTION

Perhaps the earliest to develop the Integrated Finite Difference (IFD) scheme was MacNeal (1953). Concerned with the solution of partial differential equations by means of electrical networks, he developed the method, which he termed, "an asymmetrical finite difference network", for solving second order boundary value problems. He found that the method enabled easy fitting of the mesh grid to a curved boundary and provided an efficient method of varying the mesh-size within the flow region. Subsequently, the method appears to have been used with success by workers in the field of heat transfer and a clear physical development can be found in Dusinberre (1961). Edwards (1969) essentially used the same approach and extended the method to transient as well as steady state diffusion problems in one- two- or three dimensions. The result of Edwards' efforts was the development of a sophisticated computer program called TRUMP which solves a general non-linear parabolic differential equation describing flow in various kinds of potential fields such as fields of temperature, pressure and electricity and magnetism.

The basic calculational model used in the present thesis is the same as that of TRUMP. However, TRUMP was extensively modified to include effects of gravity, stress-strain relationships of the porous medium and effects of hysteresis, so that problems of saturated-unsaturated groundwater flow could be handled. The resulting

computer program has been named TRUST, partly to indicate its development from TRUMP and partly as a mnemonic for Transient flow in Unsaturated and Strained porous media.

B. NUMERICAL FORMULATION

Consider the governing equation for transient groundwater flow:

$$\int_S \rho \frac{k\rho g}{\mu} \vec{\nabla}(z + \psi) \cdot \vec{n} \, d\sigma + G = M_c \frac{\partial \psi}{\partial t} \qquad \text{(IV.1)}$$

In (IV.1), a volume element is enclosed by the surface S and is fixed in the solid phase of the porous medium.

To solve (IV.1) numerically, we first discretize the flow region into a finite number of subregions. Each subregion has a specified volume and a specified surface area between it and contiguous subregions. We then assume that the surface integrated terms on the left hand side of (IV.1) are constant over each of the surface subsections. In particular, the quantity $\vec{\nabla}(z + \psi) \cdot \vec{n}$ must be reasonably constant along the surface $d\sigma$. Also, by definition, M_c and G represent average values for each subregion and hence, are known.

Consider then a subregion "n" and the contiguous subregions "m" as shown in figure 19. Equation (IV.1) applied over the subregion "n" can be written in difference form as,

$$\sum_m \rho_{n,m} \left(\frac{k\rho g}{\mu}\right)_{n,m} \vec{\nabla}(z + \psi)_{n,m} \cdot \vec{n} \, \sigma_{n,m} + G_n = (M_c)_n \frac{\Delta \psi_n}{\Delta t} \qquad \text{(IV.2)}$$

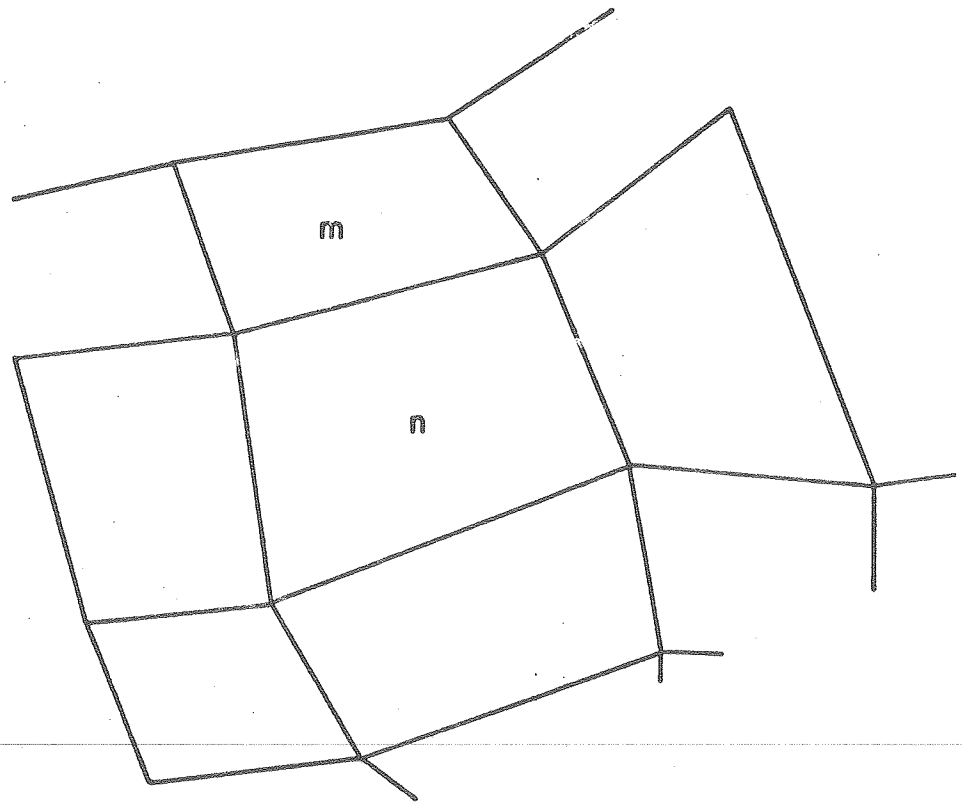

Fig. 19. Network of subregions

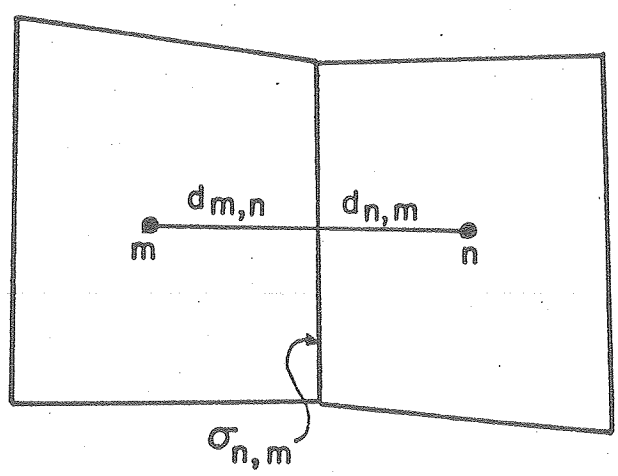

Fig. 20. Nodal points within subregions

To evaluate the coefficients, $\rho_{n,m}$ and $\left(\frac{k\rho g}{\mu}\right)_{n,m}$ we assume that the average values of ρ_n, $\left(\frac{k\rho g}{\mu}\right)_n$, ρ_m and $\left(\frac{k\rho g}{\mu}\right)_m$ apply specifically at a particular nodal point in the subregions n and m. We further assume that the subregions are so designed and the nodal points so located that the line joining the nodal points is normal to the surface in between. Consider now two adjoining subregions as in figure 20. The gradient term can now be approximated as,

$$\vec{\nabla}(z + \psi)_{n,m} \cdot \vec{n} \simeq \frac{(z_m - z_n) + (\psi_m - \psi_n)}{d_{n,m} + d_{m,n}} \qquad \text{(IV.3)}$$

To evaluate the coefficient $\left(\frac{k\rho g}{\mu}\right)_{n,m}$ we need to recognize that $\left(\frac{k\rho g}{\mu}\right)\vec{\nabla}(z + \psi) \cdot \vec{n}$ represents the flux at the interface. If there is a change in the value of $(k\rho g/\mu)$ from one subregion to another (heterogeneity), we must preserve the continuity of flux as well as potential at the interface. Designating flux by $\vec{q}$, we require,

$$\vec{q}_{n,m} = \vec{q}_{m,n} \qquad \text{(IV.4)}$$

where, $\vec{q}_{n,m}$ is the flux on the right hand side of the interface in figure 20

and $\vec{q}_{m,n}$ is the flux on the left hand side

We also require the continuity of potential $(z + \psi)_{n,m}$ at the interface $\sigma_{n,m}$.

Thus,

$$\vec{q}_{m,n} = \left(\frac{k\rho g}{\mu}\right)_m \frac{[\,(z+\psi)_m - (z+\psi)_{n,m}\,]}{d_{m,n}} \qquad \text{(IV.5)}$$

$$\text{and} \quad \vec{q}_{n,m} = \left(\frac{k\rho g}{\mu}\right)_n \frac{[(z+\psi)_{n,m} - (z+\psi)_n]}{d_{n,m}} \tag{IV.6}$$

Now, assuming a linear variation in potential between nodal points n and m we can define an effective mean value of $\left(\frac{k\rho g}{\mu}\right)_{n,m}$ such that,

$$\vec{q}_{m,n} = \vec{q}_{n,m} = \left(\frac{k\rho g}{\mu}\right)_{n,m} \frac{[(z+\psi)_m - (z+\psi)_n]}{d_{m,n} + d_{n,m}} \tag{IV.7}$$

Using (IV.7) it can be demonstrated that ,

$$\left(\frac{k\rho g}{\mu}\right)_{n,m} = \frac{[d_{m,n} + d_{n,m}]}{\dfrac{d_{m,n}}{(k\rho g/\mu)_m} + \dfrac{d_{n,m}}{(k\rho g/\mu)_n}} \tag{IV.8}$$

The quantity, $\rho_{n,m}$ in (IV.2) represents the mass density of the fluid crossing the interface $\sigma_{n,m}$. For evaluating this, we use the relation,

$$\rho_{n,m} = \frac{\rho_n \rho_m (d_{m,n} + d_{n,m})}{\rho_n d_{m,n} + \rho_m d_{n,m}} \tag{IV.9}$$

Substituting (IV.3), (IV.8), and (IV.9) into (IV.2), we get,

$$\frac{\Delta t}{(M_c)_n}\left\{\sum_m \frac{\rho_n \rho_m (d_{m,n} + d_{n,m})}{\rho_n d_{m,n} + \rho_m d_{n,m}} \times \frac{\sigma_{n,m}[(z+\psi)_m - (z+\psi)_n]}{\dfrac{d_{m,n}}{(k\rho g/\mu)_m} + \dfrac{d_{n,m}}{(k\rho g/\mu)_n}} + G_n\right\}$$

$$= \Delta\psi_n \tag{IV.10}$$

We now define a new quantity,

$$U_{n,m} = \frac{\rho_n \rho_m (d_{n,m} + d_{m,m})}{\rho_n d_{m,n} + \rho_m d_{n,m}} \times \frac{\sigma_{n,m}}{\dfrac{d_{m,n}}{(k\rho g/\mu)_m} + \dfrac{d_{n,m}}{(k\rho g/\mu)_n}} \qquad \text{(IV.11)}$$

$U_{n,m}$ can be conveniently termed the "surface conductance" of the interface between subregions n and m. Physically, $U_{n,m}$ represents the mass flux across the surface $\sigma_{n,m}$ for a unit difference in potential, $(z + \psi)$, between nodal points n and m. It will be shown later that the notion of surface conductance is very convenient in interpreting the transient flow phenomenon.

The interface $\sigma_{n,m}$ may be located entirely within the continuum or may form part of its external boundary. Since boundary conditions require special treatment, it is advisible to rewrite (IV.10), duly separating the interior and the exterior surface connections. Thus,

$$\frac{\Delta t}{(M_c)_n} \left\{ G_n + \sum_m U_{n,m}[(z+\psi)_m - (z+\psi)_n] + \sum_b U_{n,b}\,[(z+\psi)_b - (z+\psi)_n] \right\} = \Delta\psi_n \qquad \text{(IV.12)}$$

where the subscripts m and b denote, respectively, interior and exterior (boundary) nodes connected to node n. The quantities $U_{n,m}$ and $U_{n,b}$ respectively denote the conductances across interior and exterior surfaces.

1. Explicit and Implicit schemes

If, on the left hand side of (IV.12) we assume the z's to be constants, set $\psi_m = \psi_{m,t_o}$, $\psi_n = \psi_{n,t_o}$, $\psi_b = \bar{\psi}_b$, where $\bar{\psi}_b$ represents an average value for the boundary node in the interval Δt and the subscript t_o denotes the time at the start of the interval Δt, then, all the quantities on the left hand side are known and the only unknown to be determined is the change in pressure head, $\Delta\psi_n$, occurring on the right hand side. This simple scheme is known as the explicit or the forward differencing scheme.

As discussed in the last chapter, the explicit scheme would yield unstable results for a subregion if Δt exceeds some critical value for the subregion. In order to be able to use conveniently large values of Δt so that rapid advancement in the time domain may be possible, one would have to use implicit relations instead of the explicit relation mentioned above. In the implicit method of solution, ψ_m , ψ_n and ψ_b are substituted in the left hand side of (IV.12) by

$$\psi_m = \psi_{m,t_o} + \lambda\Delta\psi_m$$

$$\psi_n = \psi_{n,t_o} + \lambda\Delta\psi_n \qquad \text{(IV.13)}$$

$$\psi_b = \psi_{b,t_o} + \lambda\Delta\psi_b$$

where, λ is a parameter from 0.5 to 1. Substitution of (IV.13) into (IV.12) would result in the occurrence of the unknown quantity, $\Delta\psi_m$ on both sides of the equation and hence the solution has to be

obtained by implicit methods.

2. Explicit scheme and stability

For every subregion there exists a critical size of time interval, which, when exceeded by Δt, would render the explicit equation unstable for that subregion. This critical size of time interval can be conveniently termed the stability limit or the time constant for the particular subregion. The size of the time constant is a function of fluid mass capacity of the subregion as well as its surface conductances. We will now examine the method by which the time constant could be evaluated for a subregion. We will follow the methods of approach developed by O'Brien et al (1951) and Evans et al. (1954).

O'Brien et al. analyze the stability of the explicit solution in terms of propagation of errors. If Δ is the exact solution to the partial difference equation and N is its numerical solution, then, the conditions under which $(\Delta - N)$ remains small throughout the region of integration is the problem of stability. The von Neumann method of stability analysis followed by O'Brien et al. consists in making a Fourier expansion of a line of errors and follow the progress of the general term of expansion. Consider the simple one-dimensional problem involving a uniform mesh spacing Δx involving the difference equation,

$$\frac{\psi_j^{k+1} - \psi_j^k}{\Delta t} = \frac{K}{m_c} \left[\frac{\psi_{j-1}^k - 2\psi_j^k + \psi_{j+1}^k}{(\Delta x)^2} \right] \qquad \text{(IV.14)}$$

where, k and $k+1$ denote two succesive time steps, j is the j-th mesh point and m_c is the fluid mass capacity per unit volume.

Suppose at time $t = 0$, there was an error distribution,

$$E(x) = \sum_n A_n \exp(i\beta_n x) \qquad \text{(IV.15)}$$

Substituting this expression into the difference equation and analyzing the resulting equations, it has been shown by O'Brien et al.(1951) that the difference scheme is stable only if

$$\frac{K}{m_c} \frac{\Delta t}{(\Delta x)^2} \leq \frac{1}{2} \qquad \text{(IV.16)}$$

As suggested by Evans et. al (1954), the above instability analysis can be extended to three dimensions by writing the Fourier expansion of $E(x,y,z)$ in the form,

$$E(x,y,z) = \sum_n A_n \exp(i[\beta_n x + \gamma_n y + \varepsilon_n z]) \qquad \text{(IV.17)}$$

Using (IV.17) and the approach of O'Brien et al. it can be shown that in three dimensions, the stability condition is provided by,

$$\frac{K}{m_c} \Delta t \left[\frac{1}{(\Delta x)^2} + \frac{1}{(\Delta y)^2} + \frac{1}{(\Delta z)^2} \right] \leq \frac{1}{2} \qquad \text{(IV.18)}$$

Or,

$$\frac{K}{m_c} \Delta t \left[\frac{(\Delta y \Delta z)^2 + (\Delta x \Delta z)^2 + (\Delta x \Delta y)^2}{(\Delta x \Delta y \Delta z)(\Delta x \Delta y \Delta z)} \right] \leq \frac{1}{2} \qquad \text{(IV.19)}$$

Noting that $(\Delta x \Delta y \Delta z) = V$ of a fundamental volume element

and that $(V)(m_c) = M_c$, fluid mass capacity of a volume element, (IV.19) becomes,

$$\frac{\Delta t}{M_c} \; 2K \left[\frac{\Delta y \Delta z}{\Delta x} + \frac{\Delta x \Delta z}{\Delta y} + \frac{\Delta x \Delta y}{\Delta z} \right] \leq 1 \qquad \text{(IV.20)}$$

Or,

$$\Delta t \leq \frac{M_c}{2K \left[\frac{\Delta y \Delta z}{\Delta x} + \frac{\Delta z \Delta x}{\Delta y} + \frac{\Delta x \Delta y}{\Delta z} \right]} \qquad \text{(IV.21)}$$

An examination of the terms in square brackets in (IV.21) shows that the numerator of each addend represents surface areas of the volume element, the denominator, nodal distances and that the denominator in (IV.21) is in fact the the sum of the interface conductances of the six faces of a fundamental three dimensional block. Thus, (IV.21) could be expressed as,

$$(\Delta t)_n \leq \frac{\text{Fluid mass capacity of volume element } n}{\Sigma \text{ Interface conductance of all its bounding surfaces}} \qquad \text{(IV.22)}$$

in which $(\Delta t)_n$ is the stability limit or the time constant of the element n. Whereas the earlier mentioned conditions (IV.18) were mathematical expressions, (IV.22) has the advantage of possessing the following physical interpretation. Suppose a subregion n is connected to its immediate neighbors, m. Suppose further that the difference in potential, ϕ, between n and each m equals unity. Then, the implication of (IV.22) is that $(\Delta t)_n$ represents the time required by nodal point n to attain equilibrium with its neighbors

on the basis of the explicit scheme.

There are other ways to formulate the stability criterion as well. Dusinberre (1961) shows in a simple way that if the stability criterion (IV.22) is violated, certain coefficients in the equation may attain absurd negative values.

3. Implicit method of solution

The constraint imposed by (IV.22) is in respect of the forward differencing procedure, in which the information pertaining to a later instant of time, t_{k+1}, is determined solely from the known information for an earlier instant of time, t_k. One way to avoid this constraint, so that Δt could be chosen conveniently large is to reverse the direction of progress in time and represent that the potential at an earlier instant of time is determined by those at a later instant of time and thus replace (IV.14) by,

$$\frac{\psi_j^{k+1} - \psi_j^k}{\Delta t} = \frac{\psi_{j-1}^{k+1} - 2\psi_j^{k+1} + \psi_{j+1}^{k+1}}{(\Delta x)^2} \qquad \text{(IV.23)}$$

It has been shown that (IV.23) is unconditionally stable for all Δt (O'Brien et. al, 1951; Evans et. al, 1954) and (IV.23) is often known as the backward differencing scheme.

It was found early (Hartree et al., 1937 ; Crank and Nicholson , 1948), that to combine accuracy as well as stability, one could combine both the forward and the backward differencing procedures in the same difference equation. In order to investigate the possible restrictions on their combination, let us write,

$$\frac{\psi_j^{k+1} - \psi_j^k}{\Delta t} =$$

$$= \frac{K}{m_c} \left[\lambda \left(\frac{\psi_{j-1}^{k+1} - 2\psi_j^{k+1} + \psi_{j+1}^{k+1}}{(\Delta x)^2} \right) \right.$$

$$\left. + (1 - \lambda) \left(\frac{\psi_{j-1}^{k} - 2\psi_j^{k} + \psi_{j+1}^{k}}{(\Delta x)^2} \right) \right] \quad \text{(IV.24)}$$

Note that in (IV.24), λ is the weight given to the backward differencing procedure and $(1 - \lambda)$ is the weight given to the forward differencing procedure.

It has been shown by Evans et al. (1954) that (IV.24) will be unconditionally stable only if $\lambda \geq \frac{1}{2}$. A physical interpretation of (IV.24) is that in calculating the divergence of $\vec{q}$, instead of considering the continuous variation of potential gradient during the interval Δt, we consider the gradient field prevalent at an appropriate average instant of time, $t_o + \lambda(\Delta t)$, and assume for purposes of calculation that this gradient field remains stationary throughout the time interval. Note that in (IV.24), $\lambda = 0$ and $\lambda = 1$ give rise, respectively, to the forward and the backward differencing schemes; the case, $\lambda = \frac{1}{2}$ gives rise to the so called central-differencing or the Crank-Nicholson scheme.

Equation (IV.24) is an implicit equation and has to be solved either by matrix-inversion techniques or by iterative techniques. Since matrix-inversion techniques may become inconvenient when we

have to deal with a large number of mesh points, we will choose to use an iterative technique.

Furthermore, since the restriction imposed by (IV.22) on stability applies independently to each subregion, it is possible that in a given flow region, a chosen time step Δt may exceed the time constants for some subregions but not the others. In order to combine the simplicity of the explicit scheme and the economy of the implicit scheme, therefore, it would be advantageous to have a scheme which would employ the explicit method for all those subregions for which the time step is less than the time constant and use the implicit method for all those subregions for which the time interval exceeds the time constant, and, of course, suitably treating the special case when explicit and implicit subregions adjoin each other.

In the following discussion, a "regular" node will denote a node for which calculations are made explicitly, while a "special" node is one for which calculations are to be made implicitly.

First, we consider a regular node. For convenience, we make the substitution, $\phi = (z + \psi)$ and apply (IV.12) to a regular node. We also note that if z is constant during a time step, then, $\partial\psi/\partial t = \partial(z+\psi)/\partial t = \partial\phi/\partial t$ and so, for a regular node n, (IV.12) becomes,

$$\Delta\phi_{n,Reg} = \frac{\Delta t}{(M_c)_n} \left[\sum_b U_{n,b} (\bar{\phi}_b - \phi_{n,t_o}) + \sum_m U_{n,m} (\phi_{m,t_o} - \phi_{n,t_o}) \right] \tag{IV.25}$$

in which, b denotes a boundary node interacting with node n,

while m denotes all other internal nodes (regular and special). $\bar{\phi}_b$ representes the mean, prescribed boundary value during the time interval and t_o denotes the time at the start of the time interval, Δt. Similarly, applying (IV.12) to a special node, we get,

$$\Delta\phi_{n,spec} = \frac{\Delta t}{(M_c)_n} \Big[\sum_b U_{n,b} \left(\bar{\phi}_b - [\phi_{n,t_o} + \lambda\Delta\phi_{n,spec}] \right)$$

$$+ \sum_m^{spec} \left([\phi_{m,t_o} + \lambda\Delta\phi_{m,spec}] - [\phi_{n,t_o} + \lambda\Delta\phi_{n,spec}] \right)$$

$$+ \sum_m^{reg} \left([\phi_{m,t_o} + \lambda\Delta\phi_{m,reg}] - [\phi_{n,t_o} + \lambda\Delta\phi_{n,spec}] \right) \Big]$$

(IV.26)

By collecting similar terms and rearranging, we can split up $\Delta\phi_{n,spec}$ into a regular or explicit component, $\Delta\phi_{n,reg}$ and a set of terms for the implicit component. Thus,

$$\Delta\phi_{n,spec} = \Delta\phi_{n,reg} + \frac{\lambda\Delta t}{(M_c)_n} \Big[\Delta\phi_{n,spec} \left(- \sum_b U_{n,b} - \sum_m^{all} U_{n,m} \right)$$

$$+ \sum_m^{spec} U_{n,m} \, \Delta\phi_{m,spec} + \sum_m^{reg} U_{n,m} \, \Delta\phi_{m,reg} \Big]$$

(IV.27)

Finally, collecting all terms involving $\Delta\phi_{n,spec}$ to one side, we get,

$$\Delta\phi_{n,spec} = \frac{\Delta\phi_{n,reg} + \frac{\lambda\Delta t}{(M_c)_n}\left[\sum_m^{spec} U_{n,m}\,\Delta\phi_{m,spec} + \sum_m^{reg} U_{n,m}\,\Delta\phi_{m,reg}\right]}{\left(1 + \frac{\lambda\Delta t}{(M_c)_n} Z_n\right)} \tag{IV.28}$$

where, $Z_n = \sum_b U_{n,b} + \sum_m^{all} U_{n,m}$ is the total surface conductance of node n and $\lambda > \frac{1}{2}$.

Note that on the right hand side of (IV.28) all terms are known except $\Delta\phi_{m,spec}$, that is, the change in potentials in other special nodes connected to the special node n. Equation (IV.28) is therefore to be solved by an iterative procedure.

The iterative procedure used in the present numerical model (TRUST) is the same as that developed by Edwards (1969) for the computer program TRUMP. This procedure was adapted and generalized from the one formulated by Evans et al. (1954). Without going into details, the main feature of this procedure can be described as follows.

Suppose we know $\Delta\phi^p_{m,spec}$, where p denotes the p-th iteration and m denotes nodes connected to node n. Can we determine $\Delta\phi^{p+1}_{n,spec}$ purely as a function of $\Delta\phi^p_{m,spec}$ and $\Delta\phi^p_{n,spec}$? The analysis of Evans et al. (1954) indicates that this type of iterative procedure may become unstable under certain conditions. However, unconditional stability could be obtained if $\Delta\phi^{p+1}_n$ is determined as

a function of $\Delta\phi^{p}_{m,spec}$ and suitably weighted values of $\Delta\phi^{p}_{n,spec}$ and $\Delta\phi^{p+1}_{n,spec}$.

Thus,

$$\Delta\phi^{p+1}_{n,spec} = F\left[\Delta\phi^{p}_{m,spec}, ((1+\gamma)\Delta\phi^{p+1}_{n,spec} - \gamma\Delta\phi^{p}_{n,spec})\right] \tag{IV.29}$$

Again, Evans et al. have showed that the iteration scheme will be stable for $\gamma > 0$. Figure 21 is a diagrammatic representation of the points that enter into the computation of $\Delta\phi^{p+1}_{n,spec}$.

To formulate the iterative procedure, we use (IV.27) and make the following substitutions:

$$\Delta\phi_{n,spec}\text{, left hand side} = \Delta\phi^{p+1}_{n,spec}$$

$$\Delta\phi_{n,spec}\text{, right hand side} = (1+\gamma)\Delta\phi^{p+1}_{n,spec} - \gamma\Delta\phi^{p}_{n,spec}$$

$$\Delta\phi_{m,spec}\text{, right hand side} = \Delta\phi^{p}_{m,spec} \tag{IV.30}$$

Substituting (IV.30) into (IV.27), rearranging and collecting similar terms, we get the final expression for the (p+1) iteration,

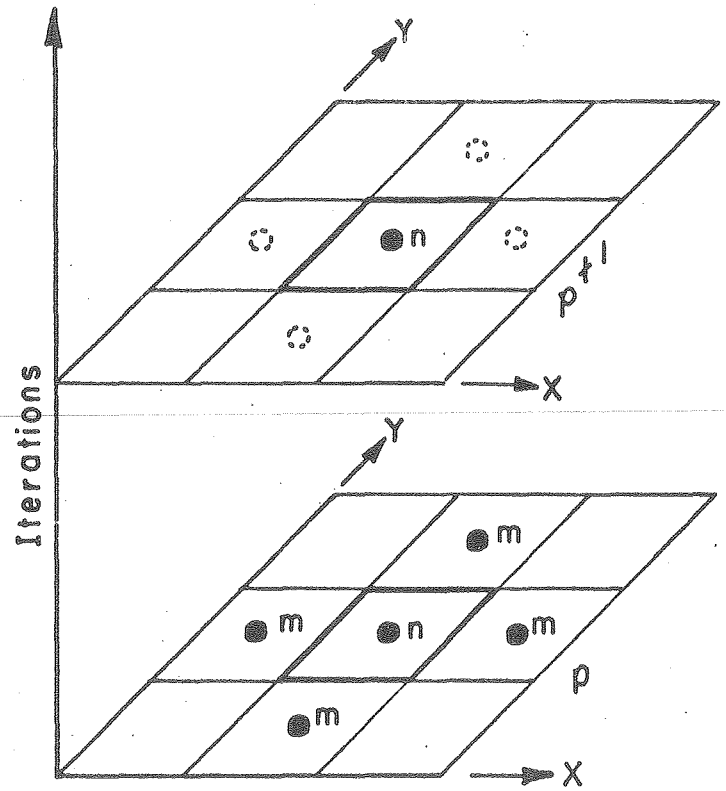

Fig. 21. Points that govern the calculation of $\Delta\phi_n^{p+1}$

$$\Delta\phi^{p+1}_{n,spec} = \frac{\Delta\phi_{n,reg} + \frac{\lambda\Delta t}{(M_c)_n}\left[\sum_m^{spec} U_{n,m}\,\Delta\phi^p_{m,spec} + \sum_m^{reg} U_{n,m}\Delta\phi_{m,reg} + Z_n\Delta\phi^p_{m,spec}\right]}{\left(1 + \frac{\lambda\Delta t}{(M_c)_n}(1+\gamma)Z_n\right)} \qquad \text{(IV.31)}$$

In order to start the iterative procedure, that is when $p = 0$, one would need to have the values of $\Delta\phi^0_{m,spec}$ and $\Delta\phi^0_{n,spec}$. An efficient way of handling this need is to estimate these values based on the past time histories at the respective nodal points.

Let the difference in the value of $\Delta\phi_{n,spec}$ between successive iterations be given by,

$$E^{p+1}_n = \Delta\phi^{p+1}_{n,spec} - \Delta\phi^p_{n,spec} \qquad \text{(IV.32)}$$

By substituting for $\Delta\phi^{p+1}_{n,spec}$ and $\Delta\phi^p_{n,spec}$ in (IV.31), we can show that ,

$$E^{p+1}_n = \frac{\sum_m^{spec} U_{n,m}\,E^p_m + \gamma Z_n\,E^p_n}{\frac{(M_c)_n}{\lambda\Delta t} + (1+\gamma)Z_n} \qquad \text{(IV.33)}$$

For the first iteration, $p = 1$, we compute $\Delta\phi^1_{n,spec}$ and E^1_n using (IV.31). Thereafter, for each iteration, we compute E^{p+1}_n using

(IV.33) and then calculate $\Delta\phi^{p+1}_{n,spec}$ by the relation,

$$\Delta\phi^{p+1}_{n,spec} = E^{p+1}_{n} + \Delta\phi^{p}_{n,spec} \qquad \text{(IV.34)}$$

The iterations are stopped whenever the maximum absolute value of E_n for any node in the region is less than a preassigned tolerance value. In the present model, the tolerance is set up in such a way that the iteration process is discontinued whenever $|E^p_n|_{max}$ is less than 10^{-4} times the maximum change in potential in the flow region allowed for each time step.

The iteration scheme is unconditionally stable, provided the coefficients in the equation are not strongly dependent on potential or on time. Convergence is generally rapid, the number of iterations being dependent on the relative number and time constants of the interconnected special nodes in the system, the relative values of conductances between such nodes and the error tolerance which is used in the convergence test.

4. The parameters λ and γ

For unconditional stability, the parameter λ should be greater than or equal to 0.5. A value of 0.5 would in fact result in the central-differencing scheme. In the present model, λ varies between 0.57 and 1, although, if desired it can be set fixed at 0, 0.5 or 1. The actual value of λ to be used in any particular time step depends on the overall behavior of the potential variation in the system. Thus, if the maximum change in potential between successive time steps does not change much, then, λ is set close to 0.57

for improved accuracy. However if the maximum time-rate of change of potential increases with time, or when steady-state is being reached necessitating large time steps, λ is shifted closer to 1 so that stability can be assured.

The acceleration parameter γ which enters into the iteration procedure, has been chosen to be 0.2. Edwards (1969) arrived at this value after studying a large number of typical problems. He found that in some problems, $\gamma = 0$ gave rise to oscillations, while, in general, $\gamma > 0.2$ gave slower rates of convergence.

5. Evaluation of non-linear coefficients

In the governing equation, (IV.2), the coefficients, ρ, k and M_c vary with the dependent variable and hence, (IV.2) is a non-linear equation. In addition, the source function, G_n and the prescribed boundary conditions may also vary with time. As a result, these parameters vary continuously during the time interval. To take this into account, we substitute in (IV.2) average values of ρ_{avg}, k_{avg} and $(M_c)_{avg}$ evaluated at a mean value of $\bar{\psi}$ for the time step. In a similar way, the source term and the boundary conditions are evaluated at an average instant of time $\bar{t}$ over the interval Δt. These mean values are evaluated with the help of λ as follows:

$$\bar{\psi} = \psi_o + \lambda \Delta t \dot{\psi}$$

$$\bar{t} = t_o + \lambda \Delta t \qquad \text{(IV.35)}$$

where $\dot{\psi}$ is a judicious estimate of the time derivative of ψ (Edwards, 1969).

6. Boundary Conditions

In general, two types of boundary conditions are encountered in potential-field problems. These are: a) prescribed potential boundary and b) prescribed flux boundary. In addition, the physics of unsaturated groundwater flow is such that the treatment of special boundary conditions are also required. Such special conditions arise in the consideration of seepage faces, evaporation and evapo-transpiration boundaries.

a. Prescribed flux and prescribed potential boundaries

In the present numerical model, fluid transfer takes place between the system and its surroundings through external fluid flow connections between a surface node and an external potential (Edwards,1969). In the following discussions, a node indicates a subregion with finite volume. For convenience, the external potential is called a boundary node. A prescribed variation of potential on the surface of the flow region may be obtained by using a very large surface conductance between the surface node and the boundary node with the prescribed variation in potential. Or, when the surface potential is either constant or changes linearly or exponentially with time, the surface node could be connected with a large interface conductance to a regular node with a large fluid mass capacity having the prescribed variation in potential.

A prescribed variation of surface fluid flux with time may be obtained by use of a very small surface conductance connecting the surface node to a boundary node with very large potential and by tabulating surface conductance with time so that the product of the

boundary potential and the surface conductance is equal to the desired flux rate across the surface. Alternatively, a thin surface node with prescribed flux generation rate could be used to provide the desired fluid input at the surface. Surface nodes should be either zero-lume nodes or very thin nodes or should have their representative nodal points at the external surface.

b. Seepage face

In saturated-unsaturated flow problems, the seepage face needs special attention. The seepage face is characterized by two features: (i) the potential at the seepage face equals z, since, at the seepage face, pressure head is atmospheric and $\psi = 0$, and (ii) the fluid can only pass through the seepage face from the flow region to the surroundings and not vice versa. At every stage of the calculations therefore, a check has to be made that should the potential just inside the flow region fall below some critical value due to the development of suction ($\psi < 0$), the seepage face is recognized as an impermeable boundary, in order to prevent fluxes from entering the flow region (See also Neuman, 1972).

Evaporation and Evapo-transpiration boundaries

In dealing with the interaction between the soil and the atmosphere one has to take into account the evaporative and evapo-transpirative transfer of water across the boundary of the soil surface. Neuman et al. (in press) have suggested a method of handling this type of boundary conditions. The amounts of moisture which the atmosphere can take in from the soil by evaporation and evapo-transpi-

ration from plants are called, respectively, potential evaporation (E_s^*) and potential evapotranspiration. These quantities can be determined with the help of appropriate micrometeorological data.

The nature of the soil-atmosphere boundary is such that the sum ($E_s^* + E_{pl}^*$) determines an upper bound for the flux that can cross a given section of the boundary. In addition, there also exist lower limits for the pressure heads that can develop at the dry soil surface (ψ_L) and the minimum pressure heads that can develop in the roots (ψ_w). ψ_w is physically the wilting pressure head for the plants. It is assumed that ψ_L and ψ_w can be determined from micrometeorological and agronomical data.

The soil-atmosphere boundary is therefore neither a prescribed potential boundary nor a prescribed flux boundary, but is one on which an upper bound for the flux and a lower bound for the surface potential are prescribed. The problem is therefore one of maximization in which one seeks to determine, by an iterative procedure, $\psi_L \leq \psi_{surface}$ and $\psi_w \leq \psi_r$ (where ψ_r is the pressure head in the root) such that the flux across the soil surface into the atmosphere is less than ($E_s^* + E_{pl}^*$). When the atmospheric demands exceed the ability of the soil to transmit, the boundary condition reduces to a prescribed potential boundary with $\psi_{surface} = \psi_L$ and $\psi_r = \psi_w$.

An infiltration boundary is the reverse of an evaporation boundary. If the rate of addition of water at the surface exceeds the ability of the soil to transmit water, as determined by its saturated permeability, then, part of the surface addition must be lost as run off.

The evaporation-evapotranspiration boundaries have not been

incorporated into the numerical model used in the present study. However, the calculational model can accomodate these conditions, in principle.

7. Control of accuracy

The accuracy of the numerical model is affected by six principal types of errors (Edwards, 1969). These are: i) modeling errors, ii) spatial truncation errors, iii) time truncation errors, iv) potential truncation errors, v) convergence errors and vi) arithmetic truncation errors.

i) Modeling errors: These arise from the use of inaccurate material properties, inaccurate initial and boundary conditions, other approximations used in modeling the real system and interpolation errors in evaluating the non-linear coefficients. Modeling errors can be estimated by comparing the results of using different models of the same system. Available material properties and boundary conditions are seldom accurate to more than two or three significant figures. Therefore, it would not be worthwhile to attempt to reduce spatial and time truncation errors much below modeling errors.

In discussing modeling errors, it is worthwhile to consider the role of mesh design. It will be recalled that in the present numerical model, the transfer of fluid across a surface between two adjoining regions is governed by the interface conductance, U. From (IV.11) it can be seen that U is a function of the surface area, σ, and the distances to the surface from the representative nodal points on either side. For improved accuracy, care should be taken to suitably select the location of the nodal points and the interconnecting surface

areas. In one-dimensional problems, surface conductances will be accurately described if all node interfaces are perpendicular to the direction of flow. In two- and three-dimensional systems, surface conductances will be accurately described only if all the node interfaces are perpendicular to the lines joining the two nodal points and intersect it at an appropriate mean position (arithmetic mean of non-divergent coordinates, log mean of cylindrical radius and geometric mean of spherical radius. This may be difficult to achieve but is an ideal to approximated as closely as possible.

An assumption made in calculating surface fluxes is that darcy velocity is constant over a given surface. This condition is best satisfied when the surface in question coincides with an isopotential line. It will be therefore advisible to design the mesh so as to conform to the expected pattern of potential distribution. Since, in transient problems the flow field changes in time, the best that could be done is to conform the mesh to the expected flow pattern as closely as possible.

ii) Spatial truncation errors: These arise from the subdivision of the system into discrete volume elements or nodes for which average values of spatially dependent variables must be estimated and for which inaccuracies in volumes, areas and distances may arise. These errors may be controlled by subdividing the system fine enough so that the nonlinear potential distributions are fitted within required accuracy by linear interpolation between the nodal points of the nodes and the variation of the non-linear properties over the volume of each node is within required limits of the average values determined for the nodal point. This may be difficult to estimate in

advance but is simple to determine after a calculation has been made. Often, a simplified version of the problem may be calculated first to help in estimating the degree of subdivision required in different parts of the system.

iii) Time truncation errors: These arise due to the use of discrete time steps for which average values of time-dependent variables must be estimated. These errors could be controlled indirectly by keeping the magnitude of timesteps within fixed, optimum limits, based on the maximum potential change that can occur within the system during a given timestep. Time steps could also be controlled so that the variation in nonlinear parameters do not vary by more than a small magnitude during a given time step.

iv) Potential truncation errors: These arise from the discrete potential changes that occur in each node at each time step, for which average values of the non-linear parameters must be estimated. These errors could be controlled by specifying a limit on the maximum change in potential that can occur any where in the flow region during a time step. Reasonable accuracy can be assured if maximum change in potential during any time step is restricted to 0.1% to 1% of the greatest potential change expected any where within the system or such that no more than 1% change occurs in a non-linear property during a time step.

v) Convergence errors: These arise from the use of an iterative method of solving the governing difference equations for connected special nodes, with arbitrary convergence criteria. The iterative procedure is stopped when the maximum difference in change in potential between two successive iterations is less than 10^{-4} times the limit on the maximum change in potential permitted for a time step.

The iterative procedure may fail to converge or may converge very slowly if the system is too finely subdivided relative to the required accuracy in space and time. Convergence may also fail if a single fluid flow connection between two nodes has very high conductance compared to the conductances of other fluid flow connections of the nodes. This problem could be avoided by lumping the two nodes. Other causes may also affect convergence. Convergence can be improved by coarser zoning or by reducing error tolerance.

vi) Arithmetic truncation errors: These arise due to accumulation of round off errors and from loss of significant figures when numerical values of widely different magnitudes are added to or when numerical values of similar magnitudes are subtracted from each other. These errors are in general minor and can be neglected.

8. Organization of computer program TRUST

As described in the preceding pages, the computer program TRUST solves non linear, parabolic differential equations in general, multidimensional systems. The data input into the program include information on the geometry of the system, system symmetry, material properties, initial conditions and boundary conditions. The geometric parameters required to be input into the system include data on nodal volumes, surface areas of nodal connections and distances between nodal points. The material properties to be input into the system principally include permeability, stress-strain relationship of the soil skeleton and saturation-moisture suction relationships in the unsaturated zone. These non linear parameters can be conveniently input into the program as tabulated properties. The hysteretic relation between saturation and moisture content in the unsaturated

zone is also input as tabulated values, with additional data on "scanning curves", which is one way in which hysteresis has been handled in the literature. Boundary conditions can also be tabulated as time dependent functions. Initial conditions may vary arbitrarily from point to point. The program as such is designed for isotropic, heterogenous media. However, extension to anisotropic media is not difficult in principle.

When certain parts of the flow region possess cylindrical or spherical symmetry, advantage could be taken of this fact in generating data on nodal volumes, surface areas and nodal distances.

The structure and organization of program TRUST is basically the same as that of TRUMP (Edwards, 1969). The program consists of a main routine, TRUST and several subroutines: THERM, HYST, FINK, GEN, SURE, SPECK, TALLY, PATCH, REFER, SEEK 1, SEEK 2, ENTER, SLOPE, LINE and MORTHAN. The program is written in standard FORTRAN IV. The main routine as well as the subroutines consist of three parts: input, parameter initialization and cycle calculations. The first two parts are called only once, at the beginning of the problem. The last part is called for each cycle of calculation. The input data begin with a problem name card and end with a problem ending card. In between these two, input information is organized into several BLOCKS. A brief description of the main routine and the different subroutines is given below:

a) TRUST

   i) logical, centre of the entire program

   ii) initialize several parameters, monitor problem time at various stages and process problem name card, end card, continuation card and BLOCK cards.

iii) Call various subroutines (THERM, GEN, FINK, SURE, SPECK and TALLY) to read input data and to solve the governing equation

iv) terminate the problem by printing suitable messages

b) THERM

i) INPUT BLOCK 2, material properties and flow region properties: total thickness of flow region, saturated soil weight, permeability, compressibility and saturation characteristics of materials.

ii) INPUT BLOCK 4, node numbers, nodal volumes and materials. node numbering may be completely arbitrary.

iii) during each cycle compute effective stresses, void ratio, porosity, fluid mass capacity, permeability, fluid density, strain rate and settlement.

iv) print out data on nodal volume, fluid mass capacity, time constant, density, saturation effective stress, strain rates and settlement

c) HYST

i) INPUT BLOCK 2, saturation versus pressure head and permeability versus pressure head data

ii) calculate specific moisture capacity; calculate limits and slopes of scanning curves to define hysteresis

iii) determine saturation and permeability for partially saturated nodes during each cycle of calculation

d) FINK

i) INPUT BLOCK 5, internal fluid flow connections between nodes described in BLOCK 4

ii) calculate surface conductance for each connection and compute explicit potential change for each node

iii) print out data on interface conductances, cumulative fluid flow across internal connections and flow rates

e) GEN

i) INPUT BLOCK 8, rate of fluid generation (sources or sinks)

ii) find explicit potential changes in nodes due to fluid generation

iii) print out data on fluid generation

f) SURE

i) INPUT BLOCK 6, external fluid flow connections

ii) INPUT BLOCK 7, boundary potentials

iii) find external surface conductances and calculate explicit changes in potentials

iv) print out data on external surface connections

g) SPECK

i) when special nodes exist in the system, use iterative procedure to find implicit corrections for changes in potential

ii) compute corrected fluxes across interfaces between nodes

iii) Make final corrections to potentials for regular nodes connected to special nodes

iv) Print out data on iterations

h) TALLY

i) INPUT BLOCK 1, problem control parameters such as print-out intervals, time limits, convergence criteria and geometrical symmetry parameters

ii) INPUT BLOCK 3, fluid properties

iii) INPUT BLOCK 9, initial conditions: distribution of potentials, distribution of preconsolidation stresses

iv) summarize input data, determine time constants for nodes, determine upper and lower limits of time step and reclassify regular nodes as special nodes if needed,

v) determine if time steps are to be repeated, fix the size of new time step; estimate time derivatives for nodes and calculate new interpolation factor

vi) print out nodal potentials, estimated time derivatives and system mass balance data

i) Subroutines PATCH, REFER, SEEK1, SEEK2, SLOPE, ENTER, LINE and MORTHAN are minor subroutines used for such purposes

as cross referencing and determining point slopes

The numerical model described in this chapter was used to solve a number of typical problems in multi-dimensional flow, involving saturated flow, consolidation and unsaturated flow. In addition to help calibrate the program, these problems establish the validity of this numerical approach to a large class of problems involving saturated-unsaturated flow in deforming porous media. The analysis of the results from these problems forms the subject matter of the next chapter.

CHAPTER V

RESULTS OBTAINED WITH THE NUMERICAL MODEL

The numerical model described in the previous chapters was used to solve nine fluid flow problems involving saturated and/or unsaturated conditions involving one-, two- or three dimensions. These solutions helped to check the validity of the numerical model and its applicability to practical problems. Each problem was chosen to investigate one of the several major features of the numerical model. The problems solved are listed below:

Saturated flow in two- or three dimensional systems

1. Radial flow to a well: comparison of results with finite element solutions

2. Continuous Point Source: verification of the ability of the model to handle three-dimensional problems with complex geometry

Consolidation in saturated systems

3. One-dimensional consolidation of London Clay: consolidation in a heterogenous clay system; comparison of results with earlier finite-difference solution

4. One-dimensional consolidation of clay slurry: consolidation of a highly deforming system; study in Lagrangian coordinates; comparison with experimental results

Unsaturated flow

5. Rainfall infiltration: one-dimensional, unsaturated flow in extremely dry sand; comparison with earlier finite difference solution

Saturated-Unsaturated flow

6. One-dimensional column drainage: drainage from a sand column; comparison with experimental results

7. Drainage from sand box: two-dimensional drainage from a sand box; comparison with experimental results

Application to hypothetical problems

8. Excavation in soft clay: consolidation and swelling in a soft clay system caused by an excavation; study pore-pressure dissipation and strain rates

9. Flow to a soil probe: unsaturated, radial flow to a soil sampler; study of the flow system around the sampler

The nature of the problems themselves, the solutions obtained, and the interpretation of results are presented below.

1. RADIAL FLOW TO A WELL

The problem of non-steady flow to a well discharging at a constant rate Q and penetrating a horizontal, infinite, homogenous, isotropic aquifer with coefficient of Transmissibility, T and Storage, S, was solved by Theis (1935). This is also the classical, continuous line source problem of heat flow. The analytical solution obtained by Theis is the well known exponential integral,

$$\phi(r,t) - \phi_o(r,t_o) = \frac{Q}{4\pi T} \int_{\frac{r^2 S}{4Tt}}^{\infty} \frac{e^{-u}}{u} du \qquad (V.1)$$

Pinder and Frind (1972) solved the Theis-equation using the Galerkin finite element method. For their purpose, they set up a pie-shaped mesh, as shown in figure 22A. They set up nine nodal

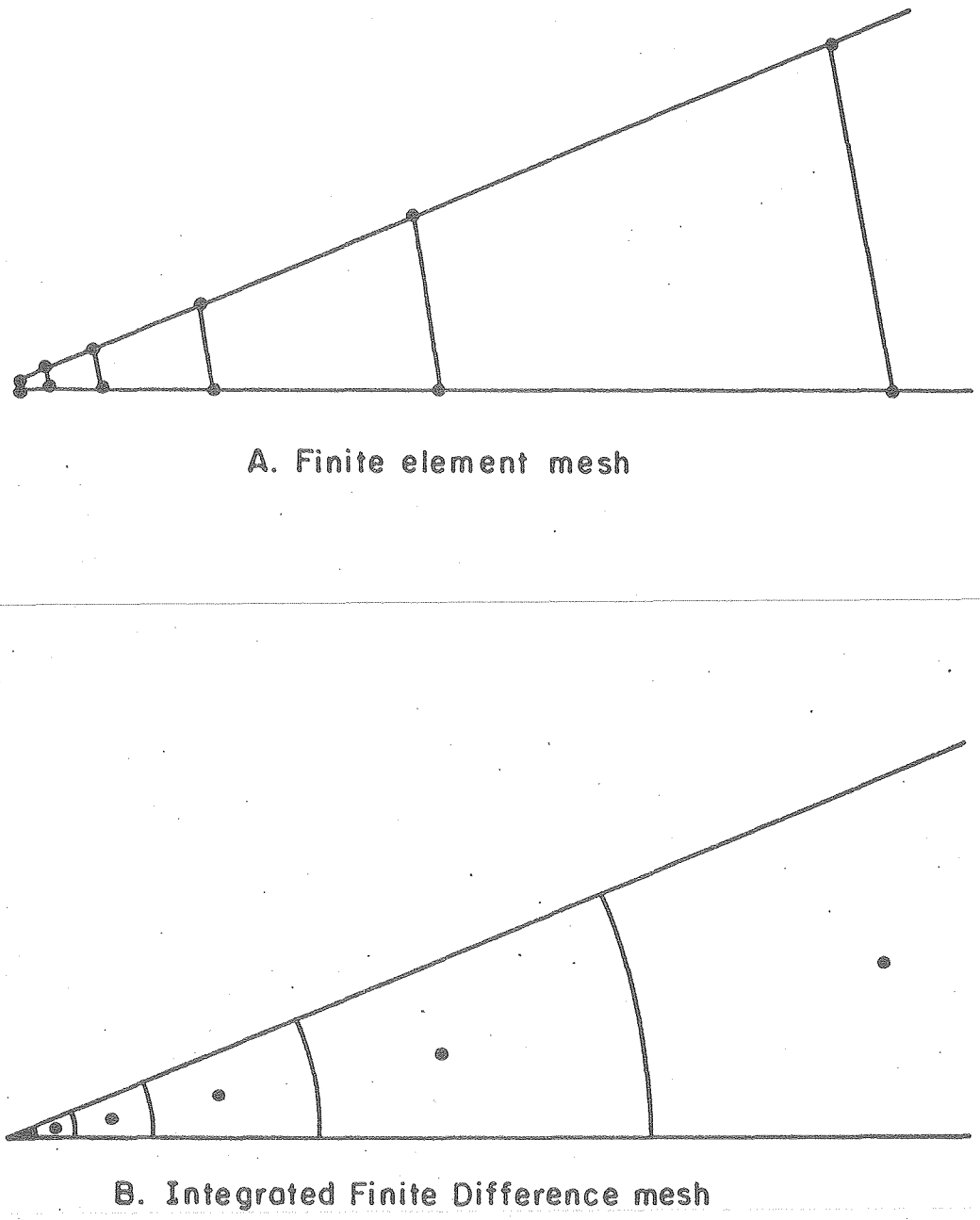

Fig. 22. Finite Element and IFD meshes for radial flow to a well

points along the x-axis, and each successive nodal spacing, along the x-axis was twice the preceding. The first nodal point was presumably one foot from the well and the last at 1000 feet.

In order to solve the same problem by the IFD method used in the present work, a similar pie-shaped region was simulated, as in figure 22B, with each nodal separation increasing by a factor of two in the radial direction.

A comparison of the results obtained by Pinder and Frind (1972), the analytical solution and the IFD results are presented in figure 23. It can be seen from the figure that the IFD results compare favorably with the analytical solution as well as with those of the finite element method.

2. CONTINUOUS POINT SOURCE

In order to test the ability of the IFD scheme to handle three-dimensional problems with complex geometry, the numerical model was used to solve the well known problem of a continuous point source in an isotripic, three-dimensional medium. Due to the spherical symmetry involved, the distribution of potential is only a function of radial distance, r and time, t. According to Carslaw and Jaeger (1959), the analytical solution for this problem is given by,

$$\phi(r,t) - \phi_o(r,t_o) = \frac{Q}{4\pi\kappa r} \operatorname{erfc}\left[\frac{r}{2\sqrt{\kappa t}}\right] \qquad \text{(V.2)}$$

where $\kappa = K/S_s$

To solve this problem with the IFD, the flow region was conceptualized as a sphere enclosed in a cube, with the spherical elements gradually grading outwards to the cube. This conceptualization was

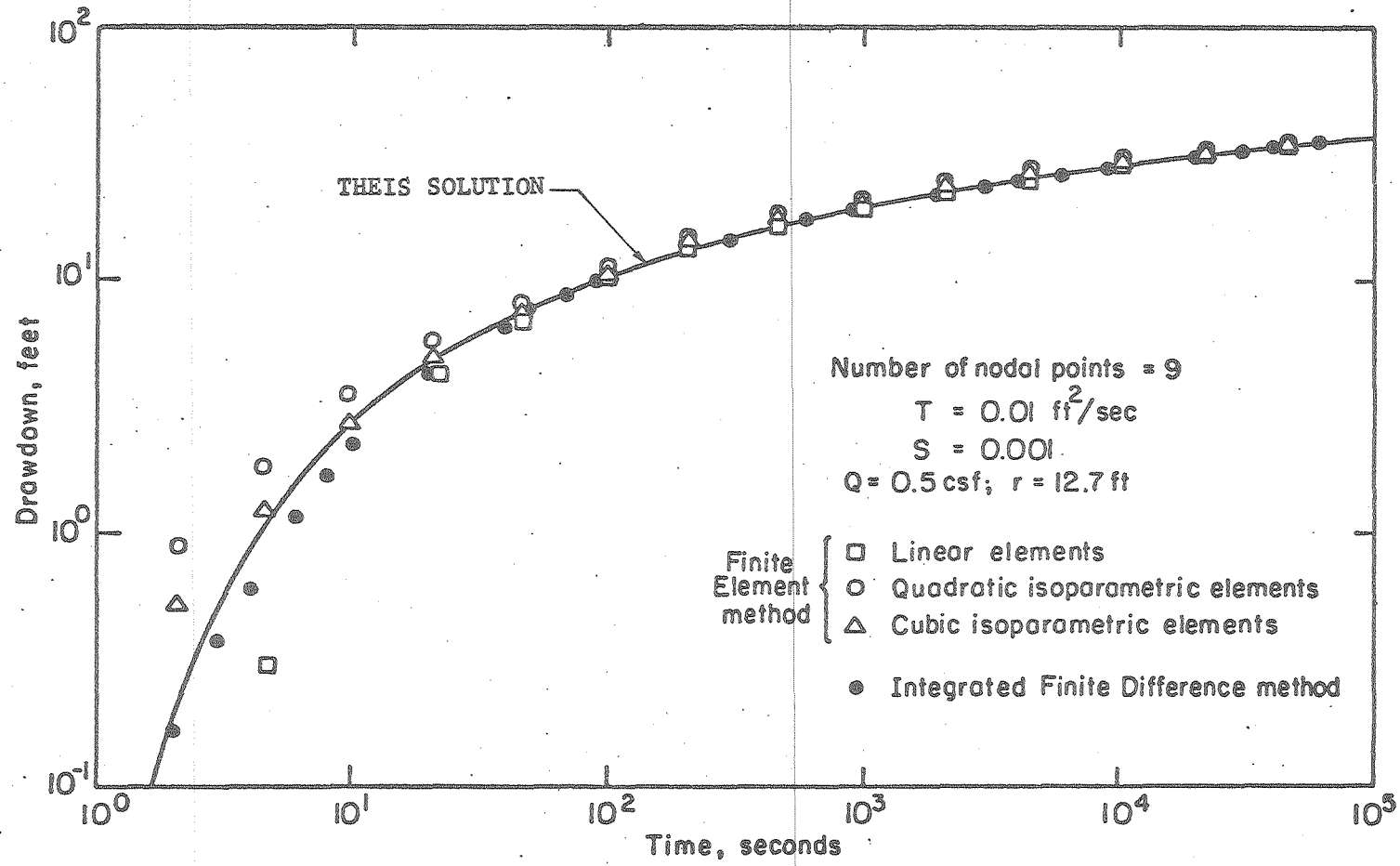

Fig. 23. Radial flow to a well; comparison of numerical and analytical results

made so that one could simulate the spherical symmetry of flow close to the point source, but allow for more general conditions of flow away from the point source. The flow region was divided into three-dimensional nodes or elements. From symmetry considerations (eight quadrants in a cube and in each quadrant symmetry exists about each of the three cartesian axes), a wedge-shaped segment of the flow region, whose volume is a twenty-fourth part of the whole cube was chosen for actual modeling. The three-dimensional mesh so set up is given in figure 24.

The distance from the point source to the surface of the cube is 400 m. The three-dimensional region is discretized into 47 volume elements and there are a total of 87 interconnecting surface areas between the elements. The nodal point closest to the point source is located at a distance of 1 m. from the source. The farthest nodal point is located at a distance of 593 m. from the centre. The nodes vary widely in volume from $0.91\ m^3$ in the case of the smallest to 9×10^3 in the case of the largest. For this problem, the following arbitrary parameters were used:

Discharge, Q	=	$10^3 m^3/sec$
Permeability, K	=	10^{-3} m/sec
Storage Coeff., S_s	=	10^{-2}

Impermeable conditions were assumed on the outer surface of the cube as well as the other symmetry faces bounding the wedge-shaped region.

The results of the computations are presented in figure 25. In figure 25A, drawdown is given as a function of time for various distances from the point source. In figure 25B, drawdown is shown

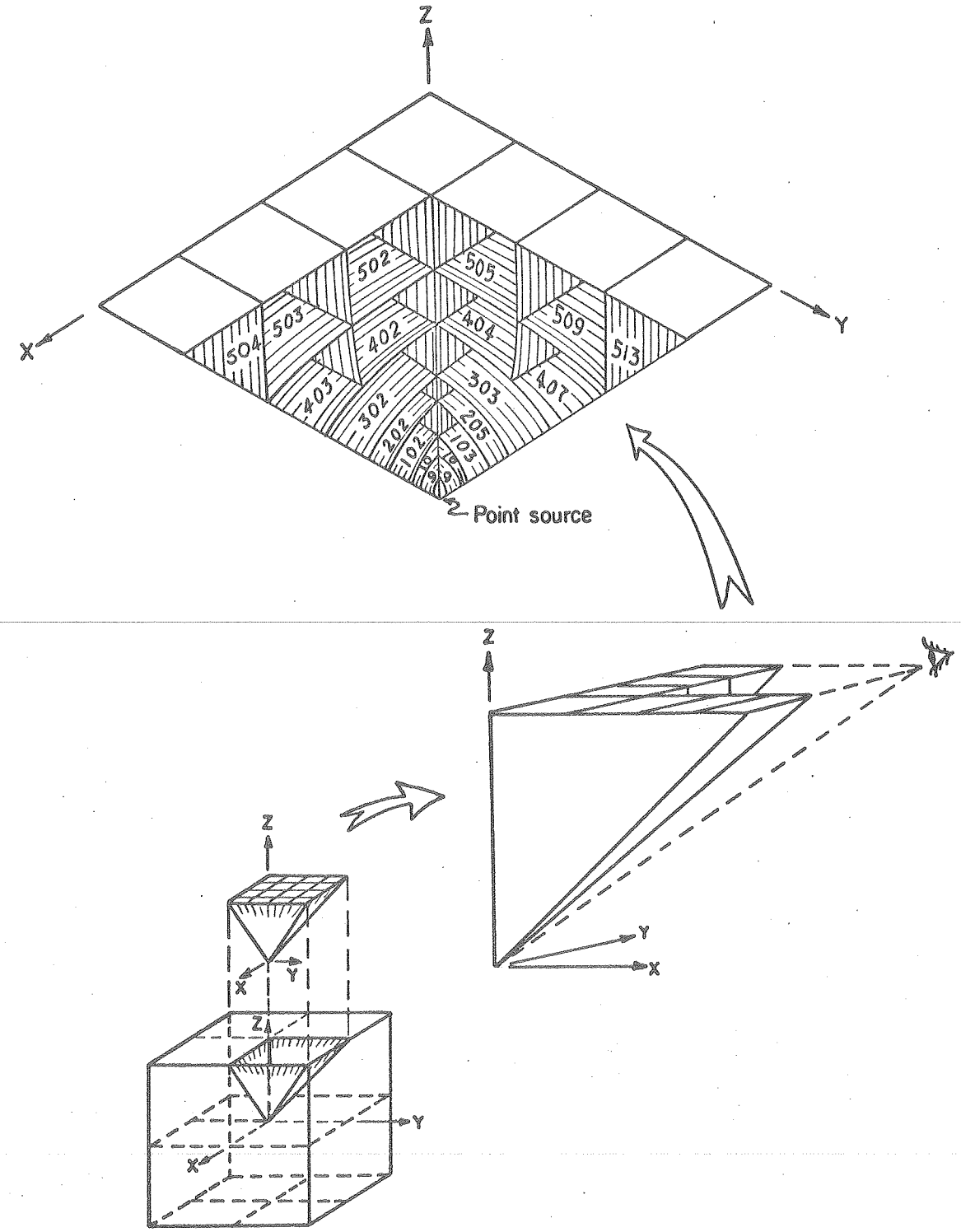

Fig. 24. Three-dimensional network of elements for the continuous point source problem

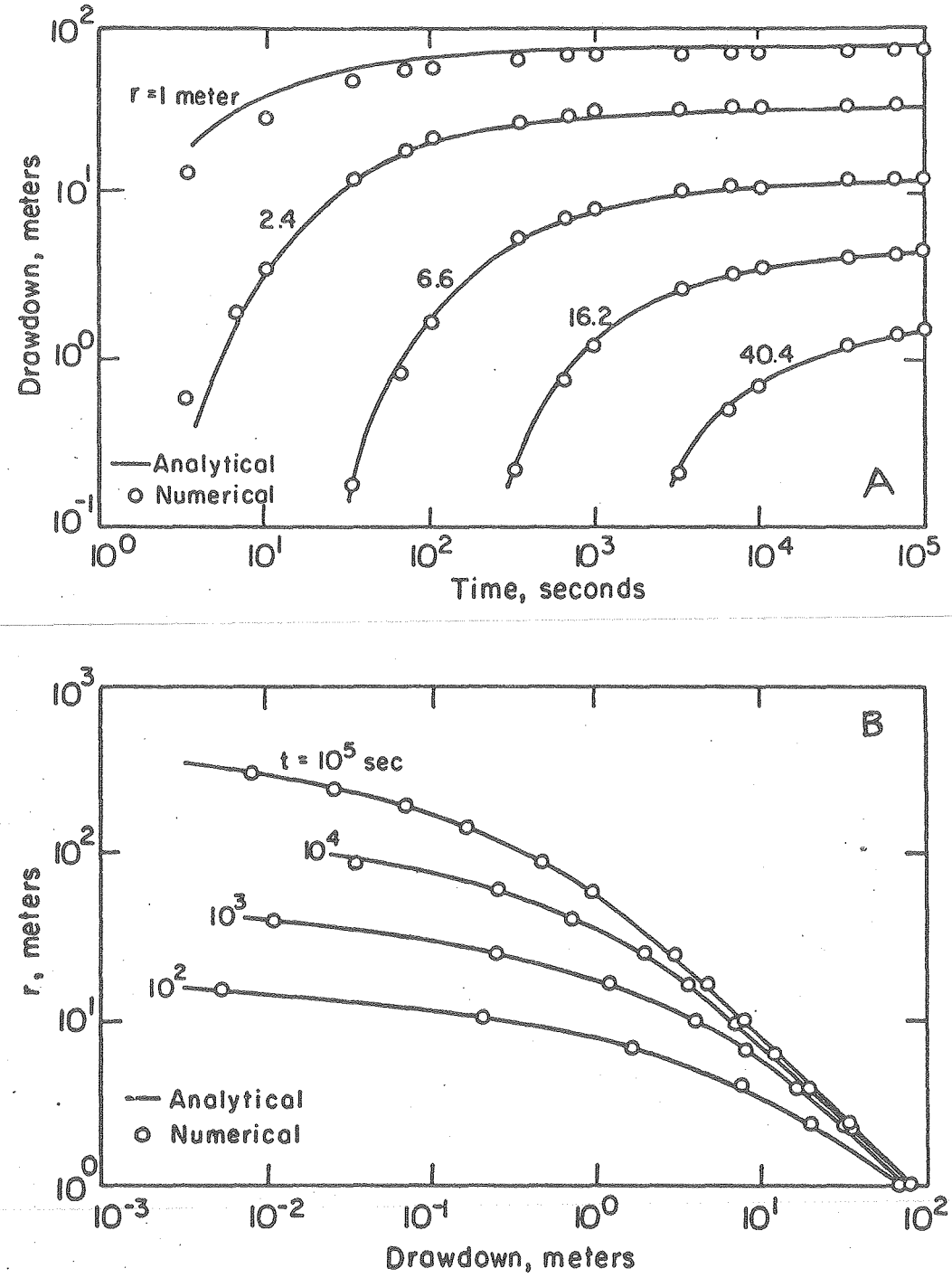

Fig. 25. Continuous point source; comparison of IFD and analytical solutions, A. time-drawdown plot, B. distance-drawdown plot

as a function of radial distance at different instants of time. It can be seen from figures 25A and 25B that the computed results deviate from the analytical solution for small values of time and small values of radial distance. However, these errors are reasonably small and hence, it is concluded that the numerical model has been able to successfully handle the three-dimensional problem in question.

3. ONE-DIMENSIONAL CONSOLIDATION OF LONDON CLAY

The problem of settlement of foundations built on soft soils is an important concern of soil engineers. In order to predict such settlement, soil engineers widely use the one-dimensional consolidation theory of Terzaghi.

In the conventional use of Terzaghi's theory, the soil layer is assumed to be homogenous, with a single coefficient of permeability and a single coefficient of compressibility. However, in practice, it is not unusual to find more rapid settlement of structures than is predicted by the conventional Terzaghi theory.

Although there could be many reasons for the observed departure from the conventional theory, Schiffman and Gibson (1964) reasoned that the non-homogenity of the clay layers with depth may contribute significantly to the observed departure. To study this, they developed a modified theory of one-dimensional consolidation of non-homogenous soils and solved their governing equation using a finite difference technique.

As a typical example, Schiffman and Gibson considered a 100-foot column of overconsolidated London Clay. Thanks to the earlier experiments of Skempton and Henkel (1957), the physical properties of this

clay were known as a function of depth. This column was assumed to be drained at the top and at the bottom (doubly drained), and subjected to a constant total stress of 1 ton/ft^2 (figure 26). The problem is to predict the consolidation of the column with time. In their calculations, Schiffman and Gibson approximated permeability, K, and compressibility, m_v , as algebraic functions of the form,

$$A\ (x) \quad = \quad A_o\ [\ 1 + \alpha\ \frac{z}{H}\ ]^{\nu} \qquad (V.3)$$

where, α and ν are some coefficients.

The problem of Schiffman and Gibson was also solved by the numerical model of the present study. In this case, instead of of expressing the variation of K and m_v as an algebraic function of depth, the column was divided into 10 different materials with step-wise change in physical properties, as shown in figure 27.

The results of the numerical calculations are presented in figures 28 and 29. In figure 28, degree of consolidation is plotted as a function of time. The term, degree of consolidation, expresses the settlement at any given time t as a fraction of the total settlement expected at t_∞ due to the existing load. The total settlement can be calculated for any volume element by multiplying its volume by its m_v and the constant load acting on it.

It can be seen from figure 28 that the IFD results differ only slightly from the earlier calculations of Schiffman and Gibson. This difference is probably to be attributed to the different methods used to approximate the physical properties. However, for the type of the problem considered, the agreement seems reasonable

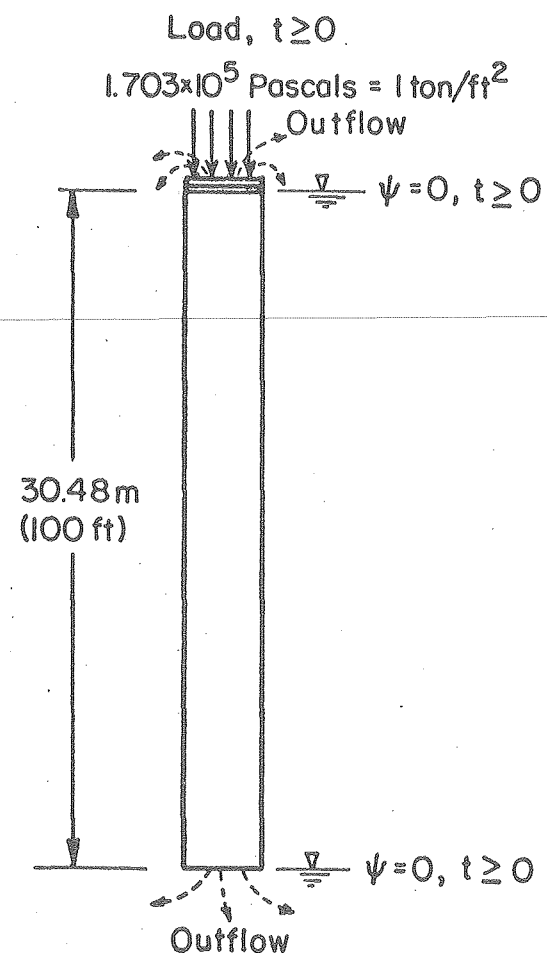

Fig. 26. Consolidation of non-homogeneous clay; initial and boundary conditions

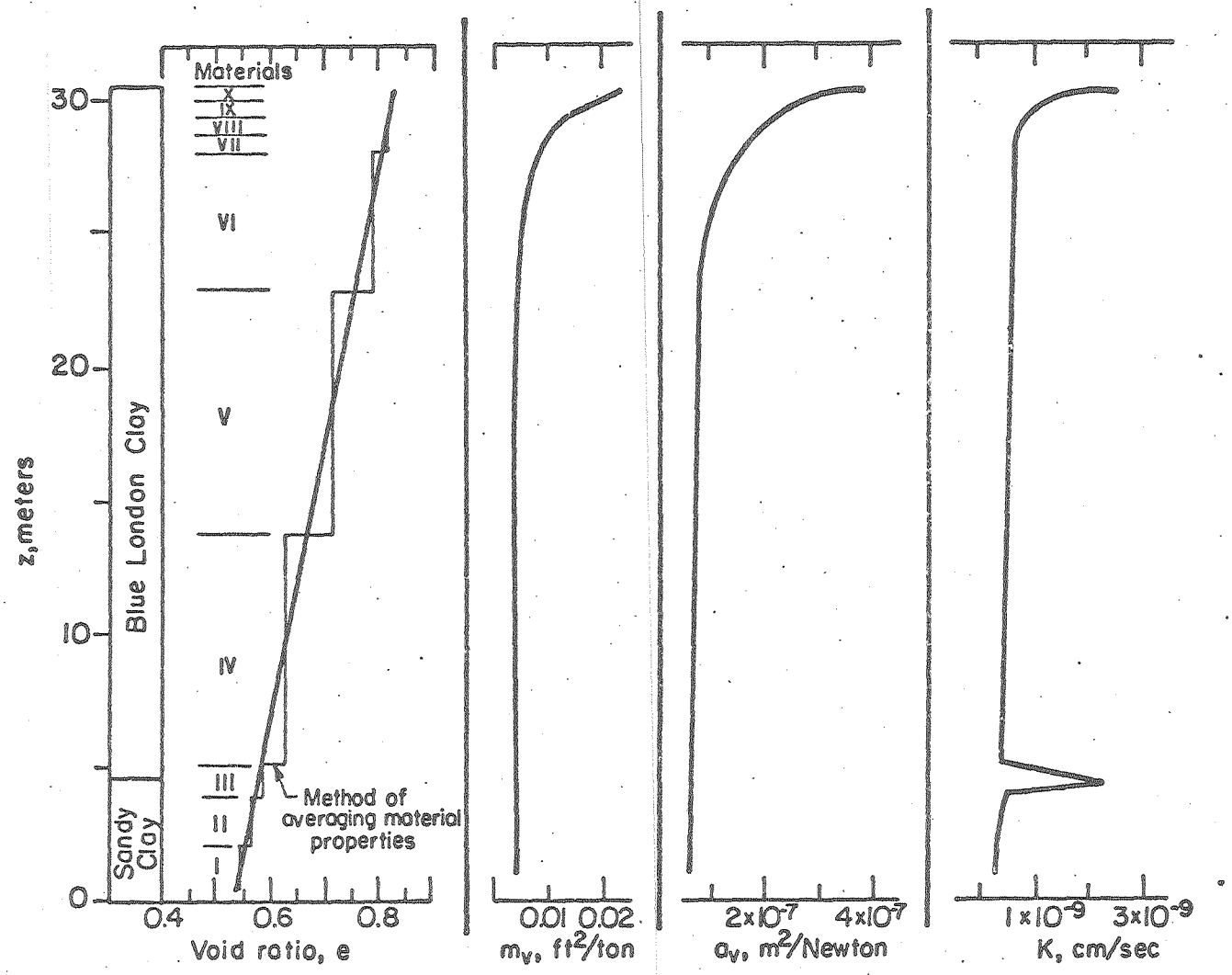

Fig. 27. Consolidation of non-homogeneous clay; material properties

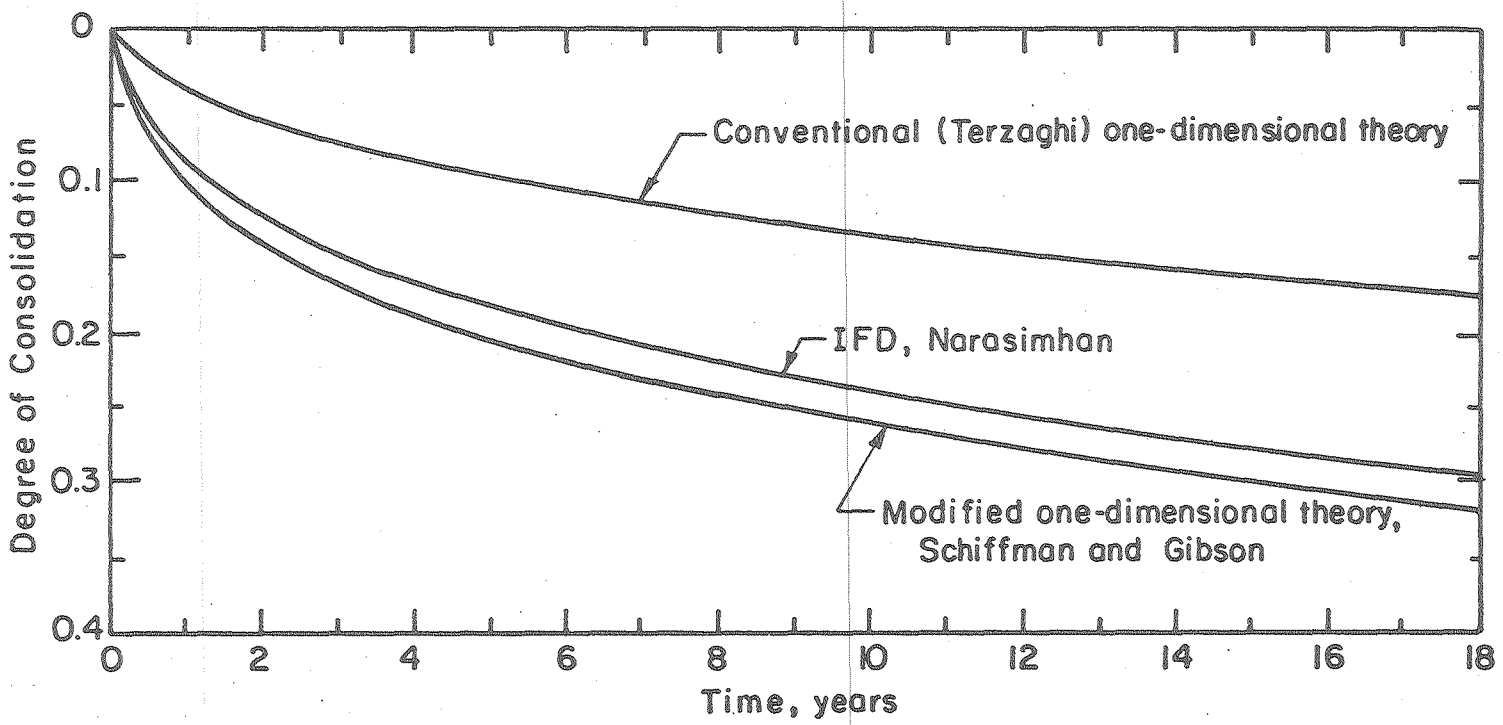

Fig. 28. Consolidation of non-homogeneous clay; comparison of numerical results

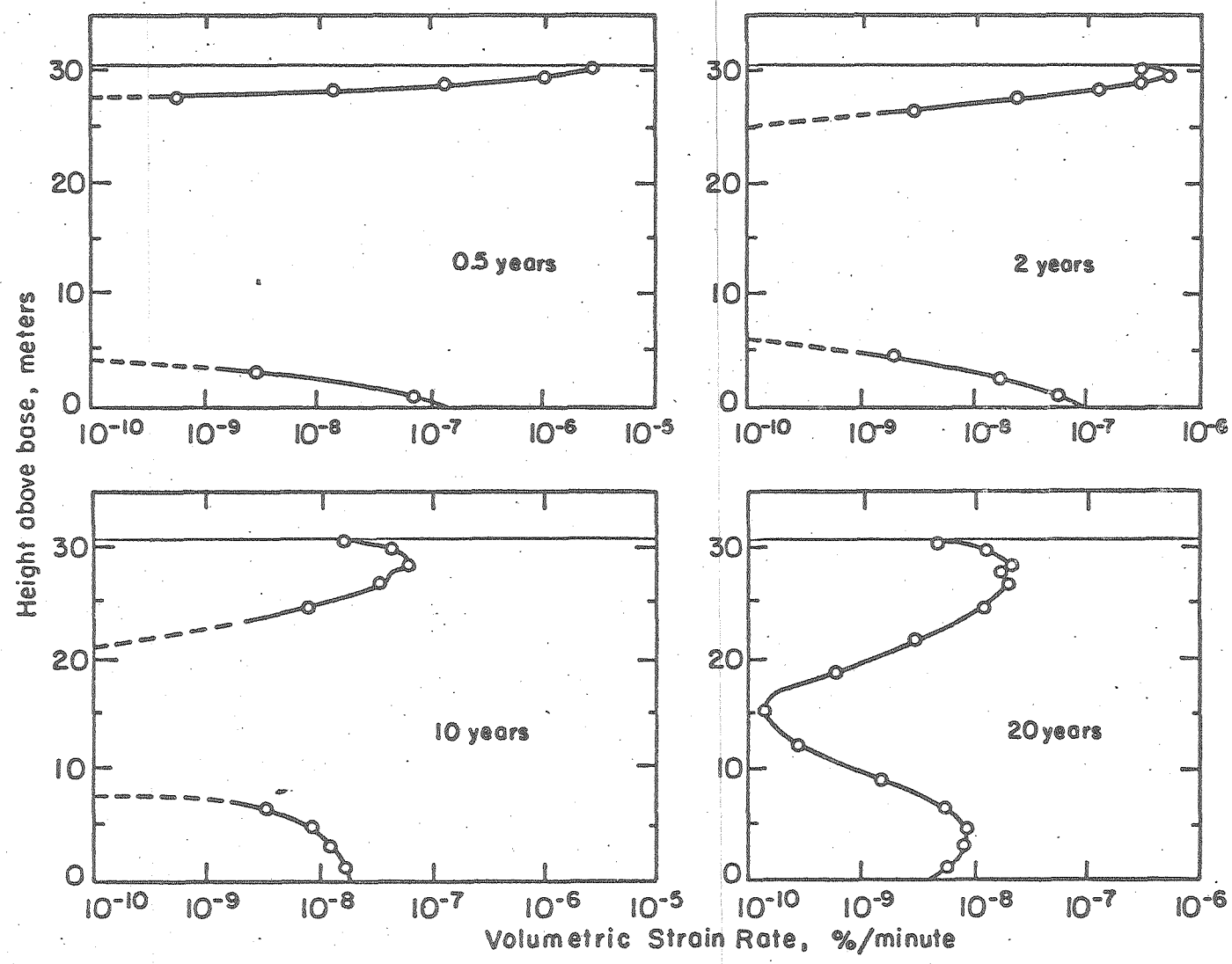

Fig. 29. Consolidation of non-homogeneous clay; Volumetric strain-rate as a function of depth

and justifies no concern for the validity of the method used. It can be seen also from figure 28 that, as Schiffman and Gibson expected, consideration of material nonhomogeneity with depth has indeed predicted faster settlement rates than that predicted by the conventional Terzaghi theory.

Figure 29 is a plot of the time-rate of volumetric strain at four intervals of time. This diagram gives an idea of the deformation history of different parts of the clay column. It can be seen from the figure that the elements at the extremities initially take up the bulk of the deformation and consolidate rapidly. With progress of time, the elements toward the middle progressively undergo greater deformation. As a result, the strain-rates of the upper elements attain peak values which gradually decline with time, as the more interior elements tend toward their peak strain-rates.

4. ONE-DIMENSIONAL CONSOLIDATION OF CLAY SLURRY

An extreme case of the phenomenon of consolidation of soil is that of the shrinkage of an active clay such as Bentonite clay. In such a material, very large changes in volume can take place during relatively small intervals of time. The movement of water in such a swelling material is of interest in the field of soil physics. An important problem is that of the determination of the hydraulic conductivity of such a material, as a function of its void ratio.

Smiles and Rosenthal (1968) developed a theory for the one-dimensional movement of water in clay-water systems that are free to swell in the direction of water movement. This theory was developed from the fact that Darcy's law describes the flow of fluid relative

to the movement of soil particles and was based on a scale of length defined with reference to the distribution of the mass of clay, rather than the more conventional fixed scale of length. They showed that in the new material scale, the appropriate equation for water movement is the diffusion equation.

To develop their theory, Smiles and Rosenthal considered the desorption (drainage) of electrolyte from a semi-infinite column of saturated clay that is restrained within smooth cylindrical walls but is free to contract in the direction of the cylindrical axis. For this system, they defined a new material scale,

$$m = \int_0^x \frac{dx}{(1 + e)} \qquad (V.4)$$

In this scale, the continuity equation with reference to an elemental volume dV is shown to be,

$$\frac{\partial}{\partial m} \left(D_m \frac{\partial e}{\partial m} \right) = \frac{\partial e}{\partial t} \qquad (V.5)$$

$$\text{where,} \quad D_m = \frac{K}{(1 + e)} \frac{\partial \psi}{\partial e} \qquad (V.6)$$

and in which, e is the void ratio and ψ is the pressure head.

The semi-infinite column is subjected to the following intial and boundary conditions,

$$\begin{aligned} e &= e_n, \quad m > 0, \quad t = 0 \\ e &= e_o, \quad m = 0, \quad t > 0 \end{aligned} \qquad (V.7)$$

Using the Boltzman-transformation, $\lambda = mt^{-\frac{1}{2}}$, as suggested by Bruce and Klute (1956), the quantity D_m could be determined experimentally by,

$$D_m(e) = -\frac{1}{2}\frac{d\lambda}{de}\int_{e_n}^{e} \lambda de \qquad (V.8)$$

This theory, if valid must lead to the following consequences.

a. the moisture content, or, equivalently, the void ratio, must be a unique function of λ

b. the cumulative outflow from the column or the change of length of the saturated column must plot as a straightline with the square root of time

c. the slope of the straightline obtained in b above should be equal to the following integral,

$$\frac{dL}{dt^{1/2}} = \int_{e_n}^{e} \lambda de$$

In order to verify the theory, Smiles and Rosenthal conducted a set of experiments with a 13.5 cm. tall perspex column filles with a slurry of Wyoming Bentonite, at an initial uniform void ratio of $e_n = 44.76$ (porosity = 97.81%). A constant air-pressure of 1.66 m. of water was applied to this column at the top, while at the bottom (m = 0), water was allowed to drain through a millipore filter (figure 30). The void ratio, e_o (m = 0, t > 0), was 15.91 (porosity = 94.08%). The non-linear relationship between void ratio and effective stress for the Bentonite was experimentally determined and this relation is presented in the form of a semi-logarithmic straightline plot in figure 31A. The slope of this straightline is the compression index, C_c of

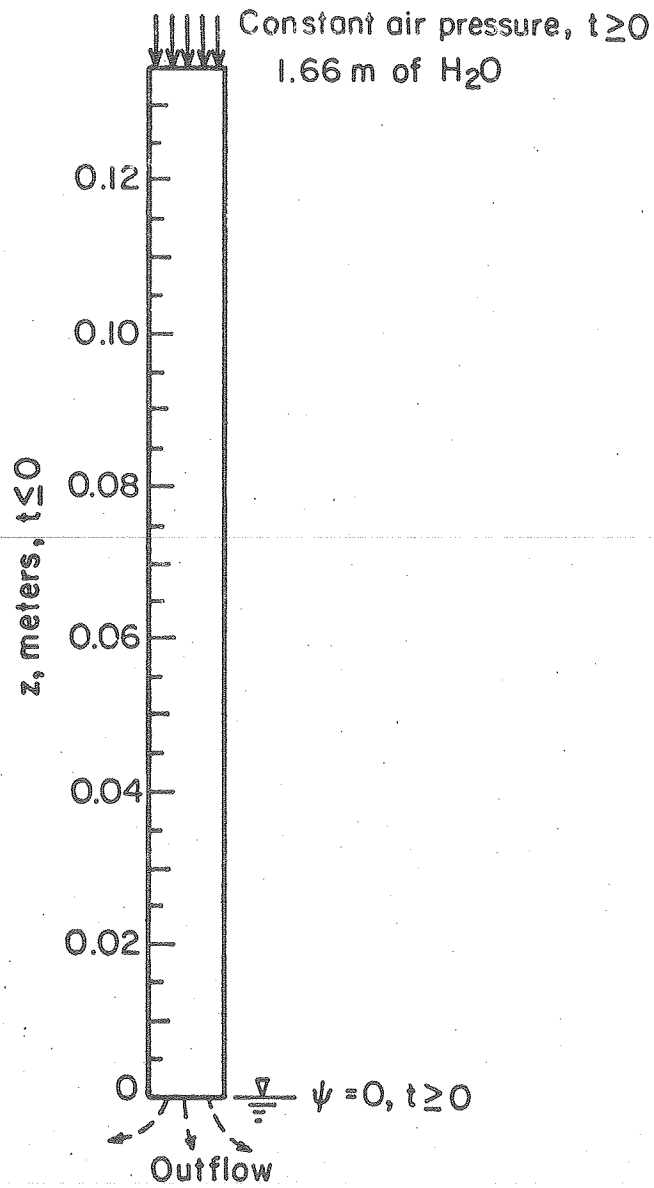

Fig. 30. Consolidation of clay slurry; initial and boundary conditions

the Bentonite used. The initial and the boundary conditions of the experiment are shown in figure 30.

The desorption experiments were carried out for three weeks. The shrinkage of the column as well as the void ratios at various points in the column were carefully measured at various times. With the data so collected, the plots of shrinkage versus $(\text{time})^{1/2}$ and e versus λ were generated. It was found that the shrinkage versus $\text{time}^{1/2}$ did indeed prove to be a reasonable straightline as predicted by theory and the slope, $(dL/dt^{1/2}) \simeq 3.8 \times 10^{-3}$ $\text{cm/sec}^{1/2}$. Also, as predicted by the theory, there was a fairly well-defined unique relation between $\lambda = mt^{-1/2}$ and void ratio. On graphical evaluation, the integral, $\int_{e_n}^{e_o} \lambda \, de$ yielded a value of 3.2×10^{-3} $\text{cm/sec}^{1/2}$. The difference between this value and the value of 3.8×10^{-3} obtained for $dL/dt^{1/2}$ was attributable to to the difficulties in the measurement of the length of the perspex column and to problems of sampling various sections of the column at different times (Smiles, personal communication, 1974).

Using the λ versus e relation, Smiles and Rosenthal then proceeded to compute the quantity, D_m (e), using the relation (V.8). The values of D_m so calculated, in conjunction with the stress-strain plot shown in figure 31A, directly leads to the evaluation of hydraulic conductivity, K, of the Bentonite, as a function of void ratio.

The numerical model developed in the present thesis was applied to the Smiles-Rosenthal problem, but, for the reverse purpose; whereas Smiles and Rosenthal calculated K from shrinkage, the aim of the numerical solution was to calculate shrinkage from the experimentally known

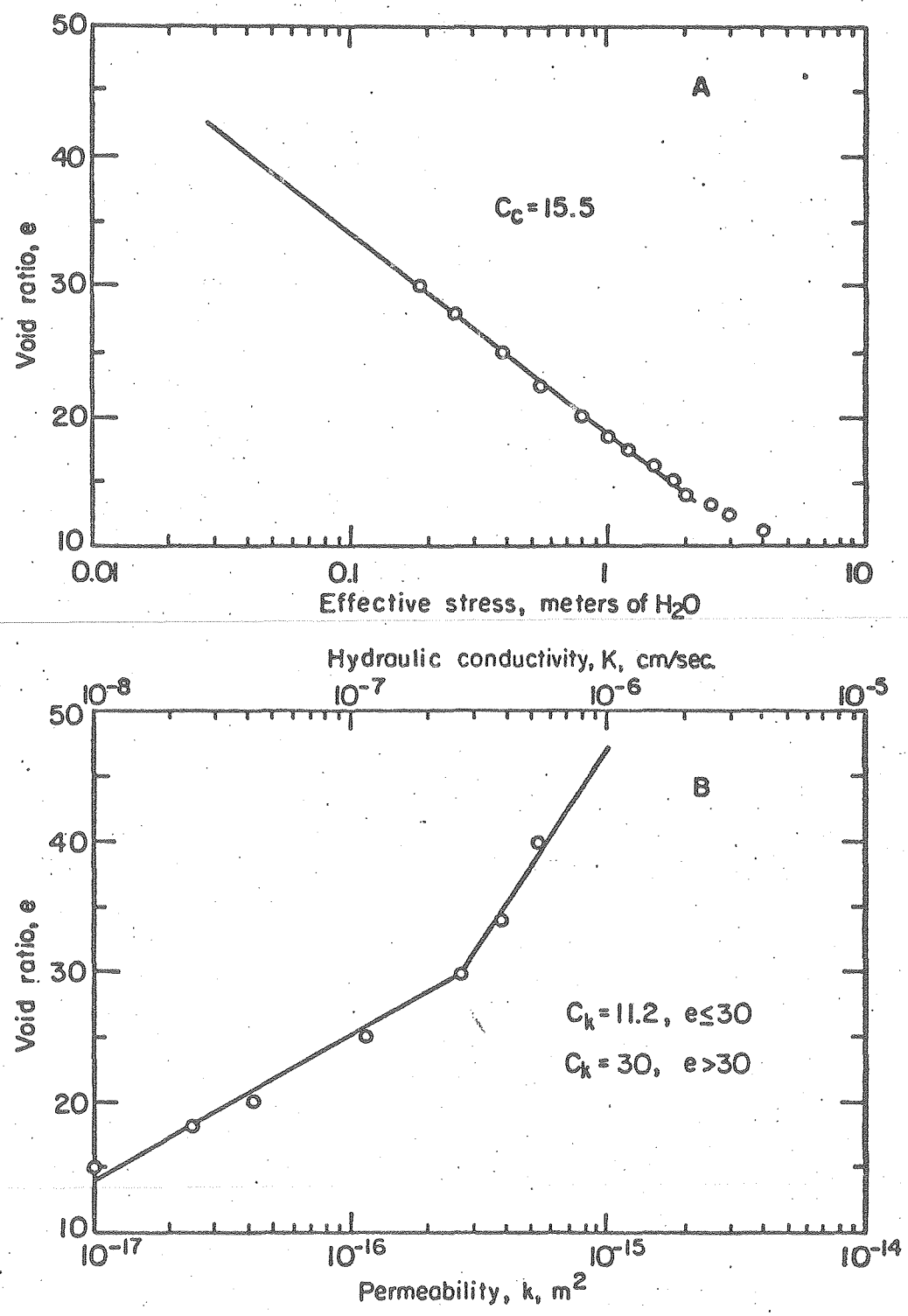

Fig. 31. Consolidation of clay slurry; material properties, A. void ratio versus effective stress, B. void ratio versus permeability

values of K and the stress-strain relationship.

It is pertinent to mention here that the Boltzman-transform method of solution of Bruce and Klute (1956) is strictly applicable to a horizontal column, in which gravitational effects are non-existent. The experiment, however, had to be conducted for convenience with a vertical column. However, the potential gradient component due to gravity was less than about 8% and hence, neglected.

The numerical experiments were carried out to investigate the following:

i) does the shrinkage predicted by the numerical model agree with the experimentally observed shrinkage ?

ii) how important is the role of gravity ? in other words, do the solutions for the horizontal and the vertical column differ appreciably ?

iii) to what extent should consideration be given to a material coordinate system in numerically calculating consolidation in the type of highly deforming system considered ?

The results, discussed below, seek to answer the above questions.

Using the D_m values computed by Smiles and Rosenthal and the moisture-characteristic plot given in figure 31A, functional dependence between permeability and void ratio was determined, using the relation (V.6) (figure 31B). The data presented in figures 31A and 31B form the basic input information on the physical properties of the swelling clay.

a. Lagrangian formulation

Under saturated flow conditions, equation (IV.2) for a node n can be written:

$$\sum_{m} K_{m,n} \frac{(z_m - z_n) + (\psi_m - \psi_n)}{(d_{n,m} + d_{m,n})} \sigma_{m,n} = (M_c)_n \frac{\Delta\psi_n}{\Delta t} \qquad (V.9)$$

We recall that (V.9) applies to a material element fixed in the soil particles; in other words, the volume of solids in a given volume element is a constant. As the void ratio of such an element changes with time, so does its total volume V and this dependence of V on time is duly taken into consideration in evaluating M_c according to the relation, $M_c = d(V\rho Sn)/d\psi$.

Now, since the volume of the element changes with time, it follows that the quantities, $\sigma_{m,n}$, surface area, $(d_{n,m} + d_{m,n})$, the distance between the nodal points, and, in the case of a vertical column, z_m and z_n , on the left hand side of (V.9) should also change with time. Normally, in slightly deforming systems, while evaluating the left hand side of (V.9), it is customary to ignore the changes in the aforesaid quantities as a function of time. Thus, we have a situation in which we are considering a deforming volume element on the right hand side of (V.9), while the element considered on the left hand side has a fixed geometry. The justification for this is that the gross effect of the change in geometry is negligible on the left hand side. While, this may be true in slightly deforming systems, can the deformation be ignored in a highly deforming system as the one we are now considering ? In order to investigate this aspect, we are led to the solution of the problem in Lagrangian coordinates.

In seeking to solve the problem in Lagrangian coordinates, we note that the deformation of the column is restricted to one direction. Hence, in this case, the surface areas $(\sigma_{m,n})$ designed perpendicular to the direction of movement of water, are constants and do not vary with time. Therefore, in considering the left hand side of (V.9), we have to take into consideration the changes of the d's and the z's only. In order to take into consideration the changes in these parameters with time, the coordinates of the nodal points were re-calculated at the end of each time step in the light of the deformation history at the respective nodal points. Along with this, the time rates of change of the d's and the z's were also estimated at the end of each time step. With the help of these data mean values of $\bar{z}_m$, $\bar{z}_n$, $\bar{d}_{m,n}$ and $\bar{d}_{n,m}$ were calculated for each time step in the same manner as evaluating the non-linear parameters (chapter IV). These values were then used to evaluate the left hand side of (V.9).

b. Horizontal and vertical columns

To start with, the consolidation problem was solved for two cases: i) with the column vertical and ii) with the column horizontal. The boundary conditions in the case of the vertical column are depicted in figure 30. In the case of the vertical column, the initial void ratio (e_n) was uniformly equal to 44.43 (porosity = 97.74%), while, at all times, the void ratio at m = 0 was constant at 14.54 (porosity = 93.58%). The condition of uniform void ratio throughout the vertical column (and hence, uniform effective stress) gave rise to a decrease in hydraulic potential towards the top; from 1.779 m. at the bottom to 1.774 m. at the top. As a result, at t = 0, there was a small

upward movement of water within the column.

In the case of the horizontal column, the initial void ratio in the column (e_n) was uniformly 44.76 (porosity = 97.81%) while the constant void ratio at m = 0 (e_o) was 15.05 (porosity = 93.78%).

The computed values of consolidation for the horizontal and the vertical cases are presented in figure 32. It can be seen from the figure that the horizontal and the vertical columns have yielded identical patterns of consolidation. Although the gross pattern of consolidation is the same in both the cases, a detailed study of the computed results indicated that the deformation patterns of individual elements within the vertical and the horizontal columns were not the same.

Thus, in the case of the vertical column, the upward movement of water persisted for over ten days, causing the elements in the upper part of the column to swell, rather than to shrink. The uppermost element did not commence to consolidate until after about 11 days. On the other hand, in the case of the horizontal column, the movement of water was always towards the drainage end and none of the elements experienced any swelling.

To get an idea of the pattern of deformation going on within the column, the time-rate of volumetric strain of four typical elements is plotted in figure 33. It can be seen from this figure that for each element, the strain-rate initially increases with time, attains a peak and then finally decreases with time. Also, the nodes located more towards the moving end of the column attain peak deformation at progressively later instants of time, showing the gradual migration of the consolidation transient away from the fixed end.

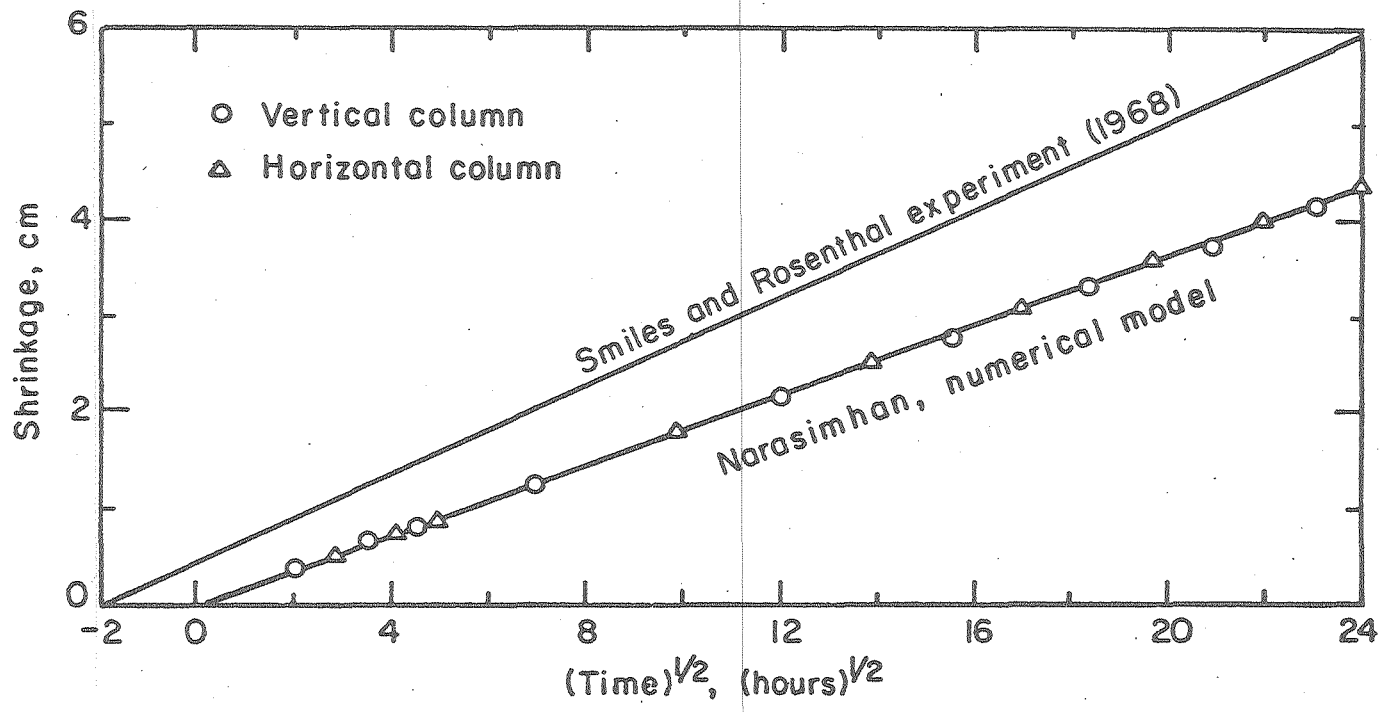

Fig. 32. Consolidation of clay slurry; comparison of numerical and experimental results

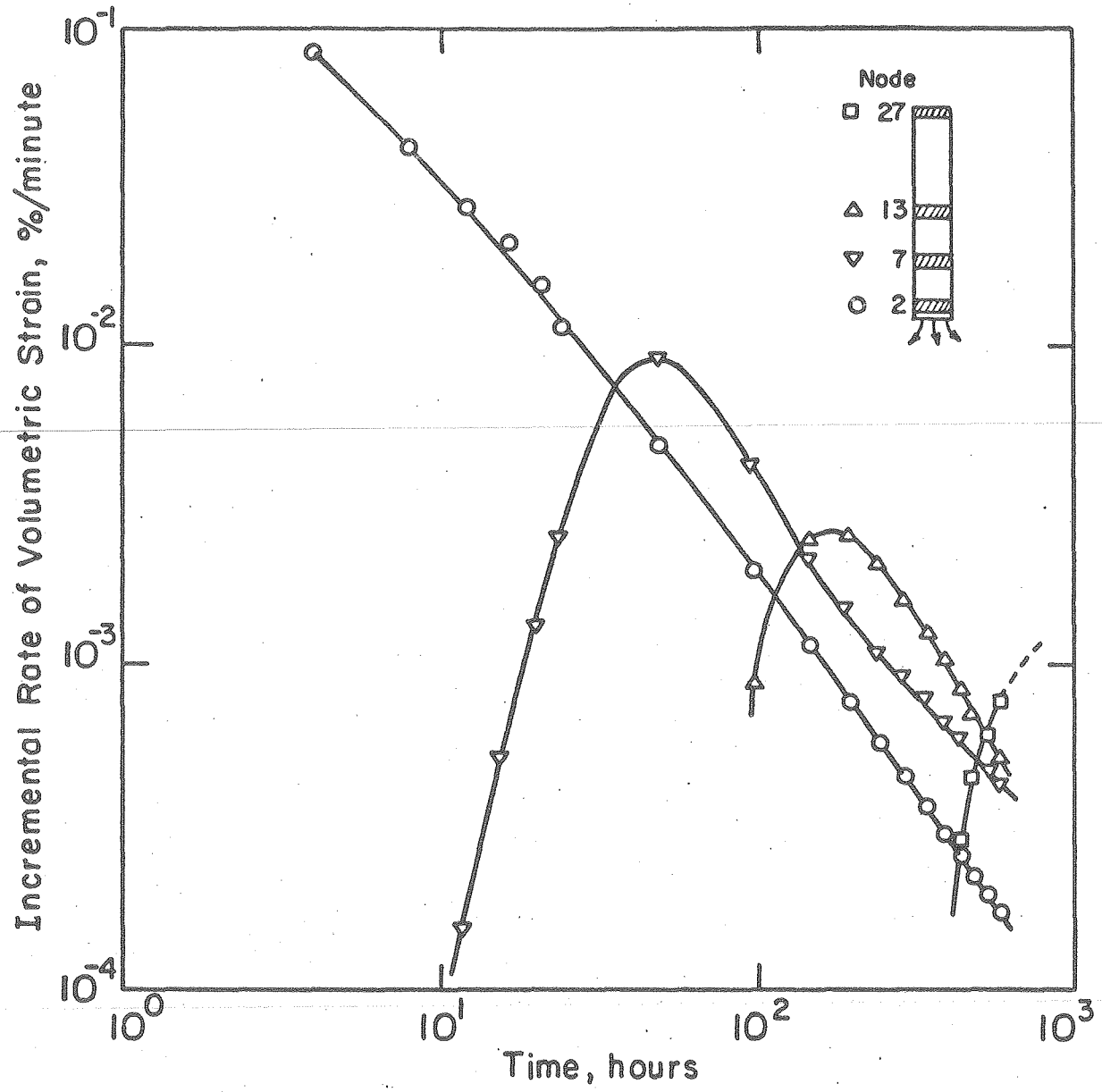

Fig. 33. Consolidation of clay slurry; volumetric strain-rates of some typical elements

c. Departure from experimental results

Referring back to figure 32, we note that the numerically computed rate of consolidation is smaller than the consolidation rate experimentally observed by Smiles and Rosenthal. In order to investigate the reason for this discrepancy, the numerical results were first checked for consistency. First, we see that the shrinkage versus $\text{time}^{1/2}$ plot (figure 32) is a straightline, passing through the origin, as to be expected from theory. Secondly, the relation between the numerically computed values of e and λ is shown plotted in figure 34 for the vertical column. It can be seen from this figure that there is a fairly well-defined unique relationship between e and λ according to theory.

Moreover, the theory predicts that the slope of the shrinkage versus $t^{1/2}$ plot must be equal to the area under the curve in figure 34 (the integral $\int_{e_n}^{e_o} \lambda \, de$. Actual evaluation shows that the area under the curve in figure 34 $\simeq 3.1 \times 10^{-3}$ cm/sec$^{1/2}$, while the slope of the line in figure 32 $\simeq 3.06 \times 10^{-3}$ cm/sec$^{1/2}$.

Having checked the consistency of the numerical results, it was reasonable to question whether the observed discrepancy was due to the input values of permeability being lower than what they should be. Some trial computations indicated that a good agreement between the computed consolidation and the observed consolidation could be obtained if the permeability input data is arbitrarily multiplied by a factor of about 2. This could be easily done by assuming the e versus $\log k$ plot to be appropriately shifted to the right in figure 31B. This indicated that the experimentally determined values

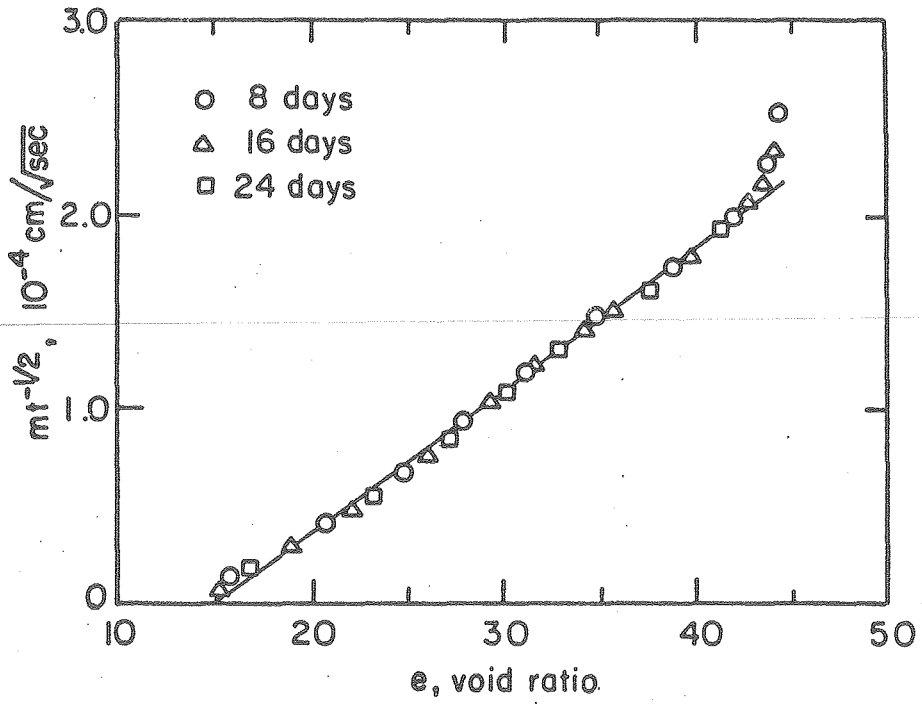

Fig. 34. Consolidation of clay slurry; relation between λ and e for vertical column

of $D_m(e)$ were too low by a factor of about 2.

A reexamination of the data (Smiles, personal communication) indicated that an experimental misclose was indeed possible due to the difficulties of measuring shrinkage through the perspex column and computing void ratios. Considering the laboratory difficulties, such an experimental misclose appears tolerable. It is also of interest to point out that in a later paper, Smiles and Harvey (1973) have suggested that the D_m values calculated earlier by Smiles and Rosenthal was suspect, since the theoritical boundary conditions were not exactly realized experimentally.

d. Accuracy and adjustments of nodal distances

In order to solve the problem in the Lagrangian coordinate system, the geometric parameters such as nodal volumes, surface areas and nodal distances must be progressively adjusted with time in accordance with the deformation history of the flow region. Now, while it is fairly easy, computationally, to make adjustments to the nodal volumes as time progresses (on the right hand side of (V.9)), it is far more cumbersome to make such progressive adjustments to nodal distances and surface areas, which occur on the left hand side of (V.9).

It is worth noting at this point that since volume involves the third power of distance, the geometric parameter likely to change by the maximum magnitude, in general, is the volume. Moreover, since, on the left hand side of (V.9) surface areas occur in the numerator and nodal distances in the denominator, one could intuitively expect that their changes due to deformation would tend to compensate each

other's effect. Therefore, it seems reasonable to infer that, except in extreme cases, ignoring adjustments to nodal distances and surface areas on the left hand side of (V.9) may not affect accuracy very adversely.

In the particular one-dimensional problem studied, all the deformation is in one direction and hence, the change of volume is of the same order as the magnitude of the change of nodal distances. This problem, therefore, poses an extreme case in which the errors due to ignoring changes in nodal distances is likely to be maximum, and hence merits further attention.

Figure 35A shows the computed consolidation rate from a model in which the nodal distances, $d_{m,n}$ and $d_{n,m}$ and the nodal elevations, z_m and z_n were held constant on the left hand side while the variation of nodal volume was properly taken into account in the fluid mass capacity term (M_c) on the right hand side of (V.9). For convenience, we will call this a rigid mesh. Now, since the column is consolidating, the nodal points get closer and closer together with time and hence, the nodal distances must continuously decrease in magnitude. In the rigid mesh, this decrease is ignored, and, as a consequence, the fluxes calculated on the left hand side of (V.9) tend to be smaller than what they should otherwise be. The result is that the rigid mesh solution indicates a much slower rate of consolidation than the rigorous solution, as seen in figure 35A.

Looking at the left hand side of (V.9), it can be reasoned that instead of applying corrections to the d's in a rigorous manner, we could, computationally speaking, keep the mesh rigid, but apply an equivalent opposite correction to the permeability term, $K_{m,n}$.

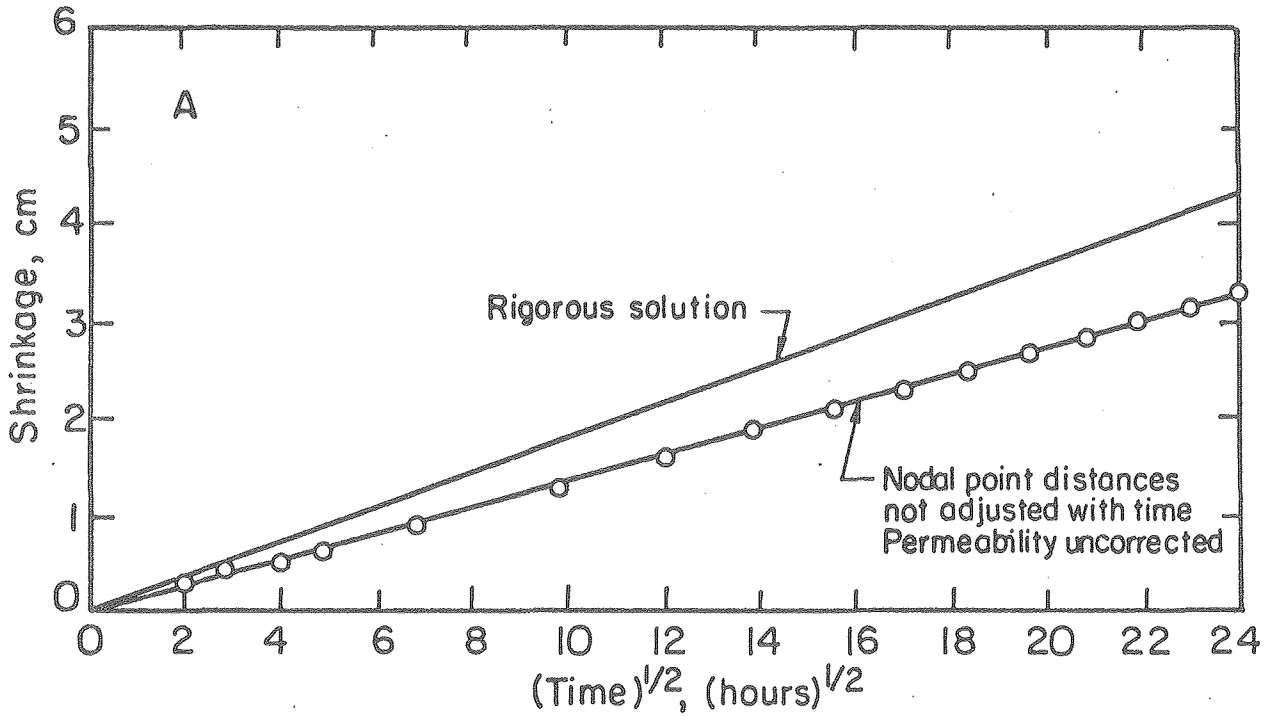

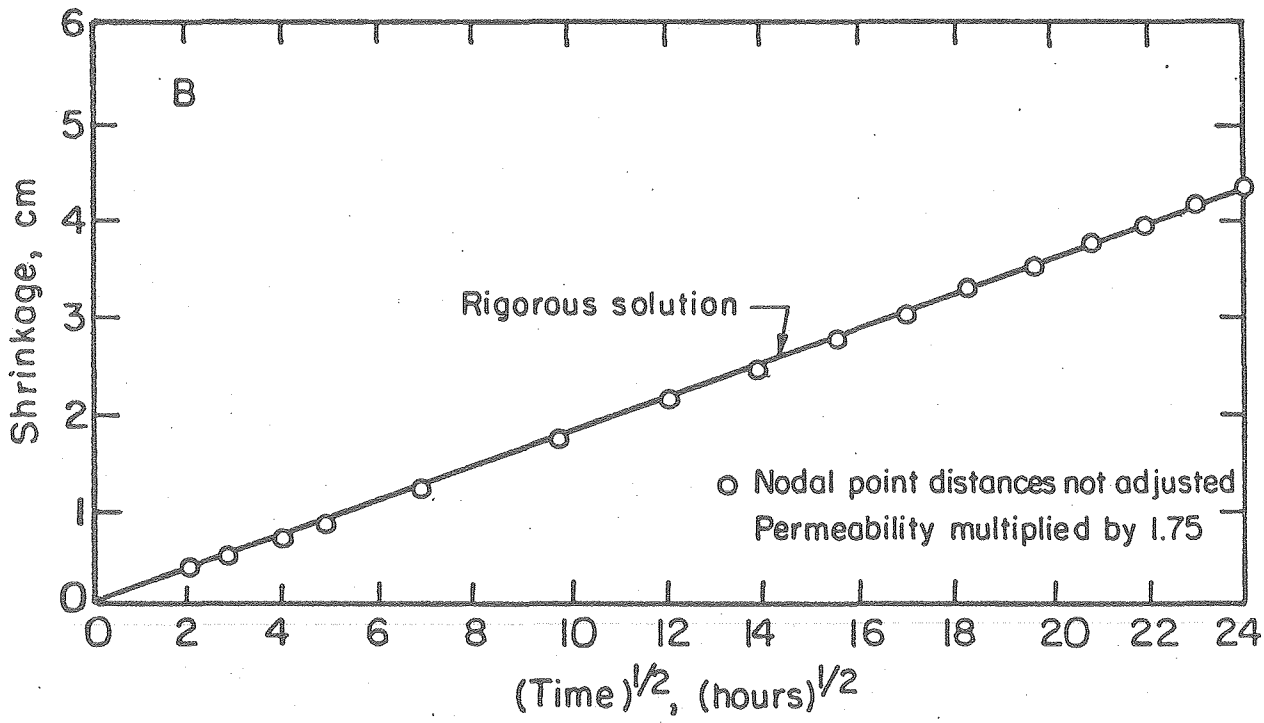

Fig. 35. Consolidation of clay slurry; effect of ignoring nodal point displacements on the rate of consolidation, A. permeability unconrrected, B. permeability multiplied by 1.75

Thus, instead of decreasing the d's, which occur in the denominator, one could increase $K_{m,n}$ by an appropriate amount and still get numerically accurate results.

With this reasoning in mind, the permeability values of the rigid mesh problem of figure 35A were arbitrarily multiplied by a factor of 1.75 (by shifting the e versus log K curve appropriately to the right in figure 31B) and the calculations were repeated. The results of these calculations are presented in figure 35B. It is readily seen from this figure that the solution for rigid mesh with increased permeability practically coincides with the rigorous solution.

These results lead to some inferences of practical interest:

i) a single, simple correction to permeability seems capable of adequately compensating for the far more complex task of deforming the mesh with time

ii) in the particular problem studied, the equivalent correction turned out to be multiplication by a factor of 1.75 (increasing permeability by 75 per cent). However, the precision of measuring the permeability function experimentally is such that an error of 100 per cent may often be considered tolerable. Thus, the error accrued using a rigid mesh as above appears to be of the same order of magnitude as that introduced due to errors in the input values of permeability, which ranged from 10^{-6} to 10^{-8} cm/sec.

iii) in the present problem, the overall shrinkage at the end of 24 days was about 32 per cent of the original length of the column. During the same period, the maximum strain in the bottom most element attained a value of about 64 per cent. Even though the deformations encountered in this problem have thus been large, the required permeability correction was only 75 per cent. In actual field problems involving soil engineering far smaller deformations are likely to be encountered. In such cases, the required permeability corrections should be expected to be so small that they would be well within the precision of the experimental measurement of permeability

iv) for most field problems, therefore, one could use a rigid mesh in the manner described above and still get reasonably accurate results. However, if it is desired to minimise the errors using the rigid mesh, one could apply appropriate corrections to permeability. For this, one

would need to know, a priori, the magnitude of correction to be applied. A possible method of determining the correction factor would be to carry out a parametric study by comparing rigorous and rigid mesh solutions in a wide variety of cases and determining the corresponding correction factors. The correction factors so obtained can be expressed as function of C_c or total deformation .

e. Deforming and non-deforming coordinates

De Wiest (1969), in discussing the concept of storage coefficient, draws attention to the fact that Jacob's (1950) derivation of the mass-conservation equation of groundwater flow considers a deformable volume element for time rate of change in potential, while, on the other side of the equation considers a non-deformable element for flux calculations. To get over this inconsistency, De Wiest then proceeds to redefine specific storage in a fixed coordinate system.

If we consider a saturated flow region and ignore the compressibility of water, it is obvious that the volume of the flow region must decrease by an amount equal to the volume of water released from storage. Therefore, we cannot assume that the overall flow region remains fixed in dimensions and does not change with time, which would be possible only if additional porous material is continuously added to the system, which is not realistic. Therefore, one cannot formulate the overall problem in a fixed coordinate system and so, physically, the formulation in terms of a deforming volume element is more logical. In the light of what we saw in the case of the rigid mesh, we can interpret Jacob's derivation as pertaining to a deforming, material volume element, but ignoring, as a reasonable approximation, the effects of deformation on surface areas and nodal distances in evaluating the fluxes. Interpreted in this fashion, Jacob's derivation is of practical utility in handling problems of groundwater flow.

5. RAINFALL INFILTRATION

An interesting problem involving unsaturated flow is that of the infiltration of rainfall into extremely dry soils. In considering soil-water relations during rain infiltration, Rubin and Steinhardt (1963) showed that ponding of water on the soil surface can result only if the rainfall intensity exceeds the saturated hydraulic conductivity of the soil. If the rainfall intensity is less than the latter, the soil would tend to attain that uniform saturation at which the rainfall intensity exactly matches the hydraulic conductivity. To demonstrate this, they considered a semi-infinite, vertical column of Rehovot sand (porosity 39.7 per cent) on whose surface, rain was assumed to fall at a constant rate (figure 36). The sand itself is initially very dry, with a saturation of about 12.6 per cent (moisture content, 0.5 per cent). The hydraulic conductivity, K, as well as moisture content, θ, are highly nonlinear functions of moisture suction, as shown in figure 37. Empirically, these functions were fitted to the following equations by Rubin et al. (1964):

$$-\psi = \text{suction in millibars}$$

$$= 11.3 + \frac{3.19}{\theta} - 0.05\, e^{15\theta} + e^{-575\theta} + 16.3 \qquad \text{(V.10)}$$

$$K = \text{Hydraulic conductivity in cm/sec}$$

$$= 8400/(-\psi^5 + 14.45^5) \qquad \text{(V.11)}$$

Because of the very strong dependence of moisture content on moisture suction, the initial pressure head distribution in the

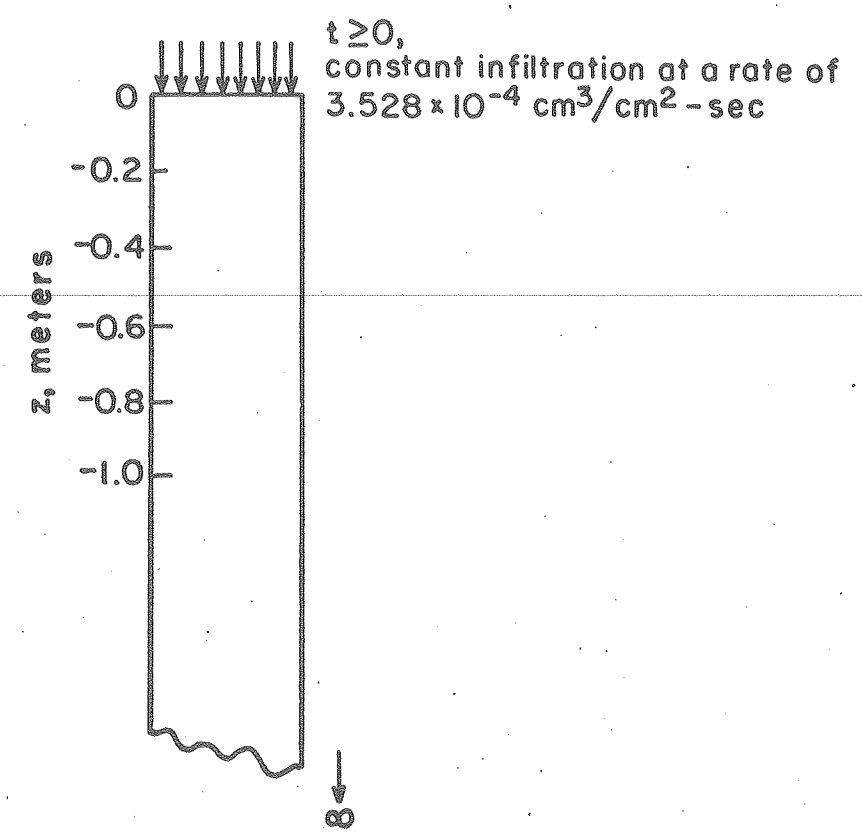

Fig. 36. Rainfall infiltration; initial and boundary conditions

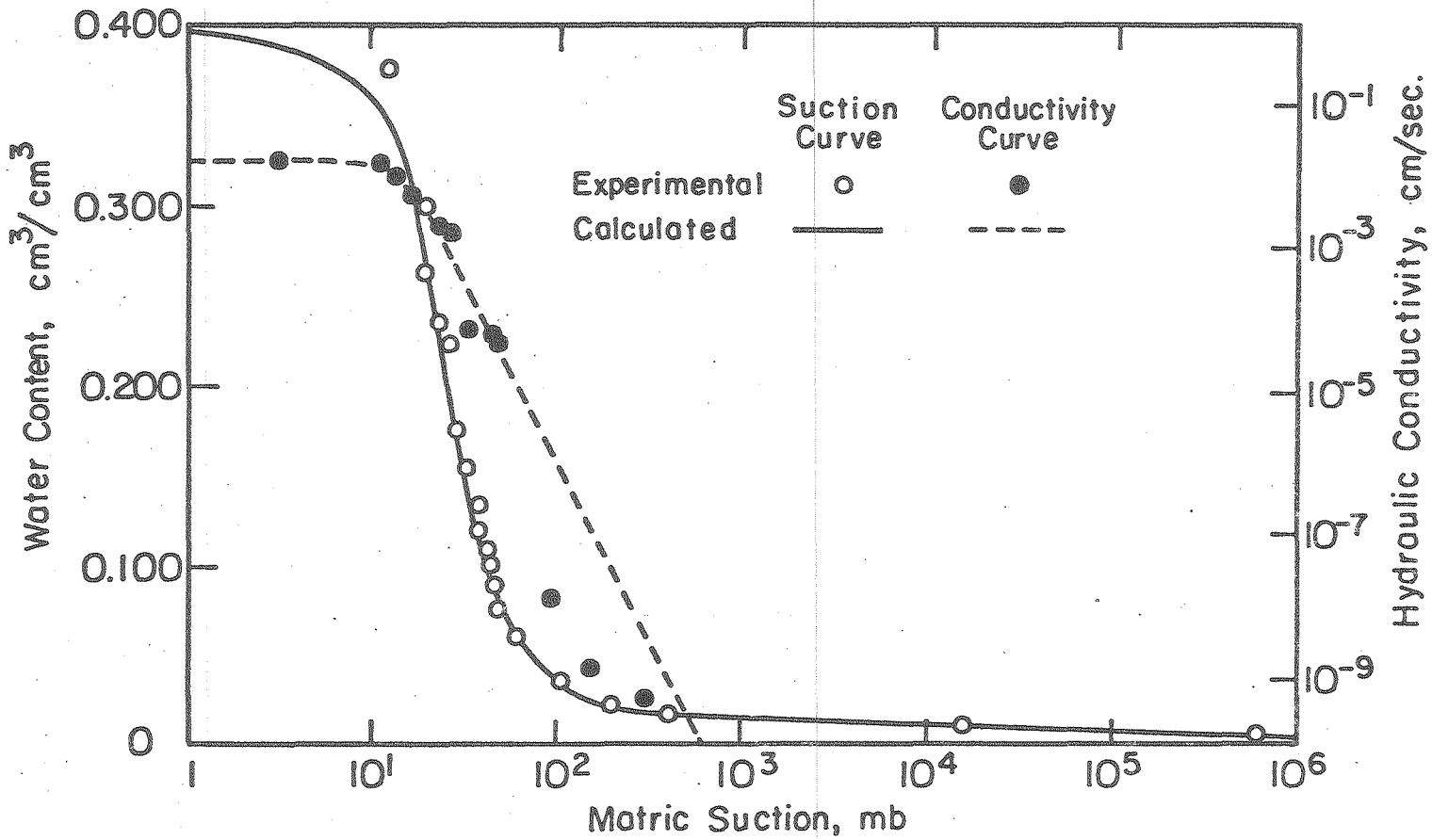

Fig. 37. Rainfall infiltration; material properties (after Rubin et. al., 1964)

semi-infinite column at time t_o had a very large negative value and was computed to be about -6.77×10^5 bars or -6.69×10^3 meters of water. Computations also indicate that at a moisture content of about 0.168 (suction head of about 30 millibars or 0.3 meters of water), the hydraulic conductivity of the soil would equal the assumed rainfall intensity of 3.528×10^{-4} cm/sec. Between the initial moisture content of 0.005 and the final moisture content of 0.168, the pressure head changes over five orders of magnitude, while the hydraulic conductivity has to change over ten orders of magnitude. Because of this, in the governing equation with ψ the dependent variable,

$$\int_S K\vec{\nabla}(z + \psi) \cdot \vec{n}\, d\sigma = \int_S (K\vec{\nabla}z + K\vec{\nabla}\psi) \cdot \vec{n}\, d\sigma = M_c \frac{\partial\psi}{\partial t} \tag{V.12}$$

K and M_c are so strongly dependent on ψ that it is extremely difficult to solve (V.12). However, the difficulty could be overcome if we can use the θ-based equation instead of (V.12):

$$\int_S [K\vec{\nabla}z + D\vec{\nabla}\psi] \cdot \vec{n} = \frac{\partial\theta}{\partial t} \tag{V.13}$$

in which, $D = K\,(d\psi/d\theta)$, is the soil moisture diffusivity.

Rubin and Steinhardt successfully used (V.13) to numerically solve the rainfall infiltration problem with a finite difference scheme.

The fact that the infiltration problem is amenable to solution

with the θ-based equation suggestes that between adjacent nodal points the variation of θ is more linear than that of ψ. Hence, in addition to the difficulty of the strong non-linearity of K and M_c, an added difficulty in the case of the ψ-based equation is that the assumption of linear variation in potential between adjoining nodal points would be incorrect.

However, since most problems of unsaturated flow can be solved using the ψ-based equation, it is of interest to investigate if the θ-based equation could be suitably transformed and incorporated into the scheme of the ψ-based equation.

Consider the second integral in (V.12). We have seen that $\vec{\nabla}\psi$ in this integral cannot be computed on the assumption of linear variation in potential between adjoining nodal points. But, since θ can be assumed to vary linearly, we could compute an equivalent $\vec{\nabla}\psi_{m,n}$ at the interface between nodal points m and n by the relation,

$$\vec{\nabla}\psi_{m,n} = (d\psi/d\theta)\vec{\nabla}\theta_{m,n} \qquad \text{(V.14)}$$

Therefore, in order to evaluate the gradient term in the second integral in (V.12), we could evaluate $d\psi/d\theta$ at the interface between the nodal points of interest and multiply it by the gradient of θ between the nodal points.

Using this procedure, the infiltration problem of Rubin and Steinhardt was solved with the IFD scheme. In the solution the sand was assumed rigid and the suction stresses were assumed to have

no effect on the density of water and hence, ρ was constant.

The computed positions of the moisture profiles, as a function of time, are shown in figure 38, along with Rubin-Steinhardt's results. A good agreement between the two results is readily seen from the figure. It can also be noticed that the sand tends to attain a constant moisture content of approximately 0.168.

Although the relation (V.14) helped avoid the difficulty due to non-linear variation of ptential between nodal points, the problem of the strong dependence of K and M_c on ψ could not be avoided in the IFD solution. Thus, the solution became either unstable or convergence could not be assured when the hydraulic conductivity or M_c varied too much between successive time steps. As a result, very small time steps had to be taken to get a smooth solution. Due to the need for choosing very small time steps, adapting the ψ-based solution in the manner suggested in (V.14) may not be economical for practical purposes. The best method of handling this type of problem would probably be to write a separate program for the θ-based equation. As pointed out at the end of chapter II, such a program would be able to handle flow regions that are composed of only one material.

6. ONE-DIMENSIONAL COLUMN DRAINAGE

The next problem we shall consider is that of drainage of water from a vertical column of sand, initially at saturation and progressively becoming unsaturated due to gravity drainage.

Liakopoulos (1965) in his doctoral work on transient flow of water through unsaturated porous media, conducted several experiments on the drainage of water from vertical columns of sand (Del Monte

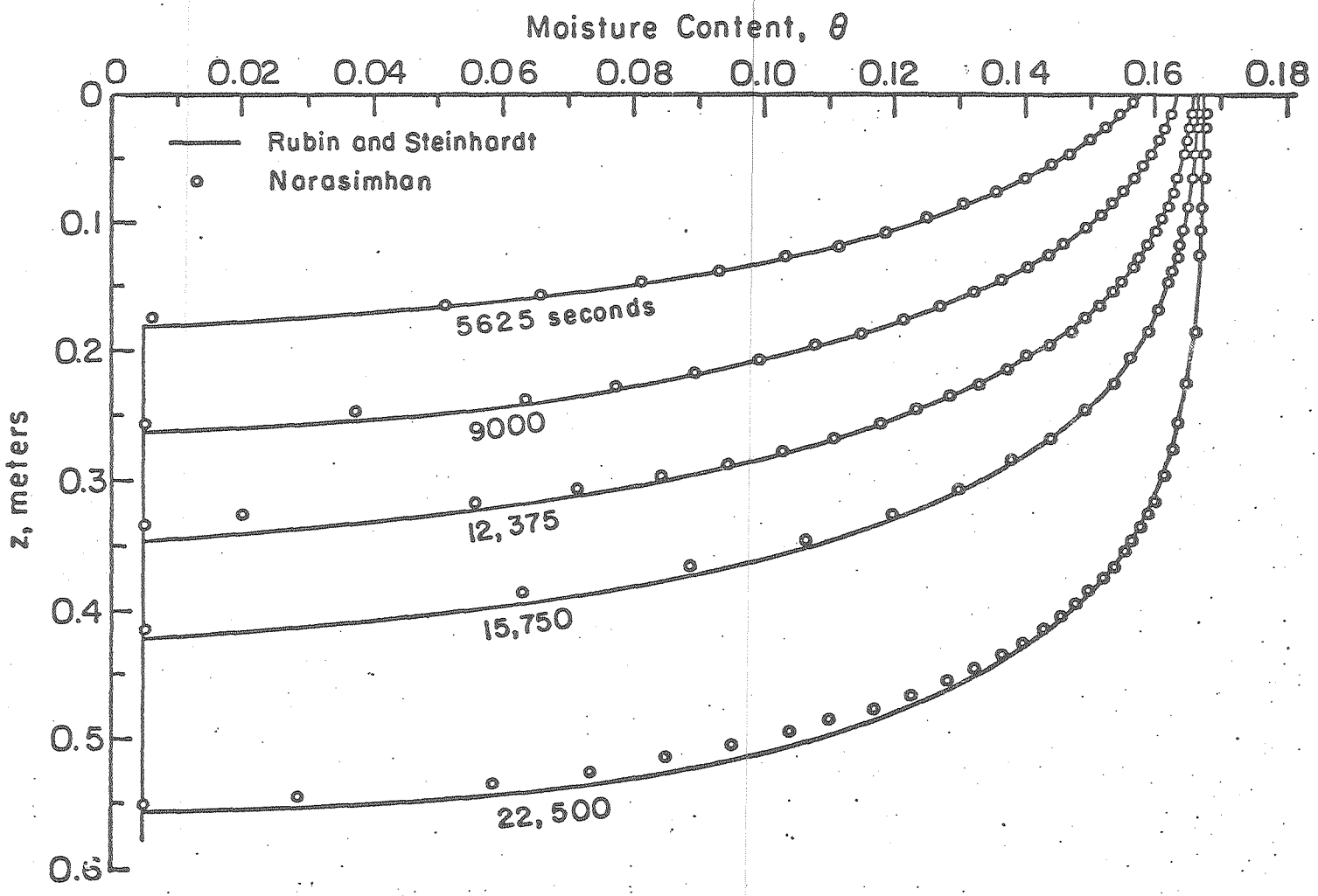

Fig. 38. Rainfall infiltration; moisture profiles as a function of time

sand). One of Liakopoulos' experiments is chosen for the present simulation with the IFD method.

The experimental set up is diagrammatically represented in figure 39. A one-meter tall perspex column was packed with Del Monte sand. At regular intervals within the column, tensiometers were placed to monitor pore pressure changes. Prior to the experiment, water was continuously added at the top of the column and was allowed to drain freely at the bottom through a micro-pore filter. The flow was regulated and continued until all the tehsiometers in the column recorded zero pore pressure. This meant that the vertical gradient in potential became unity ($\partial\phi/\partial z = 1$). On attaining this initial condition, the addition of water at the top was stopped and the upper boundary of the column was rendered impermeable. From then on, the pressure heads measured by the tensiometers were carefully noted at various instants of time. In addition, the drainage rates at the bottom of the column were also measured as a function of time. The aim of the numerical simulation is to reproduce the experimentally observed profiles of pore pressure and drainage rates.

The physical properties of the Del Monte sand were determined by Liakopoulos with a separate set of experiments. The sand had a porosity of about 29.75 per cent. The dependences of moisture content (θ), saturation (S), and permeability (k), as deduced from the experimental data are shown in figure 40. It can be seen from figure 40 that both θ and S remain unchanged in the range: -0.2 m. $\leq \psi \leq 0$ m. However, when the critical value of -0.2 m. is reached, the capillary stresses reach a maximum value and thereafter, the effective stress on the soil skeleton remains essentially constant and no further compression occurs

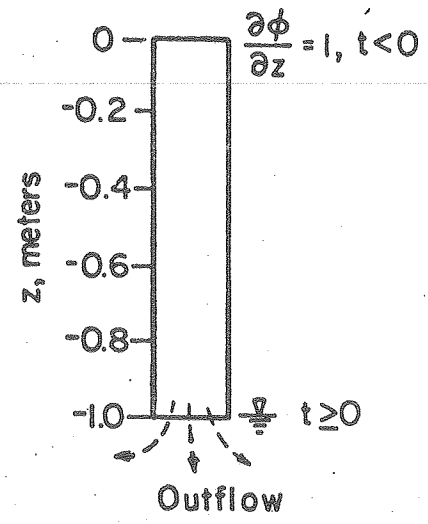

Fig. 39. Column drainage in Del Monte sand; initial and boundary conditions

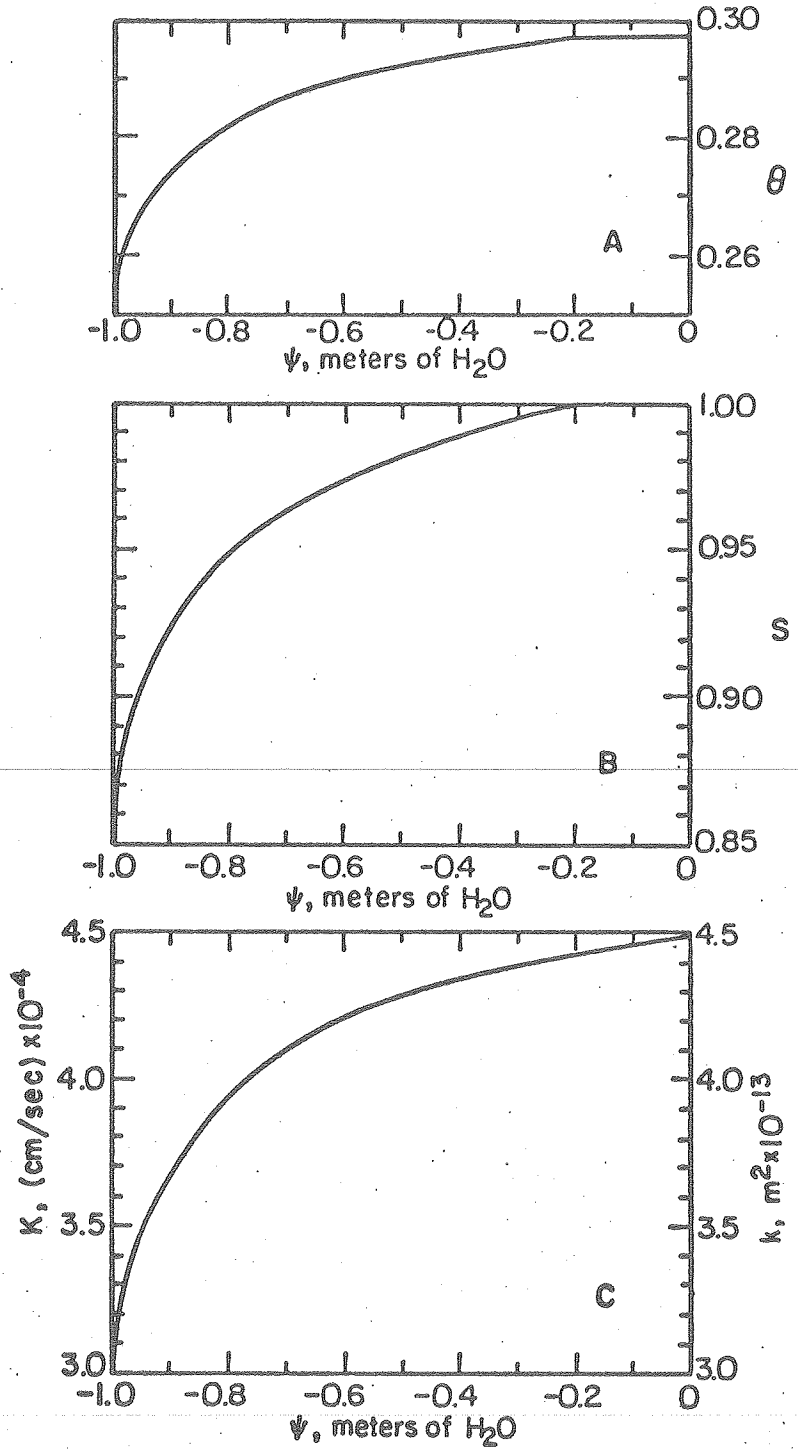

Fig. 40. Column drainage in Del Monte sand; material properties, A. moisture content versus pressure head, B. saturation versus pressure head, C. permeability versus pressure head

as desaturation commences. The critical value refered to above is sometimes called the "air-entry" value.

For purposes of numerical simulation, the column was divided into ten nodes (elements) of equal size. The results of the numerical simulation is summarized in figures 41 and 42.

As a first step in the simulation, the sand was assumed non-deformable and rigid, as is cistomarily done in dealing with unsaturated flow. The profiles of pore pressure computed with this assumption can be seen in figure 41A. It is seen from this figure that although the computed and the experimentally observed values agree fairly closely after about 10 minutes from the start of the experiment, the computed suctions are markedly greater than the observed suctions at the end of 5 minutes. In this context we note that at the end of 5 minutes, the experimentally observed pressure heads have not fallen below -0.2 m. anywhere within the column. Theoritically, therefore, no drainage should have occurred during this interval since the sand is assumed rigid and the pressure head changes are too small to allow for significant changes in water density. However, the experimental data indicate that drainage had occurred during the first five minutes. The most reasonable conclusion that one could draw from this is that during this interval the drained water was released from storage by a slight deformation of the soil skeleton and the consequent decrease in void volume.

The next step in the numerical simulation was therefore to investigate whether better simulation of experimental results could be achieved by assuming the sand to be deformable.

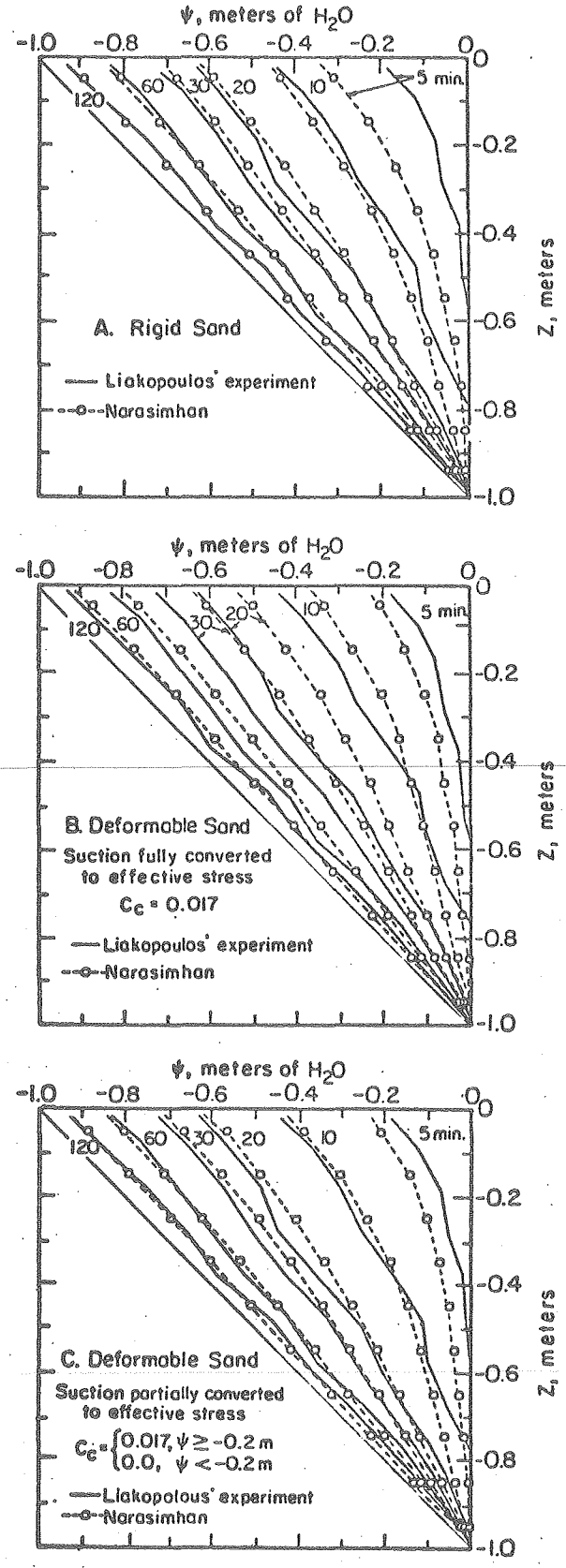

Fig. 41. Column drainage in Del Monte sand; comparison of numerical and experimental results, A. rigid sand, B and C. deformable sand

Moisture suction and effective stress

In order to assess the role of the deformation of the sand on the drainage process, the Del Monte sand was aribitrarily assigned a C_c value (compression index) of 0.017, which was assumed to be reasonable for an unconsolidated sand. At the start of the experiment, the effective stress at a nodal point 0.55 m. from the top of the column is approximately equal to 0.825 m. of water or 8.1 newtons/m^2. At this low effective stress, a C_c value of 0.017 would amount to a coefficient of compressibility (a_v) of approximately 2.1×10^{-6} m^2/newton or $m_v \simeq 1.7 \times 10^{-6} m^2$/newton.

Using the assumed value of C_c, a second simulation was carried out. In this simulation, it was assumed that whatever suction stress that may develop in a node is fully converted into effective stress. If we recall the governing equation for saturated-unsaturated groundwater flow (II.41), the above assumption would imply that the factor χ is set to 1 in the unsaturated zone also.

The results of this simulation are presented in figure 41B. It is seen from figure 41B that although there is a slightly closer agreement between the results at the end of five minutes, for larger values of time, the computed pore pressures are consistently higher than the observed values, indicating that in the numerical simulation, the porepressures are not falling as rapidly as they should. This suggests that the fluid mass capacities of the elements are probably too high, which indeed is the case since the elements are not only desaturating but also deforming.

From these we could infer that while the deformation process is important at small values of time (and hence, small values of

suction) deformation should decrease or even cease at higher magnitudes of suction. If this were so, the factor χ cannot be unconditionally set to 1 in the unsaturated zone. Instead, it should be a function of the pressure head ψ. In the absence of any data on the nature of the parameter χ for Del Monte sand, the following arbitrary assumption was made about χ for purposes of numerical simulation:

$$\chi = \begin{cases} 1, & \psi \geq -0.2 \text{ m.} \\ 0, & \psi < -0.2 \text{ m.} \end{cases} \qquad \text{(V.15)}$$

Equation (V.15) implies purely saturated conditions of flow above air-entry value and purely unsaturated conditions of flow below air-entry value.

In the third and final simulation, equation (V.15) was used in conjunction with a C_c value of 0.017. The results of this simulation are presented in figure 41C. Figure 41C clearly indicates that the experimental and the computed results agree reasonably closely at early as well as late times.

The results presented in figures 41A,B and C indicate that in the transition zone between saturated and unsaturated flow, deformation of the soil skeleton cannot be ignored.

The experimentally observed rates of drainage from the bottom of the column and the numerically computed rates are compared in figure 42. It can be seen that there is satisfactory agreement between the two.

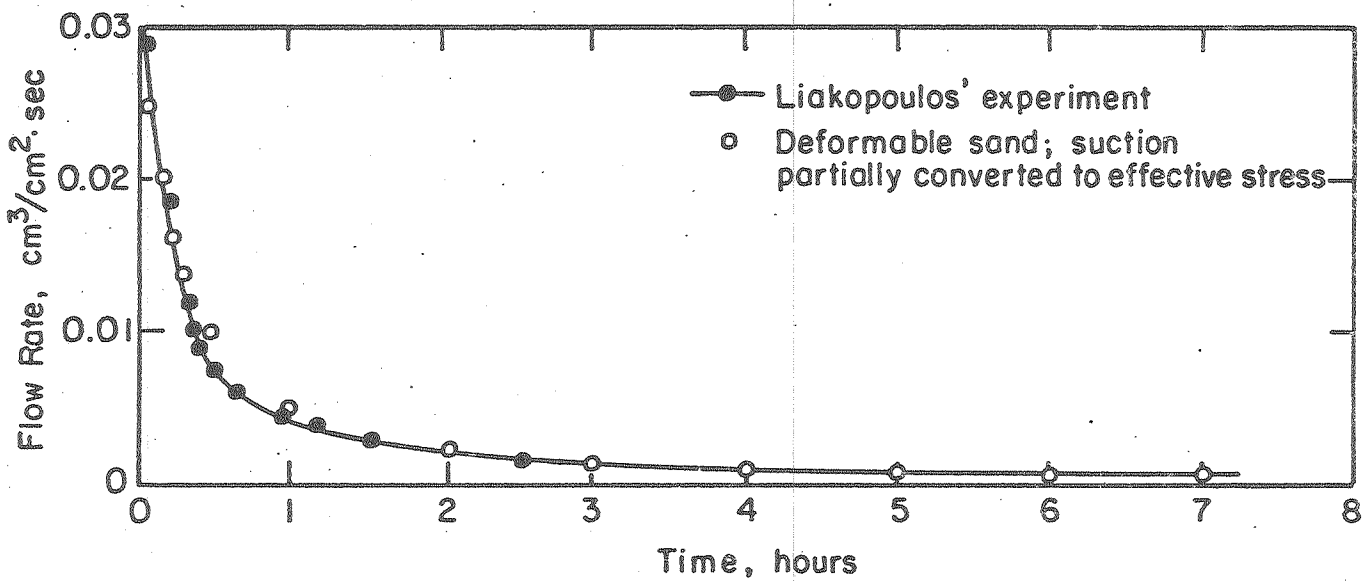

Fig. 42. Column drainage in Del Monte sand; comparison of numerical and experimental drainage rates

7. DRAINAGE FROM SAND BOX

Experimental data available in the literature on drainage or infiltration from sands usually pertain to one-dimensional models. Good quality experimental data on two dimensional models are hard to obtain , primarily because of the difficulties involved in setting up and carrying out such experiments. Recently, Vachaud and his co-workers in Grenoble, France (Vachaud et al., 1971) conducted very carefully controlled experiments on drainage and infiltration from from a two-dimensional sand box model, and their experimental data probably constitute some of the best available information on the subject. Therefore, one of the drainage experiments of Vachaud et al. was chosen for simulation by the IFD scheme used in this thesis. The results of the simulation are presented below.

The experimental sand box measures 3m. long, 2 m. tall and 0.05 m. deep (figure 43). The left hand and the right hand side of the sand box are left free to enable entry and exit of water, while the remaining four sides are rendered impermeable.

Before the start of the experiment, $t < 0$, the water table was brought to a height of 1.43 m. above the base, by letting the water levels on the left hand side and on the right hand side of the model stand at that elevation for a long period of time. At $t = 0$, the water level on the left hand side was suddenly lowered to an elevation of 0.8 m., creating a drawdown of 0.63 m., and was maintained at that elevation through the duration of the experiment. During the course of the experiment, lasting over 50 hours, the pressure heads were regularly measured with the help of 20 tensiometers distributed throughout the sand box. In addition, the distribution of moisture contents were

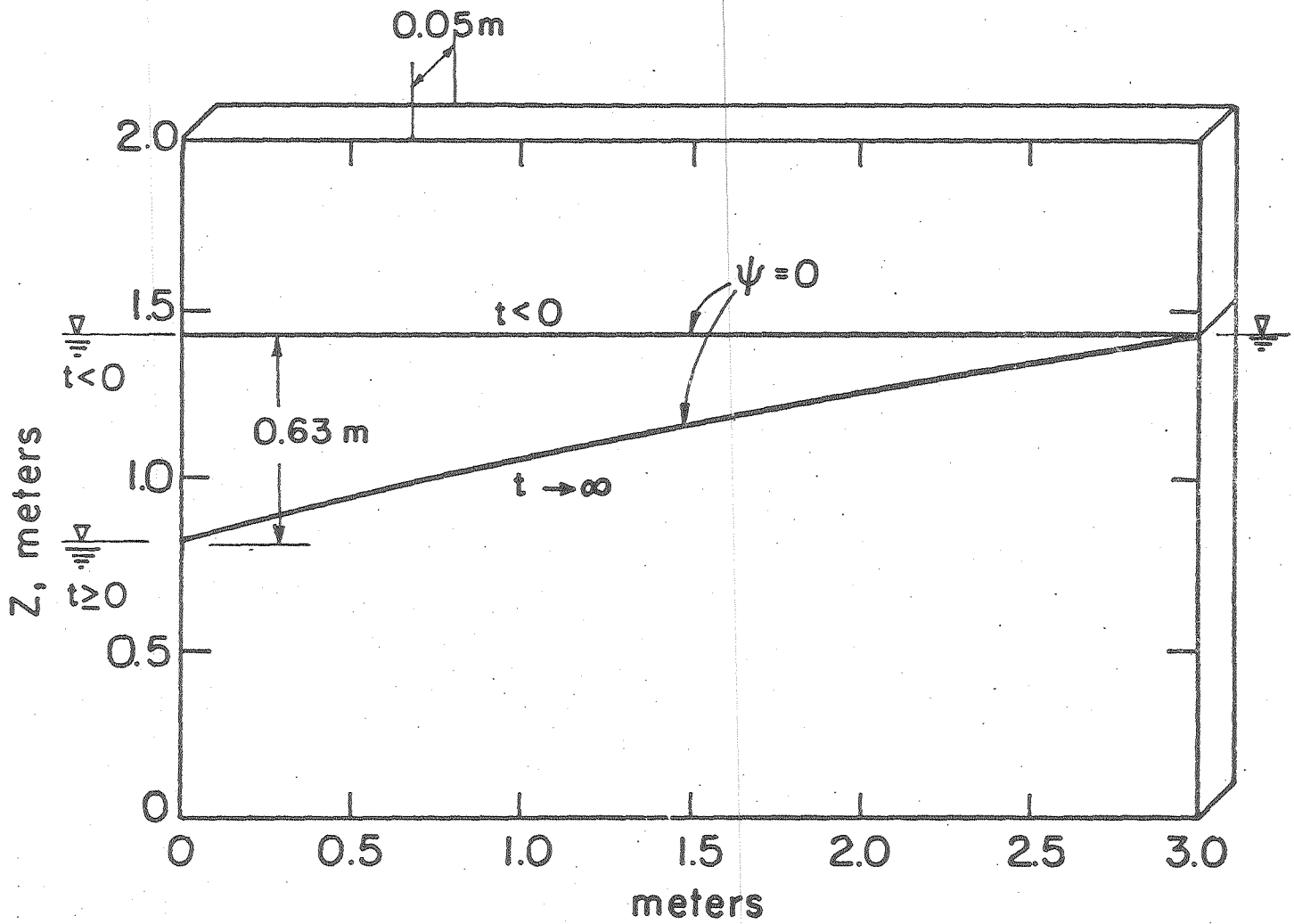

Fig. 43. Drainage from a sand box; initial and boundary conditions

also measured regularly with the help of a gamma-ray attenuation technique, using a movable platform and three sources of 241 Americium, continuously facing three photomultiplier detectors. The data collected during the experiments not only yielded information on ϕ, ψ, and θ as functions of space and time, but also provided data on the quantity of water actually removed from storage as a function of time.

The aim of the numerical simulation was to use appropriate material properties, boundary conditions, and initial conditions and to reproduce by calculation the observed distributions of ϕ, ψ, and θ and the observed rates of cumulative depletion from storage.

a. Material properties

The sand used in the experiment was a fine- to medium-grained sand, in which 10 to 90 per cent of the grains ranged in diameter from 0.1 to 0.5 mm. The median (50 percentile) was approximately 0.3 mm.

The experimentally observed relations between moisture content and pressure head, as well as those between permeability and pressure head are shown in figure 44. It can be seen from figure 44A that the porosity of the sand (θ at zero pore pressure) varied from 28 to 34 per cent. Moreover, the scatter of the data in figures 44A and 44B suggest that the physical properties of the sand within the model were appreciably varying from place to place. For purposes of numerical simulation, however, the sand was assumed to be homogenous with average values represented by the solid lines in figures 44A and 44B. These mean values are shown replotted in figure 45.

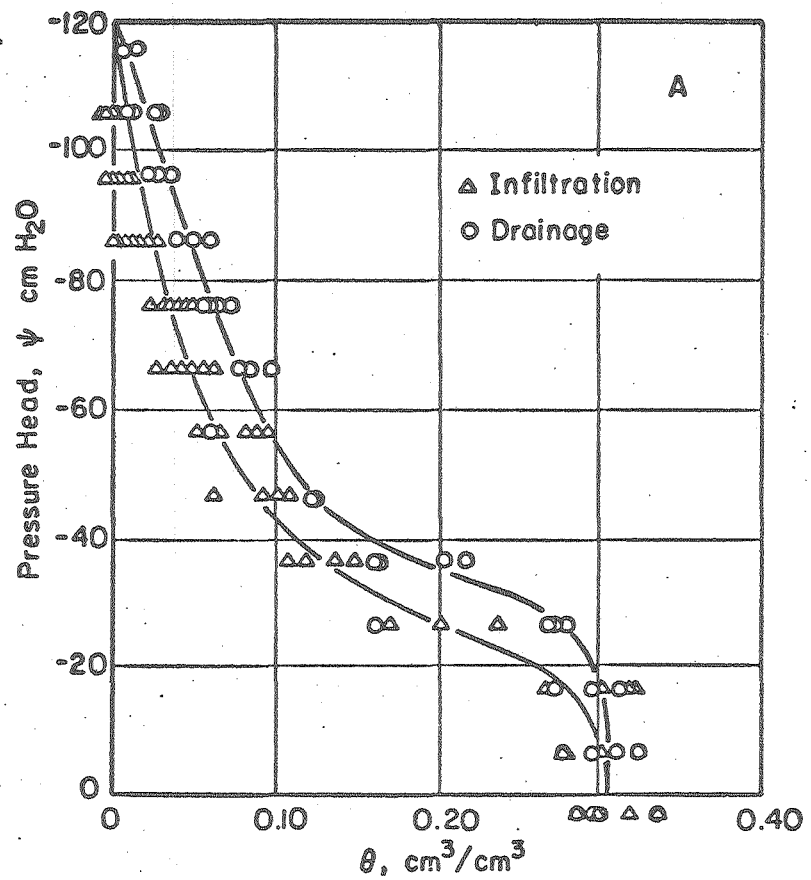

A. Mean curves of suction for infiltration and drainage.

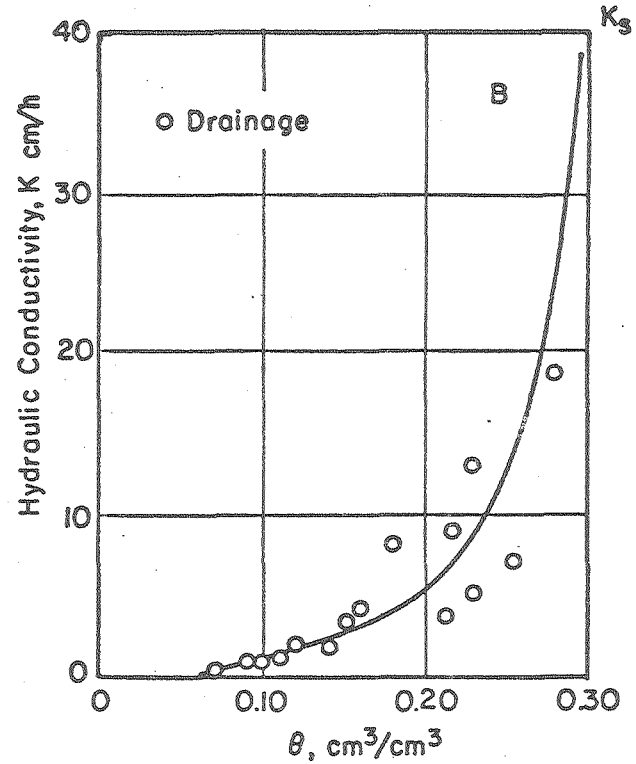

B. Mean curve of hydraulic conductivity.

Fig. 44. Drainage from a sand box; material properties, A. Mean curves of moisture content versus pressure head, B. Mean curve of permeability versus moisture content (after Vachaud et. al., 1971)

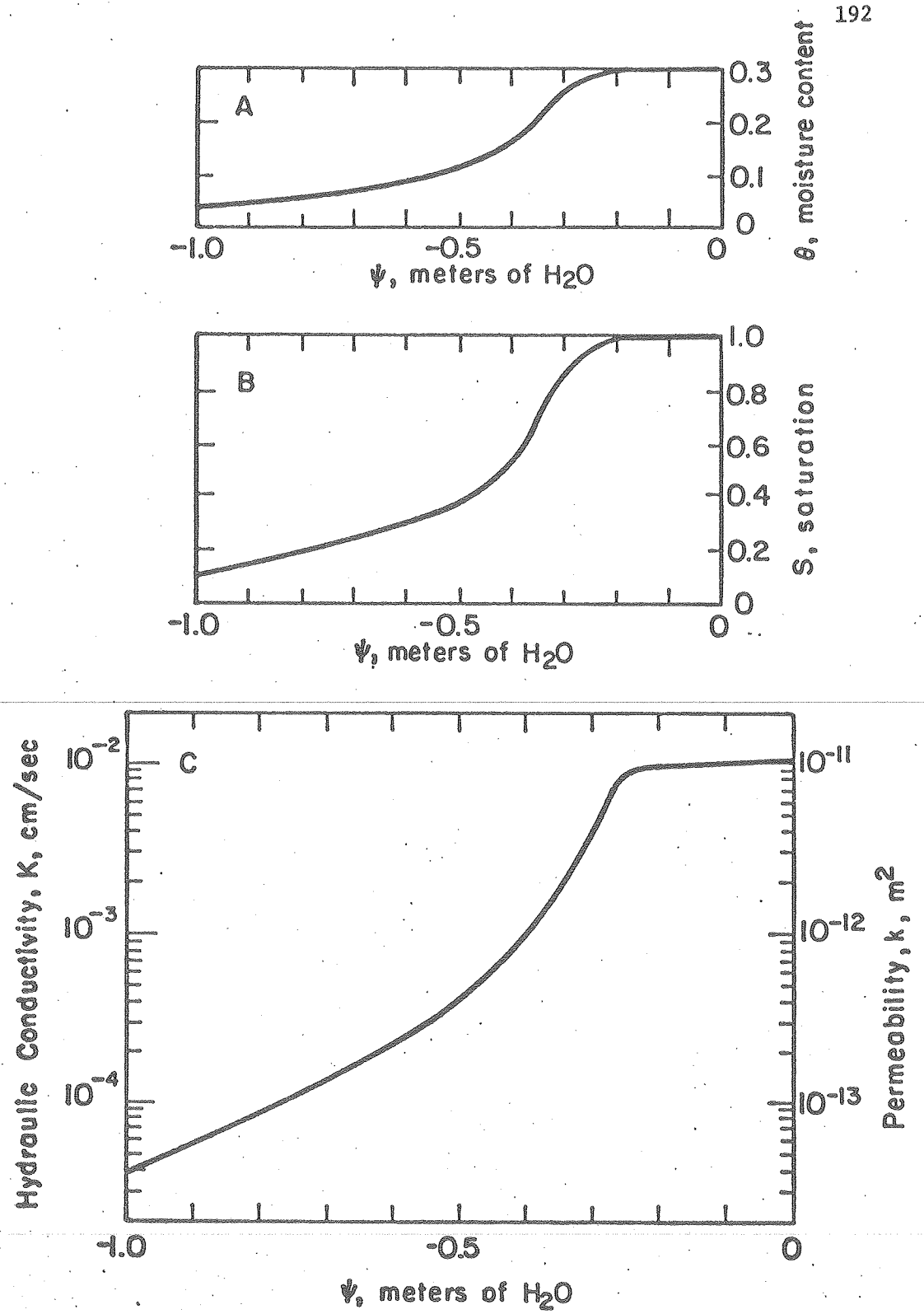

Fig. 45. Drainage from a sand box; material properties used in the simulation, A. moisture content versus pressure head, B. saturation versus pressure head, C. permeability versus pressure head

According to the authors of the experiment, hydrostatic equilibrium was initially obtained (for $t = 0$)as indicated by the profiles of pressure head in figure 46. The experimentally observed moisture profile (θ) corresponding to the initial hydraulic equilibrium is shown in figure 47. It can be seen from this figure that the saturated moisture content varies from 28 to 34 per cent in different parts of the flow region, indicating the heterogenous nature of the sand.

The hydrostatic equilibrium obtained, in conjunction with the uniform physical properties assumed for numerical simulation, gave rise to the simplified uniform initial condition as shown in figure 48, which was used in the numerical model.

In the numerical model, the flow region was discretized into 238 rectangular nodes (or elements) with a representative nodal point located at the center of each node. The boundary conditions were simulated by connecting the flow region through very thin nodes to the external, boundary potentials. Because of the initial hydrostatic equilibrium, at $t = 0$, the potential everywhere in the flow region was 1.43 m.

b. Role of deformation of the soil skeleton

An important question in connection with the numerical simulation is the treatment of flow in the saturated region. In soil physics literature, it is customary to assume the soil skeleton to be rigid when considering saturated-unsaturated flow. Vachaud and his associates have probably assumed the soil to be rigid and so have not provided any data on the deformation characteristics of the sand.

However, in order to evaluate the possible role which a deformable sand can have on the flow pattern in a situation like the present

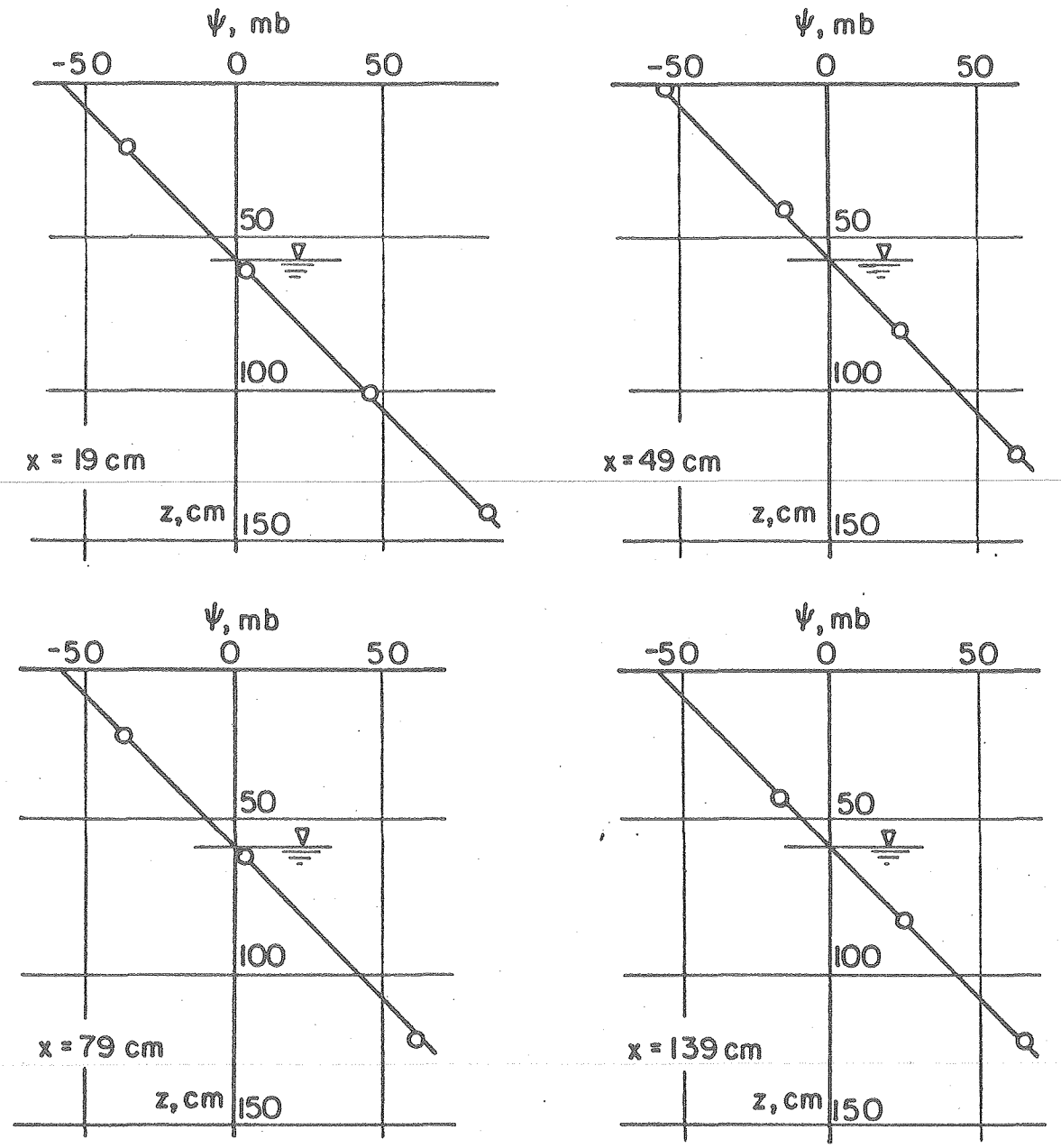

Fig. 46. Drainage from a sand box; initial distribution of pressure head at different abcissa (after Vachaud et. al., 1971)

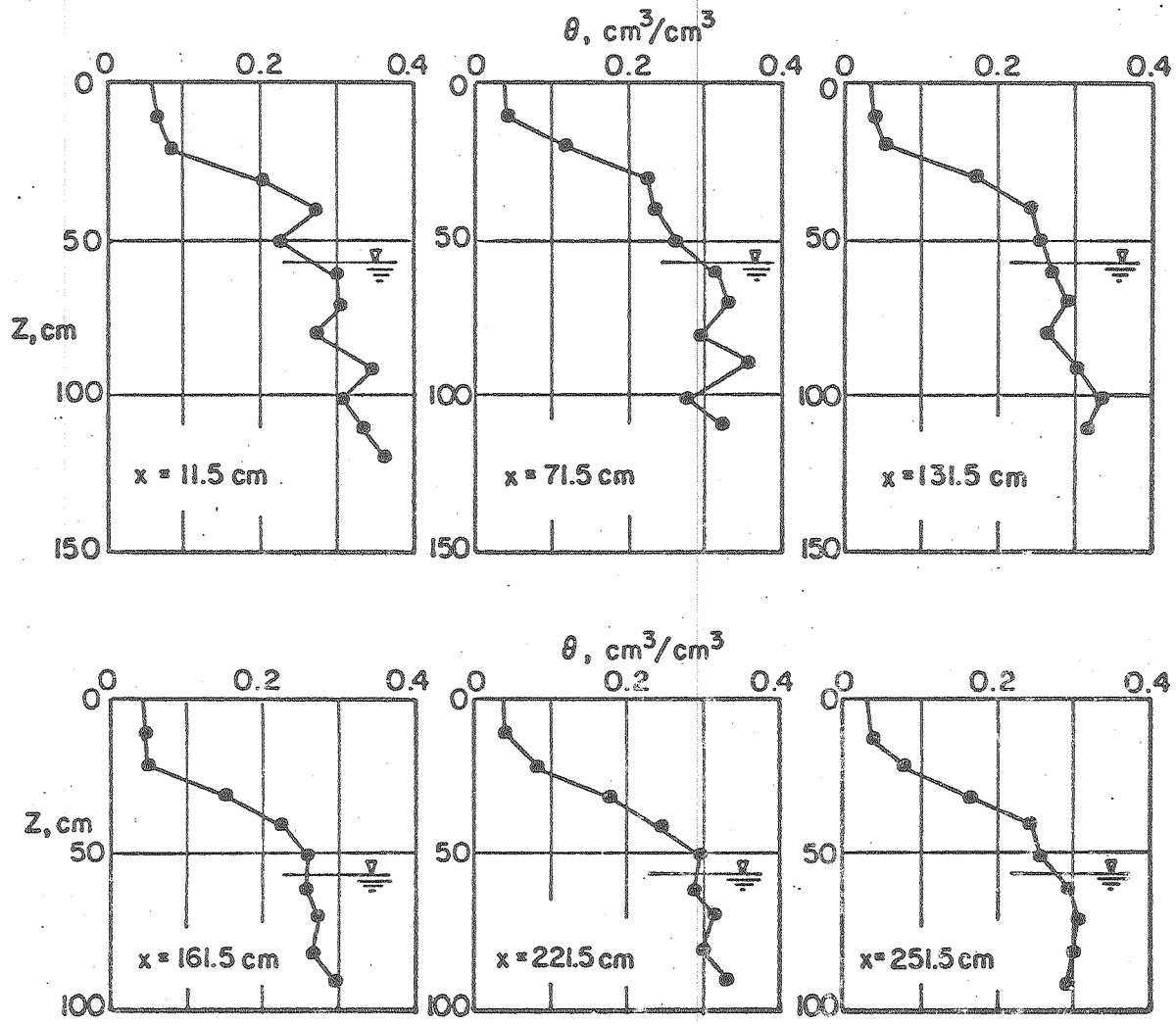

Fig. 47. Drainage from a sand box; initial distribution of moisture content at different abcissa (after Vachaud et. al., 1971)

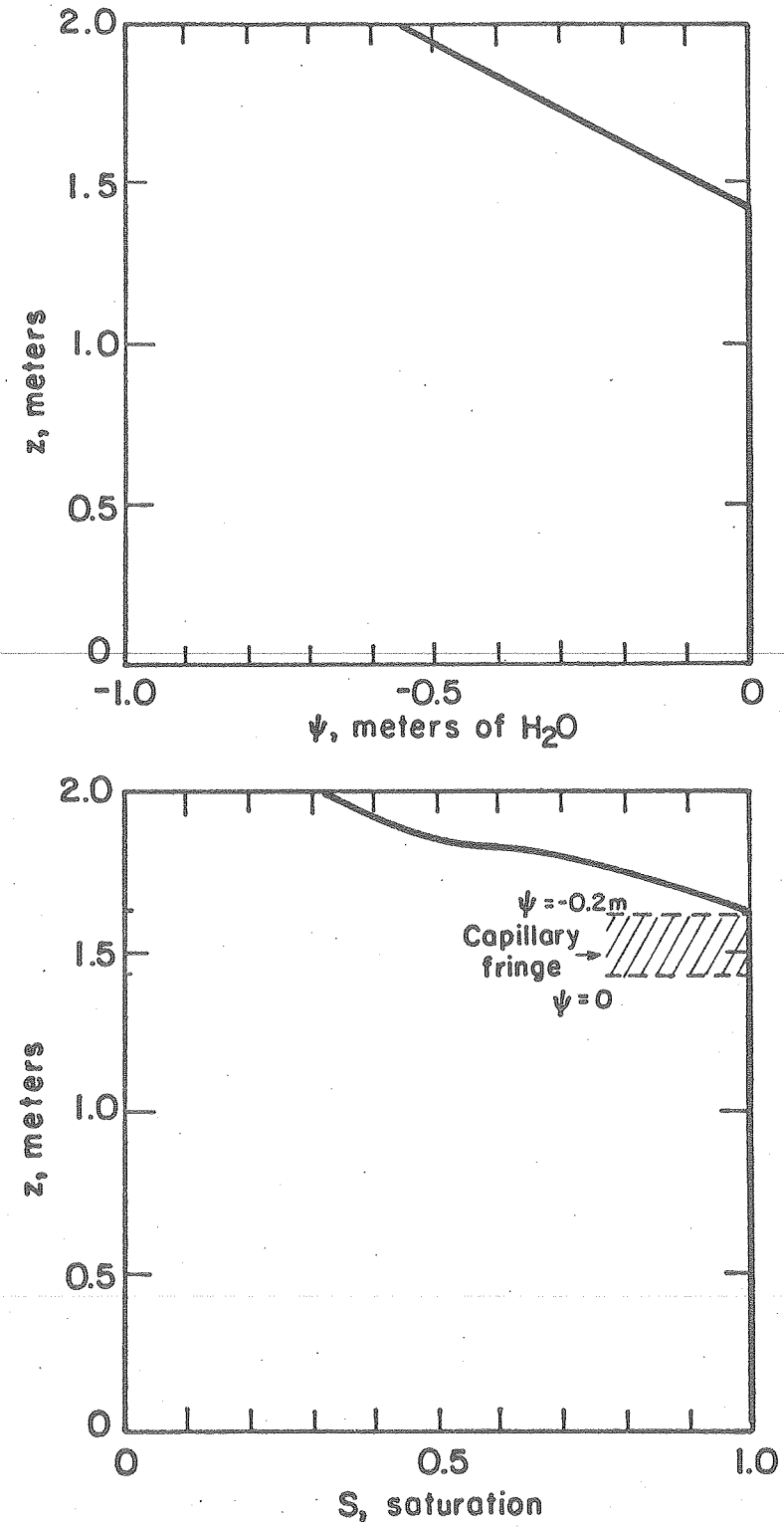

Fig. 48. Drainage from a sand box; initial distribution of pressure head and saturation used in the simulation

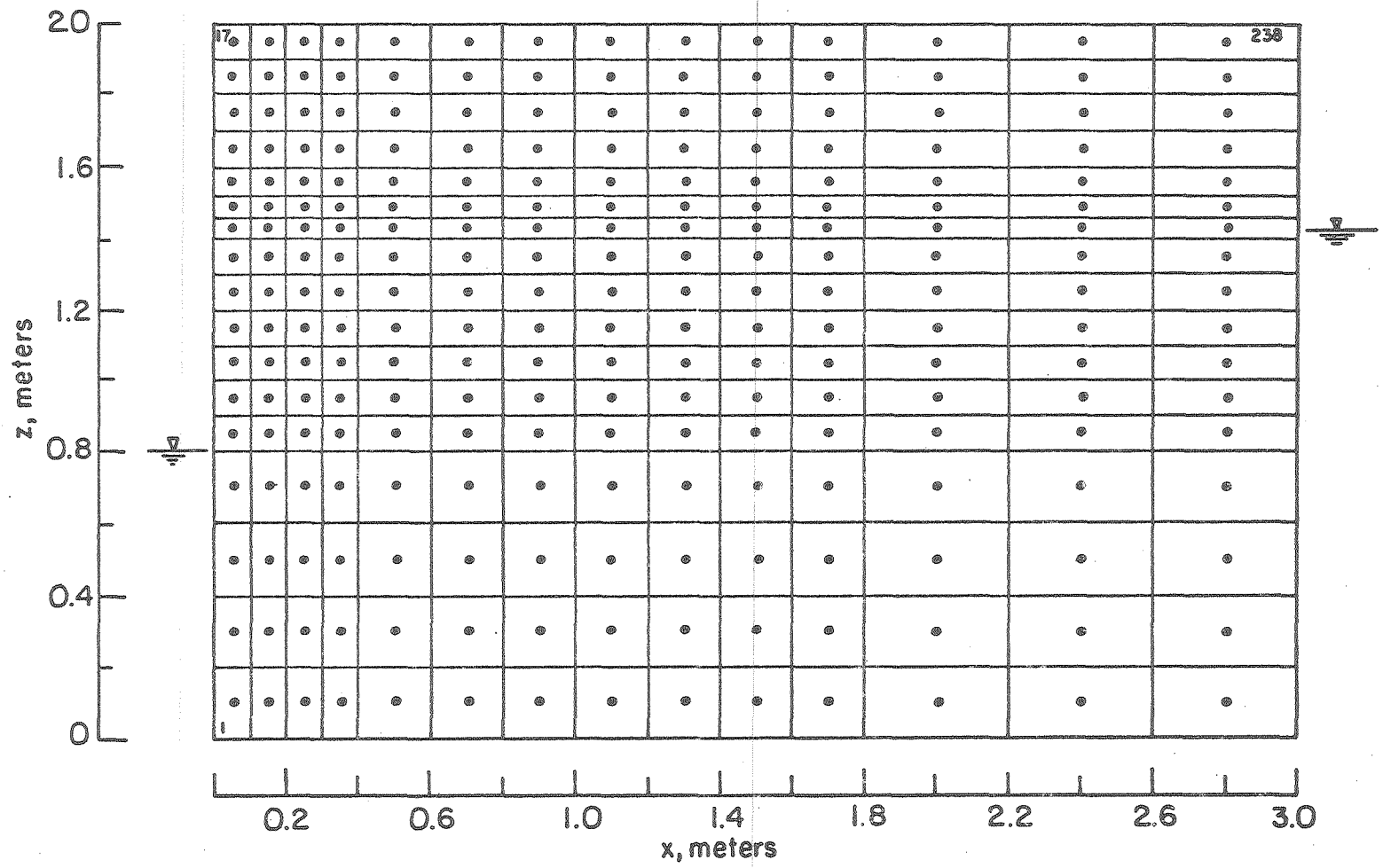

Fig. 49. Drainage from a sand box; discretization of the flow region

simulation, the numerical calculations were repeated for three hypothetical deformation characteristics assigned to the sand. These deformation characteristics ranged from $C_c = 1 \times 10^{-6}$ (rigid sand) through $C_c = 5 \times 10^{-4}$ to $C_c = 1 \times 10^{-2}$. To get a physical idea of their significance, these three values are expressed in terms of their equivalent a_v, m_v and S_s values, in Table I. The values shown on

TABLE V.I

Compressibility and related coefficients at t = 0 for a node located at an elevation of 1.05 m. above the bottom of the sand box

C_c	a_v		m_v		S_s	
	m^2/newton	ft^2/lb	m^2/newton	ft^2/lb	1/m, H_2O	1/ft, H_2O
1×10^{-6}	7.2×10^{-11}	3.4×10^{-9}	5.0×10^{-11}	2.4×10^{-9}	4.9×10^{-7}	1.6×10^{-7}
5×10^{-4}	3.6×10^{-8}	1.7×10^{-6}	2.5×10^{-8}	1.2×10^{-6}	2.5×10^{-4}	8.1×10^{-5}
1×10^{-2}	7.2×10^{-7}	3.4×10^{-5}	5.0×10^{-7}	2.4×10^{-5}	4.9×10^{-3}	1.6×10^{-3}

Table I pertain to points along a horizontal line 1.05 m. above the bottom of the sand box at time t = 0. Since, due to the process of drainage and the consequent pressure drops along this line the effective stress along this line must decrease with time, hence, the values of a_v, m_v and S_s must also decrease with time along this line and the

magnitudes tabulated in the Table represent the upper limits for the corresponding parameters.

As regards the nature of effective stress in the unsaturated zone, it was arbitrarily assumed that the sand skeleton was deformable above the air-entry value and rigid below the air-entry value. Thus,

$$\chi = \begin{cases} 1, & \psi \geq -0.2 \text{ m.} \\ 0, & \psi < -0.2 \text{ m.} \end{cases} \qquad (V.16)$$

The effect of using different deformation parameters on the development of the surface $\psi = 0$ is shown in figure 50. It is readily seen from this figure that the results obtained in all three cases fall on the same smooth curves, indicating that the system is so much dominated by desaturation that deformation of the soil skeleton has very little effect on the overall flow phenomenon. A study of the mass balance data indicated that even in the case of the largest deformation parameter used ($C_c = 0.01$), the total volume change over the entire flow region at the end of 50 hours amounted only to about 1.5 per cent of the total quantity of water drained from the system. In the other two cases, the corresponding volumetric change was but a fraction of one per cent.

c. Comparison of experimental and numerical results

As a first step in the comparison of experimental and numerical results, the computed positions of the surface, $\psi = 0$, at various times are shown in comparison with the experimental results in figure 51.

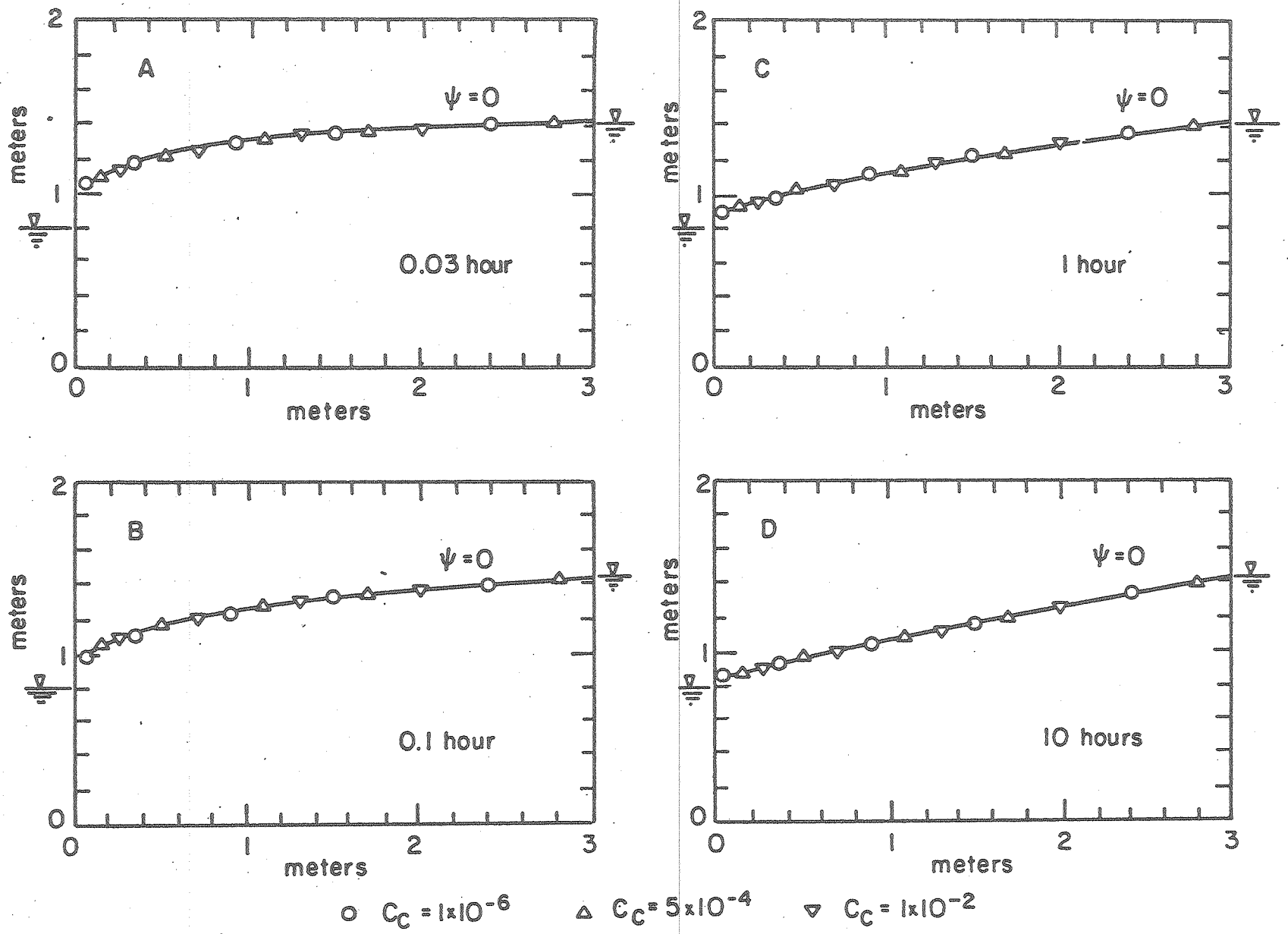

Fig. 50. Drainage from a sand box; effect of different values of C_c on the evolution of the surface, $\psi = 0$

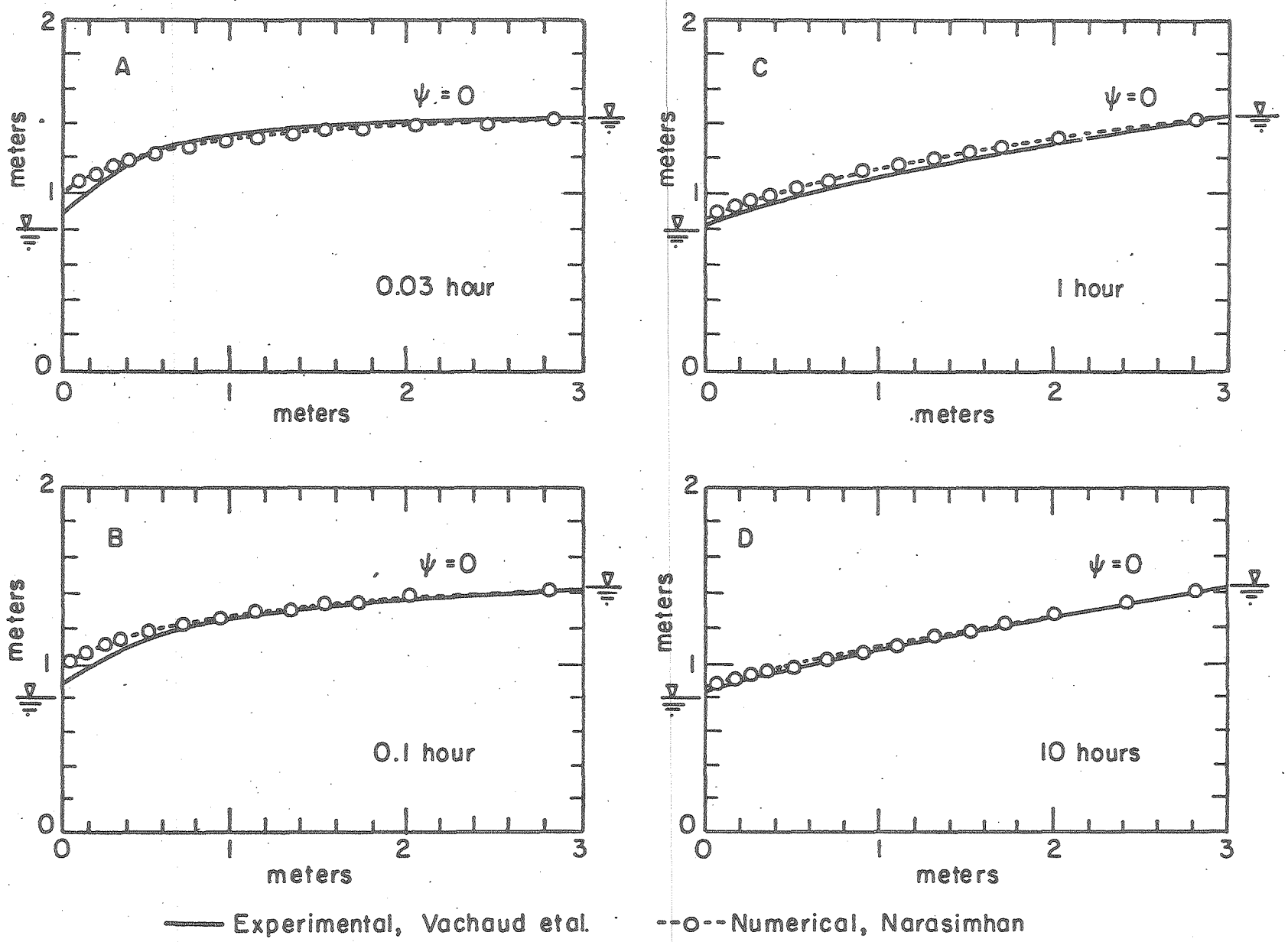

Fig. 51. Drainage from a sand box; comparison of numerical and experimental results of the evolution of the surface, $\psi = 0$

It can be seen from the figure that there is some difference between the two results at early times and within a meter of the draining end of the sand box, with the computed position remaining slightly above the observed position. The departure attenuates at larger values of time. Considering the difficulties associated with this type of experiment, it seems reasonable to assume that the departures present are tolerable.

A special feature of the Grenoble experiment was that in using the Gamma-ray attenuation technique, the total moisture content of the flow region was monitored regularly. As a result, it was possible to measure the quantity of water removed from storage as a function of time. In figure 52, this variation of cumulative depletion from storage, as measured experimentally and as computed numerically, are shown compared. It is seen from figure 52 that although the two results conspicuously approach each other for very large values of time ($t > 50$ hours), the curves depart significantly from each other in the time range, 1 to 20 hours. Thus, the numerical and the experimental models appear to tend toward the same steady-state condition, but follow different transient paths in attaining steady-state. This suggests that the mean physical properties used in the numerical simulation are probably somewhat inappropriate.

Perhaps the most rigorous test of the numerical results is to compare the evolution of the isopotential lines over the entire flow region. The experimentally observed distribution of isopotential lines at various instants of time are presented in figure 53 and the same distribution, numerically computed, are shown in figure 54. For the sake of clarity these diagrams have not been superimposed.

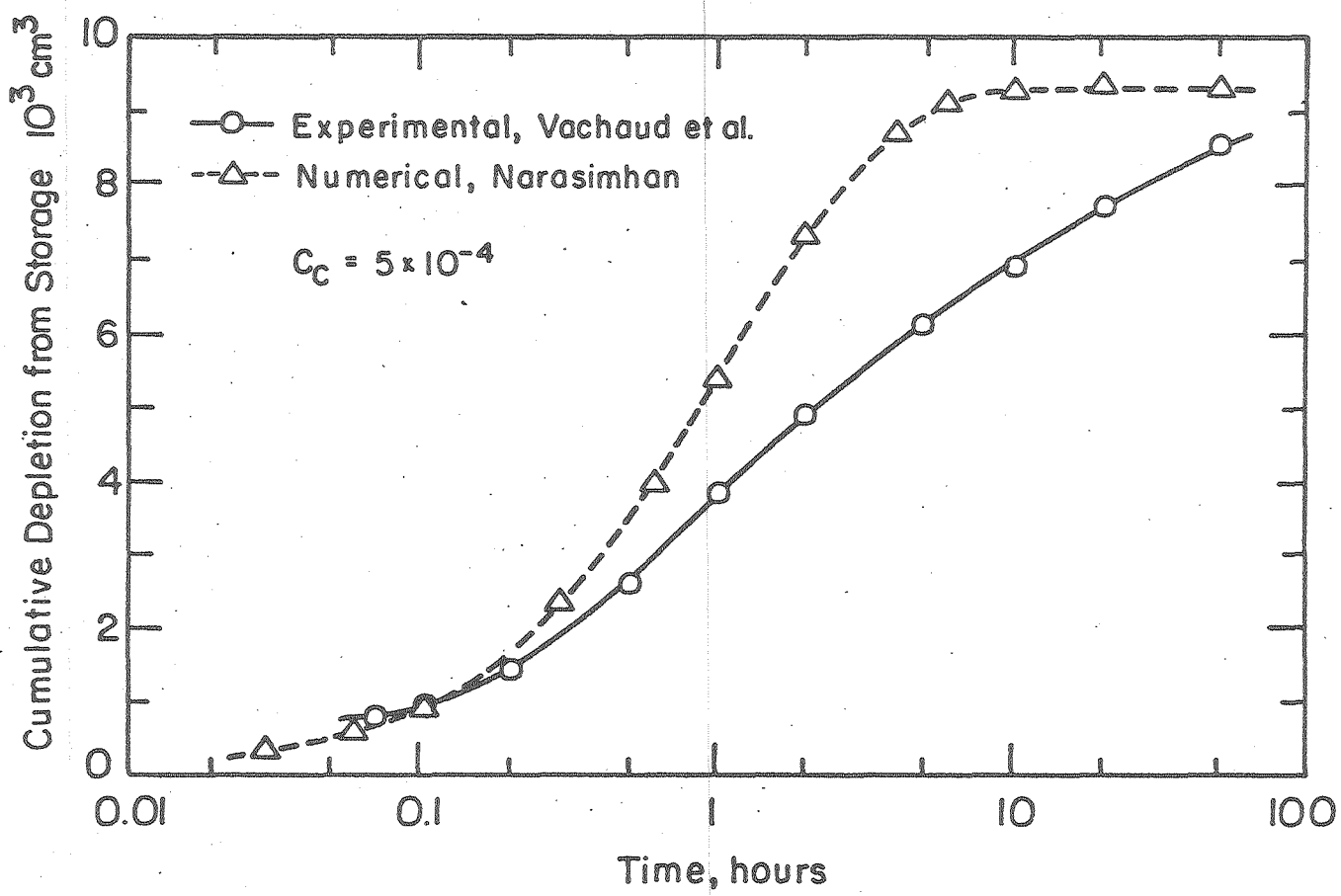

Fig. 52. Drainage from a sand box; cumulative depletion from storage as a function of time

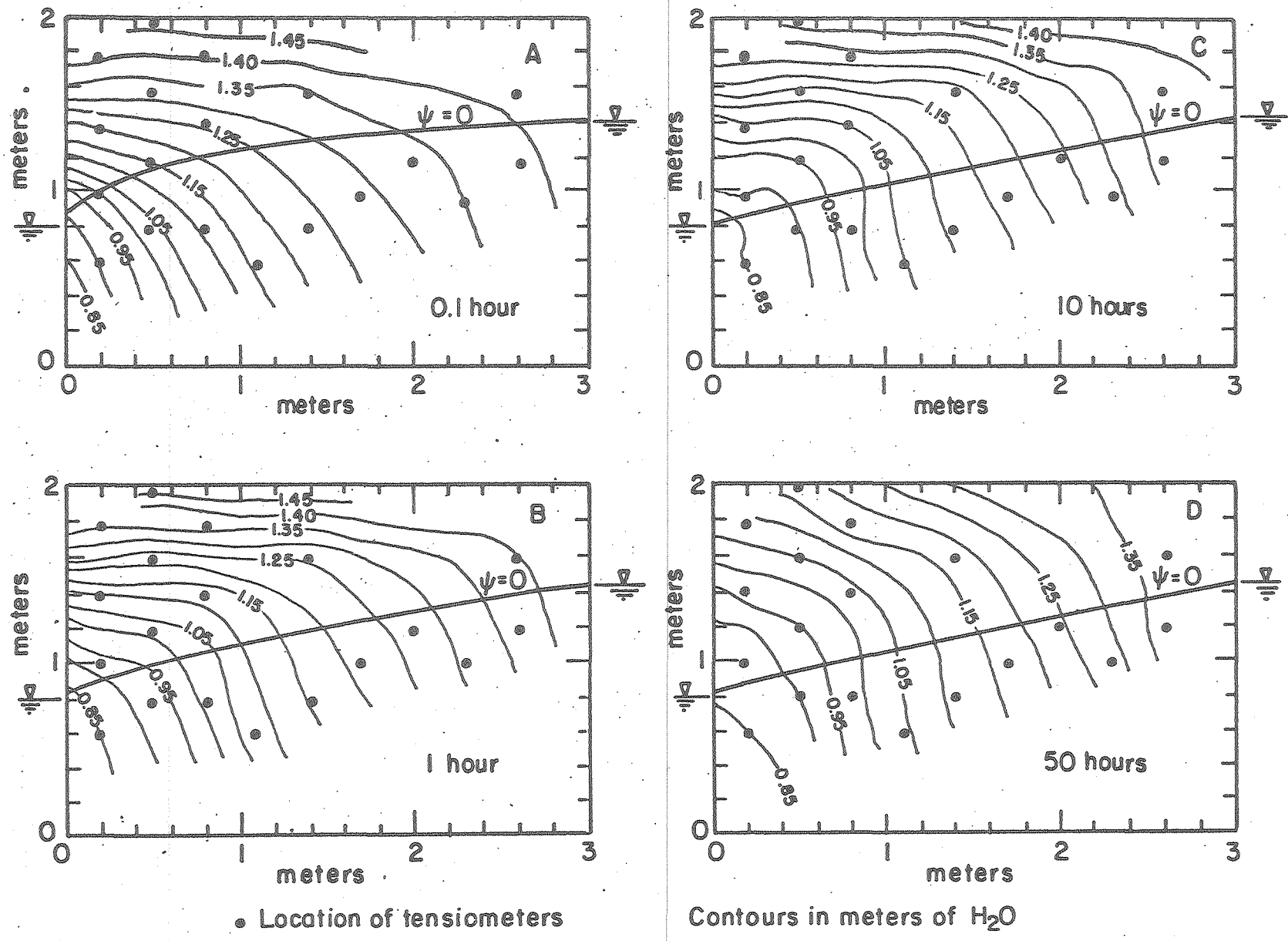

Fig. 53. Drainage from a sand box; experimentally observed evolution of isopotentials

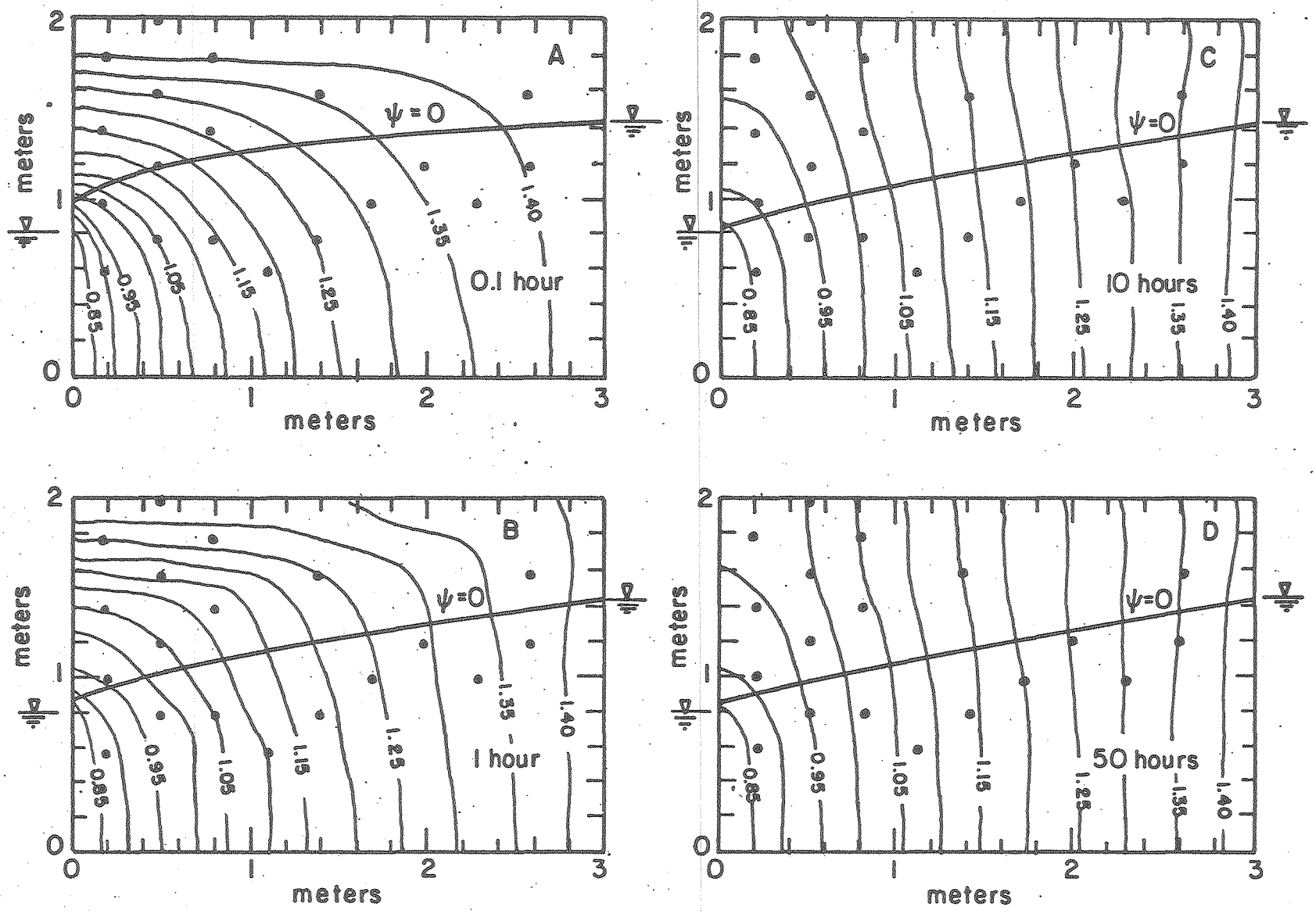

• Location of tensiometers Contours in meters of H_2O

Fig. 54. Drainage from a sand box; numerically computed evolution of isopotentials

It may be mentioned here that the isopotential lines in figure 53 were based on 19 control points, representing the 19 tensiometer locations. The numerical results on figure 54 are based on more control points.

A few features are worth noting in the experimental results presented in figure 53. First, in figures 53A and 53B one notes the presence of the 1.45 m. contour near the top boundary of the flow region. If we recall the initial conditions, we note that at t = 0 the potential throughout the flow region was equal to 1.43 m. Now, since this is a drainage problem, the potentials should be falling everywhere in the flow region and hence, the presence of the 1.45 m. isopotential line, upto as much as an hour after the start of the experiment is anamolous. This must either mean that the assumed initial conditions are somewhat incorrect near the top boundary or that the upper boundary of the flow region was not completely impermeable during the experiment. It is also worth noting here that in figures 53C and 53D. the isopotentials meet the upper boundary of the flow region obliquely. However, if the upper boundary were impermeable, the isopotentials must meet that boundary perpendicularly. If indeed these contours have been drawn correctly from experimental data, then, they should indicate the addition of water across the upper boundary during the experiment.

Comparison of figures 53C and 53D indicates that the contours are still changing position significantly and hence steady-state conditions are yet to be obtained even after 50 hours after the start of the experiment.

The principal feature worth mentioning in the case of figure 54 is that there is very little difference in the distribution of isopotentials at the end of 10 hours and 50 hours (figures 54C and 54D), indicating that the system attains steady-state after about 10 hours. Comparison of figures 53D and 54D suggests that the experimentally determined isopotentials (figure 53D) tend toward the steady-state configuration computed numerically (figure 54D).

A careful comparison of figures 53 and 54 reveals the fact that the position of the individual isopotentials show significant differences. To study these deviations more clearly, the differences between the computed values of potentials and those actually measured at the locations of the 19 tensiometers are plotted and contoured in figure 55. Negative values in figure 55 indicate that the computed potentials are less than the experimentally observed values.

Figure 55 shows that in the saturated region, the departures are mostly positive, the magnitude being less than 5 cm. at all times. These departures are small and can be ignored.

In figure 55, the position of the capillary fringe separates the deformable region below from the desaturating region above. As can be seen from figure 55A, at the end of 0.1 hours the departures throughout the flow region are small. The maximum departure increases to about -10cm. at the end of 1 hour and increases further to its largest value of -35 cm. at the end of 10 hours. Thereafter, the maximum departure decreases gradually, and attains a value of -18 cm. at the end of 50 hours. It is noteworthy that all the significant departures are restricted to the desaturating region above the capillary fringe in the upper left hand side of the model. The decrease in

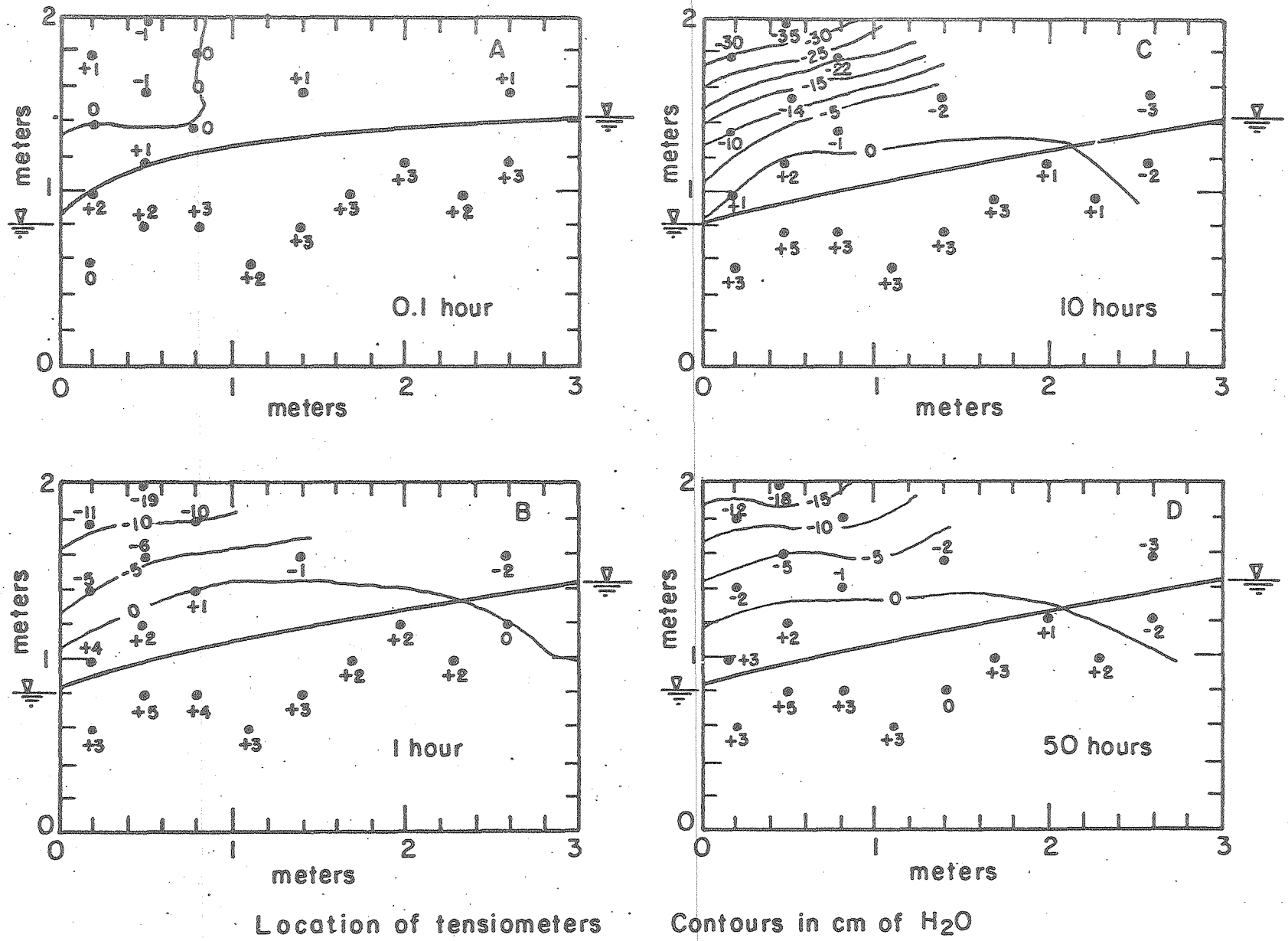

Fig. 55. Drainage from a sand box; deviation of computed potentials from observed potentials

the magnitude of the departures between 10 hours and 50 hours suggests that the steady-state solutions of the numerical and the experimental models are probably very close to each other.

In a desaturation experiment of this type, it is of particular interest to study the locations from which much of the drained water is released from storage. In order to do this, the percentage contribution to total depletion from storage by several horizontal strips in the upper left hand corner of the model is shown plotted in figure 56. This figure shows that over 55 per cent of the total depletion from storage is contributed by a region about 1 m. long and 0.7 m. high, located in the upper left hand corner of the model. Even within this region, the depletion is concentrated towards the central parts, where the values of ψ varied from slightly less than zero to less than -0.7 m. during the course of the experiment. From figure 45B it can be noticed that the S versus ψ relation shows the steepest change in the range -0.2 to -0.7 m. and hence the soil has maximum ability to desaturate in this range.

A comparison of figures 55 and 56, especially, figures 55C and 56C, shows that the departures of the computed values of potential from the experimental values are maximal in the upper left hand side of the flow region, where maximum desaturation is also taking place. Furthermore, the consistent negative values of the departures indicate that the computed potentials are falling more rapidly than the observed potentials and hence the numerical model is approaching steady-state much more rapidly than the experimental model.

That the numerical model is approaching steady-state rapidly, leads to the inference that the mean curves of material properties

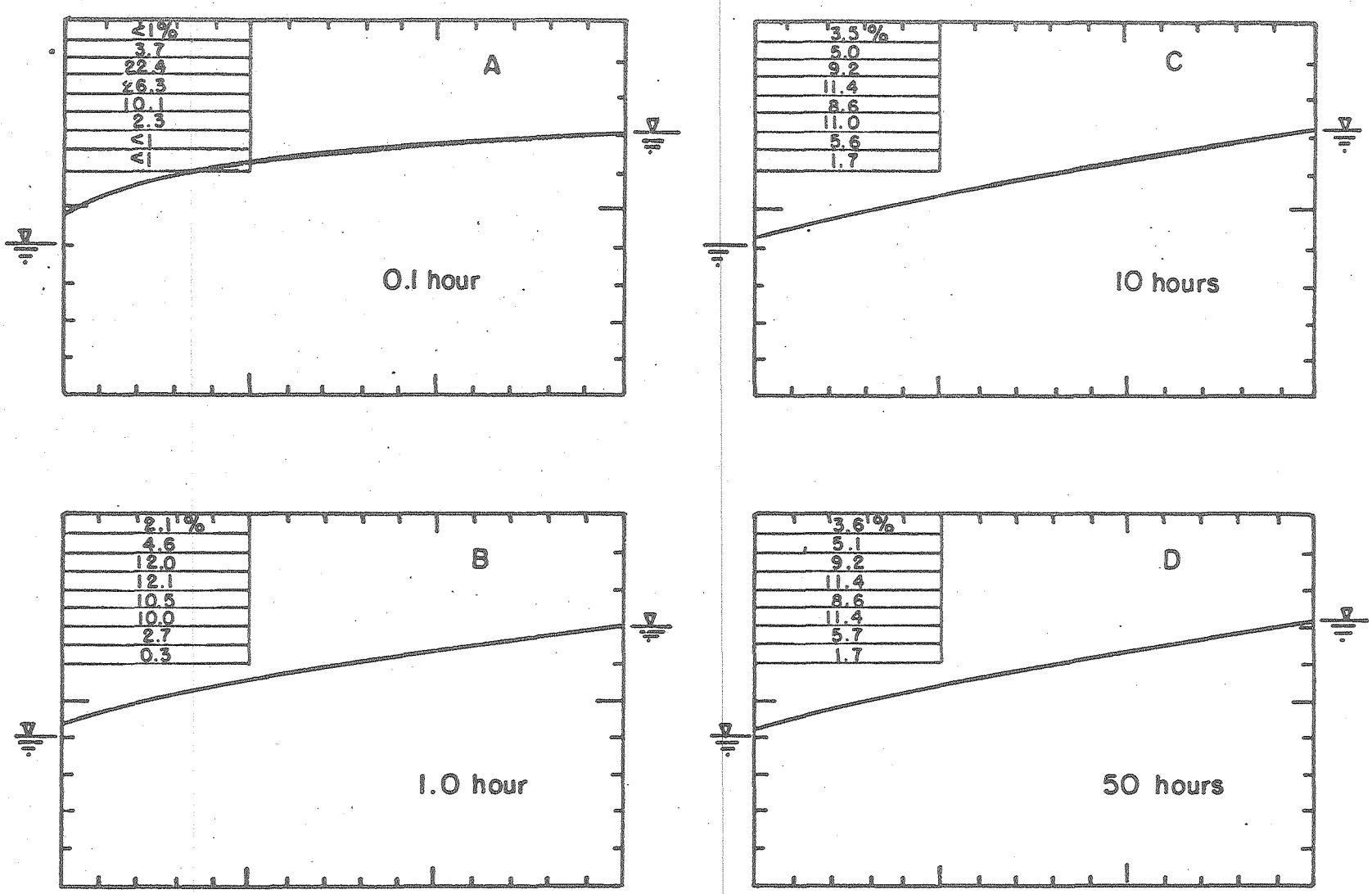

Fig. 56. Drainage from a sand box; contribution to cumulative depletion from storage by some parts of the flow region

used in the calculations (figure 44) probably do not represent the appropriate mean values, particularly for the upper left hand part of the flow region which is desaturating most. In particular, the mean curves may be providing relatively higher values of hydraulic conductivity, K and/or relatively lower values of specific moisture capacity ($d\theta/d\psi$). Or, equivalently, the mean curves may be providing, in general, higher values of diffusivity than what the experimental results would indicate.

The numerical solution shows that the transient distribution of potentials within the saturated zone, the evolution of the "free surface" ($\psi = 0$) and the cumulative depletion from storage at steady-state are all computed fairly accurately by the numerical model. However, the mathematical simulation departs appreciably from the experiment in the matter of transient potential distribution within the unsaturated zone and also the time-dependent rates of cumulative depletion from storage. A study of the experimental data shows that even in a carefully designed and executed experiment like the one under consideration, heterogenities of physical properties cannot be avoided. When a heterogenous system is to be simulated with an equivalent homogenous model, one has to statistically evaluate the mean physical properties and such a statistical evaluation may be very difficult in the case of complex nonlinear problems. The differences between the observed and the simulated behaviors of the system may be largely due to errors in the evaluation of the mean physical properties used in the numerical model.

Concluding the discussion on the sand box model, it is pertinent to mention that we are now clearly at a point when our ability to

carry out complex calculations exceeds our ability to carry out equally complex experiments. For our ultimate goal, both experiments and methematical models are essential; the former for providing the relevant physical parameters and physical basis, and the latter for predicting future effects. For maximum benefit, therefore, these two approaches should go hand in hand and complement each other.

8. EXCAVATION IN SOFT CLAY

We will now consider a problem which is of some interest to the soil and foundation engineer. In this hypothetical problem we will give consideration to the effects of arbitrary mechanical loading on the pore pressure distribution within the flow region, a phenomenon which is not generally considered by the hydrogeologist.

The problem (figure 57A) is as follows: A 20-meter bed of soft clay (San Francisco Bay Mud), fully saturated up to the ground surface, is under hydrostatic equilibrium, with fluid potential ϕ everywhere equal to 20 m. The clay bed, laterally infinite, rests on a rigid impermeable base. The upper part of the clay is assumed preconsolidated to 0.35 atm., while the remainder is normally consolidated. In this soft clay an excavation (20 m. long, 10 m. deep and very wide) is made. The problem is to study the new drainage pattern imposed within the clay bed due to the excavation and the swelling and consolidation phenomena around the excavation resulting due to the pore pressure dissipation.

Conceptually, the first step in solving this problem is to determine the effect of the unloading caused by the excavation on the antecedent hydrostatic potential distribution. In order to achieve

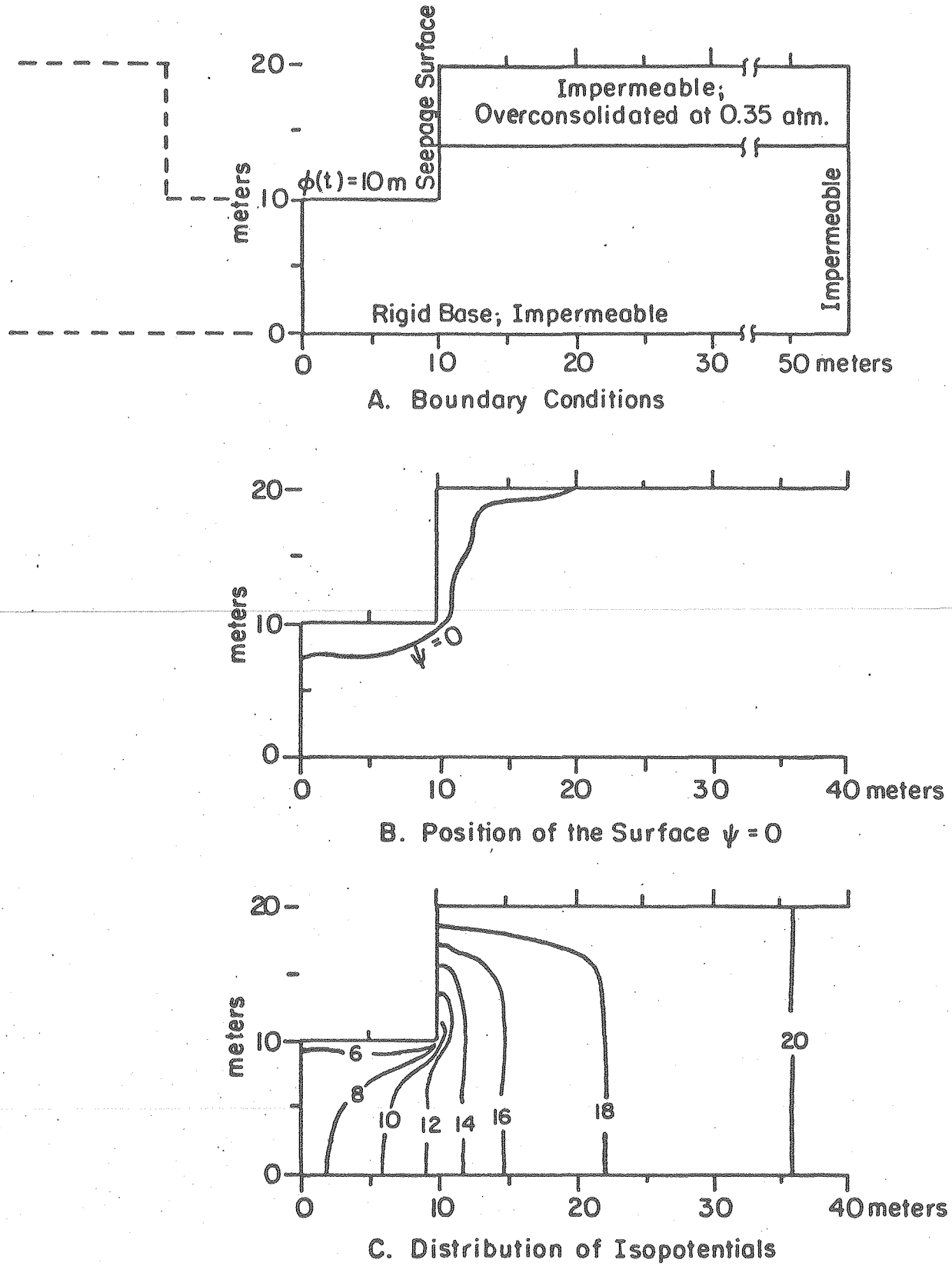

Fig. 57. Excavation in soft clay; initial and boundary conditions

this, we assume, a) that the process of excavation is very rapid and in relation to the low permeability of the clay, can be considered instantaneous and b) that the soil reacts elastically in an undrained state to the changed loading and the pore pressure changes instantaneously in such a manner that the change in loading due to the excavation is immediately compensated by the pore pressure and hence the soil skeleton does not immediately feel any change in effective stress. The soil skeleton gradually experiences change in effective stress only after pore pressures begin to dissipate, consequent upon drainage.

The new distribution of fluid potentials, caused by the excavationare shown in figures 57B and 57C. To calculate this new distribution, the following procedure was adopted. Assuming that the soft clay has a Poisson's ratio of $\nu = 0.5$, the new stress distribution was calculated at 15 control points within the flow region, using elastic theory stress distribution tables and charts from Poulose and Davis (1974). The difference between the old and the new stress distribution, as evaluated with the help of Mohr's Circle, provided the changes in the magnitudes of the principal stresses, $\Delta\sigma_1$, $\Delta\sigma_2$ and $\Delta\sigma_3$ (assuming that $\Delta\sigma_2 = \Delta\sigma_3$). These changes in stresses cause change in pore pressure within the clay. According to Skempton (1954), for elastic materials, the change in pore pressure can be related to the change in stresses by,

$$\Delta u = \frac{\Delta\sigma_1 + \Delta\sigma_2 + \Delta\sigma_3}{3} \qquad (V.17)$$

where u is the pore pressure and $\psi = u/\rho g$

The changes in the pore pressure so computed at the control points were contoured over the entire flow region to arrive at the new distribution of porepressures and potentials, which form the initial conditions for the drainage problem solved by the numerical model.

A feature worthy of note in regard to the initial conditions is that as a result of the excavation process, the portion of the flow region immediately surrounding the excavation goes into a state of negative pore pressures as shown in figure 57B. As we shall see subsequently, this zone of negative pore pressures has significant effect on the formation of the seepage face on the wall of the excavation.

The boundary conditions for the drainage problem are illustrated in figure 57A. The floor of the excavation is assumed to be constantly covered with a thin film of water so as to form a fixed potential boundary, while the wall of the excavation is partly a seepage face and partly an impermeable boundary, with the length of the seepage varying with time. All the other boundaries of the flow region are assumed impermeable.

The physical properties of the Bay Mud were experimentally determined by Prof.W.N. Houston of the University of California, Berkeley, and are presented in figure 58. These properties represent the "drained" parameters of the clay. Due to the highly plastic nature of the clay it was assumed that its air-entry value is very large and that the clay remains fully saturated throughout the range of negative pore pressures encountered in the present problem.

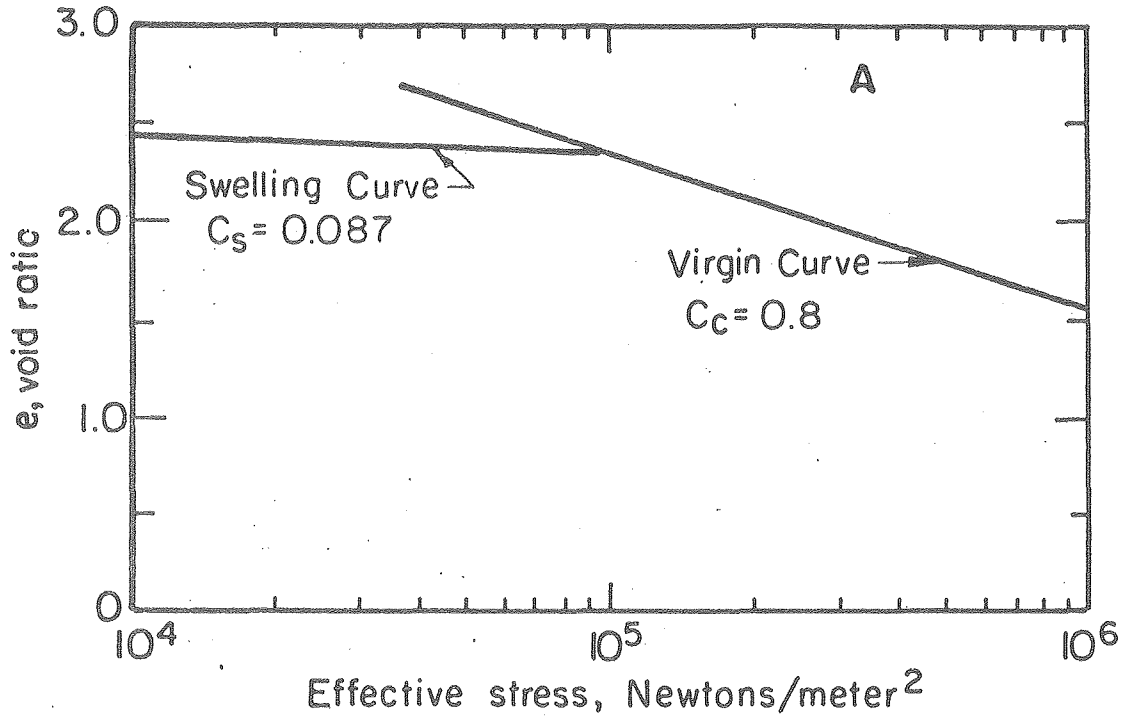

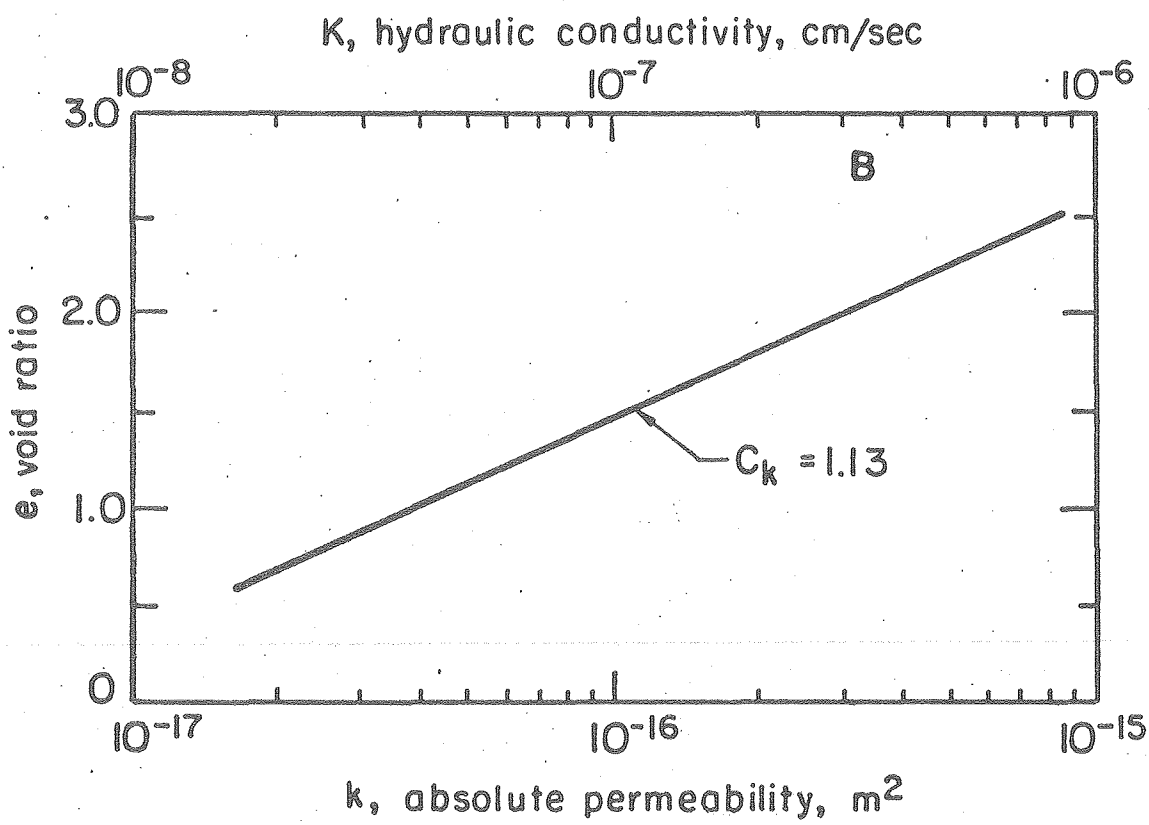

Fig. 58. Excavation in soft clay; material properties, A. void ratio versus effective stress, B. void ratio versus permeability

The flow region was discretized into a mesh of rectangles and squares, as shown in figure 59. The drainage computations were carried out for a period of 360 days from the start of the drainage process and the results of the computations are summarized in figures 60 through 62.

The time-dependent changes in the distribution of potentials and the evolution of the surface $\psi = 0$ (phreatic surface or water table) are presented in figure 60. In this figure, the disposition of the seepage face merits special attention.

By definition, a seepage face is a boundary across which water can only leave the system. From figure 57B it can be seen that at $t = 0$, the part of the flow region, immediately adjoining the wall of the excavation, is in a state of pore water suction. As a result, at $t = 0$, a seepage face could not exist along the excavation wall. The wall, therefore, formed an impermeable boundary. However, with the passage of time, as the pore pressures build up immediately behind the excavation wall, a seepage face slowly begins to grow. As can be seen from figure 60, the seepage face attains a maximum length at around 40 days and then gradually begins to decrease with time.

The numerical solution of the diffusion equation yields, for each element in the flow region, the total change in volume as a function of time. If we assume that all deformation is restricted to the vertical direction, then, the change in the volume of each node divided by its base area yields the vertical deformation of the node. The summation of the vertical deformations of all nodes along a vertical column of nodes then gives the settlement or swelling over the length of the column.

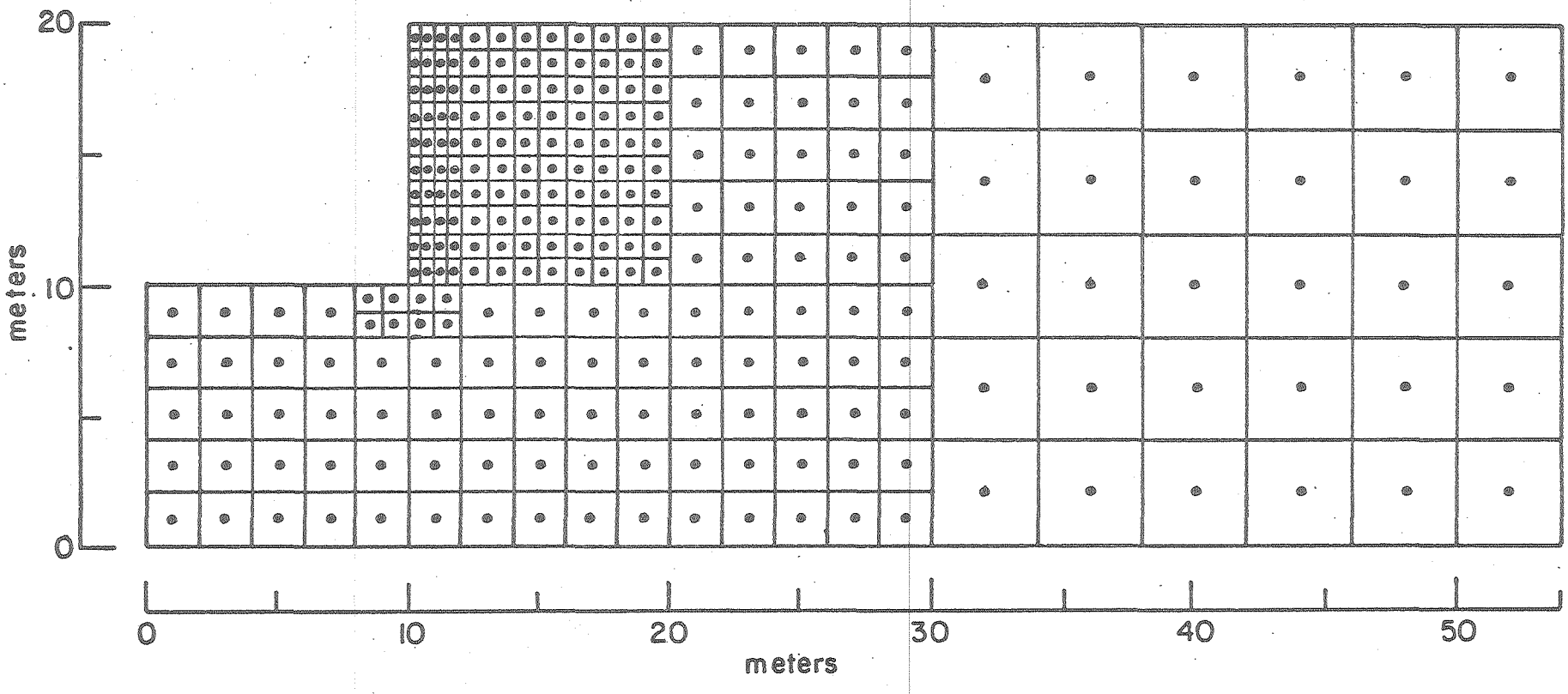

Fig. 59. Excavation in soft clay; discretization of the flow region

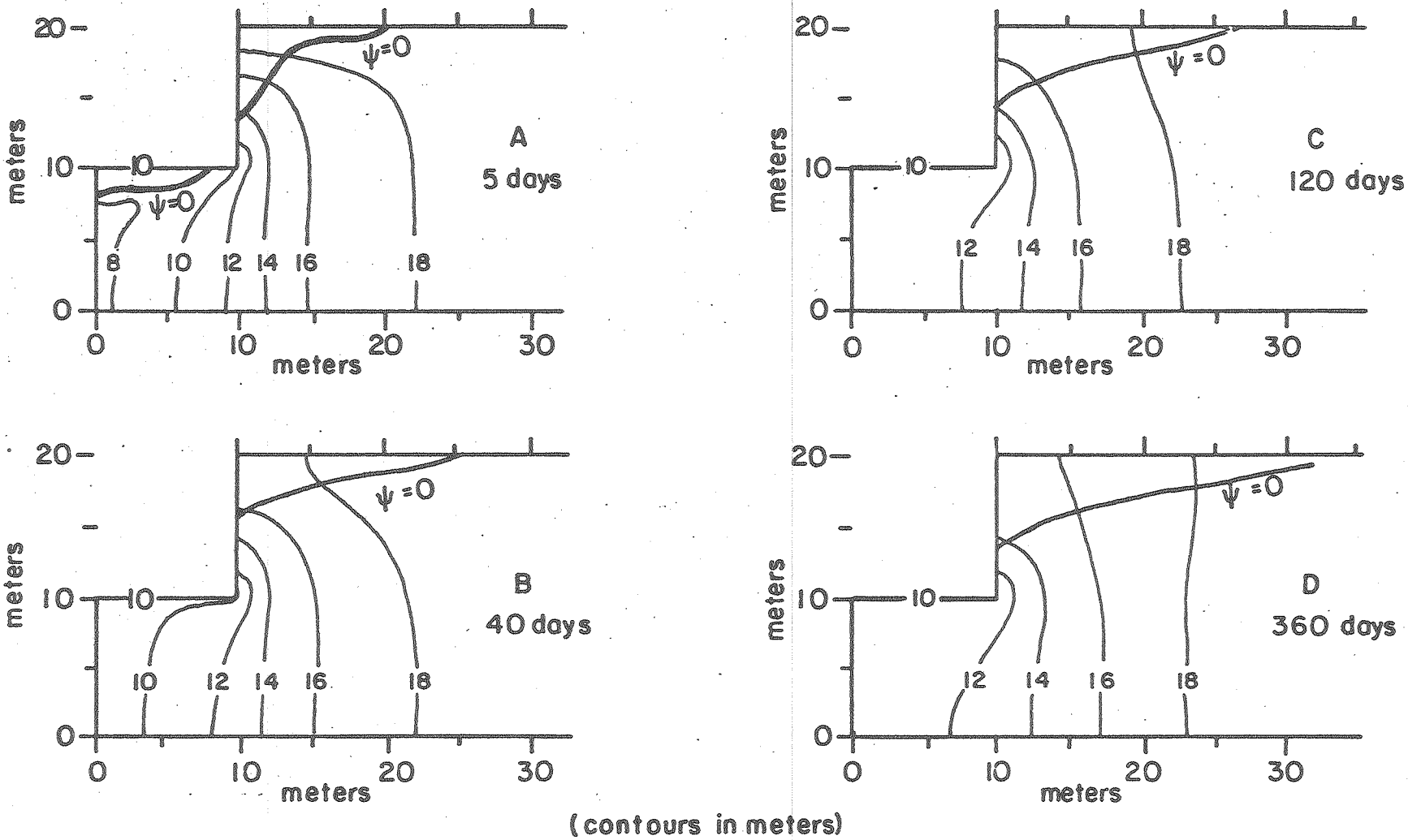

Fig. 60. Excavation in soft clay; evolution of isopotentials and the surface, $\psi = 0$

In figure 61, the pattern of consolidation and swelling around the excavation is illustrated as a function of time. It can be seen that the floor of the excavation progressively heaves up with time, the maximum rise being at the axis of the excavation.

In the region to the right of the excavation, the land surface gradually settles with time. However, it is interesting to note that the maximum settlement does not occur close to the excavation wall but a few meters inside of it. The reason for this is that due to the initial growth of the seepage face, some of the nodes close to the wall undergo swelling and it takes time before this swelling trend is reversed and consolidation sets in. Hence, the nodes close to the wall do not consolidate as much as other nodes located somewhat more interior, which determine the location of peak consolidation.

As one should expect, the magnitude of consolidation decreases as one proceeds away from the wall. However, in figure 61, one notices that the decrease is not uniform, but shows some oscillations. The cause of these oscillations is not quite clear; they could be due to the particular initital conditions used or related to the nature of the mesh or due to other causes.

Finally, we will try to gain an insight into the nature of the deformation history in different parts of the flow region. To do this, we study the time-rates of volumetric strain of some typical nodes in the flow region as shown in figure 62.

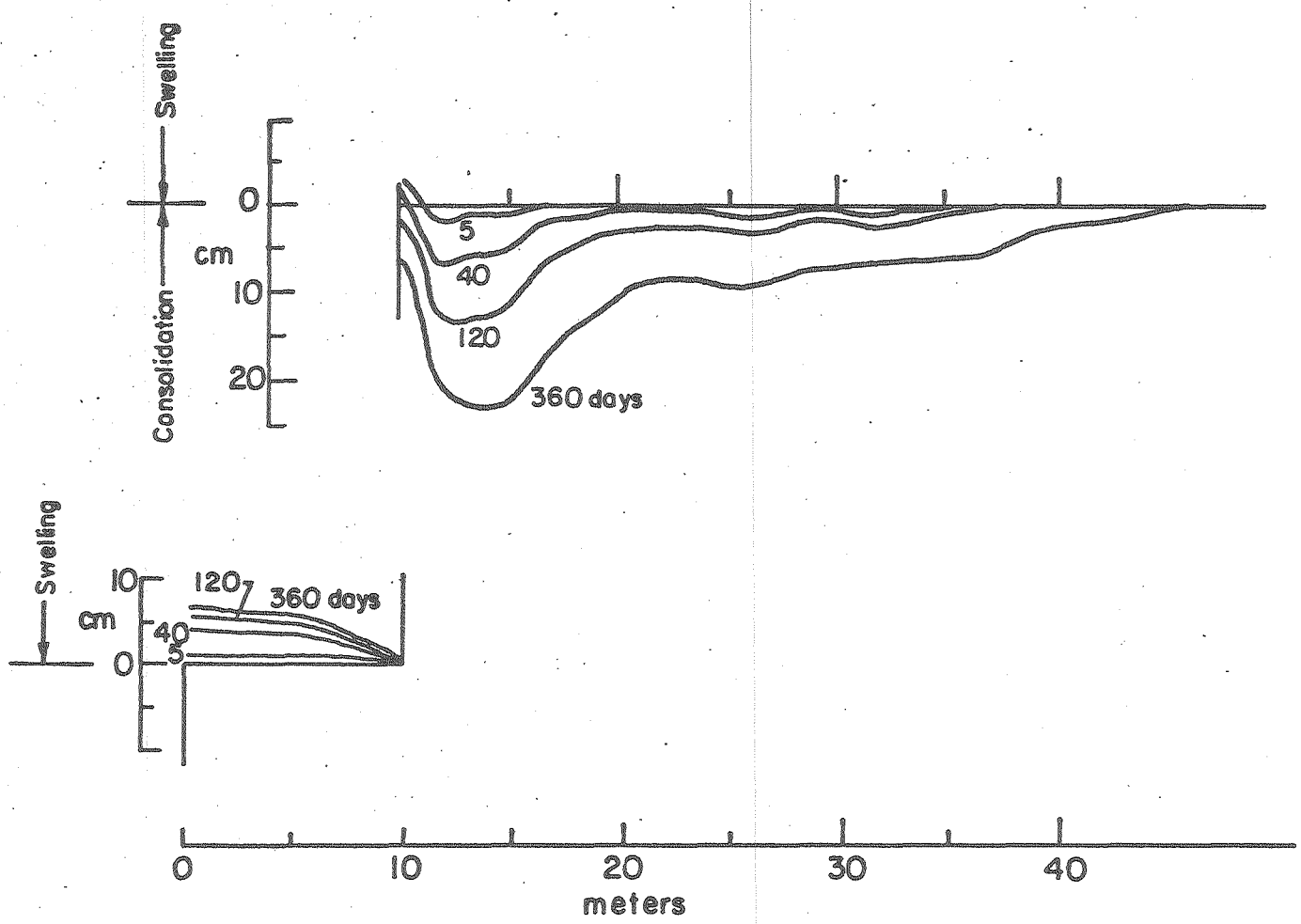

Fig. 61. Excavation in soft clay; pattern of consolidation and swelling

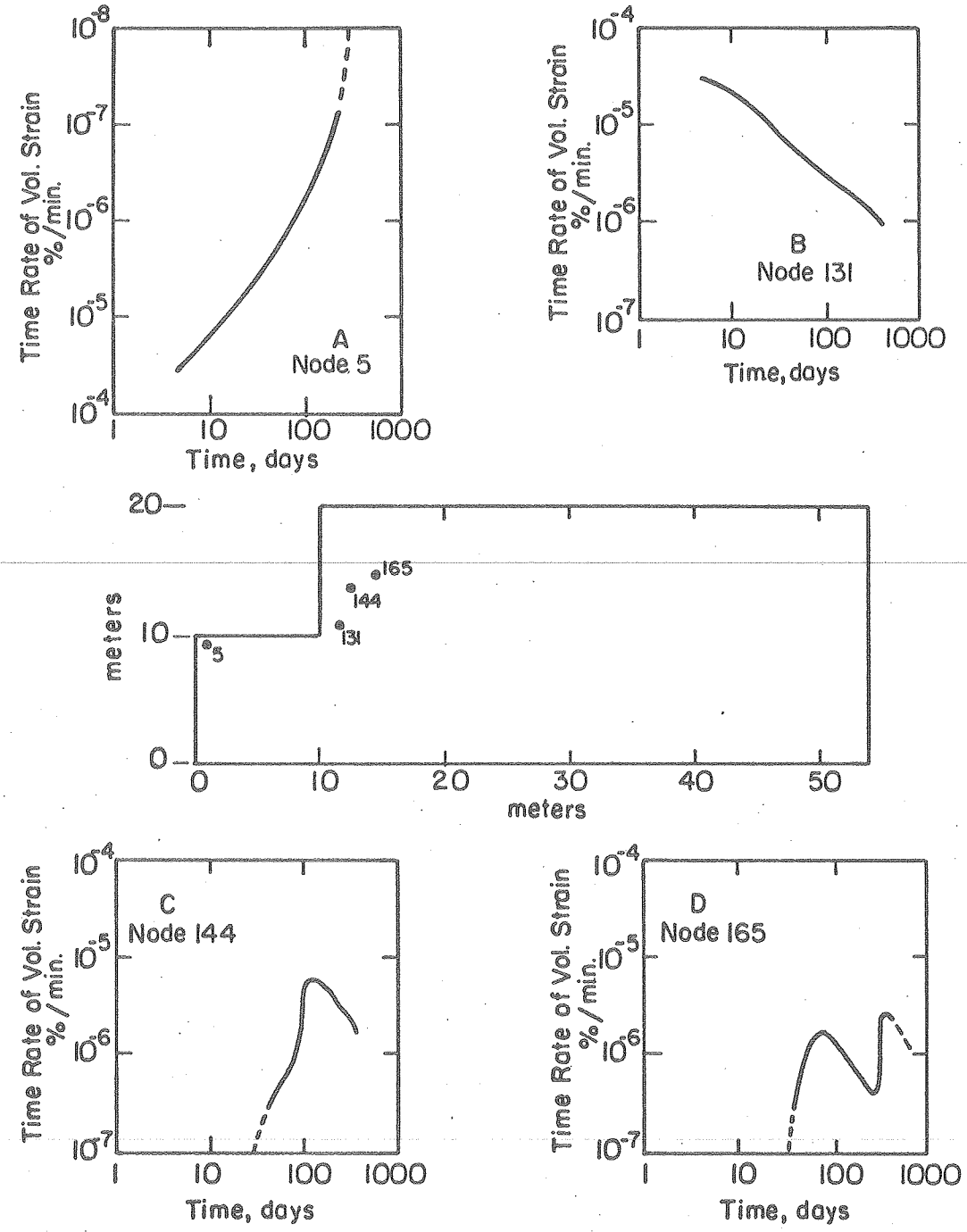

Fig. 62. Excavation in soft clay; time-rates of strain four typical elements in the flow region

Figure 62A illustrates the behavior of a node which has been undergoing swelling at a progressively decreasing rate (by convention, swelling is defined as negative). while figure 62B illustrates a node which has been consolidating since the start of the drainage process. The latter attains a peak strain-rate very early in the history and then strains at an ever decreasing rate for the rest of the time.

Figure 62C summarizes the history of a node which swells slightly to start with, reverses the trend, consolidates at increasing strain-rate, attains a peak and finally experiences ever-decreasing strain-rate. The abrupt increase in the strain-rate as evidenced by the inflection on the left limb of the curve in figure 62C, is of interest inasmuch as it indicates the transition of the node from a state of over-consolidation to one of normal consolidation.

Figure 62D illustrates the behavior of a node which passes from a state of over-consolidation to a state of normal consolidation. It can be seen that this node attains two peaks of strain-rate, one in the domain of the recompression curve and the other, in the domain of the virgin curve.

9. FLOW TO A SOIL PROBE

A practical problem encountered by soil scientist is to obtain a sample of soil solution, which effectively represents a composite of the entire solution in a small region surrounding the sampling device. Ideally, the device will perform this function satisfactorily under most conditions that are apt to be encountered in both laboratory and field.

Suction probes are being used widely as sampling devices. The present situation in respect of these probes is that they appear to work satisfactorily under some conditions, not in all. Reliable criteria that will justify confidence in the sampling procedure appear to be notably lacking. The soil, the instrument, and the technique are all involved in the problem of reliable sampling of the soil solution, particularly in circumstances in which the solution is rapidly moving past the probe.

In order to understand the influence of soil properties and the magnitude of suction applied to the probe on the inflow into the sampler, the present model was used to simulate radial flow to a soil probe in a partially saturated soil.

The physical model designed to simulate the sampling process is shown in figure 63. The diagram shows an isolated, horizontal layer of wet Geary silt loam in an impermeable cylindrical shell with a porous probe at its centre. In the model it is assumed that evaporation on the upper surface of the soil is suitably prevented to render this surface impermeable to moisture transfer.

It was further assumed that, with the help of a fairly elaborate experimental arrangement, the effluent could be withdrawn continuously for measurement of volume. At the same time, a known suction would be maintained at the probe at all times.

The following sampling routine was assumed. The soil would be saturated with water and brought to a constant suction and constant water content throughout by applying a controlled probe suction until outflow ceased. An additional known suction would then be applied to the probe and the rate of outflow would be observed. The results

would be compared with similar routines carried out with other values of suction in the soil and with other suctions in the probe.

In the mathematical model simulated, a probe. 3.7 cm. tall and 1.1 cm. in diameter, was assumed placed in a cylindrical sample of Geary silt loam, 51.1 cm. in diameter (figure 63). The physical properties of the Geary silt loam (figure 64) were obtained from Hanks and Bowers (1962). The cylindrical flow region was discretized into 30 cylindrical elements. The innermost 10 elements were 0.5 cm. wide, and the rest, 1 cm. The soil was assumed to be rigid and non-swelling. Due to the small height of the sample, gravitational effects were neglected.

Numerical solutions were obtained for various simulated sampling routines to answer the following questions: What will be the values of pressure head or suction at various points inthe soil and at various times after applying a given suction to the probe ? What will be the corresponding water contents ? What will be the rates of flow from the soil into the sampler ?

A detailed interpretation of the results will be published elsewhere (Day and Narasimhan, 1974). The results are summarized in figures 65 through 68.

Figure 65A shows a low-pressure front, which is initiated at the surface of the probe in the saturated soil and progresses outwards with its leading edge reaching the outer boundary of the system in a little more than half an hour after applying a 0.2 m. suction increment at the probe. Figure 65B shows a similar situation, where the soil was initially at a suction of 1 m. and a suction 3 m. was applied at the probe.

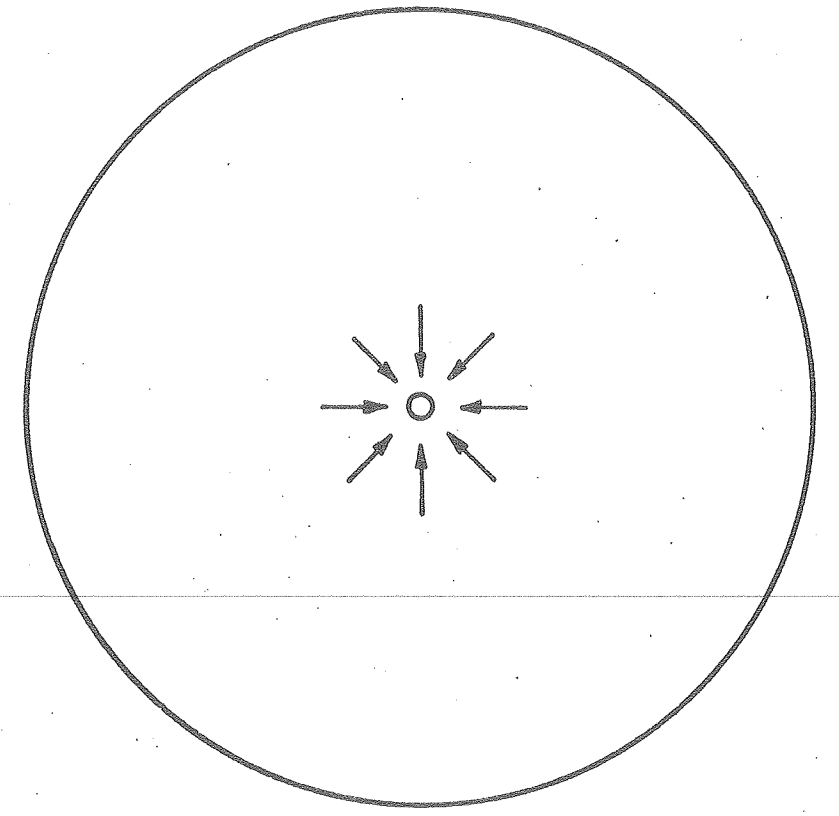

Plan View

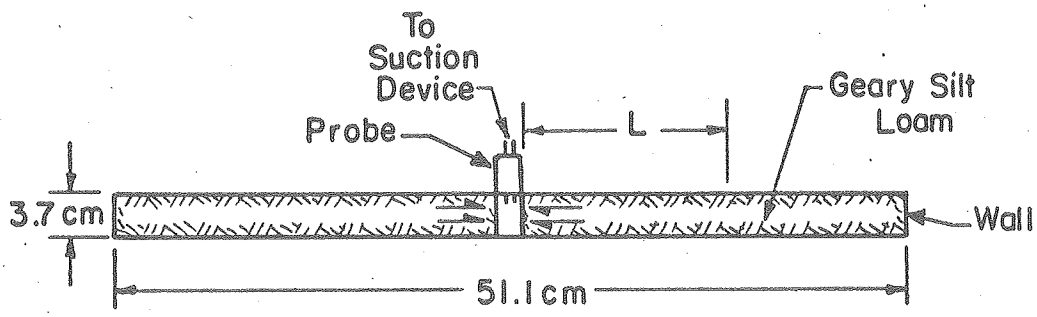

Elevation

Fig. 63. Flow to a soil probe; physical description of model

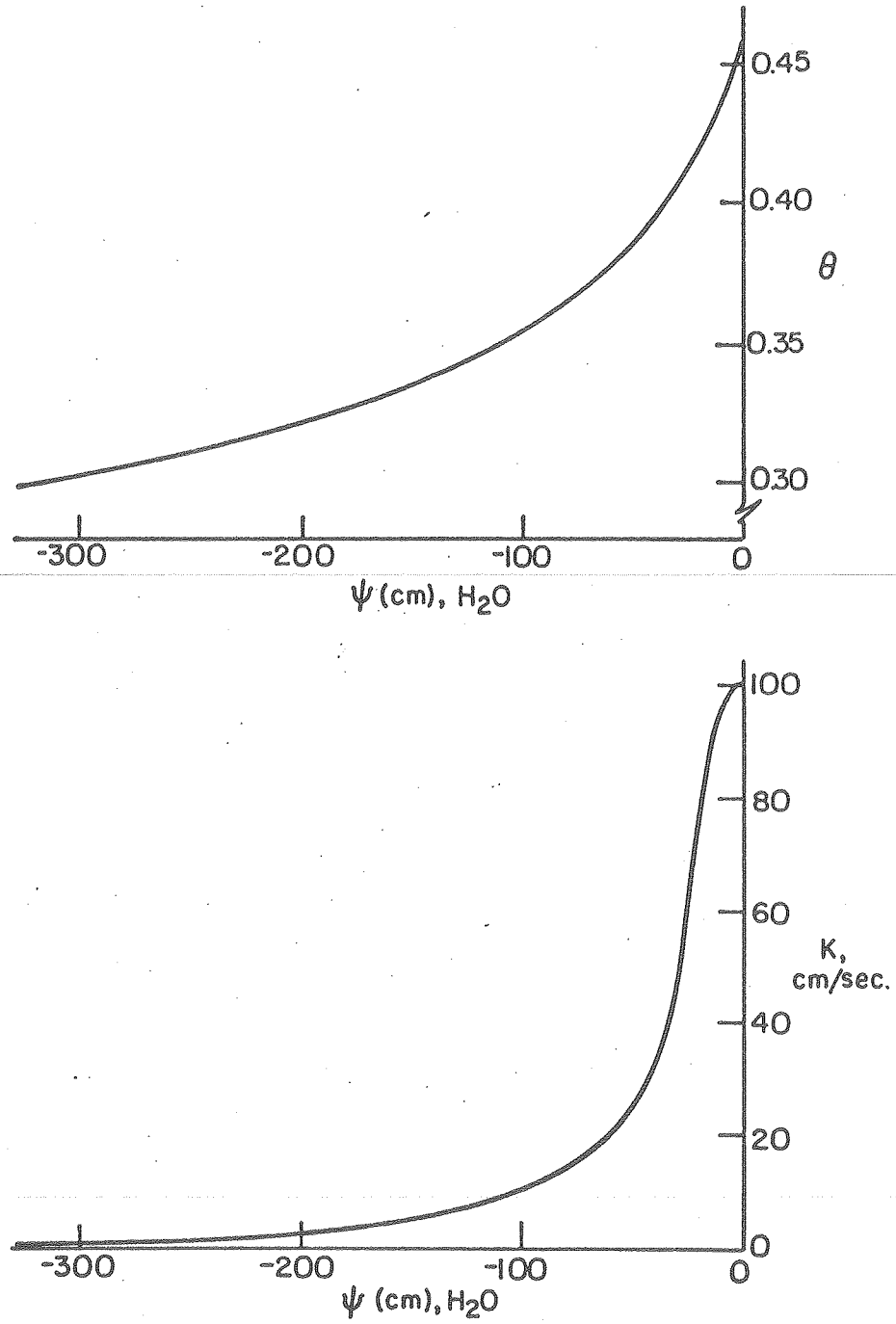

Fig. 64. Flow to a soil probe; material properties

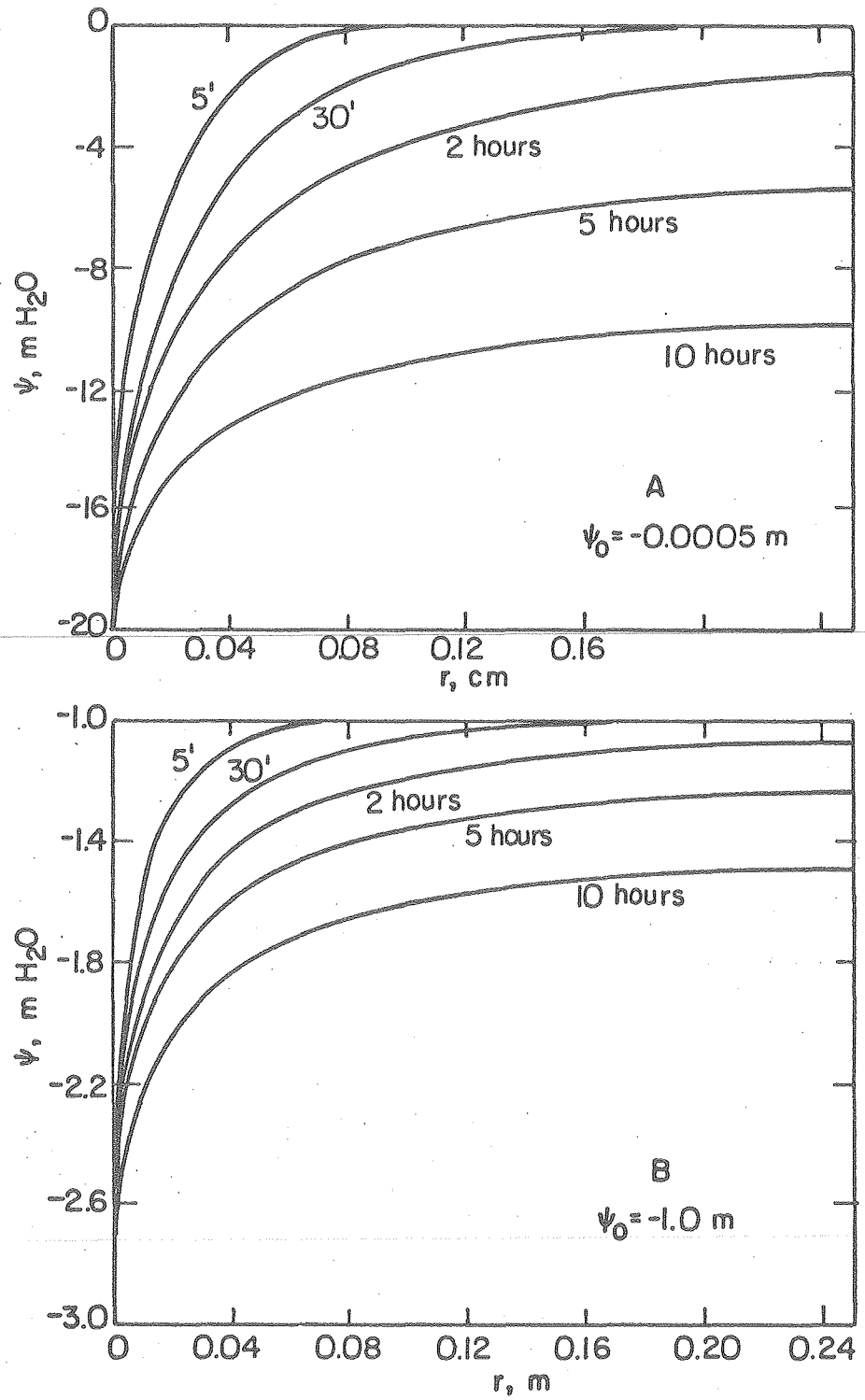

Fig. 65. Flow to a soil probe; distribution of pressure head as a function of time

Figure 66A shows the effects of sampling on the distribution of water content of the initially saturated soil at various times and at various locations in the system. Figure 66B shows that when the initial suction is greater (ψ_o = -1 m.), the effect of a differential pressure head of -0.2 m. induces the flow of only a small additional quantity of water into the probe and hence, only a small increase in the effluent.

Figure 67 shows the effect of sampling on the rate of extraction of the solution. For example. the lowest curve reflects the slow outflow of water when the soil is initially at 1 m. suction and a 1.2 m. suction is applied at the probe.

Finally, figure 68 shows the contribution to total cumulative depletion from storage from different parts of the flow region. It is seen that at early times, the bulk of cumulative drainage takes place in the immediate vicinity of the probe. As time progresses, more of the depletion from storage is contributed by regions away from the probe. After a long period of time, most of the storage depletion is contributed by the outermost shells. It may be pointed out here that due to the cylindrical symmetry of the flow region, the outer shells have far greater volume than the inner ones and hence, despite relatively small changes in moisture content, θ, the outer shells can dominate the total contribution to cumulative depletion from storage.

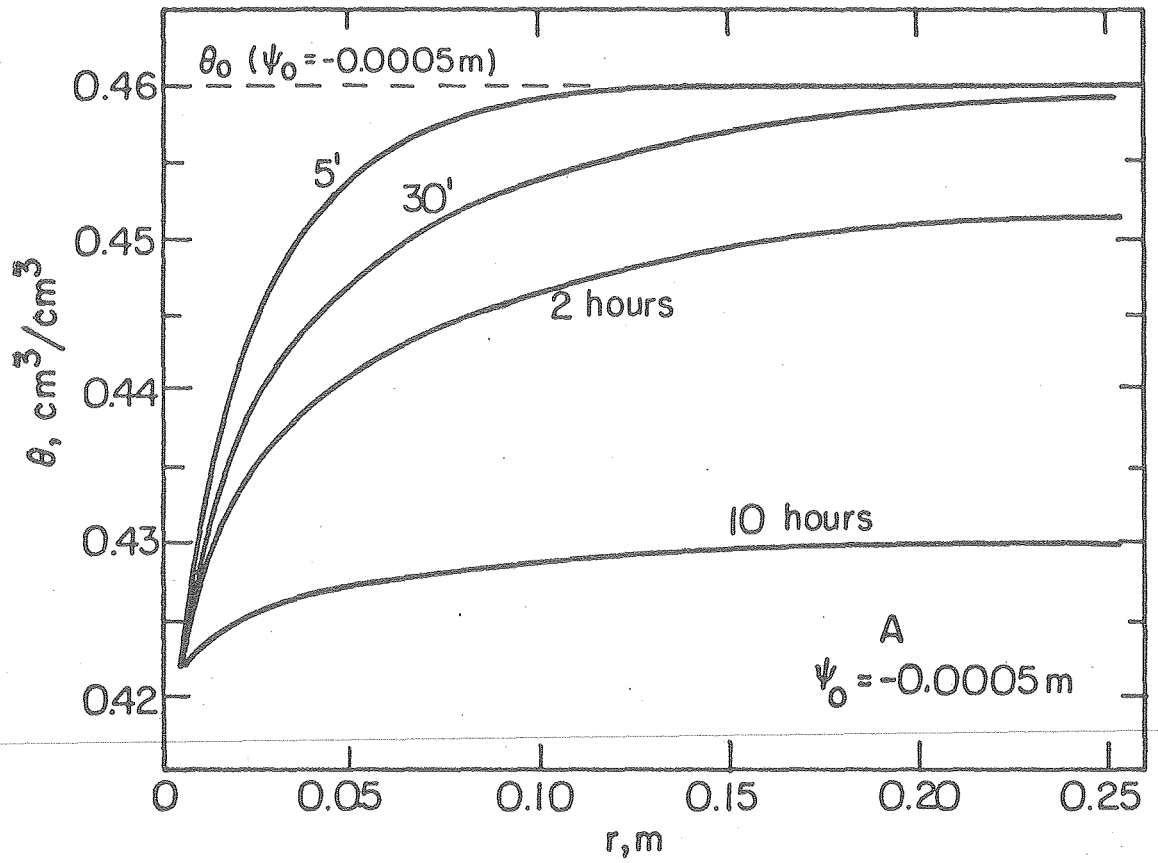

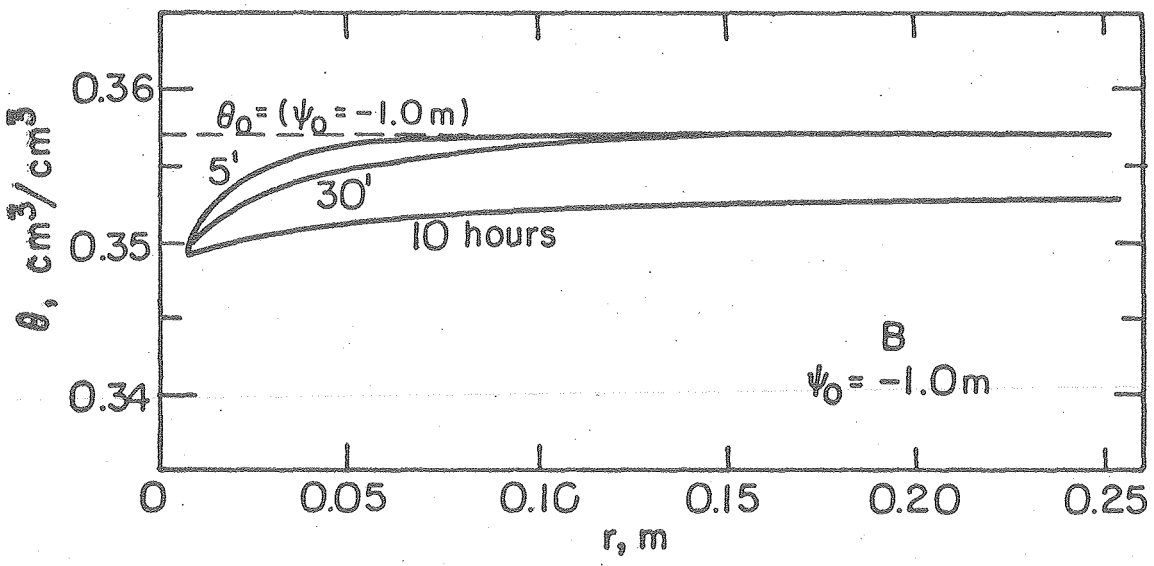

Fig. 66. Flow to a soil probe; distribution of moisture content as a function of time

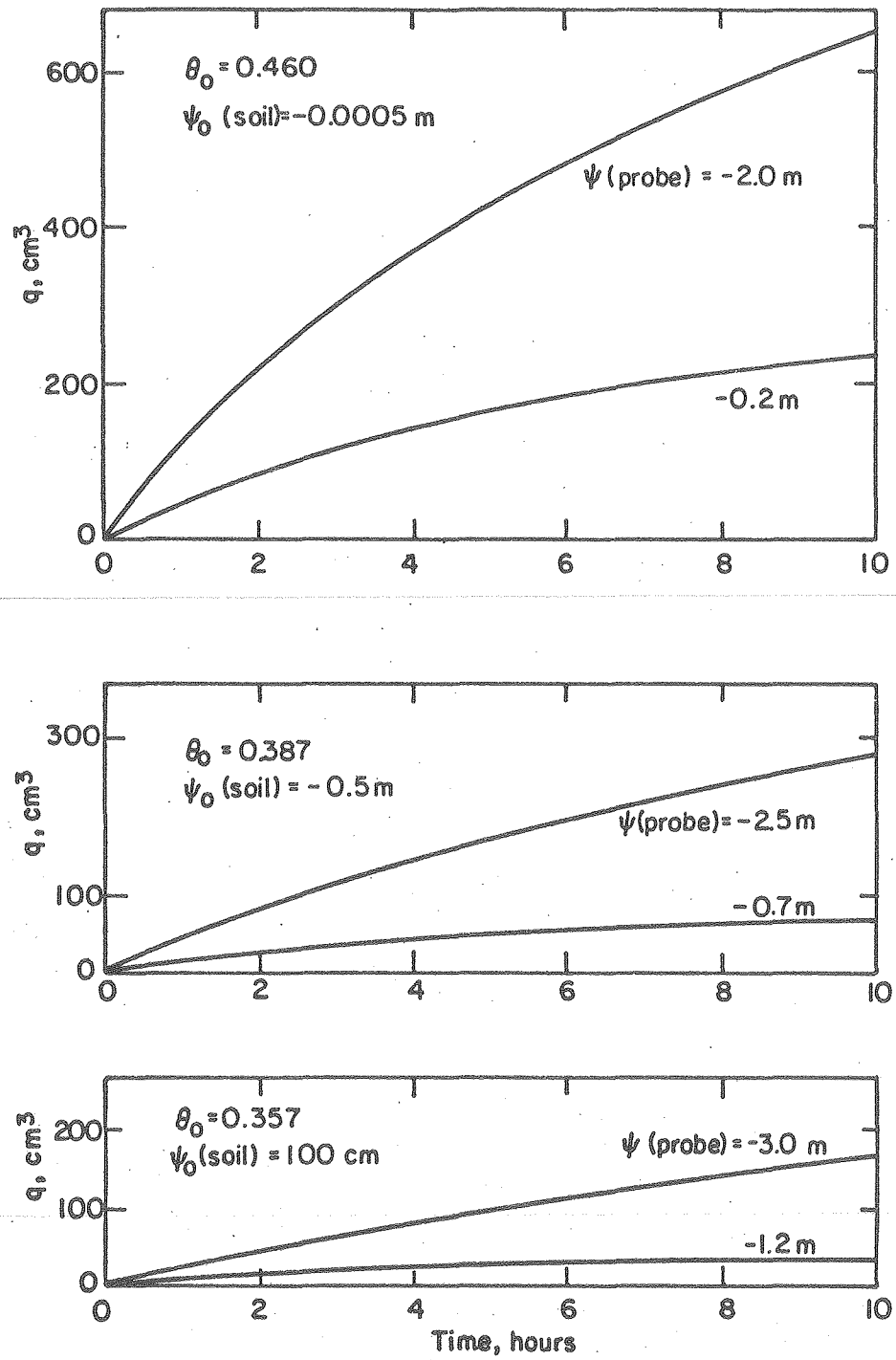

Fig. 67. Flow to a soil probe; cumulative volume of effluent as a function of time

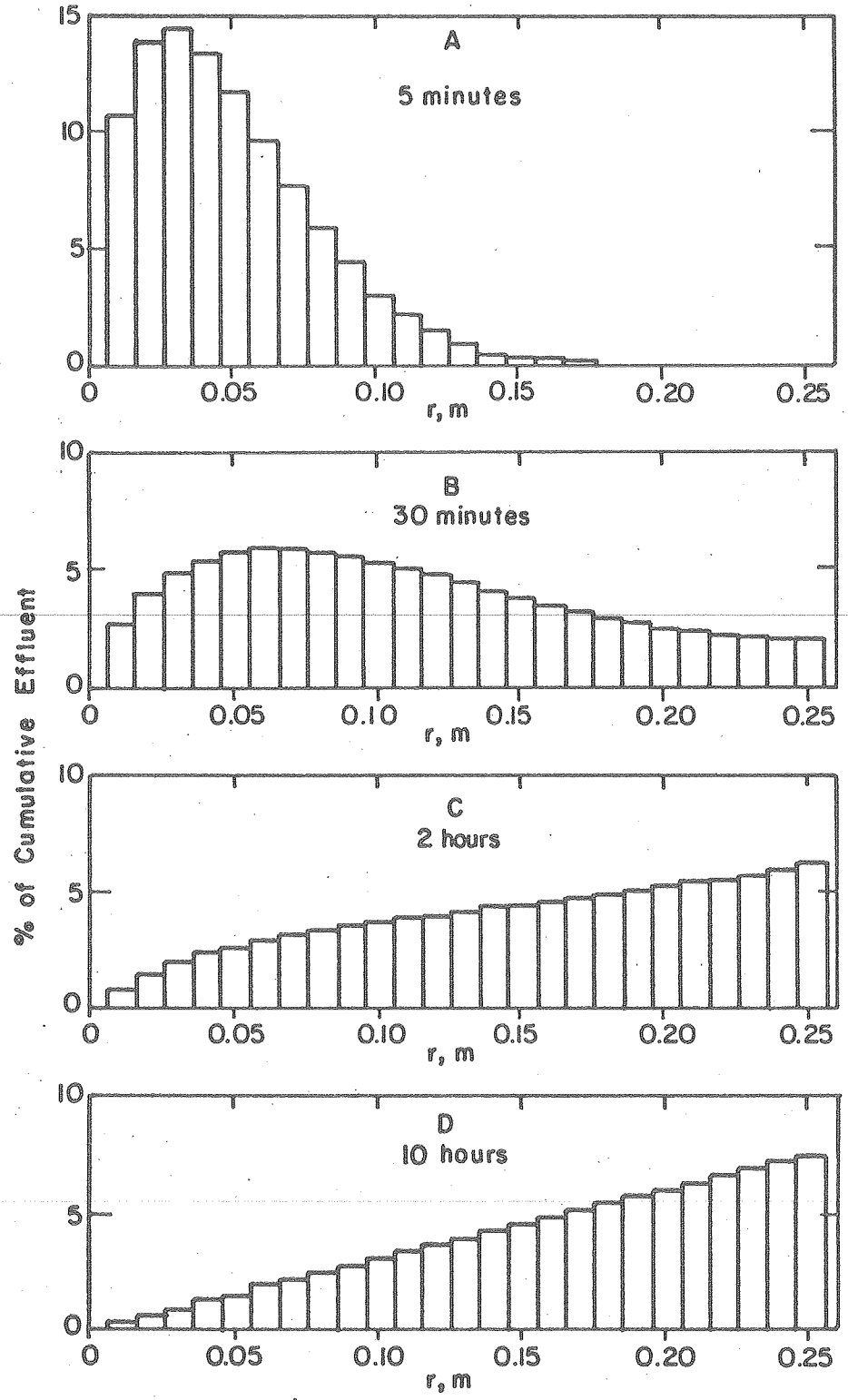

Fig. 68. Flow to a soil probe; per cent contribution to cumulative depletion from storage by one cm. wide shells of the flow region

CHAPTER VI

CONCLUSIONS AND RECOMMENDATIONS

A. CONCLUSIONS

1. Physics of the problem

The equation governing the transient, saturated-unsaturated flow of groundwater can be adequately expressed in an integral form as given in equation (II.41). This equation pertains to a material volume element which is fixed in the solid phase of the porous medium.

A special feature of this equation is that it treats the deformation of the soil skeleton rigorously, according to the one-dimensional consolidation theory of Terzaghi. Furthermore, this equation also takes into account the relationship between pore pressure and effective stress, which is particularly complex in the unsaturated zone, through the use of the parameter χ. Equation (II.41) is non-linear in that all the coefficients occurring in the equation are functions of the dependent variable, ψ.

2. Differential versus integral equations

For a long time it has been customary to formulate and teach the continuity equation in the form of a differential equation. A basic step in setting up this differential equation is to dispense with the term (dV), denoting the volume of the elemental region. This approach is convenient and justified in the case of steady-state problems or in the case of flow regions with rigid geometry. However, when the problem is that of non-steady flow and the flow region is

deformable (problems of subsidence, swelling soils) the term dV constitutes important information and its omission in setting up the differential equation renders a physical understanding of the problem considerably more difficult. On the other hand, directly formulating the mass balance equation in the form of an integral equation preserves the important information on dV and a physical understanding of the overall phenomenon becomes far more easier. Intuitively and physically, the integral formulation appears to be a direct, natural approach to the mass conservation problem.

In retrospect, it seems reasonable to speculate that the relative ease of analytically solving differential equations in comparison to integral equations and the lack of fast computational ability in the past might have been an important factor in the development and popularity of differential equations. Now that integral equations can be handled numerically, in addition to solving complex physical problems we can also gain the added benefit of easy formulation of the problem and probably, better communication with the average student.

3. Numerical methods.

Equation (II.41) is too complex to be easily solved by analytical methods. However, with the help of numerical methods, (II.41) could be successfully solved, to provide valuable insight into many complex problems of practical interest.

Of the numerical methods available, the so-called integral formulations (e.g. the Finite Element Method and the Integrated Finite Difference Method) offer the greatest power in terms of problems involving complex geometry. Basically, the integral formulations

seek to solve the mass balance equation for finite subdomains of the flow region. The average properties of these subdomains are associated with representative nodal points. The different integral formulations differ primarily in the process of averaging by which the subdomain properties are assigned to the representative nodal points.

The Integrated Finite Difference Method (IFD) is especially suited for handling multidimensional, heterogeneous flow regions with arbitrary geometry and was chosen as the basic tool of analysis for saturated-unsaturated groundwater flow studies described in the preceding chapters.

4. Development of the computer program TRUST

Using the IFD approach, a powerful computer program called TRUST has been developed. The basic calculational model for TRUST is the heat-flow computer program called TRUMP developed by Edwards (1969).

TRUST computer program helps analyze transient, saturated-unsaturated fluid flow in heterogeneous, isotropic multidimensional porous media. For advancing in the time domain, TRUST uses an optimized combination of explicit and implicit procedures in conjunction with an iterative scheme.

5. Testing the computer program and applications

TRUST computer program has successfully helped the solution of the following types of problems:

i) confined flow in two-dimensional and three-dimensional systems

ii) one-dimensional consolidation in slightly as well as highly deforming systems

iii) rainfall infiltration in dry sand

iv) saturated-unsaturated flow in one- and two-dimensional systems

v) pore pressure dissipation and deformation in arbitrarily loaded, deforming systems

vi) radial drainage from a partly saturated soil

B. RECOMMENDATIONS

The recommendations that follow the successful development of the computer program TRUST can be divided into two categories, viz., 1) the use of TRUST, as it is, to solve problems of practical interest and 2) improvements to the numerical model. We will consider each of these separately.

1. Use of computer program TRUST

The program TRUST can help solve a large class of problems ranging from purely saturated flow through saturated-unsaturated flow to purely unsaturated flow. These problems may include subsidence of geological systems, seepage through dams and embankments, flow of groundwater in complex, heterogeneous systems, saturated-unsaturated flow involved in recharge practices and, surface water-groundwater interactions and unsaturated flow in the vicinity of the root zone affecting plant growth. One cannot overemphasize the fact that the development of a computer program or a mathematical model is an end in itself; rather, it is a means to an end. The desired end is to use these tools to study practical problems of interest, hitherto beyond the grasp of detailed analysis.

In particular, the applicability of TRUST to analyze groundwater flow in the hard rock areas of India and elsewhere is worth mentioning. So far, no reliable tool is available to find reasonable answers to several important problems confronting the hydrogeologist investigating these areas. Among the chief concerns of these problems may be mentioned the following: identification of the patterns of groundwater motion in different geomorphological set ups; identification of the most significant field parameters that govern groundwater movement and development; identification of suitable criteria for defining safe yield of wells and optimum well-spacing; study of the complex factor that govern the flow towards large diameter dug wells, dug-cum-bored wells and bored wells; assessment of the zone of partial saturation in the overall groundwater budget; identification of the nature of the interaction between surface water bodies (such as ponds and lakes) and the groundwater reservoir and the possibility of coordinating the exploiting these sources towards an optimal use and conservation of the limited resources of water available. It is believed that the numerical model developed in this thesis can provide a reasonable starting point towards a rational approach to the complex problems detailed above. The use of the numerical model, as a complement to judiciously designed field studies, may prove to be extremely rewarding in the long run.

2. Improvements to the numerical model.

The numerical model developed in this thesis is versatile enough enough to be capable of modifications and extension to more general problems. These improvements could be discussed in two parts: a) improvements to the calculational model and b) improvements to the physics of the governing equation.

a. Improvements to the calculational model.

The IFD scheme, as developed in this thesis, evaluates only normal gradients across nodal surfaces. While this information is sufficient in the case of isotropic media, it is inadequate for handling anisotropy and other tensorial quantities, which require, for a complete solution, the evaluation of tangential gradients along nodal surfaces. To compute such tangential gradients, a suitable interpolation scheme would have to be incorporated into the IFD scheme. If this interpolation scheme is successfully incorporated, the range of effectiveness of the IFD would be greatly increased to include transport problems involving dispersion of the transported species (heat, soultes) as well as problems involving general stress-strain behavior of soils.

b. Improvements to the physics of the governing equation.

Perhaps the most significant area in which the physics of the governing equation can be improved is in relation to the handling of general stress-strain relationship in the soil. In the present form, the governing equation neglects lateral strain and is thus greatly simplified.

However, there exist numerous problems of interest to the soil and foundation engineer, engineering geologist and the seismologist, which deal with the reaction of water saturated systems to various types of arbitrary loading. For tackling these problems, the basic requirement is a mathematical model in which the general multidimensional equations of fluid flow and of stress-strain interaction are suitably coupled.

Once the interpolation scheme for evaluating tangential gradients along desired surfaces is incorporated into the IFD scheme, there should be no logical difficulty in handling the genral force balance equation and the general coupling of the stress equation and the fluid flow equation. When this is successfully done, three-dimensional analysis of dynamic, pore pressure dissipation problems will become practical and economic.

REFERENCES

Benthien, G.W., Semi Discrete Approximations to Linear-Boundary-Initial Value Problems, Ph.D. dissertation, Carnegie Mellon University, Department of Mathematics, 1973

Bishop, A.W., " The measurement of pore pressure in the triaxial test ", in Pore Pressure and Suction in Soils, Butterworths, London, 1961

Bishop, A.W., " The principle of effective stress ", Tek. Ukeblad, Norway, No. 39, 1959

Bishop, A.W. and G.E. Blight,"Some aspects of effective stress in saturated and partly saturated soils ", Geotechnique, 13, 177-197, 1963

Bishop, A.W. and I.B. Donald, " The experimental study of partly saturated soils in the triaxial apparatus ", Proc. Fifth Intl. Conf. on Soil Mech. and Found. Eng., 1, 13-21, 1961

Blight, G.E., " A study of effective stress for volume change ", Symposium on Moisture Equilibrium and Moisture Changes in Soils Beneath Covered Areas , Butterworths, Australia, 259-269, 1968

Braester, C., G. Dagan, S.P. Neuman and D. Zaslavski, A Survey of Equations and Solutions of Unsaturated Flow in Porous Media, Project No. A 10-SWC-77, Technion, Israel Inst. Tech., Haifa, Israel, pp. 176, 1972

Bruce, R.R. and A. Klute, " The measurement of soil water diffusivity ", Proc. Soil Sci. Soc. Am., 20, 458-462, 1956

Buckingham, E., Studies on the Movement of Soil Moisture, Bull. No. 38, U.S. Dept. Agriculture, 1907

Carslaw, H.S. and J.C. Jaeger, Conduction of Heat in Solids, Oxford University Press, London, 1959

Cooper, H.H. Jr., " The equation of groundwater flow in fixed and deforming coordinates ", Jour. Geophys. Res., 71, 4785-4790, 1966

Crank, J. and P. Nicholson, " A practical method for the numerical evaluation of partial differential equations of the heat conduction type ", Proc. Camb. Phil. Soc., 43, 50-67, 1947

Day, P.R. and W.M. Forsythe, " Effect of isotropic confining pressure on hydrostatic pressure of water in unsaturated soil ", Science, 136, 779-780, 1962

Day, P.R. and T.N. Narasimhan, " Dynamics of soil solution sampling by porous probes ", Abstracts, Soil Sci. Soc. Am., Annual Meeting, 1974

De Wiest, R.J.M., " Fundamental principles of groundwater flow ", in Flow through Porous Media, Editor, R.J.M. De Wiest, Academic Press, New York, 1959

Dusinberre, G.M., Heat Transfer Calculations by Finite Differences, International Text Book Co., Scranton, Pennsylvania, 1961

Edwards, A.L., TRUMP: A Computer Program for Transient and Steady-State Temperature Distributions in Multidimensional Systems, National Tech. Information Ser., UCRL 14754, Rev. II, Springfield Virginia , 22151, pp. 265, 1969

Emery, A.F. and W.W. Carson, An Evaluation of the Use of the Finite Element Method in the Computation of Temperature, Sandia Laboratories, Rept. No. SCL-RR-69-83, 1969

Ergatoudis, I., B.M. Irons and O.C. Zienkiewicz, " Curved isoparametric 'quadrilateral elements' for finite element analysis ", Intl. Jour. Sol. Str., 4, 31-42, 1968

Evans, G.W., R.J. Brousseau and R. Keirstead, Instability Considerations for Various Difference Equations Derived from the Diffusion Equation, Lawrence Livermore Laboratory, USRL 4476, 1954

Felippa, C.A., Refined Finite Element Analysis of Linear and Non-Linear Two-Dimensional Structures, Rept. SESM 66-22, Structural Engineering Laboratory, University of California, Berkeley, 1966

Finlayson, B.A., Method of Weighted Residuals and Variational Principles, Academic Press, New York, 1972

Freeze, R.A., " Three-dimensional transient saturated-unsaturated flow in a groundwater basin ", Water Resources Res., 7, 347-366, 1971

Gambolati, A., " Equation for one-dimensional vertical flow of groundwater - I: Rigorous theory ", Water Resources Res., 9, 1022-1028, 1973a

Gamobolati, A., " Equation for vertical one-dimensional flow of groundwater - 2. Range of validity of the diffusion equation ", Water Resources Res., 9, 1385-1396, 1973b

Hanks, R.J. and S.A. Bowers, " Numerical solution of the moisture flow equation for infiltration into layered soils ", Proc. Soil Sci. Soc. Am., 26, 530-534, 1962

Hartree, D.R. and J.R. Womerseley, " A method for the numerical or mechanical solution of certain types of partial differential equations ", Proc. Roy. Soc. London, Ser. A, 161, 353-366, 1937

Helm, D.C., " Evaluation of aquitard parameters by simulating observed compaction from known stress history ", Ph.D. dissertation, University of California, Berkeley, 1974

Hubbert, M.K., " The theory of groundwater motion ", Jour. Geol., 48, part 1, 785 - 944, 1940

Jacob, C.E., " Flow of groundwater ", in Engineering Hydraulics, editor, Hunter Rouse, John Wiley, New York, 1950

Klute, A., " The determination of hydraulic conductivity and diffusivity of unsaturated soils ", Soil Sci., 113, 264 - 276, 1972

Lambe, T.W. and R.V. Whitman, Soil Mechanics, John Wiley, 1969

Liakopoulos, A.C., " Transient flow through unsaturated porous media ", Doctor of Engineering dissertation, University of California, Berkeley, 1965

Mac Neal, R.H., " An asymmetrical finite difference network ", Quart. Appl. Math., 11, 295 - 310, 1953

Matyas, E.L. and H.S. Radhakrishna, " Volume change characteristics of partly saturated soils ", Geotechnique, 18, 432 - 449, 1968

McMurdie, J.L. and P.R. Day, " Slow tests under soil moisture suction ", Proc. Soil Sci. Soc. Am., 24, 441 - 444, 1960

Muskat, M., Flow of Homogenous Fluids, McGraw Hill, 1937

Neuman, S.P., " Saturated-Unsaturated seepage by finite elements ", Jour. Hydr. Div., ASCE, 99 (HY 12), 2233 - 2250, 1973

Neuman, S.P., " Finite element computer programs for flow in saturated-unsaturated porous media ", Project NO. A 10-SWC-77, Technion Israel Inst. Tech., Haifa, Israel, 1972

Neuman, S.P., R.A. Feddes and E. Bresler, " Finite element analysis od two dimensional flow in soils considering water uptake by roots: I. Theory ", Proc. Soil Sci. Soc. Am., (in press)

O'Brien, G.G., M.A. Hyman and S. Kaplan, " A study of the numerical solution of partial differential equations ", Jour. Math. Phys., 29, 223 - 251, 1951

Ollier, C.D., Weathering, Geomorphology Text 2, American Elsevier, 1969

Phillip, J.R., " Future problems of soil water research ",Soil Sci., 113, 294 - 300, 1972

Pinder, G.F. and E.O. Frind, " Application of Galerkin procedure to aq ifer analysis ", Water Resources Res., 8, 108-120, 1972

Poulos, H.G. and E.H. Davis, Elastic Solutions for Soil and Rock Mechanics, John Wiley, 1974

Richards, L.A., " Capillary conduction of liquids through porous mediums ", Physics, 1, 318-333, 1931

Richards, L.A., " Advances in soil physics ",

Trans., Seventh Intl. Conf. on Soil Sci., Madison, Wis., 1, 67-79, 1960

Rubin, J. and R. Steinhardt, " Soil-water relations during rain infiltration, I. Theory ", Proc. Soil Sci. Soc. Am., 27, 246-251, 1963

Rubin, J., R. Steinhardt and P. Reiniger, " Soil-water relations during rain infiltration ,II. Moisture content profiles during rains of low intensities ", Proc. Soil Sci. Soc. Am., 28, 1-5, 1964

Scheid, F., Numerical Analysis, Schaum's Outline Series, Mc Graw Hill, 1968

Schiffman, R.L. and R.E. Gibson, " Consolidation of non-homogeneous clay layers, Jour. Soil Mech. and Gound. Eng., ASCE, 90,(SM5), 1-30, 1964

Schultze, E. and A. Moussa, " Factors affecting the compressibility of sand ", Pro. Fifth Intl. Conf. on Soil Mech and Found. Eng., 1, 335-340, 1961

Sircar, P., Stress Deformation Characteristics of Compacted Clays, Ph. D. dissertation, Department of Civil Engineering, University of California, Berkeley, 1973

Skempton, A.W., " The pore pressure coefficients, A and B ", Geotechnique, 4, 143-147, 1954

Skempton, A.W. and D.J. Henkel, " Tests on London Clay from deep borings at Paddington, Victoria and South Bank ", Proc. Fourth Intl. Conf. on Soil Mech. and Found Eng., 1, 100-106, 1957

Smiles, D.E. and A.G. Harvey, " Measurement of moisture diffusivity of swelling systems ", Soil Sci., 116, 391-399, 1963

Smiles, D.E. and M.J. Rosenthal, " The movement of water in swelling materials ", Australian Jour. Soil Res., 6, 237-248, 1968

Sokolnikoff, I.S. and R.M. Redheffer, Mathematics of Physics and Modern Engineering, Mc Graw Hill, New York, 1966

Swartzendruber, D., " The flow of water in unsaturated soils ", in Flow Through Porous Media, Editor R.J.M. De Wiest, Academic Press, 1969

Terzaghi, K., "Principles of Soil Mechanics, A summary of experimental results of clay and sand ", Engineering News Record, 3-98, 1925a

Terzaghi, K., "Settlement and consolidation of clay ", Engineering News Record, 26, 1925b

Theis, C.V., "The relation between the lowering of the piezometric surface and the rate and duration of discharge of a well using groundwater storage ", Trans. Am. Geophys. Union, 16, 519-524, 1935

Todd, D.K., Ground Water Hydrology, John Wiley, New York, 1959

Vachaud, G.M., M. Vauclin, J.L. Thony and D. Khanji, Etude Experimentale du Drainage de la Recharge des Nappes a Surface Libre dans un Model Bidimenssionel, Laboratoires de Mecanique des Fluides, Universite Scientifique et Medicale de Grenoble, Cedex, 53, 38-Grenoble-Gare, 1971

Wilson, E.L., The Determination of Temperatures within Mass Concrete Structures, SESM Rept. No. 68-17, Department of Civil Engineering, Structual Engineering Laboratory, 1968

Witherspoon, P.A., J.K. Mitchell, S.P. Neuman and others, Aquitards in the Coastal Groundwater Basin of Oxnard Plain, Ventura County, Bull. No. 63-4, Dept. Water Resources, State of California, 1971

Zienkiewicz, O.C. and C.J. Parekh, " Transient field problems: Two-dimensional and three-dimensional analysis by isoparametric finite elements ", Intl. Jour. Num. Meth. Eng., 2, 61-71, 1970

U.S.GPO:1979-689-058(F)1

This report was done with support from the Department of Energy. Any conclusions or opinions expressed in this report represent solely those of the author(s) and not necessarily those of The Regents of the University of California, the Lawrence Berkeley Laboratory or the Department of Energy.

TECHNICAL INFORMATION DEPARTMENT
LAWRENCE BERKELEY LABORATORY
UNIVERSITY OF CALIFORNIA
BERKELEY, CALIFORNIA 94720